UCRL-MA-110630

DYNA2D

A Nonlinear, Explicit, Two-Dimensional Finite Element Code For Solid Mechanics - User Manual

Robert G. Whirley
Bruce E. Engelmann

Methods Development Group
Mechanical Engineering

John O. Hallquist
Originator

******* 1993 *******

DYNA2D

A Nonlinear, Explicit, Two-Dimensional Finite Element Code For Solid Mechanics - User Manual

Robert G. Whirley
Bruce E. Engelmann

Methods Development Group
Mechanical Engineering

John O. Hallquist
Originator

April, 1992

Preface

DYNA2D has been used extensively at the Lawrence Livermore National Laboratory over the past fourteen years. As a public domain code, DYNA2D has been applied to a wide variety of large deformation transient dynamic problems by analysts both at LLNL and elsewhere. DYNA2D was originated and developed by Dr. John O. Hallquist of the Methods Development Group at LLNL (Hallquist, 1978a), (Hallquist, 1988). During the period 1984-1987, he was joined by Dr. David J. Benson, who is now on the Engineering faculty at the University of California, San Diego. Dr. Hallquist continued as Lead Developer on DYNA2D until 1988, when he left LLNL to pursue a career in private business. During his time at the Laboratory, Dr. Hallquist made innumerable contributions to the field of computational mechanics; many of them by demonstration. It is with great respect for these accomplishments embodied in DYNA2D that the authors continue the expansion of DYNA2D's capabilities to meet new challenges in computational mechanics.

DYNA2D USER MANUAL

ABSTRACT

This report is the User Manual for the 1992 version of DYNA2D, and also serves as an interim User Guide. DYNA2D is a nonlinear, explicit, finite element code for analyzing the transient dynamic response of two-dimensional solids. The code is fully vectorized and is available on several computer platforms. DYNA2D incorporates a large deformation formulation to allow maximum flexibility in modeling physical problems. Many material models are available to represent a wide range of material behavior, including elasticity, plasticity, composites, thermal effects, and rate dependence. Also, a variety of equations of state are available for modeling the hydrodynamic response of many materials, including explosives and propellants. In addition, DYNA2D has a sophisticated contact interface capability, including frictional sliding, single surface contact, and a new automatic contact option. DYNA2D contains a rezoner to allow nodes to be repositioned when the finite element mesh becomes excessively distorted during a calculation. This rezoner can be used in either an interactive graphics mode or an automatic (noninteractive) mode. In addition, DYNA2D now contains a general remeshing option which allows a completely new mesh to be defined for a body during an analysis. A real-time analysis display option allows the analyst to view an evolving graphical display of the analysis results as they are calculated. A material model driver with interactive graphics display is incorporated into DYNA2D to permit accurate modeling of complex material response based on experimental data. This document provides the information necessary to apply DYNA2D to solve a wide range of engineering analysis problems.

1.0 INTRODUCTION

DYNA2D is an explicit, Lagrangian, finite element code for analyzing the transient dynamic response of two-dimensional solids. The element formulations available in this version include a 4-node constant stress element with several types of viscous and stiffness hourglass control. Many material models are available to represent a wide range of material behavior including elasticity, plasticity, composites, thermal effects, and rate dependence. A diverse equation of state library permits accurate modeling of the hydrodynamic behavior of many materials, including propellants and high explosives. In addition, DYNA2D has a sophisticated contact interface capability, including frictional sliding, tied interfaces, and single surface contact, to handle arbitrary mechanical interactions between independent bodies or between two portions of one body. An interactive ‘‘r-type’’ rezoner in DYNA2D allows nodes of distorted mesh to be repositioned, elements to be smoothed, and the calculation resumed. A new remeshing option allows an entirely new mesh to be constructed at any point in an analysis. The rezoning and remeshing options allow DYNA2D to analyze problems with very large distortions and shape changes. A material model driver with interactive graphics display is integrated into DYNA2D to allow computation of the stress response to any prescribed strain history without inertial effects. This feature allows accurate assessment of the representation of complex material behavior by the numerical constitutive model in DYNA2D.

Over the last fourteen years, DYNA2D has been widely used at LLNL and in industry. It has been applied to a wide spectrum of problems, many involving large inelastic deformations and contact. The code has evolved rapidly to meet changing engineering analysis requirements and to fully exploit current technology in computing hardware. Algorithms have been optimized, and nearly all of the code is now vectorized. Versions of DYNA2D are available for several computing platforms, including CRAY/NLTSS, CRAY/UNICOS, VAX/VMS, and workstations from SUN, Silicon Graphics, and IBM. The code has been ported to many other machines, and the use of X-Windows graphics allows the SUN version to port easily to other 32-bit UNIX-based machines such as a CONVEX. The use of a “single-source” development system assures that all new developments appear simultaneously in all supported code versions.

There are many new features and options in this release of DYNA2D which should improve its performance and versatility on a wide range of applications. Major new features in this release include a stiffness-based hourglass control option, an automatic contact algorithm which precludes the need to define master and slave slidelines, eroding slidelines for modeling material failure and

penetration, and an interactive-graphics based material model driver. Other new features include a simple ALE option for solving large distortion problems, a multiple line HE burn option, a viscous fluid material, the Armstrong-Zerilli rate-dependent constitutive model, the JWLB equation-of-state, and a variable order fit option for the Steinberg-Guinan and Steinberg-Guinan-Lund material models. In addition, this release debuts a very general remeshing option and a real-time analysis display feature which graphically depicts the progress of an analysis. A fully vectorized implementation of the two-invariant cap model with kinematic hardening has replaced the previous prototype implementation. Sense switches have been improved and made more robust. Finally, new with this release of DYNA2D is full support for the CRAY/UNICOS, IBM RS/6000, and Silicon Graphics platforms. These new developments substantially enhance the accuracy, efficiency, and user convenience of DYNA2D for a large class of engineering analysis problems.

DYNA2D is part of a set of public domain codes developed in the Methods Development Group at LLNL. Other analysis codes include the three-dimensional explicit DYNA3D code (Whirley and Hallquist, 1991), the implicit NIKE3D code (Maker, Ferencz, and Hallquist, 1990), and the implicit two dimensional code NIKE2D (Engelmann and Hallquist, 1990). TOPAZ2D (Shapiro and Edwards, 1990) and TOPAZ3D (Shapiro, 1985) are finite element codes for nonlinear heat transfer and field problem analysis. PALM2D (Engelmann, Whirley, and Shapiro, 1990) is a recently developed code for fully coupled thermomechanical analysis. Interactive graphics preprocessors and postprocessors include MAZE (Hallquist, 1983) and ORION (Hallquist and Levatin, 1985) for the two-dimensional codes and INGRID (Stillman and Hallquist, 1985) and TAURUS (Spelce and Hallquist, 1991) for the three-dimensional codes. All plotting is accomplished using the DIGLIB public domain graphics library developed by Hal Brand at LLNL.

As a public domain code, the use of DYNA2D by outside firms has been widespread, and this has played an important role in its development. Many code shortcomings have been discovered and remedied as a direct result of dialog with outside users in industry. In addition, many capabilities have been suggested or inspired by feedback obtained from Collaborators outside LLNL. It is hoped that the DYNA2D user community will continue to expand and provide feedback to the authors at LLNL, and that improvements made by others will be made available for possible incorporation into future versions of DYNA2D. This active participation provides important information for future development directions of DYNA2D.

2.0 OVERVIEW OF DYNA2D

DYNA2D is an explicit, nonlinear, finite element code for the transient dynamic response of two-dimensional solids. As an explicit code, DYNA2D is appropriate for problems where high rate dynamics or stress wave propagation effects are important. For static and low rate dynamic problems, the implicit NIKE2D code (Engelmann and Hallquist, 1991) may be more suitable. DYNA2D may be applied to quasistatic problems by simply applying the external loads slowly and integrating the dynamics equations until all significant transients have died out. In contrast to NIKE2D, DYNA2D uses a large number of relatively small time steps, with the solution being explicit (and inexpensive) at each step. Thus, DYNA2D does not form and solve the large matrix equation typical of implicit codes such as NIKE2D, and does not require iteration at each time step. This often leads DYNA2D to be compute-bound with modest memory requirements, whereas NIKE2D is often memory or I/O bound due to the assembly of a large stiffness matrix at each time step.

The algorithms and architecture are designed for speed and robustness. Nearly all of the code is now vectorized for optimal performance on vector computers such as the CRAY. DYNA2D has a 4-node continuum element formulation that handles geometric nonlinearities (large displacements and large strains) and does not lock for incompressible materials.

DYNA2D has material models that include:

- elasticity and plasticity (isotropic and anisotropic)
- finite elasticity
- volumetric compaction
- rate dependence
- thermal effects
- failure.

To model nonlinear pressure-volume behavior, DYNA2D has equations of state that include:

- polynomial functions
- high explosive models
- tabulated functions.

A variety of boundary conditions are available, including:

- prescribed velocities

- non-reflecting (transmitting) boundaries
- sliding boundaries along arbitrary planes.

Methods of prescribing loads include:

- nodal forces
- follower forces
- surface pressure loads
- body force loads
- loads due to thermal expansion
- Brode function airblast loads.

DYNA2D has a general interface contact capability which includes:

- frictional sliding
- single surface contact
- tied interfaces
- rigid walls.

The constraint modeling capabilities include:

- arbitrary nodal constraints.

The analysis capabilities of DYNA2D include:

- transient dynamic analysis

The code may be restarted with a variety of modifications to the analysis, including:

- changes in termination time
- deletion of portions of the model by element or by material
- deletion of sliding interfaces.

DYNA2D contains an ‘‘r-type’’ rezoner with interactive graphics which includes:

- smoothing of elements within a material
- smoothing or equispacing nodes on material boundaries
- ‘‘dekinking’’ of material boundaries
- display of analysis results using interactive color graphics.

DYNA2D now includes a new remeshing option which allows:

- arbitrary changes to mesh topology
- addition or deletion of materials, boundary conditions, and other model parameters
- solution of problems with very large distortions and shape changes.

An analysis display option is now available which allows:

- real-time graphics display of deforming mesh or other response quantities
- easy determination of appropriate times to rezone or remesh.

There are no inherent limits on the size of a DYNA2D analysis model, and storage allocation is dynamic within the code. Problem size is constrained only by the memory available on the computer. Current generation supercomputers have solved DYNA2D problems with almost 100,000 elements, and computing capabilities continue to expand as new generations of hardware become available.

The following sections in this chapter briefly discuss each of these capabilities and its applicability to engineering analysis problems.

2.1 NOMENCLATURE AND NOTATIONAL CONVENTIONS

This section will briefly describe the notational conventions used in the remainder of this manual. Vectors and tensors are denoted by boldface type ($\mathbf{v}$, $\mathbf{s}$), or in components by subscripted italic characters (v_i, s_{ij}), and matrices are generally indicated by boldface capital letters ($\mathbf{M}$, $\mathbf{K}$). The distinction between vectors and matrices or tensors will be clear from the context in which the symbol is used.

A set of typeface conventions is followed throughout this manual to allow the reader to easily distinguish between **commands**, *parameters*, and `computer generated text`. **Commands** appear in bold type, and should be entered verbatim. *Parameters* appear in italics, and should be given values when included in the input. `Computer generated text`, such as error messages or default file names, is printed in a typewriter-like font.

In the descriptions of input format, “column” numbers refer to character positions in the ASCII input file, “field” refers to a group of character positions which contains one item of data, and “format” specifiers suggest the FORTRAN format edit descriptor used to read that item of data. This form of input description is historical in nature, and evolves from the days when paper punch cards were the predominant medium for data input to the computer. Although those days have long past, this notation and general structure of the input definition has proved convenient and are therefore retained. Further, as modern model generation software progresses, the need for the analyst to directly interact with the DYNA2D input file diminishes. Currently, the most common reason for directly editing this file is to adjust an analysis control parameter, and these quantities are easily and quickly located in the current style of input.

2.2 UNITS

There is no unit system embedded in DYNA2D. Problems may be defined in any convenient, *consistent* set of units. The units must be consistent in that mathematical operations directly yield the correct units for the result quantity; no units conversion is done internally in the code. For example, Newton’s law states that force equals mass times acceleration, so when mass (in the chosen units) is multiplied by acceleration (derived from the chosen units), the resulting quantity must be force in the chosen units. Thus, if the force unit is lb_f, the length unit is in, and the time unit is s, then the units of acceleration are $\frac{in}{s^2}$ and the mass unit is $\frac{lb_f \cdot s^2}{in}$. This approach allows complete freedom in the choice of a units system in which to describe a problem.

2.3 GENERAL FORMULATION

DYNA2D is based on a finite element discretization of two spatial dimensions and a finite difference discretization of time. The explicit central difference method is used to integrate the equations of motion in time. The central difference method is only conditionally stable, and stability is governed by the Courant limit on the time step size Δt. Physically, this limit is essentially the time required for an elastic stress wave to propagate across the shortest dimension of the smallest element in the mesh. Equivalently, this maximum time step may be related to the period of the highest free vibration mode of the finite element mesh. DYNA2D automatically calculates

the maximum time step size at each step of the solution, and adjusts the time step accordingly to minimize the number of time steps used in a solution. This feature minimizes the cost of the analysis while assuring that stability is maintained.

DYNA2D offers two analysis geometry options: plane strain and torsionless axisymmetry. In plane strain analysis the problem is assumed to lie in the y-z plane, and the out-of-plane strain ε_{xx} is assumed zero. In axisymmetric analysis z becomes the axis of symmetry and y (or r) represents the radial direction.

For axisymmetric problems DYNA2D uses a Petrov-Galerkin formulation wherein the momentum equations are weighted by the product of the basis functions and the reciprocal of the radius. This method has proven to eliminate certain problems which arise on the axis of symmetry when the more conventional Bubnov-Galerkin formulation is used.

DYNA2D uses a lumped mass formulation for efficiency. This produces a diagonal mass matrix $\boldsymbol{M}$, which renders the solution of the momentum equation

$$\boldsymbol{M}\mathbf{a}_{n+1} = \mathbf{f}^{ext} - \mathbf{f}^{int} \tag{1}$$

trivial at each step in that no simultaneous system of equations must be solved. In the above equation, $\mathbf{f}^{ext}$ are the applied external forces, and $\mathbf{f}^{int}$ are the element internal forces. The new accelerations $\mathbf{a}_{n+1}$ are easily found, from which the updated velocity and coordinates are calculated using the central difference integration formulas.

2.4 MATERIAL MODELS

DYNA2D includes a large number of material models to represent a wide range of physical behavior. Some models are used with an equation-of-state to represent complex pressure-volume-energy behavior in a material; these are termed hydrodynamic models. The material models presently implemented are:

- elastic
- orthotropic elastic
- kinematic/isotropic plasticity
- thermo-elastic-plastic
- soil and crushable foam
- viscoelastic
- Blatz-Ko hyperelastic rubber

- high explosive burn
- fluid
- elastic-plastic hydrodynamic
- Steinberg-Guinan high rate elastic-plastic
- Johnson/Cook rate dependent elastic-plastic
- power law isotropic elastic-plastic
- viscoplastic
- Armstrong-Zerilli rate dependent elastic-plastic
- concrete/geological material
- extended two invariant geologic cap
- Frazer-Nash hyperelastic rubber
- laminated composite
- Isotropic elastic-plastic
- Steinberg-Guinan-Lund rate dependent elastic-plastic
- smooth cap model
- Bammann plasticity
- Bammann plasticity with damage

2.5 EQUATIONS OF STATE

A hydrodynamic material model requires an equation-of-state to define the pressure-volume relationship. The equations of state available in this release are:

- linear polynomial
- JWL high explosive
- Sack high explosive
- Gruneisen
- ratio of polynomials
- linear polynomial with energy deposition,
- ignition and growth of reaction in HE
- tabulated with compaction
- tabulated
- propellant
- pore collapse
- composite high explosive
- pressure vs. time via load curve
- JWLB high explosive

2.6 FINITE ELEMENT FORMULATION

The finite element formulations used in DYNA2D have been chosen for their accuracy, speed, and robustness in large deformation nonlinear problems. In an explicit analysis there are many small time steps, so it is important that the number of operations performed at each time step be minimized. This consideration has largely motivated the use of elements with one-point Gauss quadrature for the element integration. This approach gives rise to spurious zero energy deformation modes, or "hourglass modes," within the element. The element must then be stabilized to eliminate the spurious modes while retaining legitimate deformation modes. This stabilization is effectively accomplished in DYNA2D. A selection of stabilization methods is available to handle almost any situation, and the default algorithms have proven effective for most applications. All element operations are highly vectorized for optimal performance on vector computers.

The basic continuum finite element in DYNA2D is the four-node solid element with one-point integration. Spurious hourglass modes are stabilized using an "hourglass viscosity" or an "hourglass stiffness." Displacements within the element are interpolated using bilinear interpolation functions, and the constitutive equations are evaluated once per element per time step based on the state at the center of the element. This element is valid for large displacements and large strains. The element may be degenerated to a triangular element, but at the expense of accuracy. Thus, these degenerated elements should be avoided whenever possible.

2.7 LUMPED PARAMETER ELEMENTS

DYNA2D contains lumped parameter elements such as discrete springs, dampers, and lumped nodal masses. This feature allows DYNA2D to be used to solve simple spring-mass models, or to couple these simple models with complex finite element models. The lumped parameter elements were originally contributed by Dr. John Miles and colleagues at Ove Arup and Partners.

2.8 INITIAL AND BOUNDARY CONDITIONS

A transient dynamic problem requires the specification of initial conditions in order to be completely defined. In DYNA2D, initial conditions are specified as initial velocities. All initial velocities may be set to zero by setting a flag in the input, or the initial velocity of every node or a subset of nodes may be explicitly defined.

The time variation of quantities in DYNA2D is specified by "load curves." An arbitrary number of load curves may be defined, and any number of boundary conditions or loads may reference one load curve. Each load curve may have an arbitrary number of points.

DYNA2D contains a number of options for modeling the wide range of boundary conditions encountered in engineering analysis. Nodes may be constrained from translation in the global coordinate system. Nodes may be constrained to move only along an arbitrary but specified line by specifying, in the node input, the angle this line makes with the positive r-axis.

Nodes may be given prescribed velocities as a function of time in any global coordinate direction, or in an arbitrary direction specified by a given angle. In cases where prescribed velocities at $t = 0$ are not equal to defined initial velocities, significant dynamic loads are induced in the model due to the incompatibility of boundary and initial conditions.

Nonreflecting boundaries, also called "transmitting boundaries," may be defined to simulate semi-infinite domains and prevent spurious wave reflections due to the finite extent of the mesh. These boundaries are quite effective, but assume essentially linear material behavior. Thus, it is necessary to discretize the domain sufficiently far from the region of interest to contain all significant nonlinear material behavior in the analysis model.

2.9 LOADS

Several types of applied loads may be defined in DYNA2D. Most load definitions include time variation by reference to a load curve, and multiply the load curve value by a scale factor to evaluate the load to be applied. DYNA2D supports surface loads, body force loads, and thermal loads.

Surface loads may be specified as either nodal forces, follower forces, or surface pressures. Nodal forces may be defined in arbitrary directions by simply specifying the components in the two coordinate directions, and are defined as a function of time. The direction of concentrated nodal loads is fixed throughout the problem and does not evolve with the deformation. Follower forces may be defined which always act normal to a plane defined by two nodes. The direction of this force evolves with the deformation to remain normal to the specified plane throughout the analysis. Surface pressure loads may be defined, and these always act normal to the surface in the current configuration. Pressures may vary linearly over an element surface, and may be an arbitrary function of time. Alternatively, pressures may be defined to follow a Brode airblast time history shifted by a given shock wave arrival time based on the distance from the Brode origin.

Body force loads can be specified to represent physical phenomena such as gravity, electromagnetic forces, or centrifugal loads due to an angular velocity. Body force loads may be specified as arising from translational base acceleration or an angular velocity of the model about the z-axis. In DYNA2D, body force loads may be specified by a translational base acceleration $\boldsymbol{a}$, where $\boldsymbol{a}$ has components defined in the global coordinate directions. The body force density $\boldsymbol{b}$ is found from

$$\boldsymbol{b} = -\rho\boldsymbol{a}, \tag{2}$$

where ρ is the material mass density. In addition, body force loads arising from rotation about the about the z-axis may be defined. Body force density $\boldsymbol{b}$ at a point is then found from the angular velocity vector $\boldsymbol{w}$ and the radius vector $\boldsymbol{r}$ (from the origin to the point) by

$$\boldsymbol{b} = \rho\boldsymbol{w} \times (\boldsymbol{w} \times \boldsymbol{r}). \tag{3}$$

The time variation of the angular velocity component ω_z may defined using a load curve, but note that the time derivative of the angular velocity is *not* included in the body force density calculation.

Loads due to thermal expansion are applied by specifying temperature changes with material models which include thermal expansion. Nodal temperatures may be read from a TOPAZ2D (Shapiro and Edwards, 1990) plot database file, or may be individually specified and scaled by a load curve in the DYNA2D input file.

2.10 HIGH EXPLOSIVE BURN

DYNA2D contains several options for simulating the initiation and burning of high explosives. Beta burn defines a compression criteria for the ignition of HE. Programmed burn options allow the specification of lighting times or detonation points for problems where these are known. An HE ignition and growth equation-of-state allows the study of impact or temperature initiation of energetic materials, and is useful when the existence and location of detonation points must be determined by the solution of the boundary value problem. These features have proved useful on a wide range of problems from explosive metal forming to enhanced oil recovery. Each of the DYNA2D burn options is described below.

There are four options for determining the lighting time of HE materials, including ‘‘beta burn,’’ selected elements light at time zero, programmed burn, and specifying the lighting time of each element. The beta burn option does not use the concept of a lighting time, and computes a burn fraction F directly from

$$F = \beta(1 - V) = \frac{1 - V}{1 - V_{CJ}}, \quad (4)$$

where V is relative volume and V_{CJ} is the Chapman-Jouguet relative volume. Another burn option allows the specification, in the input, of elements which are lit at time zero. This option is particularly useful when a precise pattern of lighting is desired. The programmed burn option is really a family of options which determine lighting times based on specified detonation locations and geometries. These options are discussed in detail in section 4.5 on page 173. Single or multiple detonation points may be defined, and the lighting time of an element is computed based on the distance from the center of the element to the nearest detonation point. Similarly, a detonation line may be defined, and the lighting time of an element is computed based on the distance from the center of the element to the closest point on the detonation line. Multiple detonation lines may be included in the model, and each line may have a different lighting time. Alternatively, a Huygens detonation may be specified wherein a number of detonation points are defined together with ‘‘shadow surfaces,’’ and differing detonation velocities are used inside and outside the shadowed HE. The fourth burn option allows the specification, in the input, of a lighting time for each element composed of HE material. The above burn options allow considerable flexibility in defining the detonation geometry for high explosive problems. ** plot lighting times at t=0 as e-bar-p **

DYNA2D contains two equations-of-state for modeling the ignition and growth of detonation waves in high explosive materials. Equation-of-state 7, developed by Tarver and coworkers, models the behavior of single component explosives. Equation-of-state 12, developed by Nutt and coworkers, allows the modeling of two-component composite explosive materials. Equation-of-state 10 allows a simple model of the ignition and burning of propellant material. These three equations-of-state allow an analysis to determine whether an explosive will ignite and burn due to pressures and temperatures present in the solution of the boundary value problem. These models are quite complex, and care is urged in their use.

2.11 GENERAL INTERFACE CONTACT

DYNA2D contains a robust and efficient capability for modeling the mechanical interaction of two bodies or two parts of a single body. Seven different options are offered for defining the behavior of “slidelines” in a wide variety of situations. Six of these options are actually general slideline definitions, and the remaining one is a special purpose capability for treating interactions between a body and a rigid surface. All DYNA2D slidelines accommodate arbitrarily large relative motions.

There are no limits on the type or total number of slidelines defined for a DYNA2D model. In the remainder of this section, first each of the six slidelines is briefly discussed, and modeling suggestions are given. The special purpose rigid wall option is then presented.

The six types of slide surfaces supported in this release of DYNA2D are:

1. sliding only (kinematic formulation)
2. tied (kinematic formulation)
3. sliding with separation (kinematic formulation)
4. sliding with separation and friction (penalty formulation)
5. sliding with separation and no friction (penalty formulation
6. single surface slideline (penalty formulation)

A slideline is defined in the input file by a list of nodes lying along the interface. One side of the contact surface is referred to as the master surface and the other side is the slave surface. The importance of the distinction between master and slave surfaces is discussed below. *The slave surface must lie to the left of the master surface as one moves along the master surface, encountering the master nodes in the order they are defined.* Arbitrary mesh refinement on adjacent sides of the interface is permitted.

There are two basic types of slidelines in DYNA2D, and the main difference is the way in which penetrating nodes are handled. The *kinematic methods* operate at the velocity/acceleration level and modify coordinates to put the penetrating node back onto the target surface. The *penalty methods* operate at the kinetic level and apply a restoring force to the penetrating node to push it back to the target surface. This restoring force is proportional to the depth of penetration, the bulk modulus of the penetrated material, the dimensions of the penetrated element, and a scale factor specified by the user. The amount of penetration observed is inversely proportional to the chosen scale factor. Using a larger penalty scale factor reduces the observed penetration, but may make the problem more difficult to solve. Using a smaller penalty scale factor makes the problem easier to solve, but may lead to unacceptably large interpenetrations. The penalty scale factor is defined in the Control Section of the DYNA2D input file and has a default value of 0.10.

Generally, experience has indicated that the kinematic slideline methods work best in high pressure hydrodynamic applications, and the penalty methods work best in lower pressure solid mechanics applications. There are clearly problems where the choice is unclear, and experience provides the most reliable guidance.

Sliding interfaces and contact in DYNA2D are formulated using a “node on surface” concept, as described in (Hallquist, 1978) and (Hallquist, Goudreau, and Benson, 1985). *Slave* nodes are restricted from penetrating *master* surfaces. Conceptually, the two-surface algorithms could thus be thought of as looping over all slave nodes, and for each slave node checking that there is no penetration through any of the master segments defined for this slideline. The kinematic slideline formulations are not symmetric, and therefore it is important that the master surface be chosen as the more coarsely meshed surface. The penalty method formulations are symmetric treatments in that the designation of the two surfaces as slave or master are interchanged, and the contact algorithm is applied a second time. Thus, each surface goes through the penalty contact algorithm once as a master surface and once as a slave surface. This symmetric approach has been found to greatly increase the robustness and reliability of penalty method slidelines.

During the initialization phase of DYNA2D, nodes on a slideline which are initially interpenetrating are put back on the surface before the dynamic calculation is begun. A message is written to the screen and a summary printout is provided in the “hsp” file when this occurs. Initial interpenetration may result from errors in the definition of the model, or simply from curved parts of different mesh densities placed in close proximity to each other. In the latter case, the maximum distance a node was moved should be a small fraction of the minimum element dimension.

The **sliding only** (type 1) slideline is a two-surface method based on a kinematic formulation. The two surfaces are allowed to slide arbitrarily large distances without friction, but are not permitted to separate or interpenetrate. This option performs well when extremely high interface pressures are present.

The **tied** (type 2) slideline is not really a slideline at all, but is a feature for joining two parts of a mesh with differing mesh refinement. This is also a kinematic formulation, so the more coarsely meshed surface should be chosen as the master surface.

The **sliding with separation** (type 3) slideline is the most general kinematic formulation. This option allows two bodies to be either initially separate or in contact, and surfaces may separate and come together in a completely arbitrary fashion. Large relative motions are permitted. Since this is a kinematic formulation, the master surface should be chosen as the more coarsely meshed surface. There is no friction in this formulation.

The **sliding with separation and friction** (type 4) slideline is the most generally applicable option for engineering solid mechanics. This implementation is a penalty formulation, and allows two bodies to be either initially separate or in contact. Large relative motions are permitted, and rate-dependent Coulomb friction is included. Surfaces may separate and come together in a completely arbitrary fashion.

The **sliding with separation and no friction** (type 5) slideline is very similar to the type 4 slideline, but does not include friction and is slightly less expensive. This implementation is a penalty formulation, and allows two bodies to be either initially separate or in contact. Large relative motions are permitted. Surfaces may separate and come together in a completely arbitrary fashion.

The **single surface contact** (type 6) slideline is a penalty formulation used for modeling two portions of the same body which may come into contact. This situation often arises in buckling problems, where one surface often develops folds and comes into contact with itself. Frictional sliding is permitted between surfaces in contact.

"Rigid walls," also known as "stonewalls," may be defined to represent a rigid, planar, stationary surface. Rigid walls permit modeling unilateral contact without requiring discretization of the target surface, and thus are considerably less expensive than defining a type 4 slideline.

2.12 ERODING SLIDELINES AND AUTOMATIC CONTACT

DYNA2D now incorporates ''eroding slidelines'' for penetration and material failure. In addition, there is now an ''automatic contact'' feature which automatically identifies surfaces of potential contact and eliminates the need to specify master and slave surfaces. This option is currently slightly more expensive than the traditional contact algorithms, but continued development is expected to reduce this difference.

Eroding slidelines are a technique for modeling penetration events using a Lagrangian finite element method. Erosion models were developed and popularized by Johnson and coworkers (Snow, 1982), (Stecher and Johnson, 1984), (Kimsey and Zukas, 1986), (Johnson and Stryk, 1986), (Johnson and Stryk, 1987). A failure criterion is defined for the materials involved, and initial slidelines are defined between the penetrating object and the target. During the impact process, elements

on the surface of the target (and possibly the penetrator) are deleted when the material in these elements exceeds the failure criterion. The slideline is automatically redefined to include the newly exposed outer boundaries of the penetrator and target materials and the calculation continues.

To activate eroding slidelines in DYNA2D, first select automatic contact as described in section 4.1 on page 37. The material(s) which may erode must be included as active in the automatic contact definition. Next, for eroding materials, define the effective plastic strain at failure. The failure models are described in detail with the material descriptions. This version of DYNA2D allows erosion with material types 3, and 5. Other material failure options will be added in future versions of DYNA2D.

Automatic contact allows the proper modeling of interactions between two bodies without the explicit definition of slidelines between the two bodies. When automatic contact is used, algorithms in DYNA2D identify regions of possible contact and prevent interpenetration within those regions. Rate dependent Coulomb friction may be included, if desired. Automatic contact is more convenient to use than conventional slidelines, and also reduces the probability of difficulties due to input errors. This generality does make automatic contact somewhat more expensive than defining the appropriate slidelines, however, since an analyst can usually eliminate some potential contact regions from the slideline based on an intuitive understanding of the problem under consideration. Users are encouraged to report their experiences with this new feature in DYNA2D.

2.13 CONSTRAINT EQUATIONS

Constraint equations may be explicitly defined in DYNA2D. Nodal constraint equations simply specify that two or more nodes share a global degree-of-freedom. This feature is sometimes useful in defining unique boundary conditions on an analysis model.

2.14 ARBITRARY LAGRANGIAN EULERIAN (ALE) OPTION

This version of DYNA2D incorporates an arbitrary Lagrangian Eulerian (ALE) option. This capability was first developed for DYNA2D by Benson (see Benson**,** 1986 and Benson, 1989), and has been under wide study in the research community in recent years (Haber, 1984), (Liu, Belytschko, and Chang, 1986), and (Ghosh and Kikuchi, 1991). The ALE in DYNA2D is termed in the literature “Simple ALE” because each finite element is assumed to contain only one material. This assumption differentiates “Simple ALE” from “Complex ALE,” wherein each element (or finite difference zone) may contain multiple materials whose fractions and interfaces must be

tracked throughout the mesh. The simple ALE implementation in DYNA2D can appropriately be regarded as automatic rezoning, since the end effect is to move the mesh around within material boundaries to minimize mesh distortion and thereby improve computational accuracy. Although the formulation doesn't permit mixed-material elements, the DYNA2D ALE option has proven useful on a wide variety of large-deformation applications.

2.15 ANALYSIS OPTIONS

DYNA2D is most efficient for transient dynamic analysis, although it may also be used for quasi-static analysis. A transient dynamic analysis using the central difference method is performed whenever loads are given their actual, physically realistic variation with time. A quasistatic analysis may be performed by simply applying the loads very slowly and running the analysis until all significant transient oscillations have died out. The remaining solution is the quasistatic solution. This quasistatic analysis procedure may confidently be used with history dependent materials if dynamic oscillations are kept to a minimum (i.e., loads are applied sufficiently slowly).

2.16 ANALYSIS DISPLAY

DYNA2D now has the capability to display the deforming body in color as an analysis progresses. This display is updated at a specific simulation time interval, and may show any graphical display available in the rezoner such as the deformed mesh, or contour/fringe plots of element quantities such as stress or effective plastic strain. The analysis display option is activated by specifying a nonzero time interval between display updates on Control Card 6, or interactively by sense switches. The use of Analysis Display is described in section 3.6 on page 32. The analysis display option does not interfere with interactive or non-interactive rezoning in any way; the two capabilities are completely independent.

The analysis display option is a convenient new feature in DYNA2D. It allows the analyst to easily monitor the progress of an analysis, and intervene if required. This feature also allows the analyst to promptly terminate an analysis which is seen to be incorrect, thus saving both computer time and turn-around time that would have been otherwise wasted.

2.17 RESTART

DYNA2D supports a restart capability to continue calculations once they have been terminated by a user request or a computer system crash. Restart files are written at an interval specified in the input file, and are written sequentially. Standard restart files are never overwritten, and therefore the analysis may be restarted from any restart dump state. Since these files accumulate, the frequency of writing standard restart files is often limited by the amount of available disk space.

DYNA2D allows many changes to the model and analysis at a restart. These changes are specified in an optional “restart input file,” which is specified in addition to the binary “restart dump file” which contains the data from the first part of the run. The restart input file need not be supplied if nothing is to be changed. Analysis options which can be changed at restart include termination time, plot data dump interval, and restart dump intervals. In addition, the model itself may be changed during a restart, including deletion of any number of materials, elements, or slidelines.

2.18 MATERIAL MODEL DRIVER

DYNA2D incorporates a Material Model Driver to simplify fitting material models to experimental data. The driver computes the stress response to a prescribed strain path, and allows the results to displayed in an interactive graphics environment. Any stress, strain, or history variable may be plotted against any other component to allow clear insight into the material model behavior. In the Material Model Driver, the stress response is computed without inertial effects, so the true constitutive response is shown. This capability is available for all DYNA2D material models, and the material input format is identical to that used for dynamic analysis. The Material Model Driver is described in detail in Chapter 8 of this manual.

2.19 REZONING

Explicit Lagrangian codes are well suited for problems with moderate element distortions. When distortions become excessive, Eulerian approaches may become necessary. However, Lagrangian formulations are usually preferred for solid mechanics for various reasons, including good resolution of material interfaces, accurate treatment of history dependent material models, and general contact capabilities. Rezoning and remeshing may be used to extend the domain of application for Lagrangian codes to problems with large distortions. Rezoning is described below, and remeshing is described in section 2.20 on page 25.

The DYNA2D implementation for rezoning is based on (Hallquist, 1982b) and (Goudreau and Hallquist, 1982). Rezoning is performed in three phases:

1) Generate nodal values on the old mesh for all variables to be remapped.
2) Rezone one or more materials either interactively or automatically via a command file.
3) Perform the remapping by interpolating from nodal values of the old mesh.

When rezoning interactively, current results can be interactively displayed. Automatically rezoning via a command file requires some understanding of the deformations *a priori*. However, automatic rezoning has proven to be an important option for performing parameter studies.

Nodal values of all element variables, such as stress, are computed in Phase 1. A global variable to be remapped is approximated piecewise by a continuous field g, defined over each element in terms of nodal variables as

$$g = \mathbf{f}\mathbf{g}_e, \tag{5}$$

where are shape functions of the same order as those used in the finite element analysis, and $\mathbf{g}_e$ is a vector of nodal point values. Given a variable h to be remapped, a least squares fit is obtained by minimizing the functional

$$\Pi = \sum_e \int_{\Omega_e} (g - h)^2 d\Omega_e , \tag{6}$$

with respect to nodal values. The minimization

$$\frac{\partial \Pi}{\partial g_i} = 0 \qquad i = 1, 2, \ldots, n, \tag{7}$$

requires the solution of the set of linear equations

$$\mathbf{M}\mathbf{g} = \mathbf{f}, \tag{8}$$

where

$$\mathbf{M} = \sum_e \mathbf{m}^e = \sum_e \int_{\Omega_e} \mathbf{f}^T \mathbf{f} d\Omega_e \tag{9}$$

$$\mathbf{f} = \sum_e \mathbf{f}^e = \sum_e \int_{\Omega_e} \mathbf{f}^T h d\Omega_e. \tag{10}$$

If the ‘‘mass’’ matrix is lumped as

$$\hat{M}_i = \sum_{j=1}^{a} M_{ij}, \tag{11}$$

the calculation of the desired nodal values is simply

$$g_i = \frac{f_i}{\hat{M}_i}. \tag{12}$$

Equation (12) provides an initial guess for $\boldsymbol{g}$. This is used as a starting vector to iterate for a solution that ultimately satisfies (8), while avoiding matrix inversion (see Zienkiewicz, Xi-Kui, and Nakazowa, 1985). Iterations are performed using the recursive relation

$$\mathbf{g}^{i+l} = \hat{\mathbf{M}}^{-1}[\mathbf{f} - (\mathbf{M} - \hat{\mathbf{M}})\mathbf{g}^i], \tag{13}$$

where convergence is determined by

$$\frac{\|\mathbf{g}^{i+1} - \mathbf{g}^i\|}{\|\mathbf{g}^{i+1}\|} \le e_r. \tag{14}$$

The value of e_r may be specified in the input file, and has a default of 0.01. Tighter tolerances lead to nodal values that are only marginally more accurate but at the cost of many more iterations. Convergence to $e_r = 0.01$ is typically achieved in less than 5 iterations, and is monotonic. Tighter tolerances, for example $e_r = 0.0001$, can require up to forty iterations to attain convergence. Cost per iteration, however, is relatively inexpensive since the element consistent ‘‘mass’’ matrices are computed once and stored.

In the output file of DYNA2D, each element variable is compared with its interpolated value from the nodes. A percentage error is computed at each Gauss point by

$$\text{percent error} = \frac{|h_g - \tilde{g}|}{h_{max} - h_{min}} \times 100 \tag{15}$$

where h_g is the actual Gauss point value, $\tilde{g}$ is the interpolated value from the fit, h_{max} is the maximum value in the material, and h_{min} is the minimum value in the material.

An average value over all elements is computed and printed. The errors are usually under 5% which is well within the range of acceptable accuracy for most calculations.

After element consistent mass matrices are computed and stored, (8)-(13) are applied to each history variable, i.e., stress, plastic strain, energy, density, etc., for each material. This necessitates $m \times n$ applications of these latter equations where m is the number of materials used in the analysis and n is the number of history variables. The resulting $m \times n$ nodal vectors are stored for possible use in the third phase of rezoning. The efficient implementation of the first phase makes its cost insignificant relative to third phase remap.

Phase two is performed either interactively or automatically using a rezone command file. Interactive rezoning includes color graphics that can be used to study current response variables, including the capability to display:

- color fringes,
- contour lines,
- vector plots,
- principal stress lines,
- deformed meshes and material outlines,
- profile plots,
- reaction forces,
- interface pressures along slidelines.

All relevant variables can be plotted including constitutive model state variables that are not available in the output database for post-processing. Copies of the plots can be obtained as black-and-white or color postscript, or as DLI files at LLNL.

Rezoning involves dekinking slidelines and material boundaries, adjusting the spacing of boundary nodes, and moving the interior nodes to achieve a smooth mesh. The total number of nodes and elements is preserved, making this an ‘‘r-type’’ rezoner. Three methods are available in DYNA2D for smoothing interior nodes. They are the equipotential method, isoparametric interpolation, and a combination of the two obtained by a linear blending. Other methods have been proposed. The QMESH manual (Jones, 1974) provides an excellent description and evaluation of a variety of techniques. In applying the relaxation, the new nodal positions are given by

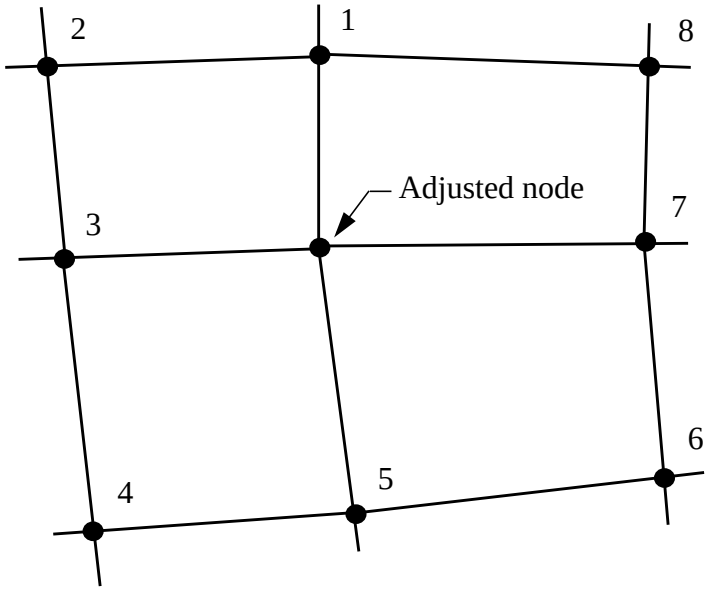

Figure 1
Nodal stencil for smoothing.

$$r = \frac{\sum_{i=1}^{8} \zeta_i r_i}{\sum_{i=1}^{8} \zeta_i}, \tag{16}$$

$$z = \frac{\sum_{i=1}^{8} \zeta_i z_i}{\sum_{i=1}^{8} \zeta_i}, \tag{17}$$

where r_i and z_i are the nodal positions relative to the node being moved as shown in Figure 1.

The weights for equipotential smoothing are

$$\zeta_1 = \zeta_5 = \frac{1}{4}[(r_7 - r_3)^2 + (z_7 - z_3)^2] \ , \tag{18}$$

$$\zeta_3 = \zeta_7 = \frac{1}{4}[(r_1 - r_5) + (z_1 - z_5)^2] \ , \tag{19}$$

$$\zeta_2 = \zeta_6 = \frac{1}{2}[(r_1 - r_5) + (z_1 - z_5)(z_7 - z_3)] \ , \tag{20}$$

$$\zeta_4 = \zeta_8 = -\zeta_2, \tag{21}$$

and for isoparametric smoothing are

$$\zeta_1 = \zeta_3 = \zeta_5 = \zeta_7 = 0.50, \tag{22}$$

$$\xi_2 = \zeta_4 = \zeta_6 = \zeta = \zeta_8 = -0.25. \tag{23}$$

Since logical regularity is not assumed in the mesh, the nodal stencil is constructed for each interior node, and then relaxed. The nodes are iteratively moved until convergence is obtained.

In phase three, new element Gauss point values in the rezoned regions are found by interpolation from the nodal values on the old mesh. Nodal quantities are likewise determined by interpolation.

2.20 REMESHING

DYNA2D now contains a powerful remeshing capability to further enlarge the class of problems that can be solved. This new feature allows the mesh to be completely redefined at any point in an analysis, and new objects can even be added to the analysis model. This capability is most useful for problems with extremely large shape changes, where element distortions become too large to correct just by moving nodes around with the standard DYNA2D rezoner. Examples of problems in this class include projectile penetration and bulk metal forming operations. This is a new feature within DYNA2D, and innovative users will doubtless find many unforeseen applications for this general capability.

The DYNA2D remeshing capability works by allowing the user to stop an analysis, enter the DYNA2D rezoner and write out MAZE line definitions defining the deformed boundary of each material. These line definitions are then read into MAZE where a completely new mesh is developed for the deformed part, along with appropriate boundary conditions, loads, and slidelines.

The resulting new analysis model is then input to DYNA2D along with the restart file from the old analysis model. All stresses, velocities, accelerations, and material history variables are initialized from the old model, and the analysis then continues using the new model.

3.0 ANALYSIS WITH DYNA2D

The typical engineering analysis process begins with a physical description of some problem or system to be studied. First, a pre-processor or mesh generator is used to construct the model. This program writes a DYNA2D input file. This input file is a standard ASCII text file, so it may be edited or modified at this stage, if desired. Next, the DYNA2D analysis is run, which generates the ASCII printout file and a number of binary plot and restart files. The analysis may be conducted all in one run, or there may be multiple DYNA2D terminations and restarts in this part of the process. Finally, a post-processor is used to read the binary plot files and create display and hardcopy graphics output of desired quantities. Each of these steps is described in the sections that follow.

3.1 PRE-PROCESSING AND MODEL GENERATION

DYNA2D does not contain any significant model generation capability, and relies totally on external software for this task. The public domain mesh generator MAZE (Hallquist, 1983) is widely used at LLNL and provides full support for all DYNA2D analysis options. The format of the DYNA2D input file is described in Chapter 4 of this manual. Since the DYNA2D input file is in ASCII text format, many users find it convenient to do all model generation on an engineering workstation, and then transfer the DYNA2D input file to a larger computer to run the analysis.

3.2 STARTING A NEW DYNA2D ANALYSIS

The execution line for DYNA2D varies slightly depending on the computing platform. On CRAY UNICOS and UNIX workstation systems, the execution line is:

DYNA2D i=*inf,* **o**=*otf,* **g**=*ptf,* **d**=*dpf,* **f**=*thf,* **t**=*tpf,* **c=***rcf,***s**=*acf,***m**=*mlf*

where

inf=input file name [**i**]
otf=printed output file name [**o**]
ptf=binary state data plot file name (for post-processing [**g**])
dpf=binary standard dump file name (for restarting [**d**])
thf=binary time history data plot file name (for post-processing [**f**])

tpf=binary TOPAZ2D plot file name (for temperature profiles [**t**])
rcf=rezoning command file name (for automatic rezoning [**c**])
acf=analysis display command file name [**s**]
mlf=file name containing line definitions for use in MAZE with the remeshing option [**m**].

On VAX (VMS) systems, the execution line is:

run DYNA2D

The user then types the file name specifications when prompted:

i=*inf*, **o**=*otf*, **g**=*ptf*, **d**=*dpf*, **f**=*thf*, **t**=*tpf*, **c**=*rcf*,**s**=*acf*,**m**=*mlf*

File names must be unique and can have up to six characters. When starting an analysis, the input file name must be specified. For example,

DYNA2D i=*inf*

is a valid execution line. The specification of other file names is optional, except as noted below.

A TOPAZ2D plot file name, **t**=*tpf*, must be specified if nodal temperatures are to be read from a TOPAZ2D plot file. A rezoning command file name, **c**=*rcf*, should be specified if automatic rezoning is desired.

Due to the large volume of data generated by a typical DYNA2D analysis, printed results output is of limited use and is not generated by default. Printed results may be obtained for nodes and elements selected in time history blocks may be obtained by *not* specifying **f**=*thf* on the DYNA2D execution line. This omission will signal DYNA2D to write the results for the selected nodes and elements into the printed output file instead of into a binary time history data plot file. A binary time history file for post-processing with ORION is produced if **f**=*thf* is specified on the DYNA2D command line.

The default file names for DYNA2D files are given in Table 1. It is expected that all file names will have a file extension of .DAT on VAX/VMS systems, however, this extension should never be specified in defining a file name. No file name extensions are expected on non-VMS systems.

Table 1:

Identifier	Default file name	Purpose
inf	(none)	input file
otf	d2hsp	printed output file
ptf	d2plot	binary plot state data file
dpf	d2dump	binary standard restart dump file
thf	d2thdt	binary time history data plot file
tpf	(none)	TOPAZ2D plot file containing temperature data
rcf	(none)	rezone command file
acf	(none)	analysis display command file
mlf	mazlin	MAZE line definition file for remesh option

File sizes are set depending on the computing platform being used. Like the other codes in the MDG set, DYNA2D uses a familied file system to control the length of individual files. In this system, a root file is augmented by additional “family members” when data to be written exceeds the set file length. New family members are named by appending a two digit number to the root name. For example, following an analysis with several state dumps written to the plot state database, the resulting family of binary files might be

```
d2plot
d2plot01
d2plot02
d2plot03.
```

If, instead of the default, the binary state data plot file name **g**=*pltdat* had been given on the command line, the resulting file family would be

```
pltdat
pltdat01
pltdat02
pltdat03.
```

Note that file families are specified by their root name, and that there is a maximum of 100 files in a family.

3.3 INPUT FILE CONVERSION

Previous versions of DYNA2D have used various input file formats. For the last five years, this format has been as described in the 1987 and 1988 DYNA2D User Manuals. This manual introduces a completely new input file format, denoted the `92` format. The new version of DYNA2D will run using input files with the old format, but it is advantageous to use the new format since more functionality is available. Since many DYNA2D users have valuable input files in the old format, an input conversion utility has been incorporated into this version of DYNA2D. The conversion utility converts input files which either follow the 1988 manual or the `87` format into the `92` format. To convert an old file, first change its name to `convert`. Then run DYNA2D using the execution line

DYNA2D i=`convert`, **s**=*nwf*.

The code will convert the old input file and terminate. The file *nwf* will contain the input data in the 92 format.

3.4 INTERACTIVE ANALYSIS STATUS QUERY

DYNA2D offers several “sense switches” to allow the brief interruption of an analysis to request a status report, request that a plot state or restart file be written at the current time, or to cleanly terminate the run. To use sense switches on CRAY/NLTSS, simply type the desired switch while DYNA2D is executing. On CRAY/UNICOS, VAX/VMS, and SUN/SGI/IBM machines, first interrupt execution by typing <`ctrl`>`c`, and then enter the desired sense switch at the prompt. The following eight sense switches are available:

Table 2: DYNA2D Sense Switches

Type	Code Response
sw1.	A restart file is written and DYNA2D terminates.
sw2.	DYNA2D responses with time and time step information.
sw3.	A restart file is written and DYNA2D continues.
sw4.	A plot state is written and DYNA2D continues.
sw5.	Enter interactive graphics and rezoning phase.
sw6.	Turns on step-by-step printout of time, time step number, and controlling element number into the hsp file. Retyping this sense switch turns this output off.
sw7.	Prompt for new graphics commands for analysis display.
sw8.	Activate or enter new time interval for analysis display.

3.5 RESTARTING A DYNA2D ANALYSIS

The execution line for restarting a DYNA2D analysis from a restart dump file is

DYNA2D i=*irf*, **r=***rtf***, o**=*otf*, **g**=*ptf*, **d**=*dpf*, **f**=*thf*, **t**=*tpf*, **c**=*rcf*, **s**=*acf*, **m**=*mlf*

and for restarting a DYNA2D analysis and immediately entering the rezoner is

DYNA2D z=rezone, i=*irf*, **r=***rtf***, o**=*otf*, **g**=*ptf*, **d**=*dpf*, **f**=*thf*, **t**=*tpf*, **c**=*rcf*, **s**=*acf*, **m**=*mlf*

where

rtf=binary restart dump file name, including the full family name (e.g., d2dump03)

irf=optional restart input file name

and the other file designations are as given in Section 3.2. The restart input file, **i**=*irf*, is optional. This file may be used to redefine output intervals for plotted and printed data and make other modifications to the analysis model. The format of the restart input file is described in Chapter 5.

Care must be taken to specify the entire name of the binary restart dump file, and not just the root name (e.g., d2dump03, not just d2dump). This is necessary since family members in a standard restart dump sequence represent different points in an analysis, and it is necessary to specify which restart dump is to be used as the starting point for the current restart run. Some very large problems require two standard restart dump file family members to store the required data for one restart dump. This case is easily recognized since DYNA2D writes to the screen the name of the first file in which a specific restart dump is written. In most cases, the first three restart dumps would produce messages to the screen like

```
 restart file d2dump01 written, 186350 words
 restart file d2dump02 written, 186350 words
 restart file d2dump03 written, 186350 words
```

For very large problems, the first three restart dumps would produce messages to the screen like

```
restart file d2dump01 written, 1586232 words
restart file d2dump04 written, 1586232 words
restart file d2dump07 written, 1586232 words
```

When restarting these very large problems, the restart dump file name specified by **r**=*rtf* on the command line should name the first restart file family member for the desired restart dump. For example, to restart the very large problem above from the second restart dump state, a valid execution line might be

DYNA2D r=d2dump04

Specifying the name of restart files is the *only* time a family file member name should be specified including the two digit suffix.

3.6 ANALYSIS DISPLAY WITH DYNA2D

The flexibility of workstation-based window systems has driven the need for a continuous display of analysis results while running DYNA2D. Results are displayed using one or a sequence of graphics commands that are described in Chapter 6. The commands available for analysis display are a subset of those available for interactive rezoning and are very similar to those used with the ORION post-processor. The specified graphics commands are executed at a user-defined time interval.

Analysis display may be activated either by specifying a nonzero value for the time interval for analysis display in the DYNA2D input file (described in Chapter 4, section 4.1 on page 37) or by specifying a nonzero value interactively using sense switch **sw8**. By default, the commands executed at the specified interval are:

g	(display mesh)
f	(resume analysis).

This effectively displays the current mesh configuration (refreshed at the specified time interval). A different graphics display can be achieved in two ways. First, an analysis display command file containing a valid graphics command sequence (see section 6.2 on page 237) can be defined and then specified as the **m**=*acf* file. Alternatively, sense switch **sw7.** may be used to temporarily halt execution and prompt the user for a new graphics command sequence. Therefore **sw7.** may be used to interactively modify the type of analysis display as the simulation evolves. Before any display occurs the user will be interactively prompted for the appropriate graphics device number.

To terminate the analysis display option at any time during an analysis, a zero value for the time interval shound be entered after typing **sw8.** On NLTSS CRAY machines, terminating the analysis display causes the TMDS to be released. The TMDS will be reselected at a later time if interactive rezoning is activated by typing **sw5.** or a nonzero time interval is specified after again typing **sw8.** On other machines with X-Windows graphics, the graphics window will remain after terminating the analysis display. This window may be iconified, but *should not be eliminated* unless no other interactive graphics (rezone or analysis display) is desired for the remainder of the analysis.

3.7 REMESHING A DYNA2D MODEL

The remeshing feature in DYNA2D allows for topologically different meshes to be used at different times during a single analysis. A discussion of the remeshing methodology, remarks on the construction of the required input files, and examples illustrating the DYNA2D remeshing capability are given in Chapter 7. In this section, the procedural steps of running a DYNA2D analysis with one remesh is given. For the purpose of this discussion, an ‘‘old mesh’’ is used for $0 \le t \le t_{remesh}$ and a ‘‘new mesh’’ is used for $t > t_{remesh}$.

There are four steps to performing a DYNA2D analysis with one remesh:

Step 1: Run the analysis with the old mesh. The analysis is started with the old mesh input file as described in section 3.2 on page 27. To perform a remesh at a time $t = t_{remesh}$, a restart dump file must be created at $t = t_{remesh}$. Restart dump files are created at the termination time (as specified in the old mesh input file), by typing sense switch **sw1.**, or as specified by a restart dump interval in the old mesh input file. Step 1 is complete when this dump file is created.

Step 2: Create MAZE line definitions corresponding to the deformed geometry at $t = t_{remesh}$. To do this, first restart the analysis and immediately enter the rezoner as described in section 3.5 on page 31. While in the rezoner, specify MAZE line definitions using the ''**ld**'' and ''**lds**'' commands as described in Chapter 6. The line definitions will be written to the file specified by **m**=*mlf* on the DYNA2D command line (this file is `mazlin` by default). After all required line definitions are generated, the ''end'' command should be used to terminate DYNA2D.

Step 3: Generate the new mesh input file with MAZE using the line definitions generated in Step 2. Guidelines for constructing the new mesh are given in Chapter 7.

Step 4: Restart the DYNA2D analysis with an immediate remesh. The execution line is

DYNA2D z=remesh, i=*inf*, **r**=*rtf*, **o**=*otf*, **g**=*ptf*, **d**=*dpf*, **f**=*thf*, **t**=*tpf*, **c**=*rcf*,**s**=*acf*,**m**=*mlf*

where *inf* is the new mesh input file.

By repeating steps 2 to 4 an arbitrary number of successive remaps can be performed.

3.8 POST-PROCESSING AND RESULTS DISPLAY

DYNA2D may write one or two binary plot databases. The state data plot file family is always created and contains information for complete states at relatively infrequent intervals; 50 to 100 states of data are typical in a state database. The time history data plot file family is created only when the **f**=*thf* option is specified on the execution line and contains information for only selected nodes and elements, but at much more frequent intervals; 1000 to 10,000 states of data are typical in a time history database.

ORION post-processes output from DYNA2D. ORION can read either of the binary plot databases produced by DYNA2D. ORION allows plotting of color contours, fringes, deformed shapes, and time histories in an interactive graphics environment. ORION can compute a variety of strain measures, momenta, and other response quantities of interest. An interactive help package describes new commands and provides assistance to new or infrequent users. ORION is supported for the same computing platforms as DYNA2D: CRAY/NLTSS, CRAY/UNICOS, VAX/VMS, and SUN, Silicon Graphics, and IBM workstations.

On all platforms except CRAY/NLTSS, ORION uses the public domain graphics library DIGLIB, developed by Hal Brand at LLNL. DIGLIB supports a large number of display and hardcopy graphics devices, including X-Windows and Sunview on the SUN/UNIX platform and Postscript (black and white or color) for hardcopy output.

4.0 INPUT FORMAT

The following sections describe the input for DYNA2D. Notational conventions are described in section 2.1 on page 7. Numerous notes and explanations are given to describe the purpose and application of specific features. The DYNA2D input file is entirely ASCII, and is completely portable across all computer platforms.

4.1 CONTROL CARDS

Following is the input description for the eight control cards. A set of notes on control card entries follows at the end of this section.

Card 1

Columns	Quantity	Format
1-72	Heading or problem title	12A6
73-74	Input format option EQ.92: input follows this 1992 manual NE.92: input follows 1988 manual	A2

Card 2

Columns	Quantity	Format
1-5	Number of materials, *NUMMAT*	I5
6-10	Number of nodes, *NUMNP*	I5
11-15	Number of elements, *NUMEL*	I5
16-20	Discrete element input option, *INPSD* EQ.0: no discrete element input EQ.1: discrete elements are defined	I5
21-25	Number of load curves	I5
26-30	Number of concentrated nodal loads and follower forces	I5
31-35	Number of element sides with pressure or shear loads applied	I5
36-40	Number of prescribed nodal velocity cards	I5
41-45	Base acceleration in r-direction (plane strain only) EQ.0: no r-acceleration EQ.1: r-acceleration is prescribed	I5
46-50	Base acceleration in z-direction EQ.0: no z-acceleration EQ.1: z-acceleration is prescribed	I5
51-55	Angular velocity about z-axis (axisymmetric only) EQ.0: no angular velocity EQ.1: angular velocity is prescribed	I5

Card 3

Columns	Quantity	Format
1-5	Initial conditions flag EQ.0: initialize all velocities to zero EQ.1: initial velocities are specified in input	I5
6-10	Number of nonreflecting boundary definitions	I5
11-15	Number of rigid walls	I5

Card 4

Columns	Quantity	Format
1-5	Number of defined slidelines, *NUMSI*	I5
6-10	Number of slidelines intersections, *NUMSIN*	I5
11-15	Automatic contact algorithm flag, *IAUTO* EQ.0: no automatic contact EQ.1: active material list input in section 4.25 on page 221 EQ.2: all materials are active for auto contact	I5
16-20	Scope of contact searching (1 to 4) EQ.0: default, set to 1 EQ.1: fastest search EQ.4: most robust search	I5
21-25	Search frequency for automatic slidelines (defaults to every 10 steps)	I5
26-35	Scale factor for automatic slideline penalty number (default=1.0)	E10.0
36-45	Low velocity friction coefficient, μ_s	E10.0
46-55	High velocity friction coefficient, μ_k	E10.0
56-65	Exponential friction decay constant, β	E10.0

Card 5

Columns	Quantity	Format
1-10	Termination time	E10.0
11-20	Initial time-step size EQ.0.0: an initial time-step size is computed	E10.0
21-25	Number of time steps between restart dumps EQ.0: restart dump is written when normal termination occurs	I5
26-35	Scale factor for computed time step size, $SFCT$ (DEFAULT =.67)	E10.0
36-45	Reduction factor, RF, to determine minimum permissible time step (< 1.0) NE.0.0: calculation terminates when $DT \le RF \times DT_I$ where DT_I is the initial time-step size.	E10.0
46-55	Time to begin automatic rezoning	E10.0
56-65	Time to end automatic rezoning	E10.0
66-75	Time interval between automatic rezoning	E10.0

Rezoning data in columns 46-65 is only used if a rezone command file is specified (**c**=*rcf*) on the execute line.

Card 6

Columns	Quantity	Format
1-10	Time interval between output of printout or time history plot data	E10.0
11-20	Time interval between output of state plot data	E10.0
21-25	Number of node time history blocks	I5
26-30	Number of element time history blocks	I5
31-35	Output option for internal energy EQ.0: internal energy is not written into state plot database EQ.1: internal energy is written into state plot database	I5
36-40	Chemistry dump option EQ.0: p^2T written to state plot database EQ.1: temperature written to state plot database	I5
41-45	History variable dump flag EQ.0: history variables are not written EQ.1: history variables are written into state plot database	I5
46-50	Peak value dump flag EQ.0: peak values are not written EQ.1: peak values of displacements, velocities, max/min principal stress and max/min pressure are written into the state plot database for each element (ORION components 71-79).	I5
51-60	Time interval between updates of analysis display EQ.0: no analysis display GT.0: simulation time interval between display refreshes.	E10.0
61-65	Number of time steps between status updates print to file.	I5

Card 7

Columns	Quantity	Format
1-5	Geometry type EQ. 0: axisymmetric EQ. 1: plane strain	I5
6-10	Brode function flag, *IBRODE* EQ.0: Brode functions are not used. EQ.1: Brode parameters are defined. EQ.2: HE parameters are defined.	I5
11-15	Number of points in density vs. depth curve for gravity stress initialization, *NUMDP*.	I5
16-20	Number of nodal constraint sets	I5
21-25	High Explosive burn option, *IHE* EQ.0: beta burn EQ.1: programmed burn - elements that are lit at time zero are designated in the element data EQ.2: programmed burn - lighting is defined in section 4.5 on page 173. EQ.3: volume burn - lighting times are specified on element cards	I5
26-30	Thermal effects option EQ.0: no thermal effects EQ.n: temperature-time history is defined by load curve *n* LT.0: nodal temperatures are defined in TOPAZ2D plot files	I5
31-35	Number of materials with ALE formulation, *NALE*	I5
36-40	Number of ALE boundary segments, *NABC*	I5
41-45	Element formulation for axisymmetric geometries, *IPETFX* EQ.0: default EQ.1: Petrov-Galerkin	I5

Card 8

Columns	Quantity	Format
1-5	Hourglass stabilization method, *IHQ* EQ.0: default set to "1" EQ.1: standard DYNA2D EQ.2: rotational EQ.3: Flanagan-Belytschko EQ.4: Hancock EQ.5: stiffness	I5
6-15	Hourglass viscosity coefficient, (Q_h, default = 0.10) *IQH*.EQ.1: $Q_h \le 0.15$ for stability *IQH*.EQ.2: $Q_h \le 0.20$ for stability *IQH*.EQ.3: $Q_h \le 0.40$ for stability *IQH*.EQ.4: $Q_h \le 0.40$ for stability	E10.0
16-20	Bulk viscosity type, *IBQ* EQ.0: default set to "1" EQ.1: standard DYNA2D EQ.2: Richards-Wilkins	I5
21-30	Quadratic shock viscosity coefficient (default = 1.5)	E10.0
31-40	Linear shock viscosity coefficient (default =.06)	E10.0
41-45	Stress rate default reset EQ.0: DYNA2D default stress rate for this material EQ.1: Jaumann rate EQ.2: Green-Naghdi rate	I5

A bulk viscosity method is used to smear shock fronts across a small number of elements. This procedure improves numerical behavior and minimizes spurious oscillations which may appear in the vicinity of strong shocks in numerical models.

The above inputs may be used to reset certain DYNA2D global defaults. These new values then become the DYNA2D defaults for the entire analysis. For any given material, these values are overridden by optional values given on the Material Control Card.

Problem Definition Notes

(card):(field)	Comments
1 : 2	Enter 92 to use the input format described in this manual. Old format input files may be converted to the 92 format using the convert utility described in section 3.3 on page 30.
2 : 1	Materials are defined as described in section 4.2 on page 51.
2 : 2	Nodal coordinates and boundary conditions are defined as described in section 4.3 on page 169.
2 : 3	Element connectivities and attributes are defined as described in section 4.4 on page 171.
2 : 4	Set this flag to 1 if discrete springs, dampers, and masses are specified as described in section 4.22 on page 209.
2 : 5	Define load curves as described in section 4.8 on page 183.
2 : 6	Define concentrated nodal loads and follower forces as described in section 4.9 on page 186.
2 : 7	Define pressure loads and shear tractions on element faces as described in section 4.10 on page 187.
2 : 8	Define specified velocity boundary conditions as described in section 4.11 on page 189.
2 : 9-10	Prescribed base acceleration may be used to apply load to a structure. Define the components of translational acceleration as described in section 4.12 on page 191. *Note that a nonzero r-component may only be specified for a plane strain geometry.*
2 : 11	A prescribed angular velocity about the z-axis may be used to apply loads to a structure. Define an angular velocity as described in section 4.13 on page 192. *Note that angular velocity may be prescribed for axisymmetric geometries only.*
3 : 1	Specify nonzero initial velocities as described in section 4.15 on page 194.
3 : 2	Nonreflecting boundaries prevent artificial stress wave reflections arising from a finite model of an infinite domain. Define nonreflecting boundaries as described in section 4.15 on page 194.
3 : 3	Rigid walls are used to define unilateral contact, such as the impact of a body into a large, rigid object. Define rigid walls as described in section 4.17 on page 197.

Problem Definition Notes (continued)

(card):(field)	Comments
4 : 1	Sliding interfaces allow general contact between bodies or parts of bodies. Define slidelines as described in section 4.18 on page 199. Slideline definitions are not required when automatic contact is used (see Control Card 5).
4 : 2	Define slideline intersections as described in section 4.19 on page 205. These are only needed for slidelines which use a nodal constraint formulation (see discussion in section 2.11 on page 14).
4 : 3	Automatic contact eliminates the need to define individual slidelines with master and slave contact surfaces. Automatic contact may be defined for a subset of materials ($IAUTO = 1$) as described in section 4.25 on page 221, or may include all materials ($IAUTO = 2$). Automatic contact is slightly more expensive than defining the required individual contact surfaces, but may be less prone to input error.
4 : 4	This option selects the level of sophistication in the closest node search in the automatic contact algorithm (default=1, maximum=4). Experience has shown the default value to work well at minimum cost for most problems, but if contact seems to be ‘‘missed’’ by the code then this parameter should be set to a higher number to obtain a more accurate search.
4 : 5	This parameter sets the number of time steps between large-domain searches in the automatic contact algorithm (default=10). Setting this parameter to a smaller value may correct poor slideline performance, while increasing cost. Increasing this value from default will decrease the cost of automatic contact.
4 : 6	This factor is used in the automatic contact algorithm to determine the magnitude of the restoring force placed on a penetrating node. In general, increasing this factor decreases interpenetration, but may adversely affect stability if the time step scale factor is not also reduced.
4 : 7-9	The automatic contact algorithms incorporate a rate-dependent Coulomb friction law. The coefficient of friction is given by $$\mu = \mu_k + (\mu_s - \mu_k)e^{-\beta v_{rel}}, \quad (24)$$ where μ_s and μ_k are the static and kinetic friction coefficients, β is a transition coefficient governing the rate of change from static friction to kinetic friction, and v_{rel} is the relative velocity between the two sliding surfaces. Note that if $\mu_k = 0$ and $\beta = 0$, then a rate-independent friction model is recovered with $\mu = \mu_s$.

Problem Definition Notes (continued)

(card):(field)	Comments
5 : 2	By default, DYNA2D chooses the initial time step. The time step size Δt in DYNA2D is governed by the Courant criterion, and may simply be thought of as $\Delta t \sim L^e{}_{min}\sqrt{\frac{\rho}{E}}$, where $L^e{}_{min}$ is the smallest distance across any element in the mesh, ρ is the mass density, and E is a material modulus.
5 : 3	Restart files are written consecutively and are not overwritten, thus allowing restart from any point at which a restart file was written. The use of restart is described in Chapter 5.
5 : 4	This factor is multiplied by the maximum stable time step to determine the time step size actually used by DYNA2D. This is useful for the (rare) situations in which the time step size is chosen based on other than stability considerations.
5 : 5	This options terminates DYNA2D when a minimum time step size is reached, and prevents the code from consuming large amounts of computer time if the time step falls to a very small value.
5 : 6	If automatic rezoning is desired, enter the solution time at which automatic rezoning is to begin. The default value is zero. Automatic rezoning may only be used if a rezone command file is specified (**c**=*rcf*) on the execute line.
5 : 7	If automatic rezoning is used, enter the solution time at which the last rezoning is to occur. The default value is the problem termination time (i.e., rezoning will continue at the specified time interval throughout the entire solution).
5 : 8	If automatic rezoning is used, enter the solution time interval between automatic rezoning operations.
6 : 1	The time history database allows plotting information to be stored frequently for a selected group of nodes and elements, thus allowing resolution of high frequency response components. Data for nodes and elements included in the time history database is output at the interval defined in this field. This data is written in binary form into the file specified by **f**=*thf, o*r printed into the file specified by **o**=*hsp* if no time history plot file is defined on the execute line.
6 : 2	The state plot database contains data for all nodes and elements of a model.
6 : 3-4	Nodes and elements are selected for inclusion in the time history database as described in section 4.6 on page 181 and section 4.7 on page 182.

Problem Definition Notes (continued)

(card):(field)	Comments
6 : 8	If this option is activated, DYNA2D keeps a running tab on the maximum values of r and z displacements, r and z velocities, maximum and minimum principal stresses, and maximum and minimum pressures. These peak values are written into the state plot database at each plot state, and may be plotted using ORION components 71-79.
6 : 9	Analysis display provides a continuous graphical display of the deforming model. This parameter specifies the interval, in simulation time, between updates of this display. Using too small an interval can significantly impact performance on vector supercomputers, but has somewhat less impact on engineering workstations. It is usually best to set this parameter to provide an update every 5 to 30 seconds of real (wall-clock) time. Analysis display is turned off by specifying a zero time interval.
7 : 1	Specify the applicable geometry: torsionless axisymmetry or plane strain. In axisymmetry analysis, the axis of symmetry is the z-axis. In plane strain analysis, the y and z axes are in-plane.
7 : 2	This option is used to define a pressure time history using the Brode function definition. Define the Brode parameters as described in section 4.21 on page 208, and the surfaces to receive the pressure loading as described in section 4.10 on page 187.
7 : 3	Density vs. depth curves are used to permit initialization of a hydrostatic stress state due to overburden and gravity. These curves are defined as described in section 4.20 on page 206.
7 : 4	Nodal constraints are used to constrain two or more nodes to share a common degree of freedom. Define nodal constraint sets as described in section 4.14 on page 193.
7 : 5	High explosive burn options are described in section 4.5 on page 173.
7 : 6	Temperatures must be defined if temperature-dependent material properties are used. Several options are available for specifying temperatures for DYNA2D. Care should be taken in the definition of the reference, or stress-free temperature.
7 : 7	ALE functions as a fully automatic rezoner in DYNA2D. The use of ALE is described in section 4.23 on page 213.
7 : 8	ALE boundary segments ***** need words here *****. Input ALE boundary segments as described in section 4.23 on page 213.

Problem Definition Notes (continued)

(card):(field)	Comments
8 : 1	Several algorithms are available for the stabilization of hourglass modes. Stabilization option $IHQ = 4$ with $Q_h \approx 0.30$ has been found by some analysts to work well at very high deformation rates.
8 : 2-5	The global default values of the hourglass viscosity and shock viscosities may be reset. These values may also be altered for a specific material in the Material Cards, as described in section 4.2 on page 51. Bulk viscosity methods are used for added stability and resolution when shock waves are present.
8 : 6	By default, DYNA2D uses a Green-Naghdi stress rate for kinematic hardening plasticity, a total-Lagrangian formulation for hyperelastic materials, and a Jaumann stress rate for all other materials. This default may be globally reset on Control Card 8, or reset for a particular material on the Material Control Card. The default stress rates are accurate and cost-effective in most applications.

4.2 MATERIALS

Repeat the following set of cards for each material definition until $NUMMAT$ materials have been defined. Materials may be input in any convenient order, but all materials must be defined. Materials are referenced by their material number, which is used for identification only. Material type refers to the material model number, such as Material Type 1 for elastic behavior.

A material model typically requires 8 cards for input, and exceptions are noted as appropriate. A brief list of notes follows the description of the Material Control Card.

Some material models, called ‘‘hydrodynamic’’ models, define only the deviatoric behavior of the material. An equation of state must be defined in conjunction with these hydrodynamic models to specify the volumetric behavior of the material. Materials requiring an equation of state are clearly identified as such by a note at the top of the first page of the input description. Following the material cards of a hydrodynamic material, the equation of state is defined. Note that different equations of state may require a different number of input cards. Also note that an equation of state is required by some material models and is not permitted by others.

Card 1

Columns	Quantity	Format
1-5	Material identification number	I5
6-10	Material type (*asterisk * indicates an equation of state is required*) EQ. 1: elasticity EQ. 2: orthotropic elasticity EQ. 3: kinematic/isotropic plasticity EQ. 4: thermo-elastic-plastic EQ. 5: soil and crushable foam EQ. 6: viscoelasticity EQ. 7: Blatz-Ko hyperelastic rubber EQ. 8: high explosive burn* EQ. 9: fluid* EQ.10: elastic-plastic hydrodynamic* EQ.11: Steinberg-Guinan high rate plasticity* EQ.12: Johnson/Cook plasticity* EQ.13: power law plasticity EQ.14: viscoplasticity EQ.15: Armstrong-Zerilli plasticity* EQ.16: concrete/geologic model* EQ.17: not currently available EQ.18: extended two invariant geologic cap EQ.19: Frazer-Nash hyperelastic rubber EQ.20: laminated composite EQ.21: isotropic elastic-plastic EQ.22: Steinberg-Guinan-Lund rate dependent plasticity* EQ.23: three-invariant viscoplastic cap model EQ.24: Bammann plasticity EQ.25: Bammann plasticity with damage EQ.26: circumferentially cracked elastoplasticity	I5
11-20	Mass density, ρ	E10.0
21-25	Equation of state type. Define only for material types 8-12, 15, 16, and 22. EQ. 1: linear polynomial EQ. 2: JWL high explosive EQ. 3: Sack high explosive EQ. 4: Gruneisen EQ. 5: ratio of polynomials EQ. 6: linear polynomial with energy deposition EQ. 7: ignition and growth of reaction in HE EQ. 8: tabulated compaction EQ. 9: tabulated EQ. 10: propellant	I5

Columns	Quantity	Format
	EQ. 11: tensor pore collapse EQ.12: shock initiation of composite HE EQ.13: pressure vs. time via load curve EQ.14: JWLB high explosive	
26-30	Hourglass stabilization method, *IHQ* EQ.1: standard DYNA2D (default) EQ.2: rotational EQ.3: Flanagan-Belytschko viscosity form EQ.4: Hancock EQ.5: stiffness	I5
31-40	Hourglass viscosity coefficient, Q_h	E10.0
41-45	Bulk viscosity type, *IBQ* EQ.1: standard DYNA2D (default) EQ.2: Richards-Wilkins	I5
46-55	Quadratic viscosity coefficient	E10.0
56-65	Linear viscosity coefficient	E10.0
66-70	Stress rate option EQ.0: DYNA2D default stress rate for this material EQ.1: Jaumann rate EQ.2: Green-Nagdi rate	I5

Material Control Card Notes

field	Comments
1	The material identification number should be between 1 and *NUMMAT*, the number of materials in the problem. Materials may be input in any order, but all materials must be defined.
2	The material type defines the mathematical model used to evaluate the material stress-strain behavior. Note that some material types ***must*** be used with an equation-of-state.
3	Define the mass density for the material in consistent units. No unit conversions are done internally in DYNA2D. See section 2.2 on page 8 for a complete discussion of units in DYNA2D.
4	Some material types (marked with an asterisk) require an equation-of-state. A nonzero value for EOS type must be specified for these materials.

5, 6	The default hourglass stabilization algorithm and parameters may be modified for this material, if desired.
7-9	Bulk viscosity methods are used for added stability and resolution when shock waves are present.
10	An objective stress rate is used in the stress update calculations for all materials except 2, 7, 8, 9, and 19. Material types 2, 7, and 19 are hyper-elastic and use a total formulation. Material type 8 has no deviatoric stresses, and material type 9 is purely viscous in deviatoric stress and therefore needs no stress rate treatment.

Card 2

Columns	Quantity	Format
1-72	Material identification	12A6

This material title will appear in the printed output. It is often helpful to use this heading to identify the physical material for which the DYNA2D material model was constructed.

Cards 3, . . . , 8

Define material cards 3, . . . , 8 as described below for the chosen material type.

Material Type 1 (Elastic)

Columns		Quantity	Format
1-10	Card 3	Young's modulus, E	E10.0
1-10	Card 4	Poisson's ratio, ν	E10.0
	Card 5	Blank	
	Card 6	Blank	
	Card 7	Blank	
	Card 8	Blank	

This model produces linear elastic material behavior.

Material Type 2 (Orthotropic Elastic)

Columns		Quantity	Format
1-10	Card 3	Elastic modulus, E_a (see Figure 2)	E10.0
11-20		Elastic modulus, E_b	E10.0
21-30		Elastic modulus, E_c	E10.0
1-10	Card 4	Poisson's ratio, ν_{ba}	E10.0
11-20		Poisson's ratio, ν_{ca}	E10.0
21-30		Poisson's ratio, ν_{cb}	E10.0
1-10	Card 5	Shear modulus, G_{ab}	E10.0
1-10	Card 6	Material axes definition option, AOPT	E10.0
		EQ.0.0: locally orthotropic with material axes determined by angle Ψ and element nodes n_1 and n_2 specified on each element card.	
		EQ.1.0: locally orthotropic with material axes determined by a point in space and the global location of the element center.	
		EQ.2.0: globally orthotropic with material axes determined by angle Ψ_G.	
1-10	Card 7	Coordinate y_p or r_p (define for AOPT = 1.0)	E10.0
11-20		Coordinate z_p (define for AOPT = 1.0)	E10.0
1-10	Card 8	Angle Ψ_G, in radians (define for AOPT = 2.0)	E10.0

The constitutive matrix $\mathbf{C}$ relating increments in stress to increments in strain is defined as

$$\mathbf{C} = \bar{\mathbf{T}}^T \mathbf{C}_L \bar{\mathbf{T}}, \tag{25}$$

where $\bar{\mathbf{T}}$ is the appropriate transformation matrix and $\mathbf{C}_L$ is the constitutive matrix defined in terms of the orthogonal material axes, a and b,

$$\mathbf{C}_L^{-1} = \begin{bmatrix} \frac{1}{E_a} & -\frac{\nu_{ba}}{E_b} & -\frac{\nu_{ca}}{E_c} & 0 \\ -\frac{\nu_{ab}}{E_a} & \frac{1}{E_b} & -\frac{\nu_{cb}}{E_c} & 0 \\ -\frac{\nu_{ac}}{E_a} & -\frac{\nu_{bc}}{E_b} & \frac{1}{E_c} & 0 \\ 0 & 0 & 0 & \frac{1}{G_{ab}} \end{bmatrix}. \quad (26)$$

Poisson's ratios are defined as

$$\nu_{ij} = \frac{-\varepsilon_j}{\varepsilon_i} \quad (27)$$

which represents the strain ratio resulting from a uniaxial stress applied in the *i-th* direction. Note that symmetry of the elastic compliance $\mathbf{C}_L^{-1}$ implies

$$\frac{\nu_{ab}}{E_a} = \frac{\nu_{ba}}{E_b}, \quad \frac{\nu_{ca}}{E_c} = \frac{\nu_{ac}}{E_a}, \text{ and } \frac{\nu_{cb}}{E_c} = \frac{\nu_{bc}}{E_b}. \quad (28)$$

Further, positive definiteness of $\mathbf{C}_L$ yields the following restrictions on the elastic constants:

$$\nu_{ba} < \left(\frac{E_b}{E_a}\right)^{\frac{1}{2}}, \quad \nu_{ca} < \left(\frac{E_c}{E_a}\right)^{\frac{1}{2}}, \text{ and } \nu_{cb} < \left(\frac{E_c}{E_b}\right)^{\frac{1}{2}}. \quad (29)$$

Nonphysical energy growth may appear in the solution if these restrictions on the elastic constants are not observed.

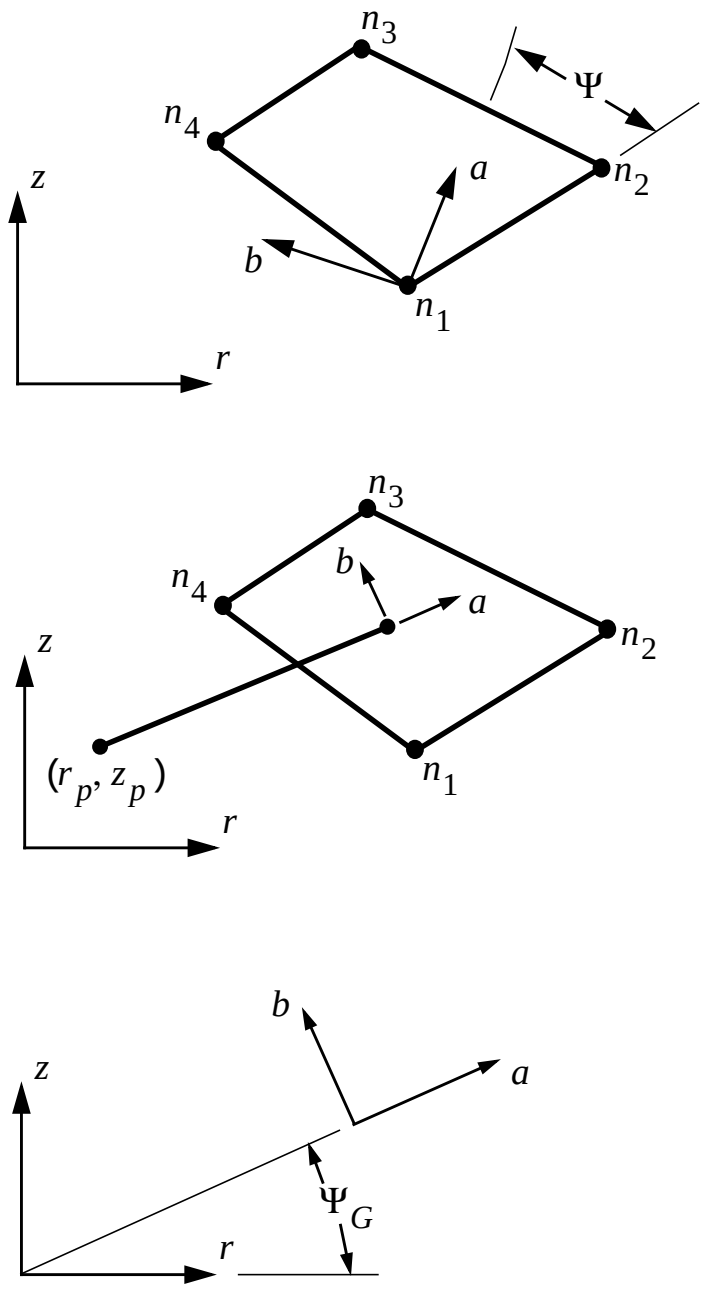

Figure 2
Options for determining the principal material axes
(a) AOPT = 0.0; (b) AOPT = 1.0; (c) AOPT = 2.0.

Material Type 3 (Kinematic/Isotropic Elastic-Plastic)

Columns		Quantity	Format
1-10	Card 3	Young's modulus, E	E10.0
1-10	Card 4	Poisson's ratio, ν	E10.0
1-10	Card 5	Yield stress, σ_0	E10.0
1-10	Card 6	Tangent modulus, E_T	E10.0
1-10	Card 7	Hardening parameter, β	E10.0
1-10	Card 8	Effective plastic strain at failure, $\bar{\varepsilon}_f^p$	E10.0

The material behavior is elastoplastic and includes linear strain hardening and material failure. The hardening parameter β specifies an arbitrary combination of kinematic and isotropic hardening; $\beta = 0.0$ yields purely kinematic hardening, while $\beta = 1.0$ gives purely isotropic hardening. Figure 3 illustrates the effect of β on the uniaxial stress-strain curve. The numerical algorithms used in this model are adapted from (Krieg and Key, 1976).

Material ''erosion'' and failure may be obtained by defining a nonzero effective plastic strain at failure $\bar{\varepsilon}_f^p$ and specifying, on Control Card 4, that this material is active for automatic contact. Erosion is discussed in detail in section 2.12 on page 17.

The yield condition can be written

$$\phi = \bar{\sigma} - \sigma_y(\bar{\varepsilon}^p), \tag{30}$$

where $\bar{\sigma}$ is the effective stress and σ_y is the current yield stress, which may be a function of the effective plastic strain $\bar{\varepsilon}^p$ if strain hardening is included. For isotropic hardening, the effective stress $\bar{\sigma}$ is given by

$$\bar{\sigma} = \left\{\frac{3}{2} s_{ij} s_{ij}\right\}^{\frac{1}{2}}, \tag{31}$$

where s_{ij} is the deviatoric stress tensor. For kinematic hardening,

$$\bar{\sigma} = \left\{\frac{3}{2} \eta_{ij} \eta_{ij}\right\}^{\frac{1}{2}} \tag{32}$$

where the translated stress η_{ij} is defined as

$$\eta_{ij} = s_{ij} - \alpha_{ij}, \tag{33}$$

and α_{ij} is the (deviatoric) back stress tensor.

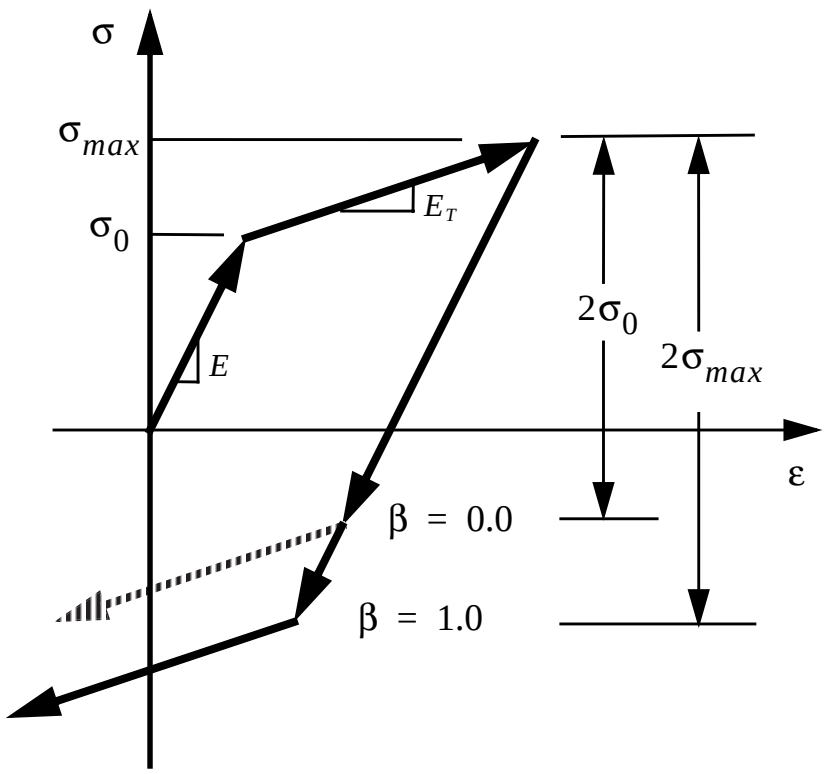

Figure 3
Uniaxial stress-strain curve showing elastic-plastic material behavior for kinematic hardening ($\beta = 0$) and isotropic hardening ($\beta = 1.0$).

The linear isotropic hardening law has the form

$$\sigma_y = \sigma_0 + \beta E_p \bar{\varepsilon}^p, \tag{34}$$

where σ_y is the current yield stress, σ_0 is the initial yield stress, and E_p is the plastic modulus.

The effective plastic strain $\bar{\varepsilon}^p$ is given by

$$\bar{\varepsilon}^p = \int_0^t d\bar{\varepsilon}^p, \tag{35}$$

where the incremental effective plastic strain $d\bar{\varepsilon}^p$ is found from the incremental plastic strain tensor $d\varepsilon_{ij}$ as

$$d\bar{\varepsilon}^p = \left(\frac{2}{3} d\bar{\varepsilon}^p_{ij} d\bar{\varepsilon}^p_{ij}\right)^{\frac{1}{2}}. \tag{36}$$

The plastic modulus is found from Young's modulus E and the tangent modulus E_T using

$$E_p = \frac{E E_T}{E - E_T}. \tag{37}$$

The plastic hardening modulus E_p is the slope of the inelastic portion of the effective stress $\bar{\sigma}$ vs. effective plastic strain $\bar{\varepsilon}^p$ curve. Similarly, the tangent modulus E_T is the slope of the inelastic part of a uniaxial stress vs. strain curve (or equivalently, the effective stress vs. effective strain curve).

Kinematic and isotropic hardening elastoplastic models yield identical behavior under monotonic loading. Under reversed loading from a maximum stress σ_{max}, kinematic hardening predicts reverse yielding when the stress has unloaded by an amount $2\sigma_0$, and isotropic hardening predicts that reverse yielding occurs when the stress reaches $-\sigma_{max}$. Thus, under cyclic loading conditions where many stress reversals may occur, kinematic hardening predicts a hysteretic energy dissipation, while isotropic hardening predicts no energy dissipation after the first cycle. The isotropic model is slightly faster in computation speed, however.

Material Type 4 (Thermo-Elastic-Plastic)

Columns		Quantity	Format
1-10	Card 3	First temperature, T_1	E10.0
11-20		Second temperature, T_2	E10.0
.		.	.
.		.	.
.		.	.
71-80		Eighth temperature, T_8	E10.0
1-10	Card 4	Young's modulus at first temperature, E_1	E10.0
11-20		Young's modulus at second temperature, E_2	E10.0
.		.	.
.		.	.
.		.	.
71-80		Young's modulus at eighth temperature, E_8	E10.0
1-10	Card 5	Poisson's ratio at first temperature, ν_1	E10.0
11-20		Poisson's ratio at second temperature, ν_2	E10.0
.		.	.
.		.	.
.		.	.
71-80		Poisson's ratio at eighth temperature, ν_8	E10.0
1-10	Card 6	Secant coefficient of thermal expansion, $\overline{\alpha_1}$	E10.0
11-20		Secant coefficient of thermal expansion, $\overline{\alpha_2}$	E10.0
.		.	.
.		.	.
.		.	.
71-80		Secant coefficient of thermal expansion, $\overline{\alpha_8}$	E10.0

Columns		Quantity	Format
1-10	Card 7	Yield stress at first temperature, σ_{y1}	E10.0
.		Yield stress at second temperature, σ_{y2}	E10.0
.		.	.
.		.	.
.		.	.
71-80		Yield stress at eighth temperature, σ_{y8}	E10.0
1-10	Card 8	Plastic modulus at first temperature, E_{p1}	E10.0
11-20		Plastic modulus at second temperature, E_{p2}	E10.0
.		.	.
.		.	.
.		.	.
71-80		Plastic modulus at eighth temperature, E_{p8}	E10.0

At least two temperatures and their corresponding material properties must be defined. The analysis will be terminated if a material temperature falls outside the range defined in the input. If a thermo-elastic material is desired (i.e., no plasticity effects), leave Cards 7 and 8 blank.

The plastic hardening modulus E_p is the slope of the effective stress vs. effective plastic strain curve (or equivalently, the uniaxial stress vs. effective plastic strain curve). The plastic hardening modulus may be found from the tangent modulus E_T as

$$E_p = \frac{EE_T}{E - E_T}, \tag{38}$$

where the tangent modulus E_T is the slope of the post-yield portion of the uniaxial stress - strain curve.

Thermal expansion due to temperature change is included when nonzero values of $\bar{\alpha}$ are specified. The *secant* coefficient of thermal expansion $\bar{\alpha}$ can also be a function of temperature, and is defined with respect to the reference temperature at the beginning of the calculation for that material. Total thermal strain ε_{ij}^{T} is defined in terms of the secant thermal expansion coefficient $\bar{\alpha}$ as

$$\varepsilon_{ij}^{T} = \bar{\alpha}(T - T_{ref})\delta_{ij}, \tag{39}$$

where T is the current temperature and T_{ref} is the reference temperature. Therefore, temperature dependent secant coefficients of thermal expansion should be defined as the value *to* that temperature, not the value *at* that temperature. The secant coefficient $\bar{\alpha}$ is related to the tangent coefficient of thermal expansion α by

$$\bar{\alpha} = \frac{1}{T - T_{ref}} \int_{T_{ref}}^{T} \alpha(T)dT . \tag{40}$$

For temperature independent coefficients of thermal expansion, $\bar{\alpha}$ is identical to α, and the classical definition of thermal expansion is valid.

Since this model is temperature dependent, the thermal effects option on Control Card 7 must be nonzero. Care should be taken to define secant coefficients of thermal expansion consistent with the reference temperature. The reference temperature in this model is chosen as the first temperature in the TOPAZ2D plot files, or the temperature at time $t = 0.0$ if temperature is specified by a load curve.

This model is applicable to materials exhibiting elastic or elastoplastic behavior where thermal effects are important. Both thermal strains and temperature-dependent material properties are included.

Material Type 5 (Soil and Crushable Foam)

Columns		Quantity	Format
1-10	Card 3	Shear modulus, G	E10.0
11-20		Bulk unloading modulus, K_u	E10.0
21-30		First yield function constant, $a_0 > 0$, or alternatively, set $a_0 < 0$ to select load curve option	E10.0
31-40		Second yield function constant, a_1, or load curve no. NC_1 giving pressure vs. volumetric strain	E10.0
41-50		Third yield function constant, a_2, or load curve no. NC_2 giving yield stress vs. pressure	E10.0
51-60		Pressure cutoff for tensile fracture, p_{cut}	E10.0
1-10	Card 4	First (most tensile) tabulated volumetric strain, ε_{v1} (see Figure 4)	E10.0
11-20		First tabulated pressure, p_1 ($p_1 < 0$)	E10.0
21-30		Second tabulated volumetric strain, ε_{v2}	E10.0
31-40		Second tabulated pressure, p_2	E10.0
1-10	Card 5	Third tabulated volumetric strain, ε_{v3}	E10.0
11-20		Third tabulated pressure, p_3	E10.0
21-30		Fourth tabulated volumetric strain, ε_{v4}	E10.0
31-40		Fourth tabulated pressure, p_4	E10.0
1-10	Card 6	Fifth tabulated volumetric strain, ε_{v5}	E10.0
11-20		Fifth tabulated pressure, p_5	E10.0
21-30		Sixth tabulated volumetric strain, ε_{v6}	E10.0
31-40		Sixth tabulated pressure, p_6	E10.0
1-10	Card 7	Seventh tabulated volumetric strain, ε_{v7}	E10.0
11-20		Seventh tabulated pressure, p_7	E10.0
21-30		Eighth tabulated volumetric strain, ε_{v8}	E10.0
31-40		Eighth tabulated pressure, p_8	E10.0

Columns		Quantity	Format
1-10	Card 8	Ninth tabulated volumetric strain, ε_{v9}	E10.0
11-20		Ninth tabulated pressure, p_9	E10.0
21-30		Modified elliptical surface flag, *AMOD* EQ.0.0: unmodified surface EQ.1.0: failure surface is constant at high pressures	E10.0

This model is based on the formulation suggested in (Key, 1974). This model has two options: one using an analytical function to describe the variation of yield stress with pressure, and one using a load curve to define a pressure-dependent yield stress. The analytical form is obtained if the constant a_0 is input as a positive number (which is required for a physically meaningful analytical model), and the load curve form is obtained if a_0 is input as a negative number. If the load curve form is chosen, data on Cards 4-8 is ignored, and load curve NC_1 is used for to describe the pressure p vs. volumetric strain ε_v curve. Load curve NC_2 is then used to directly specify the yield stress σ_y as a function of pressure.

Pressure is positive in compression, and volumetric strain is negative in compression. Volumetric strain is given by the natural logarithm of the relative volume. The tabulated pressure-volumetric strain data may contain up to nine pairs of points, and must be given in order of *increasing* compression. If the pressure drops below (i.e., becomes more tensile than) the cutoff value p_{cut}, then the pressure is reset to the cutoff value.

The deviatoric perfectly plastic yield function ϕ is defined as

$$\phi = J_2 - [a_0 + a_1 p + a_2 p^2], \tag{41}$$

where a_0, a_1, and a_2 are constants, p is pressure, and J_2 is the second invariant of the deviatoric stress tensor $\boldsymbol{s}$ given by

$$J_2 = \frac{1}{2} s_{ij} s_{ij}. \tag{42}$$

Plastic flow is nonassociative if a_1 or a_2 are nonzero.

On the yield surface, $J_2 = \frac{1}{3}\sigma_y^2$, where σ_y is the uniaxial yield stress. Thus, the yield stress at any pressure p is given by

$$\sigma_y = [3(a_0 + a_1 p + a_2 p^2)]^{\frac{1}{2}}. \tag{43}$$

There is no strain hardening in this model, so the yield stress is completely determined by the pressure.

To eliminate the pressure dependence of the yield strength, set $a_1 = a_2 = 0$ and $a_0 = \frac{1}{3}\sigma_y^2$. This approach is useful when a von Mises type elastic-plastic model is desired for use with tabulated volumetric data. Note $\varepsilon_v = \ln\left(\frac{V}{V_o}\right)$.

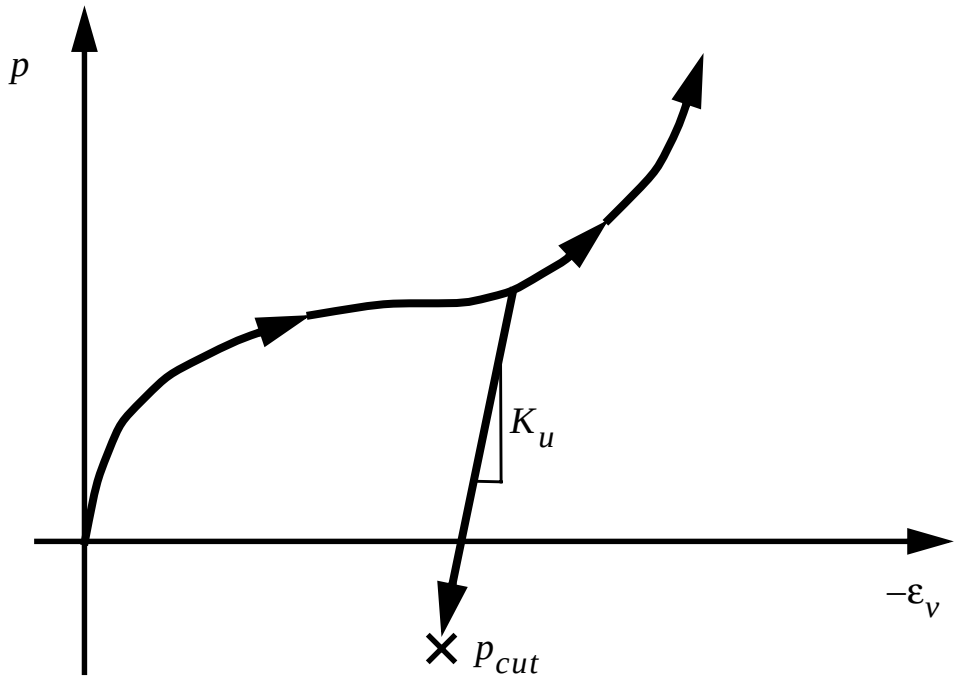

Figure 4
Pressure vs. volumetric strain curve for soil and crushable foam model.

The variation of σ_y as a function of p has three conical forms which depend on the parameter a_2: elliptic ($a_2 < 0$), parabolic ($a_2 = 0$), or hyperbolic ($a_2 > 0$). These three forms are shown in Figure 5 in terms of J_2 vs. p. Figure 6 shows the corresponding forms in a more familiar engineering form of σ_y vs. p. The elliptic yield function curves back toward the p axis at higher pressures and predicts a softening behavior which is not often observed in test data. If the modified elliptical yield surface flag *AMOD* is nonzero, then the elliptical yield surface is used up to the point of maximum J_2. For higher pressures, the yield surface is extended as a von Mises surface. The resulting yield surface is depicted in Figure 5 and Figure 6. This modification yields much improved agreement with a test data for many geologic materials such as concrete, as discussed in (Schwer, Rosinsky, and Day, 1988).

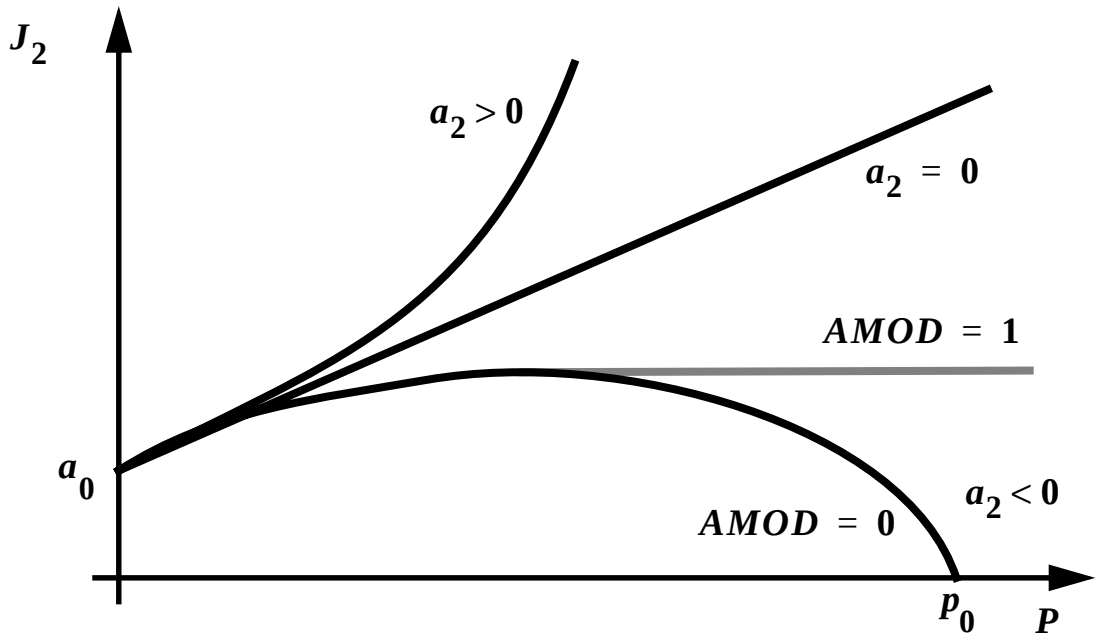

Figure 5
Material type 5 failure surface forms in J_2 vs. p space.

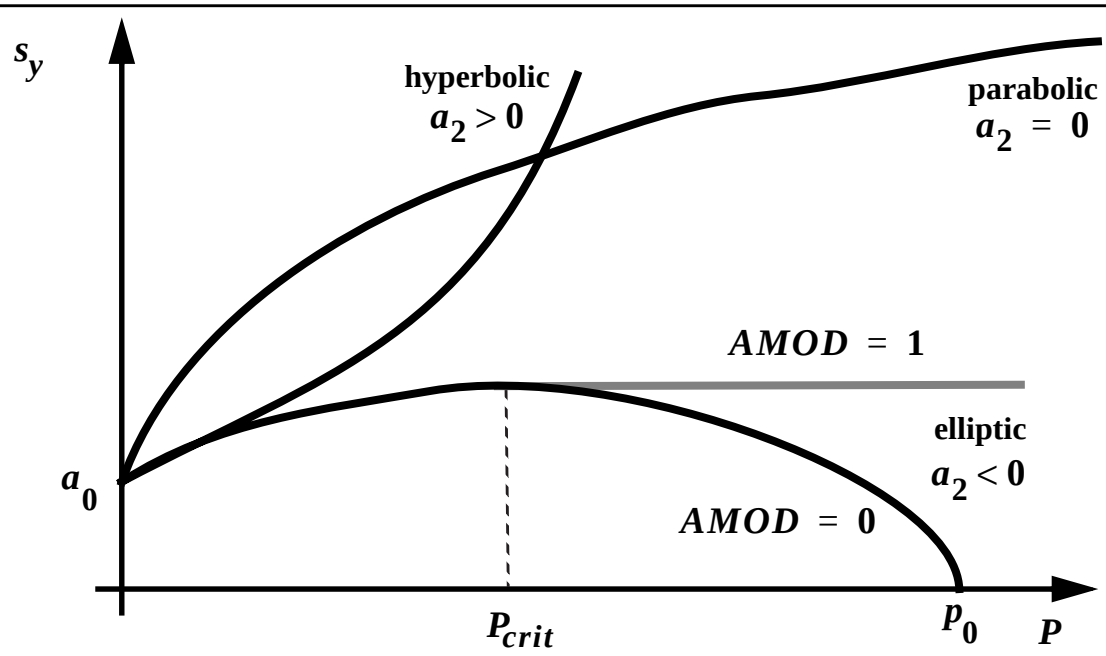

Figure 6
Material type 5 failure surface forms in σ_y vs. p space.

The unmodified elliptic yield surface crosses the $\sigma_y = 0$ at a pressure p_0, as shown in Figure 6. Thus, p_0 is the maximum pressure at which the unmodified elliptic failure surface may be used. It is easily shown that

$$p_0 = \frac{-a_1 + \sqrt{a_1^2 - 4a_0a_2}}{2a_2}. \tag{44}$$

The modified elliptic yield surface transitions to a von Mises surface at pressures greater than p_{crit}, where

$$p_{crit} = -\frac{a_1}{2a_2}. \tag{45}$$

This material model is useful as a simple representation of pressure hardening, where the deviatoric yield strength of a material increases as the hydrostatic pressure increases. At any constant pressure, the deviatoric behavior is elastic perfectly-plastic. This model permits a general representation of the material volumetric behavior via a tabulated pressure-volumetric strain curve. Such flexibility makes this model useful for representing materials with a stiffening pressure-volume curve, such as porous materials like wood or foam. This model is also often used as a simplified model for concrete or soil.

Material ‘‘erosion’’ and failure may be obtained by defining a nonzero pressure cutoff p_{cut} and specifying, on Control Card 4, that this material is active for automatic contact. If erosion is active, then the material erodes whenever the pressure becomes more tensile than p_{cut}. Erosion is discussed in detail in section 2.12 on page 17.

******* Currently, must input pcut>0 (and still interpreted as tensile value) to get erosion of the element.******

****** Also should add strain-based erosion criterion as per G R-P? *****

Material Type 6 (Viscoelastic)

Columns		Quantity	Format
1-10	Card 3	Elastic bulk modulus, K	E10.0
1-10	Card 4	Short-time shear modulus, G_0	E10.0
1-10	Card 5	Long-time shear modulus, G_∞	E10.0
1-10	Card 6	Decay constant, β	E10.0
	Card 7	Blank	
	Card 8	Blank	

This implementation of viscoelasticity is based on (Key, 1974). The deviatoric stresses are found from

$$s_{ij} = 2\int_0^t G(t-\tau)\dot{e}_{ij}d\tau\ , \tag{46}$$

where the shear relaxation behavior is described by

$$G(t) = G_\infty + (G_0 - G_\infty)e^{-\beta t} \tag{47}$$

and $\dot{e}_{ij}$ is the deviatoric strain rate. The volumetric response is elastic, so the pressure p is computed from the current volumetric strain ε_v using

$$p = -K\varepsilon_v, \tag{48}$$

where K is the elastic bulk modulus. The viscoelastic model is useful for modeling rate-dependent elastic materials. It is also effectively used whenever viscous dissipation is desired with deviatoric (shear) deformations.

Material Type 7 (Blatz - Ko Hyperelastic Rubber)

Columns		Quantity	Format
1-10	Card 3	Shear modulus, G	E10.0
	Card 4	Blank	
.			.
.			.
.			.
	Card 8	Blank	

This model is a hyperelastic model based on the implementation in (Key, 1974), and is appropriate for materials undergoing moderately large strains. In this formulation, the second Piola-Kirchhoff stress $\boldsymbol{t}$ is computed as

$$\tau_{ij} = G\left[\frac{1}{\nu}C_{ij} - V^{\frac{-1}{1-2\nu}}\delta_{ij}\right], \tag{49}$$

where V is the relative volume, C_{ij} is the right Cauchy-Green strain tensor, and ν is Poisson's ratio which is set to.463 internally. The Cauchy stress $\mathtt{s}$ is then found from $\mathtt{t}$ using

$$\mathtt{s} = \frac{1}{J}\boldsymbol{F}\mathtt{t}\boldsymbol{F}^{T}, \tag{50}$$

where $\boldsymbol{F}$ is the deformation gradient and J is the Jacobian of the deformation.

The Blatz-Ko hyperelastic model is often used to represent the behavior of rubber at moderately large strains. The Blatz-Ko formulation yields a slightly compressible material. Only one input parameter is required, and therefore this model may be useful when detailed test data is not available for the material of interest.

Material Type 8 (High Explosive Burn)

An equation of state must be used with this model.

Columns		Quantity	Format
1-10	Card 3	Detonation velocity, D	E10.0
11-20		Chapman-Jouguet pressure, P_{CJ}	E10.0
	Card 4	Blank	
	.		.
	.		.
	.		.
	Card 8	Blank	

This model is based on work described in (Giroux, 1973), and is used in conjunction with the HE burn option (see Control Card 7 in section 4.1 on page 37) to model the burning of explosives. The detonation velocity D is the velocity of a detonation or burn front. The Chapman-Jouguet pressure P_{CJ} is the maximum pressure realizable in a constant volume adiabatic burn.

During DYNA2D initialization, the lighting time of each element is computed using the selected algorithm. These lighting times may be directly specified in the input, or may be calculated from specified detonation points or lines using the programmed burn options. If detonation points are defined, then the lighting time t_L for an element is computed based on the distance from the center of the element to the nearest detonation point divided by the detonation velocity D. This option is described in greater detail in section 4.5 on page 173.

Burn fractions are computed to control the release of chemical energy for simulating high explosive detonations. If the ‘‘beta burn’’ option ($IHE = 0$ on Control Card 7) is selected, then the burn fraction F is computed from

$$F = \beta(1 - V) = \frac{1 - V}{1 - V_{CJ}}, \tag{51}$$

where V is the current relative volume, V_{CJ} is the Chapman-Jouget relative volume, and

$$\beta = \frac{1}{1 - V_{CJ}}. \tag{52}$$

This model is useful to detect initiation due to shock compression of HE.
For other burn options, the burn fraction is computed from

$$F = max(F_1, F_2), \tag{53}$$

where

$$F_1 = ((t - t_L)D)/(1.5h) \tag{54}$$

if $t > t_L$, and $F_1 = 0$ if $t < t_L$, and h is a characteristic dimension of the element under consideration. F_2 is computed from

$$F_2 = \beta(1 - V) = \frac{1 - V}{1 - V_{CJ}}. \tag{55}$$

If the above equations produce a burn fraction that is greater than one, then it is reset to one.

The burn front propagates by multiplying the pressure computed from an equation-of-state by the current burn fraction,

$$p = F p_{EOS}(V, E), \tag{56}$$

where $p_{EOS}(V, E)$ is the pressure computed from the equation-of-state at the current relative volume V and energy E. High explosives typically have large initial internal energies, E_0, which yield large pressures as $F \rightarrow 1$.

Material Type 9 (Fluid)

An equation of state must be used with this model.

Columns		Quantity	Format
1-10	Card 3	Pressure cutoff, p_{cut} (positive in compression)	E10.0
11-20		Viscosity coefficient, μ	E10.0
	Card 4.	Blank	
	.		.
	.		.
	.		.
	Card 8	Blank	

The fluid material has no stiffness, and must be used with an equation-of-state. A viscous stress is computed from

$$s_{ij} = \mu \dot{e}_{ij}, \tag{57}$$

where $\dot{e}_{ij}$ is the deviatoric strain rate and s_{ij} is the deviatoric stress.

Materials with no viscosity may reach large distortions under very small shear loads, so a nonzero viscosity should always be used.

The pressure cutoff, p_{cut}, is negative in tension. If the pressure becomes more tensile than p_{cut}, then it is reset to that value. Thus, the pressure cutoff can be interpreted as an approximate model of cavitation. The deviatoric stresses arising from viscous effects are unaffected by the tensile pressure cutoff.

This model is most useful for analyzing structures with contained fluids. Large distortions in the fluid make some free-surface and fluid flow problems more amenable to analysis using other analysis codes employing an Eulerian formulation. Caution should therefore be used when applying this material model in situations where large distortions are expected.

Material Type 10 (Isotropic-Elastic-Plastic-Hydrodynamic)

An equation of state must be used with this model.

Columns		Quantity	Format
1-10	Card 3	Shear modulus, G	E10.0
11-20		Yield stress, σ_0	E10.0
21-30		Plastic modulus, E_p	E10.0
31-40		Pressure cutoff, p_{cut} (positive in compression) EQ.0.0: cutoff of $-\infty$ is assumed (no cutoff)	
41-50		Linear pressure hardening coefficient, a_1	E10.0
51-60		Quadratic pressure hardening coefficient, a_2	E10.0
61-70		Spall model, *ISPALL* EQ.0.0: default set to 1.0 EQ.1.0: pressure limit model EQ.2.0: maximum principal stress spall criterion EQ.3.0: hydrostatic tension spall criterion	
1-10	Card 4	Effective plastic strain at failure, $\bar{\varepsilon}_f^p$	E10.0
1-10	Card 5	First tabulated effective plastic strain, $\bar{\varepsilon}_1^p$	E10.0
11-20		$\bar{\varepsilon}_2^p$	E10.0
.		.	.
.		.	.
.		.	.
71-80		$\bar{\varepsilon}_8^p$	E10.0
1-10	Card 6	$\bar{\varepsilon}_9^p$	E10.0
.		.	.
.		.	.
.		.	.
71-80		$\bar{\varepsilon}_{16}^p$	E10.0
1-10	Card 7	First tabulated yield stress, σ_{y1}	E10.0
.		.	.
.		.	.
.		.	.

Columns		Quantity	Format
71-80		σ_{y8}	E10.0
1-10	Card 8	σ_{y9}	E10.0
.		.	.
.		.	.
.		.	.
71-80		σ_{y16}	E10.0

If a tabulated yield stress vs. effective plastic strain curve is not given (Cards 5-8 are blank), then the initial yield stress σ_0, plastic hardening modulus E_p, and pressure hardening coefficients a_1 and a_2 are taken from Card 3. In this case, a pressure hardening bilinear stress-strain curve similar to that shown in Figure 3 is obtained with linear isotropic strain hardening ($\beta = 1.0$).

The yield condition can be written

$$\phi = \bar{\sigma} - \sigma_y(\bar{\varepsilon}^p, p), \tag{58}$$

where $\bar{\sigma}$ is the effective stress and σ_y is the current yield stress, which may be a function of the effective plastic strain $\bar{\varepsilon}^p$ and pressure p. The effective stress $\bar{\sigma}$ is given by

$$\bar{\sigma} = \left\{\frac{3}{2} s_{ij} s_{ij}\right\}^{\frac{1}{2}}, \tag{59}$$

where s_{ij} is the deviatoric stress tensor.

The hardening law has the form

$$\sigma_y = \sigma_0 + E_p \bar{\varepsilon}^p + (a_1 + a_2 p)\hat{p}, \tag{60}$$

where p is the pressure (positive in compression), and $\hat{p}$ is the tension-limited pressure found from

$$\hat{p} = max(p, 0). \tag{61}$$

The effective plastic strain $\bar{\varepsilon}^p$ is given by

$$\bar{\varepsilon}^p = \int_0^t d\bar{\varepsilon}^p, \tag{62}$$

where the incremental effective plastic strain $d\bar{\varepsilon}^p$ is found from the incremental plastic strain tensor $d\varepsilon_{ij}$ as

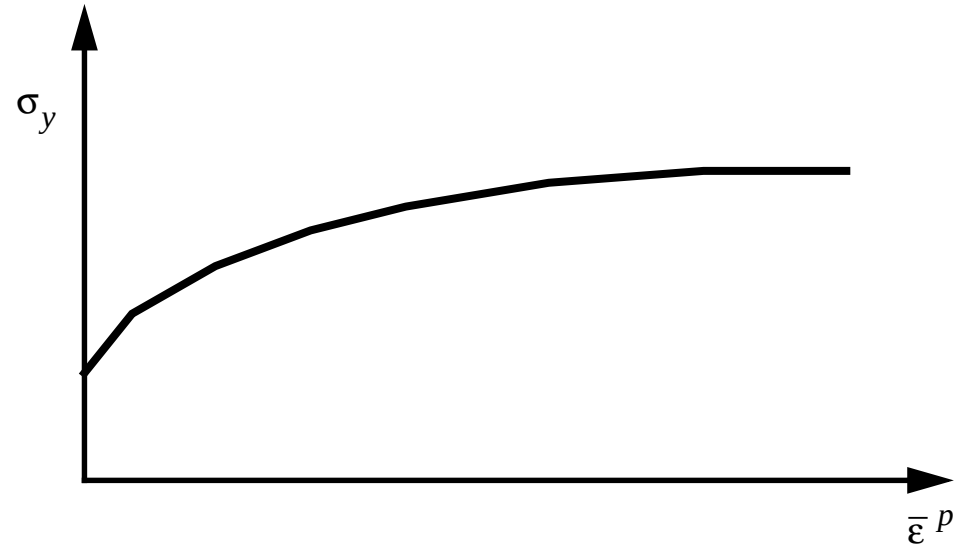

Figure 7
Tabulated yield stress vs. effective plastic strain curve.

$$d\bar{\varepsilon}^p = \left(\frac{2}{3} d\bar{\varepsilon}^p_{ij} d\bar{\varepsilon}^p_{ij}\right)^{\frac{1}{2}}. \tag{63}$$

The plastic modulus can be related to Young's modulus E and the tangent modulus E_T using

$$E_p = \frac{E E_T}{E - E_T}. \tag{64}$$

The plastic modulus E_P is the slope of the inelastic portion of the effective stress $\bar{\sigma}$ vs. effective plastic strain $\bar{\varepsilon}^p$ curve, and the tangent modulus E_T is the slope of the inelastic part of a uniaxial stress vs. strain curve (or equivalently, the effective stress vs. effective strain curve).

If tabulated values of yield stress vs. effective plastic strain are specified on Cards 5-8, a nonlinear strain hardening curve like that shown in Figure 7 may be defined. In this case the plastic hardening modulus and pressure hardening coefficients input on Card 3 are not used, and the yield stress is given as

$$\sigma_y = f(\bar{\varepsilon}^p), \tag{65}$$

where $f(\bar{\varepsilon}^p)$ is interpolated from the specified yield stress vs. effective plastic strain curve. Any number of points, from 2 to 16, may be used to define the hardening curve. This option permits additional detail to be included in the nonlinear strain hardening law, but pressure hardening is not modeled with this approach.

A choice of three spall models is offered to represent material splitting, cracking, and failure under tensile loads. The pressure limit model, $(ISPALL = 1)$, limits the hydrostatic tension to the specified value, p_{cut}. If pressures more tensile than this limit are calculated, the pressure is reset to p_{cut}. This option is not strictly a spall model, since the deviatoric stresses are unaffected by the pressure reaching the tensile cutoff, and the pressure cutoff value p_{cut} remains unchanged throughout the analysis. The maximum principal stress spall model, $(ISPALL = 2)$, detects spall if the maximum (most tensile) principal stress σ_{max} exceeds the limiting value $-p_{cut}$. Note that the negative sign is required because p_{cut} is measured positive in compression, while σ_{max} is positive in tension. Once spall is detected with this model, the deviatoric stresses are set to zero, and no hydrostatic tension $(p < 0)$ is permitted. If tensile pressures are calculated, they are reset to 0 in the spalled material. Thus, the spalled material behaves as a rubble or incohesive material. The hydrostatic tension spall model, $(ISPALL = 3)$, detects spall if the pressure becomes more tensile than the specified limit, p_{cut}. Once spall is detected the deviatoric stresses are set to zero, and the pressure is required to be compressive. If hydrostatic tension $(p < 0)$ is subsequently calculated, the pressure is reset to 0 for that element.

This model is applicable to a wide range of materials, including those with pressure-dependent yield behavior. The use of 16 points in the yield stress vs. effective plastic strain curve allows complex post-yield hardening behavior to be accurately represented. In addition, the incorporation of an equation of state permits accurate modeling of diverse volumetric behavior. The spall model options permit incorporation of material failure, fracture, and disintegration effects under tensile loads.

Material ‘‘erosion’’ and failure may be obtained by defining a nonzero effective plastic strain at failure $\bar{\varepsilon}_f^p$ and specifying, on Control Card 4, that this material is active for automatic contact. Erosion is discussed in detail in section 2.12 on page 17.

Material Type 11 (Steinberg-Guinan High Rate Elastic-Plastic)

An equation of state must be used with this model.

Columns		Quantity	Format
1-10	Card 3	Shear modulus constant, G_0	E10.0
11-20		Yield stress constant, σ_0	E10.0
21-30		Strain hardening law constant, β	E10.0
31-40		Strain hardening exponent, n	E10.0
41-50		Initial plastic strain, γ_i	E10.0
1-10	Card 4	Yield stress work hardening limit, σ_m	E10.0
11-20		Shear modulus pressure constant, b	E10.0
21-30		Yield stress pressure constant, b'	E10.0
31-40		Energy coefficient, h	E10.0
41-50		Energy exponential coefficient, f	E10.0
1-10	Card 5	Atomic weight, A (if $A = 0$, R' must be defined)	E10.0
11-20		Melting temperature constant, T_{mo}	E10.0
21-30		Thermodynamic gamma, γ_0	E10.0
31-40		Thermodynamic constant, a	E10.0
41-50		Pressure cutoff, p_{cut}	E10.0
51-60		Room temperature, T_{room} EQ.0.0: default set to 300.0	E10.0
61-70		Debye coefficient, θ EQ.0.0: Debye correction ignored.	E10.0
1-10	Card 6	Spall model, *ISPALL* EQ.0.0: default set to 2.0 EQ.1.0: Pressure limit model EQ.2.0: Maximum principal stress spall criterion EQ.3.0: Hydrostatic tension spall criterion	E10.0
11-20		R' (if $R' \neq 0$, the atomic weight A is not used)	E10.0
21-30		Effective plastic strain at failure, $\bar{\varepsilon}_f^p$	E10.0
31-40		Polynomial order for fit, $NFIT$ $(1 \leq NFIT \leq 9)$	E10.0

Columns		Quantity	Format
41-50		Cold compression energy polynomial flag, *IVAR* EQ.0.0: Polynomial coefficients given or fit in terms of η EQ.1.0: Polynomial coefficients given or fit in terms of μ	E10.0
51-60		Optional minimum limit for energy fit Input η_{min} if $IVAR = 0$ Input μ_{min} if $IVAR = 1$	E10.0
61-70		Optional maximum limit for energy fit Input η_{max} if $IVAR = 0$ Input μ_{max} if $IVAR = 1$	E10.0
1-16	Card 7	First cold compression polynomial coefficient, EC_0	E16.0
17-32		EC_1	E16.0
33-48		EC_2	E16.0
49-64		EC_3	E16.0
65-80		EC_4	E16.0
1-16	Card 8	EC_5	E16.0
17-32		EC_6	E16.0
33-48		EC_7	E16.0
49-64		EC_8	E16.0
65-80		EC_9	E16.0

The formulation of this model is described by Steinberg and Guinan (1978), and some notes on the implementation are given in (Woodruff, 1973).

In terms of the foregoing input parameters, we define the shear modulus, G, before the material melts as:

$$G = G_0\left[1 + bpV^{\frac{1}{3}} - h\left(\frac{E_i - E_c}{3R'} - 300\right)\right]e^{-\frac{fE_i}{E_m - E_i}} \tag{66}$$

where p is the pressure, V is the relative volume, E_i is the current energy, E_c is the cold compression energy, and E_m is the melting energy. The cold compression energy is calculated using

$$E_c(x) = \int_0^x p dx, \tag{67}$$

where $x = 1 - V$. The equation is integrated using initial energy E_o and pressure P_o conditions that correspond to zero K and are given by

$$E_o = -3R'T_{room} \tag{68}$$

and

$$P_o = \gamma_o E_o \text{Debye}\left(\frac{\theta}{T_{room}}\right). \tag{69}$$

Here Debye is the Debye correction factor, and has a default value of 1 when $\theta = 0$. (For values of θ, see Zemansky, 1951.) The melting energy is found from the cold compression energy and the melting temperature using

$$E_m(x) = E_c(x) + 3R'T_m(x), \tag{70}$$

where the melting temperature T_m is given by

$$T_m(x) = \frac{T_{mo} exp(2ax)}{V^{2\left(\gamma_0 - a - \frac{1}{3}\right)}} \tag{71}$$

and T_{mo} is the melting temperature at the initial density, ρ_0.

In the above equations, R' is defined by

$$R' = \frac{R\rho}{A}, \tag{72}$$

where R is the universal gas constant and A is the atomic weight. **Note that if R' is not defined, DYNA2D computes it with R in the cm-gram-microsecond system of units.** Thus, this option should not be used unless the entire analysis model is defined in the cm-gram-microsecond second system of units.

If E_m exceeds E_i (i.e., the material has not melted), then the yield strength σ_y is given by:

$$\sigma_y = \sigma'_0 \left[1 + b'pV^{\frac{1}{3}} - h\left(\frac{E_i - E_c}{3R'} - 300\right)\right] e^{-\frac{fE_i}{E_m - E_i}} \quad . \tag{73}$$

The work-hardened yield stress σ'_0 is found from the initial yield stress σ_0 and the accumulated effective plastic strain $\bar{\varepsilon}^p$ using the hardening law

$$\sigma'_0 = \sigma_0 [1 + \beta(\gamma_i + \bar{\varepsilon}^p)]^n, \tag{74}$$

where γ_i is the initial plastic strain. If the work-hardened yield stress σ_0 exceeds the limiting value σ_m, then σ'_0 is reset to σ_m. After the materials melts ($E_i > E_m$), the yield stress σ_y and shear modulus G are reset to one half their initial value.

The evaluation of the cold compression energy $E_c(x)$ using (67) is too expensive to perform at each step of a calculation. As an approximation, many codes (including DYNA2D) use a polynomial to interpolate cold compression energy data during execution. The independent variable is chosen as η, and the polynomial takes the form

$$E_c = \sum_{i=0}^{9} EC_i \eta^i. \tag{75}$$

Note that the density and compression variables are related by

$$x = 1 - V = \frac{\mu}{\mu + 1} = 1 - \frac{1}{\eta}. \tag{76}$$

The coefficients EC_0 through EC_9 may be defined in the input if they are known. If they are not specified in the input, DYNA2D will fit the cold compression energy with up to a ten term polynomial expansion using a least squares method. If the order of the polynomial is not specified, DYNA2D will automatically pick the best polynomial order that fits the EOS generated data. Otherwise, DYNA2D will attempt to fit the data to the polynomial order desired. When DYNA2D performs any fit, the exact cold compression energy is compared with the cold compression energy found using the fitted polynomial at selected values of x, and the results printed in the “hsp” output file. These results should be examined closely to verify that a reasonably accurate polynomial fit has been obtained.

A Debye correction can be applied to the cold compression energy to improve the model’s temperature response. This option is activated by specifying a non-zero value of the Debye coefficient θ.

A choice of three spall models is offered to represent material splitting, cracking, and failure under tensile loads. The pressure limit model, $(ISPALL = 1)$, limits the hydrostatic tension to the specified value, p_{cut}. If pressures more tensile than this limit are calculated, the pressure is reset to p_{cut}. This option is not strictly a spall model, since the deviatoric stresses are unaffected by the pressure reaching the tensile cutoff, and the pressure cutoff value p_{cut} remains unchanged throughout the analysis. The maximum principal stress spall model, $(ISPALL = 2)$, detects spall if the maximum (most tensile) principal stress σ_{max} exceeds the limiting value $-p_{cut}$. Note that the negative sign is required because p_{cut} is measured positive in compression, while σ_{max} is positive in tension. Once spall is detected with this model, the deviatoric stresses are set to zero, and no hydrostatic tension $(p < 0)$ is permitted. If tensile pressures are calculated, they are reset to 0 in

the spalled material. Thus, the spalled material behaves as a rubble or incohesive material. The hydrostatic tension spall model, $(ISPALL = 3)$, detects spall if the pressure becomes more tensile than the specified limit, p_{cut}. Once spall is detected the deviatoric stresses are set to zero, and the pressure is required to be compressive. If hydrostatic tension $(p < 0)$ is subsequently calculated, the pressure is reset to 0 for that element.

The Steinberg-Guinan model is applicable to metals at high strain rates (near $10^5 s^{-1}$), where the enhancement of the yield stress due to strain rate effects has reached a limiting value and compression heating effects are becoming important. Model predictions may become substantially less accurate at low strain rates (below $10^3 s^{-1}$). Examples of problems in this high strain rate regime include some explosive forming operations, metal penetration problems, and the simulation of high velocity ballistic impact.

Material ‘‘erosion’’ and failure may be obtained by defining a nonzero effective plastic strain at failure $\bar{\varepsilon}_f^p$ and specifying, on Control Card 4, that this material is active for automatic contact. Erosion is discussed in detail in section 2.12 on page 17.

Material Type 12 (Johnson/Cook Elastic-Plastic)

An equation of state must be used with this model.

Columns		Quantity	Format
1-10	Card 3	Shear modulus, G	E10.0
11-20		Yield stress constant, A	E10.0
21-30		Strain hardening coefficient, B	E10.0
31-40		Strain hardening exponent, n	E10.0
41-50		Strain rate dependence coefficient, C	E10.0
51-60		Temperature dependence exponent, m	E10.0
61-70		Melt temperature, T_m, (deg. K)	E10.0
71-80		Room temperature, T_r, (deg. K)	E10.0
1-10	Card 4	Reference strain rate, $\dot{\varepsilon}_0$	E10.0
11-20		Specific heat, c_v	E10.0
21-30		Pressure cutoff, p_{cut}, or failure stress, σ_m	E10.0
31-40		Spall model, *ISPALL* EQ.1.0: Pressure limit model (default) EQ.2.0: Maximum principal stress spall criterion EQ.3.0: Hydrostatic tension spall criterion	
41-50		Plastic strain iteration flag, *ITER* EQ.0.0: fast approx. solution for plastic strain (default) EQ.1.0: accurate iterative solution for plastic strain (More expensive than default.)	E10.0
51-60		Effective plastic strain at failure, $\bar{\varepsilon}_f^p$	E10.0
61-70		Element deletion controlled by damage level, *FSD* EQ.0.: Damage level does not control element deletion GT.0.: Element deletion based upon damage, D	E10.0
1-10	Card 5	First failure parameter, D_1	E10.0
11-20		D_2	E10.0
21-30		D_3	E10.0
31-40		D_4	E10.0
41-50		D_5	E10.0

Columns	Quantity		Format
.	Card 6	Blank	
.	Card 7	Blank	
.	Card 8	Blank	

The formulation of this model is described and constants for many materials are given in (Johnson and Cook, 1983).

The yield stress is written as

$$\sigma_y = [A + B(\bar{\varepsilon}^p)^n][1 + C ln(\dot{\varepsilon}^*)][1 - (T^*)^m] \quad , \tag{77}$$

where A, B, C, n and m are input constants, $\bar{\varepsilon}^p$ is the effective plastic strain, $\dot{\varepsilon}^*$ is the nondimensional strain rate, and T^* is the homologous temperature. The effective plastic strain $\bar{\varepsilon}^p$ is given by

$$\bar{\varepsilon}^p = \int_0^t d\bar{\varepsilon}^p, \tag{78}$$

where the incremental effective plastic strain $d\bar{\varepsilon}^p$ is found from the incremental plastic strain tensor $d\varepsilon_{ij}$ as

$$d\bar{\varepsilon}^p = \left\{ \frac{2}{3} d\bar{\varepsilon}^p_{ij} d\bar{\varepsilon}^p_{ij} \right\}^{\frac{1}{2}} . \tag{79}$$

The nondimensional strain rate $\dot{\varepsilon}^*$ is calculated from

$$\dot{\varepsilon}^* = \frac{\dot{\bar{\varepsilon}}^p}{\dot{\varepsilon}_0} \tag{80}$$

where $\dot{\bar{\varepsilon}}^p$ is the effective plastic strain rate and $\dot{\varepsilon}_0$ is the reference strain rate defined in the input. The homologous temperature T^* is the ratio of the current temperature to the melting temperature when both are expressed in degrees Kelvin. Temperature change in this model is computed assuming adiabatic conditions, i.e., no heat transfer between elements. This is usually a good assumption since transient dynamic problems typically occur over such a short time interval that the actual heat transfer is negligible. Heat is generated in an element by plastic work, and the resulting temperature rise is computed using the specific heat for the material.

Material constants for a variety of materials are provided in (Johnson and Cook, 1983).

Due to the nonlinearity in the dependence of the yield stress on plastic strain, an accurate value of the yield stress requires expensive iteration for calculation of the increment in plastic strain. However, by using a Taylor series expansion with linearization about the current state, σ_y can be approximated with sufficient accuracy to avoid iteration and achieve optimum execution speed.

This implementation of the Johnson-Cook model also contains a damage model. The strain at fracture ε_f is given by

$$\varepsilon_f = [D_1 + D_2 exp(D_3 \sigma^*)][1 + D_4 ln(\dot{\varepsilon}^*)][1 + D_5 T^*] \tag{81}$$

where σ^* is the ratio of pressure divided by effective stress

$$\sigma^* = \frac{p}{\bar{\sigma}}, \tag{82}$$

and effective stress $\bar{\sigma}$ is found from

$$\bar{\sigma} = \left\{ \frac{3}{2} s_{ij} s_{ij} \right\}^{\frac{1}{2}}. \tag{83}$$

Note that this definition of σ^* may be reversed in sign from convention in the original publications of Johnson and Cook; the sign of D_3 should be chosen carefully.

Fracture occurs when the damage parameter D exceeds the value of 1. The evolution of the damage parameter is given by

$$D = \sum \frac{\Delta \bar{\varepsilon}^p}{\varepsilon_f}, \tag{84}$$

where the summation is performed over all time steps in the analysis. When fracture occurs, all stresses are set to zero and remain zero for the rest of the calculation.

A choice of three spall models is offered to represent material splitting, cracking, and failure under tensile loads. The pressure limit model, $(ISPALL = 1)$, limits the hydrostatic tension to the specified value, p_{cut}. If pressures more tensile than this limit are calculated, the pressure is reset to p_{cut}. This option is not strictly a spall model, since the deviatoric stresses are unaffected by the pressure reaching the tensile cutoff, and the pressure cutoff value p_{cut} remains unchanged throughout the analysis. The maximum principal stress spall model, $(ISPALL = 2)$, detects spall if the maximum (most tensile) principal stress σ_{max} exceeds the limiting value σ_m. Once spall is detected with this model, the deviatoric stresses are set to zero, and no hydrostatic tension $(p < 0)$ is permitted. If tensile pressures are calculated, they are reset to 0 in the spalled material. Thus, the spalled material behaves as a rubble or incohesive material. The hydrostatic tension spall model, $(ISPALL = 3)$, detects spall if the pressure becomes more tensile than the specified limit, p_{cut}.

Once spall is detected, the deviatoric stresses are set to zero and the pressure is required to be compressive. If hydrostatic tension $(p < 0)$ is calculated, then the pressure is reset to 0 for that element.

Material Type 12 is applicable to the high rate deformation of many materials, including most metals. Unlike the Steinberg-Guinan model (Material Type 11), the Johnson-Cook model remains valid down to lower strain rates, and even into the quasistatic regime. Typical applications include explosive metal forming, ballistic penetration, and impact.

Material ‘‘erosion’’ and failure may be obtained by defining a nonzero effective plastic strain at failure $\bar{\varepsilon}_f^p$ and specifying, on Control Card 4, that this material is active for automatic contact. Erosion is discussed in detail in section 2.12 on page 17. Alternatively, by specifying a positive FSD and nonzero damage parameters, material ‘‘erosion’’ will be controlled by the accumulated damage parameter D. Both material erosion methods can be used simultaneously. In this case which every condition is satisfied first will determine erosion.

Material Type 13 (Power Law Isotropic Elastic-Plastic)

Columns		Quantity	Format
1-10	Card 3	Young's modulus, E	E10.0
11-20		Poisson's ratio, ν	E10.0
21-30		Yield stress coefficient, k	E10.0
31-40		Strain hardening exponent, n	E10.0
1-10	Card 4	Effective plastic strain at failure, $\bar{\varepsilon}_f^p$	E10.0
	Card 5	Blank	
	.		
	.		
	.		
	Card 8	Blank	

The material behavior is elastoplastic with nonlinear isotropic strain hardening given by a power law expression. The yield condition can be written

$$\phi = \bar{\sigma} - \sigma_y(\bar{\varepsilon}^p), \tag{85}$$

where $\bar{\sigma}$ is the effective stress and σ_y is the current yield stress. The hardening law has the form

$$\sigma_y = k(\varepsilon_0 + \bar{\varepsilon}^p)^n, \tag{86}$$

where ε_0 is the initial yield strain given by

$$\varepsilon_0 = \left(\frac{E}{k}\right)^{\frac{1}{n-1}}. \tag{87}$$

This model is generally applicable to ductile materials such as metals. Although similar to Material Type 3, this model provides additional flexibility in specifying the post-yield behavior with a nonlinear isotropic hardening law.

Material ‘‘erosion’’ and failure may be obtained by defining a nonzero effective plastic strain at failure $\bar{\varepsilon}_f^p$ and specifying, on Control Card 4, that this material is active for automatic contact. Erosion is discussed in detail in section 2.12 on page 17.

Material Type 14 (Viscoplastic)

Columns		Quantity	Format
1-10	Card 3	Young's modulus E	E10.0
11-20		Poisson's ratio ν	E10.0
21-30		Initial temperature T in $^{\circ}K$	E10.0
31-40		Density x specific heat ρC_v	E10.0
41-50		Hardening parameter β	E10.0
1-10	Card 4	Rate dependent yield stress coefficient C_1	E10.0
11-20		Rate dependent yield stress exponent C_2	E10.0
21-30		Rate independent yield stress coefficient C_3	E10.0
31-40		Rate independent yield stress exponent C_4	E10.0
1-10	Card 5	Transition coefficient C_5	E10.0
11-20		Transition exponent C_6	E10.0
21-30		Hardening coefficient C_7	E10.0
31-40		Hardening exponent C_8	E10.0
1-10	Card 6	Dynamic recovery coefficient C_9	E10.0
11-20		Dynamic recovery exponent C_{10}	E10.0
21-30		Diffusion recovery coefficient C_{11}	E10.0
31-40		Diffusion recovery exponent C_{12}	E10.0
	Card 7	Blank	
	Card 8	Blank	

This model represents a modified implementation of a unified creep plasticity model proposed by Bamman (1984). The original implementation is described by Hallquist (1986), and recent results and modifications are discussed by Bamman (1990), and Flower and Nikkel (1990). The current model implementation is briefly described below.

The history dependence of this model is characterized through the introduction of two internal state variables, a scalar κ, and a second order tensor $\mathbf{a}$. The governing constitutive equations are of the form

$$\dot{\mathbf{s}} = \frac{E\nu}{(1+\nu)(1-2\nu)} tr(\dot{\mathbf{e}})\mathbf{1} + \frac{E}{1+\nu}(\dot{\mathbf{e}} - \dot{\mathbf{e}}^p) \quad , \tag{88}$$

$$\dot{\mathbf{e}}^p = f(T)\sinh\left[\frac{|\boldsymbol{\eta}| - \kappa - Y(T)}{V(T)}\right]\frac{\boldsymbol{\eta}}{|\boldsymbol{\eta}|} \, , \tag{89}$$

$$\dot{\boldsymbol{\alpha}} = k(T)(1-\beta)\dot{\mathbf{e}}^p - \frac{(g(T) + h(T)|\dot{\boldsymbol{e}}^p|)|\boldsymbol{\alpha}|\boldsymbol{\alpha}}{1-\beta} \quad , \tag{90}$$

$$\dot{\kappa} = k(T)\beta|\dot{\boldsymbol{e}}^p| - \frac{(g(T) + h(T)|\dot{\boldsymbol{e}}^p|)\kappa^2}{\beta} \quad , \tag{91}$$

where the translated stress $\boldsymbol{\eta}$ is given by

$$\boldsymbol{\eta} = \mathbf{s} - \boldsymbol{\alpha} \, , \tag{92}$$

and $\mathbf{s}$ is the deviatoric stress. The inelastic behavior of the model is governed by six temperature dependent parameter functions *V(T)*, *Y(T)*, *f(T)*, *h(T)*, *k(T)*, and *g(T)*. Each of the functions is an exponential and defined by two material parameters as follows:

$$V(T) = C_1 e^{-C_2/T} \quad \text{(rate dependent yield stress)}, \tag{93}$$

$$Y(T) = C_3 e^{C_4/T} \quad \text{(rate independent yield stress)}, \tag{94}$$

$$f(T) = C_5 e^{-C_6/T} \quad \text{(transition to rate dependent behavior)}, \tag{95}$$

$$h(T) = C_7 e^{-C_8/T} \quad \text{(hardening)}, \tag{96}$$

$$k(T) = C_9 e^{-C_{10}/T} \quad \text{(dynamic recovery)}, \tag{97}$$

$$g(T) = C_{11} e^{-C_{12}/T} \quad \text{(diffusion controlled static or thermal recovery)}. \tag{98}$$

The specification of hardening parameter β, where $0.0 \le \beta \le 1.0$, results in either kinematic, isotropic, or a combination of kinematic and isotropic hardening. Purely kinematic or purely isotropic hardening is obtained by setting $\beta = 0.0$ or $\beta = 1.0$, respectively. For these cases,

numerical perturbations are used to prevent the governing equations from becoming singular. The model also accounts for adiabatic heating due to plastic work. Temperature rate $\dot{T}$ is defined in terms of the density ρ and specific heat C_v as

$$\dot{T} = \frac{0.95}{\rho C_v} \sigma_{ij} \dot{\varepsilon}^{p}_{ij} \tag{99}$$

To help illustrate the use of this model, a sample set of material parameters for 21-6-9 stainless steel is given as follows.

Sample values for 21-6-9 stainless steel

Young's modulus E	2.00e+5	[*MPa*]
Poisson's ratio ν	0.30	
Initial temperature T	373	[$^\circ K$]
Density x specific heat ρC_v	2.68e-01	[*MKg*] or [(m^3 $^\circ K$/*MJ*)]
Hardening parameter β	0.0	
Rate dependent yield stress coefficient C_1	5.58e+01	[*MPa*}
Rate dependent yield stress exponent C_2	8.67e+01	[$^\circ K$]
Rate independent yield stress coefficient C_3	1.67e+01	[*MPa*]
Rate independent yield stress exponent C_4	4.68e+02	[$^\circ K$]
Transition coefficient C_5	1.02e+04	[s^{-1}]
Transition exponent C_6	3.48e+03	[$^\circ K$]
Hardening coefficient C_7	4.72e-03	[1/*MPa*]
Hardening exponent C_8	2.55e+02	[$^\circ K$]
Dynamic recovery coefficient C_9	1.81e+03	[*MPa*]
Dynamic recovery exponent C_{10}	5.23e+01	[$^\circ K$]
Diffusion recovery coefficient C_{11}	0.0	[1/*MPa* $\cdot$ *s*]
Diffusion recovery exponent C_{12}	1.0	[$^\circ K$]

Material Type 15 Generalized Armstrong-Zerilli Elastic-Plastic

An equation of state must be used with this model.

Columns		Quantity	Format
1-10	Card 3	Shear modulus at reference temperature, G_0	E10.0
11-20		Crystal geometry flag, *IXTAL* EQ.-1: BCC EQ. 1: FCC	E10.0
21-30		Polycrystal grain diameter, L	E10.0
1-10	Card 4	Yield stress constant, $\Delta\sigma_G$	E10.0
11-20		Temperature coefficient, B_0	E10.0
21-30		Temperature exponent, β_0	E10.0
31-40		Strain rate thermal exponent, β_1	E10.0
1-10	Card 5	Strain hardening coefficient, K_0	E10.0
11-20		Strain hardening exponent, n	E10.0
21-30		Strength constant, K_1	E10.0
31-40		Grain size coefficient, K_ε	E10.0
1-10	Card 6	Shear modulus ratio constant, a_0 EQ.0: default set to 1.0	E10.0
11-20		Shear modulus ratio coefficient, a_1	E10.0
21-30		Specific heat constant, b_0	E10.0
31-40		Specific heat coefficient, b_1	E10.0
1-10	Card 7	Pressure cutoff (negative in tension), p_{cut}	E10.0
11-20		Effective plastic strain at failure, $\bar{\varepsilon}_f^p$	E10.0
1-10	Card 8	Initial temperature, T_0	E10.0

The theoretical derivation of this model is described in (Armstrong and Zerilli, 1988). The application of this model to high strain rates and large strains are further discussed in (Goldthorpe, 1991). The present implementation was adapted from work described in (Church and Cullis, 1991).

The Armstrong-Zerilli model is a strain rate and temperature dependent elastic plastic model for metals undergoing large strains over a wide range of strain rates. The yield function has two forms depending on the crystal structure of the material. For BCC materials ($IXTAL = -1$), the yield function may be written as

$$\sigma_y = \Delta\sigma_G + B_0 exp\left[(-\beta_0 + \beta_1 ln(\dot{\bar{\varepsilon}}))T\right] + \left[K_0(\bar{\varepsilon}^p)^n + K_1\right]\frac{\mu_T}{\mu_0} + K_\varepsilon L^{-1/2} \quad , \qquad (100)$$

and for FCC materials ($IXTAL = 1$) the yield function becomes

$$\sigma_y = \Delta\sigma_G + B_0\sqrt{\bar{\varepsilon}^p} exp\left[(-\beta_0 + \beta_1 ln(\dot{\bar{\varepsilon}}))T\right] + \left[K_0(\bar{\varepsilon}^p)^n + K_1\right]\frac{\mu_T}{\mu_0} + K_\varepsilon L^{-1/2} \quad , \qquad (101)$$

where $\bar{\varepsilon}^p$ is effective plastic strain, $\dot{\bar{\varepsilon}}$ is the effective strain rate, μ_T is the shear modulus at the current temperature T, μ_0 is the shear modulus at the initial temperature T_0, and $\Delta\sigma_G$, B_0, β_0, β_1, K_0, K_1, and K_ε are material constants, and L is the grain size of the material. The shear modulus ratio is approximated as a linear function of temperature,

$$\frac{\mu_T}{\mu_0} = a_0 + a_1 T \qquad (102)$$

where a_0 and a_1 are constants.

Temperature change in this model is computed assuming adiabatic conditions, i.e., no heat transfer between elements. This is usually a good assumption since transient dynamic problems typically occur over such a short time interval that the actual heat transfer is negligible. Heat is generated in an element by plastic work, and the resulting temperature rise is computed using the specific heat for the material at the current temperature. The specific heat is approximated as a linear function of temperature,

$$c_p(T) = b_0 + b_1 T \, , \qquad (103)$$

where b_0 and b_1 are constants.

The pressure cutoff feature limits the hydrostatic tension to the specified value, p_{cut}. If pressures more tensile than this limit are calculated, the pressure is reset to p_{cut}.

Material ‘‘erosion’’ and failure may be obtained by defining a nonzero effective plastic strain at failure $\bar{\varepsilon}_f^p$ and specifying, on Control Card 4, that this material is active for automatic contact. Erosion is discussed in detail in section 2.12 on page 17.

Material Type 16 (Concrete/Geologic Material)

This model must be used with equation of state type 8**,** 9, or 11.

Columns		Quantity	Format
1-10	Card 3	First elastic constant Poisson's ratio, ν, for constant ν model Negative of shear modulus, $-G$, for constant G model	E10.0
11-20		Maximum principal stress at failure, σ_{cut}	E10.0
21-30		Cohesion, a_0	E10.0
31-40		Pressure hardening coefficient, a_1	E10.0
41-50		Pressure hardening coefficient, a_2	E10.0
51-60		Damage scaling factor, b_1	E10.0
61-70		Cohesion for failed material, a_{0f}	E10.0
71-80		Pressure hardening coefficient for failed material, a_{1f}	E10.0
1-10	Card 4	Percent reinforcement, $\hat{f}_r$ $(0 \le \hat{f}_r \le 100\%)$	E10.0
11-20		Elastic modulus for reinforcement, E_r	E10.0
21-30		Poisson's ratio for reinforcement, ν_r	E10.0
31-40		Initial yield stress, σ_0	E10.0
41-50		Tangent modulus, E_T	E10.0
51-60		Load curve giving rate sensitivity for principal material, N_1	E10.0
61-70		Load curve giving rate sensitivity for reinforcement, N_2	E10.0
1-10	Card 5	First tabulated effective plastic strain, $\bar{\varepsilon}_1^p$, or pressure, p_1	E10.0
.		.	.
.		.	.
.		.	.
71-80		$\bar{\varepsilon}_8^p$ or p_8	E10.0
1-10	Card 6	$\bar{\varepsilon}_9^p$ or p_9	E10.0
.		.	.
.		.	.
.		.	.
71-80		$\bar{\varepsilon}_{16}^p$ or p_{16}	E10.0

Columns		Quantity	Format
1-10	Card 7	First tabulated yield stress, σ_{y1}	E10.0
.		.	.
.		.	.
.		.	.
71-80		σ_{y8}	E10.0
1-10	Card 8	σ_{y9}	E10.0
.		.	.
.		.	.
.		.	.
71-80		σ_{y16}	E10.0

Material Type 16 was developed to give concrete and geological material modeling capabilities to DYNA2D. It can be used in two major modes - a fairly simple tabular pressure-dependent yield surface, and a potentially complex model featuring two yield versus pressure functions with various means of migrating from one curve to the other. For both modes, load curve N_1 is taken to be a strain rate multiplier for the yield strength.

Note that this model must be used with Equation-of-State type 8, 9 or 11.

Response Mode I. Tabulated Yield Stress Versus Pressure

This mode is well suited for implementing standard geologic models like the Mohr-Coulomb yield surface with a Tresca limit, as shown in Figure 8. Examples of converting conventional triaxial compression data to this type of model are found in (Desai and Siriwardane, 1984). Note that under conventional triaxial compression conditions, the DYNA2D input corresponds to an ordinate of $\sigma_1 - \sigma_3$ rather than the more widely used $\frac{\sigma_1 - \sigma_3}{2}$, where σ_1 is the maximum principal stress and σ_3 is the minimum principal stress.

Using Material Type 16 combined with Equation-of-State Type 9 (saturated materials) or Type 11 (air filled porous materials), this approach has been very successfully used to model ground shocks and soil/structure interactions at pressures up to 100 kbar (approximately 1.5×10^6 psi).

To invoke Mode I of this model, set a_0, a_1, a_2, b_1, a_{0f}, and a_{1f} to zero. The tabulated values of pressure should then be specified on cards 5 and 6, and the corresponding values of yield stress should be specified on cards 7 and 8. The parameters relating to reinforcement properties, initial yield stress, and tangent modulus are not used in this response mode, and should be set to zero.

Simple tensile failure

Note that a_{1f} is reset internally to 1/3 even though it is input as zero; this defines a failed material curve of slope $3p$, where p denotes pressure (positive in compression). In this case the yield strength is taken from the tabulated yield vs. pressure curve until the maximum principal stress (σ_1) in the element exceeds the tensile cut-off (σ_{cut}). For every time step that $\sigma_1 > \sigma_{cut}$ the yield strength is scaled back by a fraction of the distance between the two curves until after 20 time steps the yield strength is defined by the failed curve. The only way to inhibit this feature is to set σ_{cut} arbitrarily large.

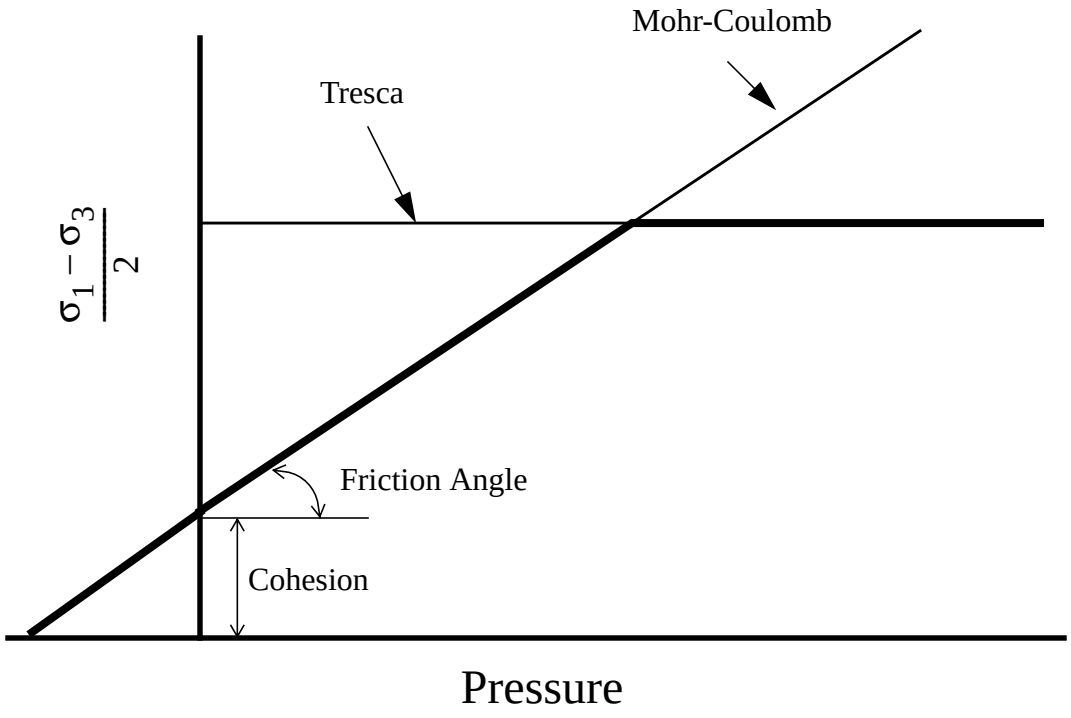

Figure 8
Mohr-Coulomb surface with a Tresca limit.

Response Mode II. Two Curve Model with Damage and Failure

This approach uses two yield versus pressure curves of the form

$$\sigma_y = a_0 + \frac{p}{a_1 + a_2 p}. \tag{104}$$

The upper curve is best described as the maximum yield strength curve and the lower curve is the failed material curve. There are a variety of ways of moving between the two curves, and each is discussed below.

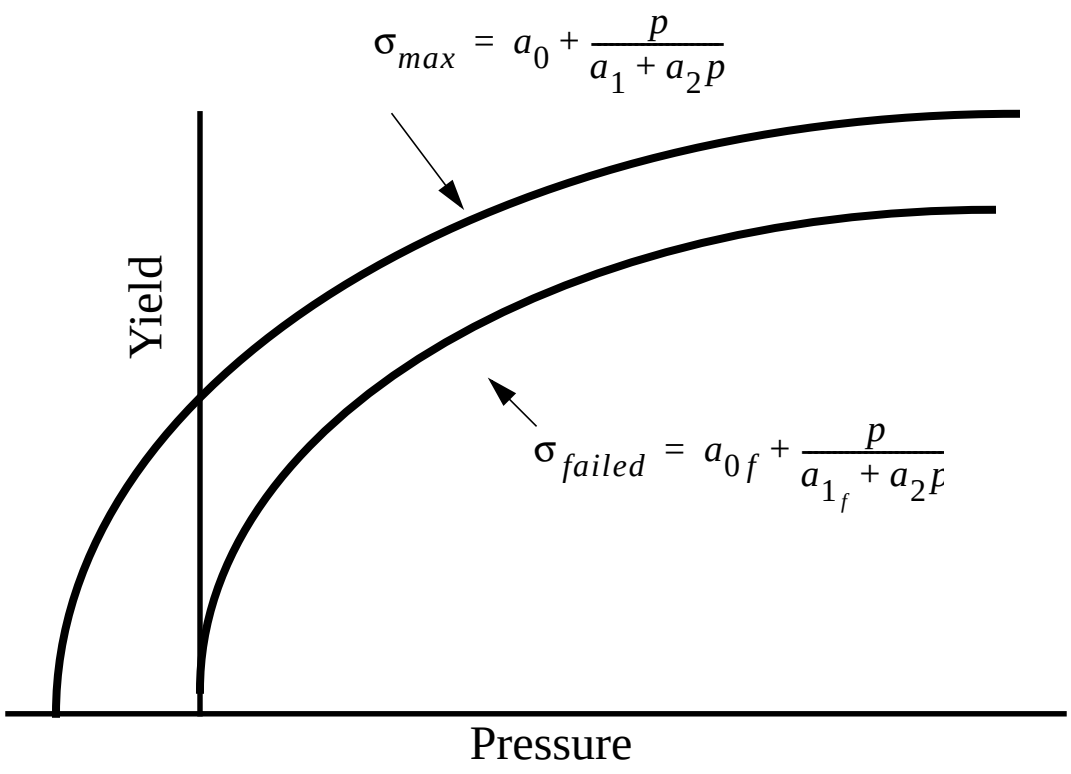

Figure 9
Two-curve concrete model with damage and failure.

Mode II.A: Simple tensile failure

Define a_0, a_1, a_2, a_{0f} and a_{1f}, set b_1 to zero, and leave cards 5 through 8 blank. In this case the yield strength is taken from the maximum yield curve until the maximum principal stress (σ_1) in the element exceeds the tensile cut-off (σ_{cut}). For every time step that $\sigma_1 > \sigma_{cut}$ the yield strength is scaled back by a fraction of the distance between the two curves until after 20 time steps the yield strength is defined by the failed curve.

Mode II.B: Tensile failure plus plastic strain scaling

Define a_0, a_1, a_2, a_{0f} and a_{1f}, set b_1 to zero, and use cards 5 through 8 to define a scale factor, η, versus effective plastic strain. DYNA2D evaluates η at the current effective plastic strain and then calculates the yield stress as

$$\sigma_{yield} = \sigma_{max} - \eta(\sigma_{max} - \sigma_{failed}), \tag{105}$$

where σ_{max} and σ_{failed} are found as shown in Figure 9.
This yield strength is then subject to scaling for tensile failure as described above. This type of model allows the description of a strain hardening and/or softening material such as concrete.

Mode II.C: Tensile failure plus damage scaling

The change in yield stress as a function of plastic strain arises from physical mechanisms such as internal cracking, and the extent of this cracking is affected by the hydrostatic pressure when the cracking occurs. This mechanism gives rise to the "confinement" effect on concrete behavior. To account for this phenomenon a "damage" function was defined and incorporated into Material Type 16. The damage function is given the form

$$\lambda = \int_0^{\bar{\varepsilon}^p} \frac{d\bar{\varepsilon}^p}{\left(1 + \frac{p}{\sigma_{cut}}\right)^{b_1}} \tag{106}$$

Define a_0, a_1, a_2, a_{0f}, a_{1f}, and b_1. Cards 5 through 8 now give η as a function of λ and scale the yield stress as

$$\sigma_{yield} = \sigma_{max} - \eta(\sigma_{max} - \sigma_{failed}) \tag{107}$$

and then apply any tensile failure criteria.

Mode II Concrete Model Options

Material Type 16 in Mode II provides for the automatic internal generation of a simple "generic" model for concrete. If a_0 is negative, then σ_{cut} is assumed to be the unconfined concrete compressive strength (f_c') and $-a_0$ is assumed to be a conversion factor from DYNA pressure units to psi. In this case the parameter values generated internally are:

$$\sigma_{cut} = 1.7\left(\frac{(f_c')^2}{-a_0}\right)^{1/3} \tag{108}$$

$$a_0 = \frac{f_c'}{4} \tag{109}$$

$$a_1 = \frac{1}{3} \tag{110}$$

$$a_2 = \frac{1}{3f'_c} \tag{111}$$

$$a_{0f} = 0 \tag{112}$$

$$a_{1f} = 0.385 \tag{113}$$

Note that these a_{0f} and a_{1f} defaults will be overridden by nonzero entries on Card 3. If plastic strain or damage scaling is desired, Cards 5 through 8 and b_1 should be specified in the input. When a_0 is input as a negative quantity, the Equation-of-State can be given as 0 and a trilinear EOS Type 8 model will be automatically generated from the unconfined compressive strength and Poisson's ratio. The EOS 8 model is a simple pressure versus volumetric strain model with no internal energy terms, and should give reasonable results for pressures up to 5 kbar (approximately 75,000 psi).

Mixture model

A reinforcement fraction, $\hat{f}_r$, can be defined along with properties of the reinforcement material. The bulk modulus, shear modulus, and yield strength are then calculated from a simple mixture rule. This feature is *experimental* and should be used with caution. It gives an isotropic effect in the material instead of the true anisotropic material behavior. A reasonable approach would be to use mixture elements only where the reinforcing exists and plain elements elsewhere. When the mixture model is being used, the strain rate multiplier for the principal material is taken from load curve N_1 and the multiplier for the reinforcement is taken from load curve N_2.

A Suggestion

Moor (1991) suggests using the damage function (Mode II.C.) in Material Type 16 with the following set of parameters:

$$a_0 = \frac{f'_c}{4} \tag{114}$$

$$a_1 = \frac{1}{3} \tag{115}$$

$$a_2 = \frac{1}{3f'_c} \tag{116}$$

$$a_{0f} = \frac{f'_c}{10} \tag{117}$$

$$a_{1f} = 1.5 \quad (118)$$

$$b_1 = 1.25 \quad (119)$$

and a damage table of:

Card 5	0.0	8.62e-06	2.15e-05	3.14e-05	3.95e-05	5.17e-04	6.38e-04	7.98e-04
Card 6	9.67e-04	1.41e-03	1.97e-03	2.59e-03	3.27e-03	4.00e-03	4.79e-03	0.909
Card 7	0.309	0.543	0.840	0.975	1.00	0.790	0.630	0.469
Card 8	0.383	0.247	0.173	0.136	0.114	0.086	0.056	0.0

This set of parameters should give results consistent with (Dilger, Koch, and Kowalczyk, 1984) for plain concrete. It has been successfully used for reinforced structures where the reinforcing bars were modeled explicitly. The model does not incorporate the major failure mechanism - separation of the concrete and reinforcement leading to catastrophic loss of confinement pressure. However, experience indicates that this physical behavior will occur when this model shows about 4% strain.

Material Type 17 (Not Available)

Material type 17 is not available in this release of DYNA2D.

Material Type 18 (Extended Two Invariant Geologic Cap)

Columns		Quantity	Format
1-10	Card 3	Initial bulk modulus, K	E10.0
11-20		Initial shear modulus, G	E10.0
1-10	Card 4	Failure envelope parameter, α	E10.0
11-20		Failure envelope linear coefficient, θ	E10.0
21-30		Failure envelope exponential coefficient, γ	E10.0
31-40		Failure envelope exponent, β	E10.0
41-50		Cap surface axis ratio, R	E10.0
1-10	Card 5	Hardening law exponent, D	E10.0
11-20		Hardening law coefficient, W	E10.0
21-30		Hardening law parameter, X_0	E10.0
31-40		Kinematic hardening coefficient, $\bar{c}$	E10.0
41-50		Kinematic hardening parameter, N	E10.0
1-10	Card 6	Plot database flag, *IPLOT* EQ.1.0: Hardening variable, κ EQ.2.0: Cap - J_1 axis intercept, $X(\kappa)$ EQ.3.0: Volumetric plastic strain, ε_v^p EQ.4.0: First stress invariant, J_1 EQ.5.0: Second stress invariant, $\sqrt{J_{2D}}$ EQ.6.0: Not used EQ.7.0: Not used EQ.8.0: Response mode number EQ.9.0: Number of iterations	E10.0
1-10	Card 7	Formulation flag, *ITYPE* EQ.1.0: Soil or Concrete (Cap surface may contract) EQ.2.0: Rock (Cap surface does not contract)	E10.0
11-20		Vectorization flag, *IVEC* EQ.0.0: Vectorized (fixed number of iterations) EQ.1.0: Fully iterative	E10.0
1-10	Card 8	Tension cutoff, $T < 0$ (positive in compression)	E10.0

This implementation of an extended two invariant cap model was developed by Whirley and Engelmann (1991) based on the formulations of Simo, Ju, Pister, and Taylor (1988), Simo, Ju, and Taylor (1990), and Sandler and Rubin, (1979). In this model, the two invariant cap theory is extended to include nonlinear kinematic hardening as suggested in (Isenberg, Vaughn, and Sandler, 1978). A brief discussion of the extended cap model and its parameters is given below.

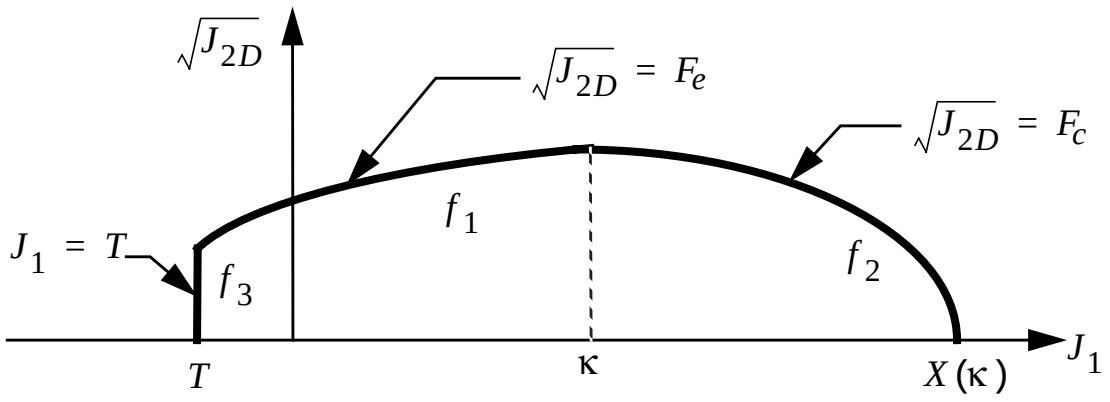

Figure 10
The yield surfaces of the two invariant cap model in $\sqrt{J_{2D}}$ - J_1 space. Surface f_1 is the failure envelope, f_2 is the cap surface, and f_3 is the tension cutoff.

The cap model is formulated in terms of the invariants of the stress tensor. The square root of the second invariant of the deviatoric stress tensor, $\sqrt{J_{2D}}$, is found from the deviatoric stresses $\boldsymbol{s}$ as

$$\sqrt{J_{2D}} \equiv \sqrt{\frac{1}{2} s_{ij} s_{ij}} \tag{120}$$

and is an objective scalar measure of the distortional or shearing stress. The first invariant of the stress, J_1, is simply the sum of the normal stresses, or equivalently, three times the pressure.

The cap model consists of three surfaces in $\sqrt{J_{2D}}$ - J_1 space, as shown in Figure 10. First, there is a failure envelope surface, denoted f_1 in the figure. The functional form of f_1 is

$$f_1 = \sqrt{J_{2D}} - min\left(F_e(J_1), T_{mises}\right), \tag{121}$$

where F_e is given by

$$F_e(J_1) \equiv \alpha - \gamma exp(-\beta J_1) + \theta J_1 \tag{122}$$

and $T_{mises} \equiv |X(\kappa_n) - L(\kappa_n)|$. This failure envelope surface is fixed in $\sqrt{J_{2D}}$ - J_1 space, and therefore does not harden, unless kinematic hardening is present. Next, there is a cap surface, denoted f_2 in the figure, with f_2 given by

$$f_2 = \sqrt{J_{2D}} - F_c(J_1, \kappa), \tag{123}$$

where F_c is defined by

$$F_c(J_1, \kappa) \equiv \frac{1}{R}\sqrt{[X(\kappa) - L(\kappa)]^2 - [J_1 - L(\kappa)]^2} \quad , \tag{124}$$

$X(\kappa)$ is the intersection of the cap surface with the J_1 axis,

$$X(\kappa) = \kappa + RF_e(\kappa) , \tag{125}$$

and $L(\kappa)$ is defined by

$$L(\kappa) \equiv \begin{matrix} \kappa \text{ if } \kappa > 0 \\ 0 \text{ if } \kappa \le 0 \end{matrix} . \tag{126}$$

The hardening parameter κ is related to the plastic volume change ε_v^p through the hardening law

$$\varepsilon_v^p = W\{1 - exp[-D(X(\kappa) - X_0)]\} \quad . \tag{127}$$

Geometrically, κ is seen in the figure as the J_1 coordinate of the intersection of the cap surface and the failure surface. Finally, there is the tension cutoff surface, denoted f_3 in the figure. The function f_3 is given by

$$f_3 \equiv T - J_1, \tag{128}$$

where T is an input material parameter which specifies the maximum hydrostatic tension sustainable by the material. The elastic domain in $\sqrt{J_{2D}}$ - J_1 space is then bounded by the failure envelope surface above, the tension cutoff surface on the left, and the cap surface on the right.

An additive decomposition of the strain into elastic and plastic parts is assumed:

$$\mathbf{e} = \mathbf{e}^e + \mathbf{e}^l, \tag{129}$$

where $\mathbf{e}^e$ is the elastic strain and $\mathbf{e}^p$ is the plastic strain. Stress is found from the elastic strain using Hooke's law,

$$\mathbf{s} = \boldsymbol{C}(\mathbf{e} - \mathbf{e}^p), \tag{130}$$

where $\mathbf{s}$ is the stress and $\boldsymbol{C}$ is the elastic constitutive tensor.

The yield condition may be written

$$\begin{aligned} f_1(\mathbf{s}) &\le 0 \\ f_2(\mathbf{s}, \kappa) &\le 0 \\ f_3(\mathbf{s}) &\le 0 \end{aligned} \tag{131}$$

and the plastic consistency condition requires that

$$\begin{matrix} \dot{\lambda}_k f_k = 0 \\ \dot{\lambda}_k \ge 0 \end{matrix} \quad k = 1, 2, 3, \tag{132}$$

where λ_k is the plastic consistency parameter for surface k. If $f_k < 0$, then $\dot{\lambda}_k = 0$ and the response is elastic. If $f_k > 0$, then surface k is active and $\dot{\lambda}_k$ is found from the requirement that $\dot{f}_k = 0$.

Associated plastic flow is assumed, so using Koiter's flow rule the plastic strain rate is given as the sum of contributions from all of the active surfaces,

$$\dot{\boldsymbol{\varepsilon}}^p = \sum_{k=1}^{3} \dot{\lambda}_k \frac{\partial f_k}{\partial \boldsymbol{\sigma}}. \tag{133}$$

One of the major advantages of the cap model over other classical pressure-dependent plasticity models is the ability to control the amount of dilatancy produced under shear loading. Dilatancy is produced under shear loading as a result of the yield surface having a positive slope in $\sqrt{J_{2D}}$ - J_1 space, so the assumption of plastic flow in the direction normal to the yield surface produces a plastic strain rate vector that has a component in the volumetric (hydrostatic) direction (see Figure 10). In models such as the Drucker-Prager and Mohr-Coulomb, this dilatancy continues as long as shear loads are applied, and in many cases produces far more dilatancy than is experimentally observed in material tests. In the cap model, when the failure surface is active, dilatancy is produced just as with the Drucker-Prager and Mohr-Coulomb models. However, the hardening law permits the cap surface to contract until the cap intersects the failure envelope at the stress point, and the cap remains at that point. The local normal to the yield surface is now vertical, and therefore the normality rule assures that no further plastic volumetric strain (dilatancy) is created. Adjustment of the parameters that control the rate of cap contraction permits experimentally observed amounts of dilatancy to be incorporated into the cap model, thus producing a constitutive law which better represents the physics to be modeled.

Another advantage of the cap model over other models such as the Drucker-Prager and Mohr-Coulomb is the ability to model plastic compaction. In these models all purely volumetric response is elastic. In the cap model, volumetric response is elastic until the stress point hits the cap surface. Thereafter, plastic volumetric strain (compaction) is generated at a rate controlled by the hardening law. Thus, in addition to controlling the amount of dilatency, the introduction of the cap surface adds another experimentally observed response characteristic of geological materials into the model.

The inclusion of kinematic hardening will result in hysteretic energy dissipation under cyclic loading conditions. Following the approach of (Isenberg, Vaughn, and Sandler, 1978), a nonlinear kinematic hardening law is used for the failure envelope surface when nonzero values of $\bar{c}$ and N are specified. In this case, the failure envelope surface is replaced by a family of yield surfaces

bounded by an initial yield surface and a limiting failure envelope surface. Thus, the shape of the yield surfaces described above remains unchanged, but they may translate in a plane orthogonal to the J_1 axis.

Translation of the yield surfaces is permitted through the introduction of a "back stress" tensor, $\boldsymbol{\alpha}$. The formulation including kinematic hardening is obtained by replacing the stress $\boldsymbol{s}$ with the translated stress tensor $\eta \equiv s - \alpha$ in all of the above equations. The history tensor $\boldsymbol{\alpha}$ is assumed deviatoric, and therefore has only 5 unique components. The evolution of the back stress tensor is governed by the nonlinear hardening law

$$\overset{\nabla}{\alpha} = \bar{c}\bar{F}(s, \boldsymbol{\alpha})\dot{\boldsymbol{e}}^p, \tag{134}$$

where $\bar{c}$ is a constant, $\bar{F}$ is a scalar function of s and α, and $\dot{\boldsymbol{e}}^p$ is the rate of deviatoric plastic strain. The constant $\bar{c}$ may be estimated from the slope of the shear stress - plastic shear strain curve at low levels of shear stress.

The function $\bar{F}$ is defined as

$$\bar{F} \equiv max\left\{0, 1 - \frac{(s - \alpha) \bullet \alpha}{2NF_e(J_1)}\right\}, \tag{135}$$

where N is a constant defining the size of the yield surface. The value of N may be interpreted as the radial distance between the outside of the initial yield surface and the inside of the limit surface. In order for the limit surface of the kinematic hardening cap model to correspond with the failure envelope surface of the standard cap model, the scalar parameter α must be replaced with $\alpha - N$ in the definition of F_e.

The cap model contains a number of parameters which must be chosen to represent a particular material, and are generally based on experimental data. The parameters α, β, θ, and γ are usually evaluated by fitting a curve through failure data taken from a set of triaxial compression tests. The parameters W, D, and X_0 define the cap hardening law. The value of W represents the void fraction of the uncompressed sample and D governs the slope of the initial loading curve in hydrostatic compression. The value of R is the ratio of major to minor axes of the quarter ellipse defining the cap surface. Additional details and guidelines for fitting the cap model to experimental data are found in (Chen and Baladi, 1985).

This model represents a new implementation of the two-invariant cap model into DYNA2D. This version is highly vectorized and more reliable than the experimental implementation available in previous releases. In addition, this new implementation incorporates nonlinear kinematic hardening to model cyclic energy dissipation due to shear hysteresis.

Material Type 19 (Frazer-Nash Hyperelastic Rubber)

Columns		Quantity	Format
1-10	Card 3	First strain energy density coefficient, C_{001}	E10.0
11-20		Second strain energy density coefficient, C_{010}	E10.0
21-30		Third strain energy density coefficient, C_{020}	E10.0
31-40		Fourth strain energy density coefficient, C_{100}	E10.0
41-50		Fifth strain energy density coefficient, C_{101}	E10.0
1-10	Card 4	Sixth strain energy density coefficient, C_{110}	E10.0
11-20		Seventh strain energy density coefficient, C_{200}	E10.0
21-30		Eighth strain energy density coefficient, C_{210}	E10.0
31-40		Ninth strain energy density coefficient, C_{300}	E10.0
41-50		Tenth strain energy density coefficient, C_{400}	E10.0
1-10	Card 5	Strain limit option, *ILIMIT* EQ.0.0: stop if strain limits are exceeded EQ.1.0: continue if strain limits are exceeded	E10.0
1-10	Card 6	Maximum strain limit, E_{max}	E10.0
11-20		Minimum strain limit, E_{min}	E10.0
	Card 7	Blank	
	Card 8	Blank	

This model implements a hyperelastic constitutive law described in (Kenchington, 1988). It is useful for representing the behavior of rubber-like materials at moderate to large strains. An alternative hyperelastic model is Material Type 7 (Blatz-Ko).

The strain energy density function is of the form

$$\begin{aligned} W \;=\; & C_{100}I_1 + C_{200}I_1^2 + C_{300}I_1^3 + C_{400}I_1^4 \\ & + C_{010}I_2 + C_{020}I_2^2 + C_{110}I_1I_2 + C_{210}I_1^2I_2 \\ & + C_{001}I_3 + C_{101}I_1I_3 \end{aligned} \tag{136}$$

where I_1, I_2, and I_3 are the strain invariants defined in terms of engineering components of the Green-Lagrange strain tensor $\boldsymbol{E}$ by

$$I_1 \;=\; E_{11} + E_{22} + E_{33}, \tag{137}$$

$$I_2 = (E_{11}E_{22} + E_{11}E_{33} + E_{22}E_{33}) - \frac{1}{4}(E_{12}^2 + E_{23}^2 + E_{31}^2), \tag{138}$$

and

$$I_3 = \left[E_{11}E_{22}E_{33} + \frac{1}{4}E_{12}E_{23}E_{31}\right] - \frac{1}{4}(E_{11}E_{23}^2 + E_{22}E_{31}^2 + E_{33}E_{12}^2). \tag{139}$$

The second Piola-Kirchhoff stress $\mathtt{t}$ is found by differentiating the strain energy density function W with respect to the Green-Lagrange strain,

$$\mathtt{t} = \frac{\partial W}{\partial \boldsymbol{E}}. \tag{140}$$

Cauchy stress $\mathtt{s}$ is then found from the second Piola-Kirchhoff stress using

$$\mathtt{s} = \frac{1}{J}\boldsymbol{F}\mathtt{t}\boldsymbol{F}^T, \tag{141}$$

where $\boldsymbol{F}$ is the deformation gradient and J is its determinant.

The values of the ten C coefficients in the strain energy density function must be determined from experimental data on the material. A procedure is described in (Kenchington, 1988) to determine these parameters using data from a uniaxial stress test, a biaxial stress or strain test, and a shear test.

The model input includes a maximum strain limit E_{max}, a minimum strain limit E_{min}, and a strain limit option flag, $ILIMIT$. This feature is particularly useful if the model has been fitted to data only over a limited range, and therefore caution should be exercised if strains outside this range are encountered. At each step, the maximum and minimum normal strains are tested against the limit criteria. If the maximum normal strain is greater than E_{max} or the minimum normal strain is less than E_{min}, then a message is written to the screen and hsp printout file, and execution terminates if $ILIMIT = 0$ or continues if $ILIMIT = 1$.

Material Type 20 (Laminated Composite)

Columns		Quantity	Format
1-10	Card 3	Elastic modulus - fiber direction, E_a (see Figure 2)	E10.0
11-20		Elastic modulus - transverse direction, E_b	E10.0
21-30		Elastic modulus - thickness direction, E_c	E10.0
31-40		Poisson's ratio, ν_{ab}	E10.0
41-50		Poisson's ratio, ν_{ac}	E10.0
51-60		Poisson's ratio, ν_{bc}	E10.0
1-10	Card 4	Shear modulus, G_{ab}	E10.0
11-20		Shear modulus, G_{ac}	E10.0
21-30		Shear modulus, G_{bc}	E10.0
31-40		Lamina thickness, t	E10.0
41-50		Lamination axes option, $Aopt$	E10.0
		EQ.1.0: planar laminate defined by normal $\boldsymbol{n}$ and interior surface point $\boldsymbol{P}$ (see Figure 11).	
		EQ.2.0: spherical laminate with interior radius R and center $\boldsymbol{P}$ (see Figure 11).	
51-60		Number of laminae, $NUMLAY$	E10.0
	Card 5	$Aopt$.EQ.1.0:	
1-10		Coordinate y_p or r_p	E10.0
11-20		Coordinate z_p	E10.0
21-30		Coordinate y_n or r_n	E10.0
31-40		Coordinate z_n	E10.0
	Card 5	$Aopt$.EQ.2.0:	
1-10		Coordinate y_p or r_p	E10.0
11-20		Coordinate z_p	E10.0
21-30		Interior radius R	E10.0
	Card 6	Blank	
	Card 7	Blank	
	Card 8	Blank	

Define $NUMLAY$ lamina orientation angles, θ, (in degrees) . Repeat the following card until all $NUMLAY$ angles have been defined.

Cards 8,...,8+NUMLAY/8

Columns	Quantity	Format
1-10	θ_1 (in degrees)	E10.0
11-20	θ_2 (in degrees)	E10.0
21-30	θ_3 (in degrees)	E10.0
.	.	
.	.	
.	.	
71-80	θ_8 (in degrees)	E10.0

Repeat this card until all lamina angles are defined.

This model simulates an elastic laminated composite by calculating the effective laminate properties, $\overline{\boldsymbol{C}}$, based upon the lamina present in each element. The effective laminate properties are calculated using the first order approach developed by Pagano (1974).

The material properties are specified in the lamina coordinate system **a-b-c**, where **a**, **b**, and **c** are the fiber, transverse, and through-thickness directions, respectively. The lamina orientation angle, θ, is the angle that the fibers make with the plane of the mesh, i.e. the $r-z$ or $y-z$ plane. For example, in axisymmetric geometries hoop lamina have $\theta = \pm 90^o$ while an axial lamina has $\theta = 0$ or $\theta = 180^o$. More specifically, θ is the angle between the vector **a** and the plane formed by the element vectors **A** and **C**, shown in Figure 11. Note that the through-thickness direction **c** of the lamina is always parallel to the element direction **C**.

The laminate geometry is based upon the lamination option and the assumption that each lamina is t thick. In the planar option, the i-th lamina ($i \neq 1$) exists in the region that is bound by lines that are perpendicular to **n** and pass through the points $\boldsymbol{P} + (i-1)t \times \boldsymbol{n}$ and $\boldsymbol{P} + i \times t \times \boldsymbol{n}$. In the spherical option, the i-th lamina ($i \neq 1$) exists in the region bound by two circles whose centers are **P** and radii are $R + (i-1) \times t$ and $R + i \times t$, respectively.

The laminae present in each element are determined by constructing a ‘‘slice’’ that 1) spans the entire element, 2) is parallel to the element vector **C,** and 3) passes through the element centroid. This slice is then overlaid on the laminate geometry, and the lamina number and fraction of each lamina present in the slice are determined.

The constitutive matrix $\mathbf{C}$ relating increments in stress to increments in strain in the lamina coordinate system **a-b-c** is defined as

$$C_L^{-1} = \begin{vmatrix} \frac{1}{E_a} & -\frac{\nu_{ba}}{E_b} & -\frac{\nu_{ca}}{E_c} & 0 & 0 & 0 \\ -\frac{\nu_{ab}}{E_a} & \frac{1}{E_b} & -\frac{\nu_{cb}}{E_c} & 0 & 0 & 0 \\ -\frac{\nu_{ac}}{E_a} & -\frac{\nu_{bc}}{E_b} & \frac{1}{E_c} & 0 & 0 & 0 \\ 0 & 0 & 0 & \frac{1}{G_{ab}} & 0 & 0 \\ 0 & 0 & 0 & 0 & \frac{1}{G_{bc}} & 0 \\ 0 & 0 & 0 & 0 & 0 & \frac{1}{G_{ca}} \end{vmatrix} . \tag{142}$$

Poisson's ratios are defined as $\nu_{ij} = \frac{-\varepsilon_j}{\varepsilon_i}$ (143)

which represents the strain ratio resulting from a uniaxial stress applied in the *i-th* direction. Note that symmetry of the elastic compliance $\mathbf{C}_L^{-1}$ implies

$$\frac{\nu_{ab}}{E_a} = \frac{\nu_{ba}}{E_b} , \frac{\nu_{ca}}{E_c} = \frac{\nu_{ac}}{E_a} , \text{ and } \frac{\nu_{cb}}{E_c} = \frac{\nu_{bc}}{E_b} . \tag{144}$$

Further, positive definiteness of $\mathbf{C}_L$ yields the following restrictions on the elastic constants:

$$\nu_{ba} < \left(\frac{E_b}{E_a}\right)^{\frac{1}{2}} , \nu_{ca} < \left(\frac{E_c}{E_a}\right)^{\frac{1}{2}} , \text{ and } \nu_{cb} < \left(\frac{E_c}{E_b}\right)^{\frac{1}{2}} . \tag{145}$$

Nonphysical energy growth may appear in the solution if these restrictions on the elastic constants are not observed.

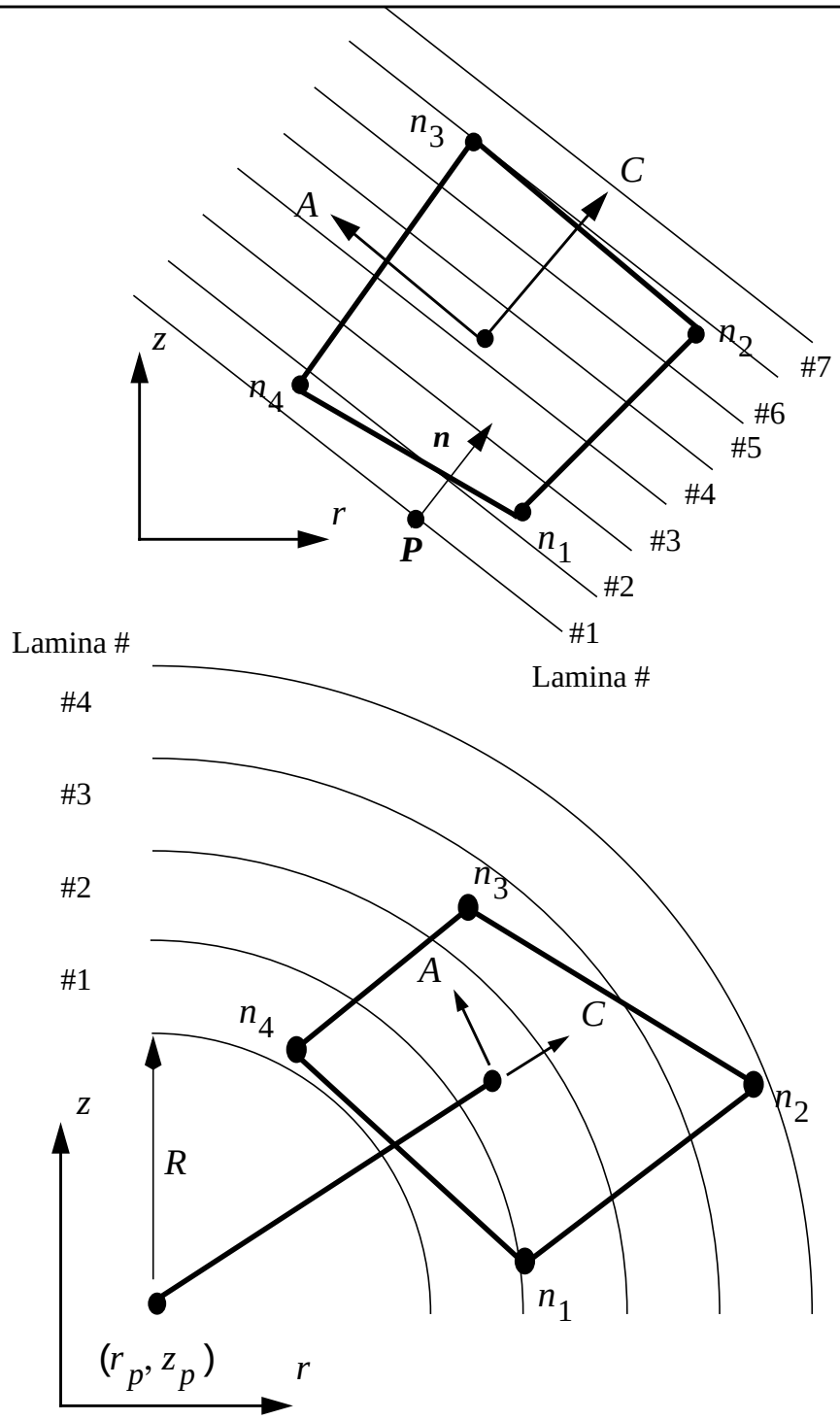

Figure 11
Options for determining the lamination axes
(a) AOPT = 1.0; (b) AOPT = 2.0.

Based upon the laminate option $Aopt$, an elemental coordinate system, **A-B-C**, is constructed at each element centroid. (See Figure 11.) The unit vector **C** is parallel to: **n** for $Aopt = 1.0$, and to the vector that connects the reference point **P** to the element centroid for $Aopt = 2.0$. For each lamina present within the element, the *i*-th lamina constitutive matrix $\mathbf{C}_i$ is rotated from the **a-b-c** lamina coordinate system to an intermediate $\boldsymbol{a}'\text{-}\boldsymbol{b}'\text{-}\boldsymbol{c}'$ sytem.The angle between the **a** and $\boldsymbol{a}'$ vectors (as well as between the **b** and $\boldsymbol{b}'$ vectors) is θ_i, the lamina orientation angle. Using each lamina's individual stiffness matrix, expressed in it own $\boldsymbol{a}'\text{-}\boldsymbol{b}'\text{-}\boldsymbol{c}'$ system, all lamina present within the element are homogenized (Pagano, 1974) and yield an effective 6×6 stiffness matrix, $\overline{\boldsymbol{C}}$. This matrix is then reduced to the required two-dimensional 4×4 stiffness matrix by *discarding* all unnecessary components. (Although the components $\overline{C}_{14} = \overline{C}_{24} = \overline{C}_{34} = 0$ always, the remaining discarded stiffnesses are only zero if the layup across the element is symmetric. See cautionary note below.) Finally, the reduced 4×4 effective stiffness matrix is then rotated from the **A-B-C** element system into the global $r - z$ or $x - z$ system, and its components are stored as history variables.

Pagono's homogenization assumes that the effective elemental stresses σ_{CC}, σ_{AC}, and σ_{AB}, and the strains ε_{AA}, ε_{BB}, and γ_{AB} are constant in the entire homogenization "slice." The corresponding 3 lamina stresses and 3 lamina strains are the same as the elemental stresses σ_{CC}, σ_{AC}, and σ_{AB}, and the strains ε_{AA}, ε_{BB}, and γ_{AB} strains, when expressed in the **A-B-C** elemental coordinate system. Care should be exercised when interpreting the global stresses and strains since, in general, they do not directly correspond to the actual lamina stresses and strains.

Caution should be exercised when interpreting results. The two-dimensional assumptions used to reduce the full 6×6 stiffness matrix, $\overline{\boldsymbol{C}}$, to a 4×4 stiffness matrix are that the elemental shear stresses σ_{AB} and σ_{bc}, and strains γ_{AB} and γ_{BC} equal zero. For symmertic layups, this conditions is satisfied trivially since no off diagonal stiffness terms exit in $\overline{\boldsymbol{C}}$ to couple the AB and BC components to each other or to any other components. However, for nonsymmetric layups, non-zero off diagonal terms render it impossible to satisfying all four assumptions simultaneously.

When nonsymmetric layups exist, it is assumed that $\sigma_{BC} = \gamma_{AB} = 0$, and consequently $\sigma_{AB} \neq 0$ and $\gamma_{BC} \neq 0$. (This is consistent with Pagano's homogenization theory.) This implies that an applied external torque *exists* to resists the net σ_{AB} contribution and that out-of-plane deformation occurs. Note that these two three-dimensional effects are not consistent with conventional two-dimensional FE assumptions. Therefore, this material model is suggested for use only with symmetric layups.

Material Type 21 (Isotropic-Elastic-Plastic)

Columns		Quantity	Format
1-10	Card 3	Young's modulus, E	E10.0
1-10	Card 4	Poisson's ratio, ν	E10.0
1-10	Card 5	Yield stress, σ_0	E10.0
1-10	Card 6	Tangent modulus, E_T	E10.0
	Card 7	Blank	
	Card 8	Blank	

This model produces bilinear elastoplastic behavior which is identical to Material Type 3 with $\beta = 1.0$, but is somewhat faster and requires less storage.

The theoretical foundations of this model are similar to those described for Material Type 3. The numerical algorithms are based on those described in (Krieg and Key, 1976).

Material Type 22 (Strain Rate Dependent Steinberg-Guinan-Lund)

An equation of state must be used with this model.

Columns		Quantity	Format
1-10	Card 3	Shear modulus constant, G_0	E10.0
11-20		Yield stress constant, σ_0	E10.0
21-30		Strain hardening law constant, β	E10.0
31-40		Strain hardening exponent, n	E10.0
41-50		Initial plastic strain, γ_i	E10.0
51-60		First thermal activation constant, C_1	E10.0
61-70		Twice the dislocation kink energy, $2U_K$	E10.0
1-10	Card 4	Yield stress work hardening limit, σ_m	E10.0
11-20		Shear modulus pressure constant, b	E10.0
21-30		Yield stress pressure constant, b'	E10.0
31-40		Energy coefficient, h	E10.0
41-50		Energy exponential coefficient, f	E10.0
51-60		Peierl's stress, Y_P	E10.0
61-70		Second thermal activation constant, C_2	E10.0
71-80		Maximum athermal yield stress, σ_{am}	E10.0
1-10	Card 5	Atomic weight, A (if $A = 0$, R' must be defined)	E10.0
11-20		Melting temperature constant, T_{mo}	E10.0
21-30		Thermodynamic gamma, γ_0	E10.0
31-40		Thermodynamic constant, a	E10.0
41-50		Pressure cutoff, p_{cut}	E10.0
51-60		Room temperature, T_{room} EQ.0.0: default set to 300.0	E10.0
61-70		Debye coefficient, θ EQ.0.0: Debye correction ignored.	E10.0

Columns		Quantity	Format
1-10	Card 6	Spall model, *ISPALL* EQ.0.0: default set to 2.0 EQ.1.0: Pressure limit model EQ.2.0: Maximum principal stress spall criterion EQ.3.0: Hydrostatic tension spall criterion	E10.0
11-20		R' (if $R' \neq 0$, the atomic weight A is not used)	E10.0
21-30		Effective plastic strain at failure, $\bar{\varepsilon}_f^p$	E10.0
31-40		Polynomial order for fit, $NFIT$ $(1 \leq NFIT \leq 9)$	E10.0
41-50		Cold compression energy polynomial flag, *IVAR* EQ.0.0: Polynomial coefficients given or fit in terms of η EQ.1.0: Polynomial coefficients given or fit in terms of μ	E10.0
51-60		Optional minimum limit for energy fit Input η_{min} if $IVAR = 0$ Input μ_{min} if $IVAR = 1$	E10.0
61-70		Optional maximum limit for energy fit Input η_{max} if $IVAR = 0$ Input μ_{max} if $IVAR = 1$	E10.0
1-16	Card 7	First cold compression polynomial coefficient, EC_0	E16.0
17-32		EC_1	E16.0
33-48		EC_2	E16.0
49-64		EC_3	E16.0
65-80		EC_4	E16.0
1-16	Card 8	EC_5	E16.0
17-32		EC_6	E16.0
33-48		EC_7	E16.0
49-64		EC_8	E16.0
65-80		EC_9	E16.0

The formulation of this model is described in Steinberg and Lund (1989), and essentially consists of a strain rate modification to the Steinberg-Guinan model (material type 11) to extend the range of validity down to lower strain rates. The following description of this complex model is necessarily brief, and users are referred to the papers by Steinberg and coworkers for a complete description of the model and its derivation. Material constants are given in (Steinberg, 1991).

In terms of the foregoing input parameters, we define the shear modulus, G, before the material melts as:

$$G = G_0\left[1 + bpV^{\frac{1}{3}} - h\left(\frac{E_i - E_c}{3R'} - 300\right)\right]e^{-\frac{fE_i}{E_m - E_i}} \tag{146}$$

where p is the pressure, V is the relative volume, E_i is the current energy, E_c is the cold compression energy, and E_m is the melting energy. The cold compression energy is calculated using

$$E_c(x) = \int_0^x p\,dx\,, \tag{147}$$

where $x = 1 - V$. The equation is integrated using initial energy E_o and pressure P_o conditions that correspond to zero K and are given by

$$E_o = -3R'T_{room} \tag{148}$$

and

$$P_o = \gamma_o E_o \mathrm{Debye}\left(\frac{\theta}{T_{room}}\right). \tag{149}$$

Here Debye is the Debye correction factor, and has a default value of 1 when $\theta = 0$. The melting energy is found from the cold compression energy and the melting temperature using

$$E_m(x) = E_c(x) + 3R'T_m(x)\,, \tag{150}$$

where the melting temperature T_m is given by

$$T_m(x) = \frac{T_{mo}\exp(2ax)}{V^{2\left(\gamma_0 - a - \frac{1}{3}\right)}} \tag{151}$$

and T_{mo} is the melting temperature at the initial density, ρ_0.

In the above equations, R' is defined by

$$R' = \frac{R\rho}{A}, \tag{152}$$

where R is the universal gas constant and A is the atomic weight. **Note that if R' is not defined, DYNA2D computes it with R in the cm-gram-microsecond system of units.** Thus, this option should not be used unless the entire analysis model is defined in the cm-gram-microsecond second system of units.

The yield strength σ_y is decomposed into a thermally activated part σ_{yT} and an athermal part σ_{ya},

$$\sigma_y = \sigma_{yT}(\dot{\bar{\varepsilon}}^p, T)G(P, T) + \sigma_{ya}, \tag{153}$$

where G is a dimensionless function that relates the shear modulus at the current pressure P and temperature T to the shear modulus under standard conditions.

The effective plastic strain rate is written in terms of the thermally activated yield stress and known functions as

$$\dot{\bar{\varepsilon}}^p = \frac{1}{C_1} exp\left[\frac{2U_k}{kT}\left(1 - \frac{\sigma_{yT}}{Y_P}\right)^2\right] + \frac{C_2}{\sigma_{yT}}^{-1}, \tag{154}$$

where Y_P is the Peierls stress, $2U_k$ is the energy to form a pair of kinks in a dislocation segment of length L, and k is the Boltzmann constant. The constant C_2 is the drag coefficient D divided by the dislocation density ρ_d times the square of the Burger's vector b. The constant C_1 is given by

$$C_1 = \frac{\rho_d L a b^2 \nu}{2w^2}, \tag{155}$$

where a is the distance between Peierls valleys, w is the width of a kink loop, and ν is the Debye frequency. Equation (154) is solved iteratively to find σ_{YT}, but the additional restriction

$$\sigma_{YT} \le Y_P \tag{156}$$

is also imposed.

If E_m exceeds E_i (i.e., the material has not melted), then the athermal part of the yield strength σ_{ya} is given by:

$$\sigma_{ya} = \sigma_0'\left[1 + b'pV^{\frac{1}{3}} - h\left(\frac{E_i - E_c}{3R'} - 300\right)\right]e^{-\frac{fE_i}{E_m - E_i}}. \tag{157}$$

The work-hardened yield stress σ'_0 is found from the initial yield stress σ_0 and the accumulated effective plastic strain $\bar{\varepsilon}^p$ using the hardening law

$$\sigma'_0 = \sigma_0[1 + \beta(\gamma_i + \bar{\varepsilon}^p)]^n, \tag{158}$$

where γ_i is the initial plastic strain. If the work-hardened yield stress σ_0 exceeds the limiting value σ_m, then σ'_0 is reset to σ_m. After the materials melts ($E_i > E_m$), the athermal yield stress σ_{ya} and shear modulus G are reset to one half their initial value.

The evaluation of the cold compression energy $E_c(x)$ using (67) is too expensive to perform at each step of a calculation. As an approximation, many codes (including DYNA2D) use a polynomial to interpolate cold compression energy data during execution. The independent variable is chosen as η, and the polynomial takes the form

$$E_c = \sum_{i=0}^{NFIT-1} EC_i \eta^i \tag{159}$$

where $NFIT$ is the chosen order of the polynomial fit. Users are cautioned from using high order polynomial fits as these may oscillate significantly and introduce errors into the calculation. Note that the density and compression variables are related by

$$x = 1 - V = \frac{\mu}{\mu + 1} = 1 - \frac{1}{\eta}. \tag{160}$$

The coefficients EC_0 through EC_9 may be defined in the input if they are known. If they are not specified in the input, DYNA2D will fit the cold compression energy with up to a ten term polynomial expansion using a least squares method. If the order of the polynomial is not specified, DYNA2D will automatically pick the best polynomial order that fits the EOS generated data. Otherwise, DYNA2D will attempt to fit the data to the polynomial order desired. When DYNA2D performs any fit, the exact cold compression energy is compared with the cold compression energy found using the fitted polynomial at selected values of x, and the results printed in the "hsp" output file. These results should be examined closely to verify that a reasonably accurate polynomial fit has been obtained.

A Debye correction can be applied to the cold compression energy to improve the model's temperature response. This option is activated by specifying anon-zero value of the Debye coefficient θ.

A choice of three spall models is offered to represent material splitting, cracking, and failure under tensile loads. The pressure limit model, $(ISPALL = 1)$, limits the hydrostatic tension to the specified value, p_{cut}. If pressures more tensile than this limit are calculated, the pressure is reset to p_{cut}. This option is not strictly a spall model, since the deviatoric stresses are unaffected by the pressure reaching the tensile cutoff, and the pressure cutoff value p_{cut} remains unchanged throughout the analysis. The maximum principal stress spall model, $(ISPALL = 2)$, detects spall if the maximum (most tensile) principal stress σ_{max} exceeds the limiting value $-p_{cut}$. Note that the negative sign is required because p_{cut} is measured positive in compression, while σ_{max} is positive in tension. Once spall is detected with this model, the deviatoric stresses are set to zero, and no hydrostatic tension $(p < 0)$ is permitted. If tensile pressures are calculated, they are reset to 0 in

the spalled material. Thus, the spalled material behaves as a rubble or incohesive material. The hydrostatic tension spall model, $(ISPALL = 3)$, detects spall if the pressure becomes more tensile than the specified limit, p_{cut}. Once spall is detected the deviatoric stresses are set to zero, and the pressure is required to be compressive. If hydrostatic tension $(p < 0)$ is subsequently calculated, the pressure is reset to 0 for that element.

The Steinberg-Guinan-Lund model is applicable to materials over a range of strain rates. Constants for this model for a wide range of materials are given in a valuable recent publication by Steinberg (1991).

Material ‘‘erosion’’ and failure may be obtained by defining a nonzero effective plastic strain at failure $\bar{\varepsilon}_f^p$ and specifying, on Control Card 4, that this material is active for automatic contact. Erosion is discussed in detail in section 2.12 on page 17.

Material Type 23 (Three-Invariant Viscoplastic Cap Model)

Columns		Quantity	Format
1-10	Card 3	Shear modulus, G	E10.0
11-20		Bulk modulus, K	E10.0
21-30		Gruneisen ratio (optional), Γ	E10.0
31-40		Shock parameter (optional), S_l	E10.0
41-50		Pore compression flag, $IPRES$ EQ.0.0: Explicit pore compression EQ.1.0: Constant bulk modulus	E10.0
1-10	Card 4	Shear failure surface constant, α	E10.0
11-20		Shear failure surface linear coefficient, θ	E10.0
21-30		Shear failure surface exponential coefficient, γ	E10.0
31-40		Shear failure surface exponent, β	E10.0
41-50		Tensile pressure cutoff (negative in tension)	E10.0
51-60		Tensile return mapping mode	E10.0
61-70		Kinematic hardening parameter, N^{α}	E10.0
71-80		Kinematic hardening coefficient, c^{α}	E10.0
1-10	Card 5	Initial ellipticity, R_0	E10.0
11-20		Initial J_1-axis intercept, X_0	E10.0
21-30		Cap contraction option, $IROCK$ EQ.0.0: Contraction allowed (soils) EQ.1.0: Contraction omitted (rocks) EQ.2.0: Contraction w/ hardening (rocks)	E10.0
31-40		Shear-enhanced compaction parameter	E10.0
1-10	Card 6	Maximum plastic volume strain, W	E10.0
11-20		Exponent D_1	E10.0
21-30		Exponent D_2	E10.0
31-40		Plot variable output option (see Table 3)	E10.0
41-50		Maximum strain increment	E10.0
1-10	Card 7	Three-invariant parameter Q_1	E10.0

Columns		Quantity	Format
11-20		Three-invariant parameter Q_2 GE.0.0: Formulation parameter LE.0.0: Friction angle, φ (degrees)	E10.0
21-30		Rounded vertices parameter, $\Delta\beta_0$ (degrees)	E10.0
31-40		Rounded vertices parameter, δ	E10.0
41-50		Viscoplasticity fluidity parameter	E10.0
51-60		Viscoplastic flow function form, *NFORM* LT.0.0: $\phi(f) = (f/f_0)^N$, where $N = \|NFORM\|$ GT.0.0: $\phi(f) = exp(f/f_0)^N - 1$	E10.0
	Card 8	Blank	

This model was developed by Len Schwer and Yvonne Murray and is described in (Schwer and Murray, 1994). For additional information on the viscoplastic aspects of this model see (Schwer, 1994).

Table 3: Output variables for NPLOT plotting option.

NPLOT	Function	Description
1	$L(\kappa)$	J_1 value at cap-shear surface intersection
2	$X(\kappa)$	J_1 intercept of cap surface
3	$R(\kappa)$	Cap surface ellipticity
4	$\bar{\varepsilon}_v^p$	Plastic volume strain
5	J_1	First stress invariant
6	J_2'	Second invariant of deviatoric stress
7	J_3'	Third invariant of deviatoric stress
8	$\hat{J}_3'$	$(3\sqrt{1.5}J_3')/(J_2')^{3/2} = -\sin(3\beta)$
9	β	Lode angle (degrees)
10	R	Octahedral plane radius
11	J	Relative volume
12	ϕ	Porosity

Table 3: Output variables for NPLOT plotting option.

NPLOT	Function	Description
13	ϕ_{cs}	Relative change in volume of solid phase
14	P_{hs}	Pressure in the solid phase
15	E_{hs}	Energy in the solid phase
16	nsubs	Number of strain subincrements
17	$1-(R^2F_f^2F_c)/J_2'$	Deviation from failure surface
18	G^{α}	Kinematic hardening limiting function
19*	J_2^{α}	Kinematic hardening backstress

Material Type 24 (Bammann Plasticity Model)

Columns		Quantity	Format
1-10	Card 3	Young's modulus, E	E10.0
11-20		Poisson's ratio, ν	E10.0
21-30		Initial temperature, T_0	E10.0
31-40		Heat generation coefficient, HC	E10.0
1-10	Card 4	C_1	E10.0
11-20		C_2	E10.0
21-30		C_3	E10.0
31-40		C_4	E10.0
1-10	Card 5	C_5	E10.0
11-20		C_6	E10.0
21-30		C_7	E10.0
31-40		C_8	E10.0
41-50		C_{13}	E10.0
51-60		C_{14}	E10.0
1-10	Card 6	C_9	E10.0
11-20		C_{10}	E10.0
21-30		C_{15}	E10.0
31-40		C_{16}	E10.0
41-50		C_{11}	E10.0
51-60		C_{12}	E10.0
61-70		C_{17}	E10.0
71-80		C_{18}	E10.0
1-10	Card 7	Initial tensor internal variable, α_{xx}	E10.0
11-20		Initial α_{yy}	E10.0
21-30		Initial α_{xy}	E10.0
31-50		Blank	

Columns		Quantity	Format
51-60		Initial scalar internal variable, κ_0	E10.0
1-10	Card 8	Effective plastic strain at failure, $\bar{\varepsilon}_f^p$	E10.0

This model is described in (Bammann, 1990) and (Bammann, Johnson, and Chiesa, 1990). It is a phenomenological plasticity model using a set of internal state variables whose evolution is based on micromechanics. The model includes rate and temperature dependence, and heat generation due to plastic work. Since internal state variables are used to track the deformation, the history effects of strain rate and temperature are correctly captured.

The number of material parameters may seem prohibitive, but rarely are all of the constants used. The model reduces to linear strain hardening with only two required parameters. For rate insensitive materials the number of parameters is reduced by four. If temperature dependence is not required (i.e. when heat generation is not important), then the number of parameters is reduced by a factor of two. All of the parameters can be determined using simple tension and compression data.

The evolution of the Cauchy stress $\mathbf{s}$ is governed by an equation of the form

$$\dot{\mathbf{s}} = \lambda Tr(\boldsymbol{d}^e)\mathbf{1} + 2G\boldsymbol{d}^e, \tag{161}$$

where $\boldsymbol{d}^e$ is the elastic part of the rate of deformation, λ is the elastic Lame parameter given by

$$\lambda = \frac{E\nu}{(1+\nu)(1-2\nu)}, \tag{162}$$

and G is the elastic shear modulus. The rate of deformation $\boldsymbol{d}$ (symmetric part of the velocity gradient) is decomposed as

$$\boldsymbol{d} = \boldsymbol{d}^e + \boldsymbol{d}^p + \boldsymbol{d}^{th}, \tag{163}$$

where $\boldsymbol{d}^p$ is the deviatoric plastic part, and $\boldsymbol{d}^{th}$ is the thermal expansion part. The deviatoric plastic part of the rate of deformation is given by

$$\boldsymbol{d}^p = f(T)\sinh\left[\frac{|\mathbf{x}| - \kappa - Y(T)}{V(T)}\right]\frac{\mathbf{x}}{|\mathbf{x}|} \quad \text{for } |\mathbf{x}| - \kappa - Y(T) \geq 0 \tag{164}$$

and

$$\boldsymbol{d}^p = 0 \text{ for } (|\mathbf{x}| - \kappa - Y(T)) < 0, \tag{165}$$

where T is temperature, κ is a scalar hardening variable, $\mathbf{x}$ is the translated stress found from the deviatoric Cauchy stress $\mathbf{s}$ and the tensor hardening variable $\mathbf{a}$ as

$$\chi \equiv \sigma - \frac{2}{3}\alpha, \tag{166}$$

and $f(T)$, $Y(T)$, and $V(T)$ are scalar functions. Assuming isotropic thermal expansion with coefficient $\hat{a}$, the thermal part of the rate of deformation can be written

$$\boldsymbol{d}^{th} = \hat{a}\dot{T}\mathbf{1}. \tag{167}$$

The evolution of the internal plasticity variables α and κ is found from

$$\dot{\alpha} = h(T)\boldsymbol{d}^{p} - [r_d(T)\bar{d} + r_s(T)]\bar{\alpha}\alpha \tag{168}$$

$$\dot{\kappa} = H(T)|\boldsymbol{d}^{p}| - [R_d(T)\bar{d} + R_s(T)]\kappa^2 \quad , \tag{169}$$

where $h(T)$ and $H(T)$ are hardening moduli (which may be functions of temperature),

$$\bar{d} = \sqrt{\frac{2}{3}}|\boldsymbol{d}^{p}|, \tag{170}$$

$$\bar{\alpha} = \sqrt{\frac{2}{3}}|\alpha|, \tag{171}$$

and $r_s(T)$, $R_s(T)$, $r_d(T)$, and $R_d(T)$ are scalar functions.

To compute temperature change, it is assumed that no heat is conducted out of an element and 90% of the plastic work is dissipated as heat, so it follows that

$$\dot{T} = \frac{0.9}{\rho c_v}(\sigma \bullet \boldsymbol{d}^{p}), \tag{172}$$

where ρ is the material density and c_v is the specific heat. To include this effect the heat generation coefficient, HC, should be defined in the input:

$$HC = \frac{0.9}{\rho c_v}. \tag{173}$$

Nine functions are used to describe the inelastic response. They can be grouped into three classes: those associated with the initial yield stress, the hardening functions, and the recovery functions. The temperature dependence of the yield functions are given by

$$V(T) = C_1 exp(-C_2/T) \tag{174}$$

$$Y(T) = C_3 exp(C_4/T) \tag{175}$$

$$F(T) = C_5 exp(-C_6/T). \tag{176}$$

The function $Y(T)$ describes the rate independent yield strength as a function of temperature. The function $F(T)$ determines the rate at which the material transitions from rate-insensitive to rate-dependent, and $V(T)$ describes the amount of rate dependence.

Two internal state variables are used to model hardening. The tensor variable α is used to describe the translation of the yield surface and the scalar variable κ is used to track growth of the yield surface. These two history variables evolve independently, and their evolution is characterized by a hardening contribution minus a recovery contribution. The hardening functions $h(T)$ and $H(T)$ are given by

$$h(T) = C_9 exp(C_{10}/T) \tag{177}$$

$$H(T) = C_{15} exp(C_{16}/T) . \tag{178}$$

Without recovery terms the model reduces to linear hardening with a tangent modulus of

$$E_T = (E(h + H))/(E + h + H) . \tag{179}$$

There are two recovery functions associated with each of the state variables α and κ. Larger values of recovery result in faster deviation from linear hardening and lower saturation stresses. The dynamic recovery function results in rate-independent hardening while the static (or thermal) recovery results in rate-dependent hardening.

The recovery functions are strongly temperature-dependent, and their form is given by

$$r_d(T) = C_7 exp(-C_8/T) \tag{180}$$

$$r_s(T) = C_{11} exp(-C_{12}/T) \tag{181}$$

$$R_d(T) = C_{13} exp(-C_{14}/T) \tag{182}$$

$$R_s(T) = C_{17} exp(-C_{18}/T) . \tag{183}$$

At higher strain rates and lower temperatures the dynamic recovery is dominant while at lower strain rates and higher temperatures the static recovery is dominant.

For high rate problems there can be a significant temperature increase due to plastic work. This allows the model to calculate thermal softening and thermal instabilities. Note that the heat generation coefficient HC will have no effect unless the functions are temperature-dependent. Typically, for strain rates less than 1.0 $\frac{1}{\text{sec}}$ the problem is not adiabatic and therefore the heat generation coefficient should *not* be included.

The parameters that give initial values to the components of the internal variable α may often be defined as zero. Nonzero values may be used to describe a material that is not initially isotropic, such as material deformed by a rolling process.

Material ‘‘erosion’’ and failure may be obtained by defining a nonzero effective plastic strain at failure $\bar{\varepsilon}_f^p$ and specifying, on Control Card 4, that this material is active for automatic contact. Erosion is discussed in detail in section 2.12 on page 17.

Material Type 25 (Sandia Damage Model)

Columns		Quantity	Format
1-10	Card 3	Young's modulus, E	E10.0
11-20		Poisson's ratio, ν	E10.0
21-30		Initial temperature, T_0	E10.0
31-40		Heat generation coefficient, HC	E10.0
1-10	Card 4	C_1	E10.0
11-20		C_2	E10.0
21-30		C_3	E10.0
31-40		C_4	E10.0
1-10	Card 5	C_5	E10.0
11-20		C_6	E10.0
21-30		C_7	E10.0
31-40		C_8	E10.0
41-50		C_{13}	E10.0
51-60		C_{14}	E10.0
1-10	Card 6	C_9	E10.0
11-20		C_{10}	E10.0
21-30		C_{15}	E10.0
31-40		C_{16}	E10.0
41-50		C_{11}	E10.0
51-60		C_{12}	E10.0
61-70		C_{17}	E10.0
71-80		C_{18}	E10.0
1-10	Card 7	Initial tensor internal variable, α_{xx}	E10.0
11-20		Initial α_{yy}	E10.0
21-30		Initial α_{xy}	E10.0
31-50		Blank	

Columns		Quantity	Format
51-60		Initial scalar internal variable, κ_0	E10.0
61-70		Damage exponent, $\bar{m}$	E10.0
71-80		Initial void volume fraction (porosity), D_0	E10.0
1-10	Card 8	Effective plastic strain at failure, $\bar{\varepsilon}_f^p$	E10.0
11-20		Element deletion controlled by damage level, *FSD* EQ.0.: Damage level does not control element deletion GT.0.: Element deletion based upon damage, $\dot{D}$	E10.0

The constitutive equations of this model are described in (Bammann, 1990) and (Bammann, Johnson, and Chiesa, 1990). The damage model is described in (Bammann, Chiesa, McDonald, Kawahara, Dike, and Revelli, 1990) and (Bammann, Chiesa, Horstemeyer, and Weingarten, 1993). This is a phenomenological plasticity model using a set of internal state variables whose evolutionis based on micromechanics. The model includes rate and temperature dependence, and heat generation due to plastic work. Since internal state variables are used to track the deformation, the history effects of strain rate and temperature are correctly captured. Ductile failure in materials is predicted by the model using a void growth evolution law.

The number of material parameters may seem prohibitive, but rarely are all of the constants used. The model reduces to a linear strain hardening with only two required parameters. For rate insensitive materials the number of parameters is reduced by four. If temperature dependence is not required (i.e. when heat generation is not important), then the number of parameters is reduced by a factor of two. All of the parameters (except for the two associated with damage) can be determined using simple tension and compression data.

The evolution of the Cauchy stress $\mathbf{s}$ is governed by an equation of the form

$$\dot{\mathbf{s}} = \lambda(1-D)Tr(\mathbf{d}^e)\mathbf{1} + 2G(1-D)\mathbf{d}^e - \frac{\dot{D}}{1-D}\mathbf{s} \quad , \tag{184}$$

where $\mathbf{d}^e$ is the elastic part of the rate of deformation, D is a scalar damage variable, λ is the elastic Lame parameter given by

$$\lambda = \frac{E\nu}{(1+\nu)(1-2\nu)} \quad , \tag{185}$$

and G is the elastic shear modulus. The rate of deformation $\mathbf{d}$ (symmetric part of the velocity gradient) is decomposed as

$$\mathbf{d} = \mathbf{d}^e + \mathbf{d}^p + \mathbf{d}^v + \mathbf{d}^{th}, \tag{186}$$

where $\mathbf{d}^p$ is the deviatoric plastic part, $\mathbf{d}^v$ is the dilatational plastic part, and $\mathbf{d}^{th}$ is the thermal expansion part. The deviatoric plastic part of the rate of deformation is given by

$$\mathbf{d}^p = f(T)\sinh\left[\frac{|\mathbf{x}| - \kappa - Y(T)(1-D)}{V(T)(1-D)}\right]\frac{\mathbf{x}}{|\mathbf{x}|} \quad \text{for} \quad |\mathbf{x}| - \kappa - Y(T)(1-D) \geq 0 \tag{187}$$

and

$$\mathbf{d}^p = 0 \text{ for } \quad (|\mathbf{x}| - \kappa - Y(T)(1-D)) < 0 \quad , \tag{188}$$

where T is temperature, κ is a scalar hardening variable, $\mathbf{x}$ is the translated stress found from the deviatoric Cauchy stress $\mathbf{s}$ and the tensor hardening variable $\mathbf{a}$ as

$$\mathbf{x} \equiv \mathbf{s} - \frac{2}{3}\mathbf{a}, \tag{189}$$

and $f(T)$, $Y(T)$, and $V(T)$ are scalar functions. The diliational plastic part of the rate of deformation depends only on the damage variable and is given by

$$\mathbf{d}^v = \frac{D}{1-D}\mathbf{1}. \tag{190}$$

Assuming isotropic thermal expansion with coefficient $\hat{a}$, the thermal part of the rate of deformation can be written

$$\mathbf{d}^{th} = \hat{a}\dot{T}\mathbf{1}. \tag{191}$$

The evolution of the internal plasticity variables $\mathbf{a}$ and κ is found from

$$\dot{\mathbf{a}} = h(T)\mathbf{d}^p - [r_d(T)\bar{d} + r_s(T)]\bar{\alpha}\mathbf{a} \tag{192}$$

$$\dot{\kappa} = H(T)|\mathbf{d}^p| - [R_d(T)\bar{d} + R_s(T)]\kappa^2 \quad , \tag{193}$$

where $h(T)$ and $H(T)$ are hardening moduli (which may be functions of temperature),

$$\bar{d} = \sqrt{\frac{2}{3}}|\mathbf{d}^p|, \tag{194}$$

$$\bar{\alpha} = \sqrt{\frac{2}{3}}|\mathbf{a}|, \tag{195}$$

and $r_s(T)$, $R_s(T)$, $r_d(T)$, and $R_d(T)$ are scalar functions.

The evolution of the damage parameter D is given by

$$\dot{D} = \chi\left[\frac{1}{(1-D)^{\bar{m}}} - (1-D)\right]|\mathbf{d}^p| \quad , \tag{196}$$

where χ is a stress triaxiality factor given by

$$\chi = \sinh\left[\frac{2(2\bar{m}-1)p}{(2\bar{m}+1)\bar{\sigma}}\right], \tag{197}$$

$\bar{m}$ is a void growth constant, p is pressure, and $\bar{\sigma}$ is effective stress.

To compute temperature change, it is assumed that no heat is conducted out of an element and 90% of the plastic work is dissipated as heat, so it follows that

$$\dot{T} = \frac{0.9}{\rho c_v}(\mathbf{s} \bullet \mathbf{d}^p), \tag{198}$$

where ρ is the material density and c_v is the specific heat. To include this effect the heat generation coefficient, HC, should be defined in the input:

$$HC = \frac{0.9}{\rho c_v}. \tag{199}$$

Nine functions are used to describe the inelastic response. They can be grouped into three classes: those associated with the initial yield stress, the hardening functions, and the recovery functions. The temperature dependence of the yield functions are given by

$$V(T) = C_1 exp(-C_2/T) \tag{200}$$

$$Y(T) = C_3 exp(C_4/T) \tag{201}$$

$$F(T) = C_5 exp(-C_6/T). \tag{202}$$

The function $Y(T)$ describes the rate independent yield strength as a function of temperature. The function $F(T)$ determines the rate at which the material transitions from rate-insensitive to rate-dependent, and $V(T)$ describes the amount of rate dependence.

Two internal state variables are used to model hardening. A tensor variable α is used to describe the translation of the yield surface and a scalar variable κ is used to track growth of the yield surface. These two history variables evolve independently, and their evolution is characterized by a hardening contribution minus a recovery contribution. The hardening functions $h(T)$ and $H(T)$ are given by

$$h(T) = C_9 exp(C_{10}/T) \tag{203}$$

$$H(T) = C_{15} exp(C_{16}/T). \tag{204}$$

Without recovery terms the model reduces to linear hardening with a tangent modulus of

$$E_T = (E(h+H))/(E+h+H). \tag{205}$$

There are two recovery functions associated with each of the state variables α and κ. Larger values of recovery result in faster deviation from linear hardening and lower saturation stresses. The dynamic recovery function results in rate-independent hardening while the static (or thermal) recovery results in rate-dependent hardening.

The recovery functions are strongly temperature-dependent, and their form is given by

$$r_d(T) = C_7 exp(-C_8/T) \tag{206}$$

$$r_s(T) = C_{11} exp(-C_{12}/T) \tag{207}$$

$$R_d(T) = C_{13} exp(-C_{14}/T) \tag{208}$$

$$R_s(T) = C_{17} exp(-C_{18}/T)\,. \tag{209}$$

At higher strain rates and lower temperatures the dynamic recovery is dominant while at lower strain rates and higher temperatures the static recovery is dominant.

For high rate problems there can be a significant temperature increase due to plastic work. This allows the model to calculate thermal softening and thermal instabilities. Note that the heat generation coefficient HC will have no effect unless the functions are temperature-dependent. Typically, for strain rates less than 1.0 $\frac{1}{\text{sec}}$ the problem is not adiabatic and therefore the heat generation coefficient should *not* be included.

The parameters that give initial values to the components of the internal variable α may often be defined as zero. Nonzero values may be used to describe a material that is not initially isotropic, such as material deformed by a rolling process.

The evolution of the damage internal state variable D is motivated by the Cocks-Ashby solution for the growth of a spherical void in a rate-dependent plastic material. Note that there is strong dependence on the ratio of mean stress to effective stress. Based on microscopic measurements of initial void volume fractions for metals, a value of 0.0001 is typically used for D_0. The value for $\bar{m}$ must be determined from test data, but unfortunately a simple procedure has not been found. Typically a notch tensile test is modeled and $\bar{m}$ is varied through a trial-and-error process until the correct strain to failure is produced. Other notch tests can then be used as validation. If no notch data exists, then a standard tensile test may be modeled and the strain at failure can be used (although this is less accurate). Most metals will fail at void fractions of several percent. However, at five percent damage, the growth rate is usually so large that a damage fraction of one (total material failure) is usually reached in a few time steps. For this reason the damage is limited to

0.99, at which point failure is assumed. The element stress and stiffness are inversely proportional to the damage, and at a damage level of 0.99 the element is essentially removed from the calculation.

Material ‘‘erosion’’ and failure may be obtained by defining a nonzero effective plastic strain at failure $\bar{\varepsilon}_f^p$ and specifying, on Control Card 4, that this material is active for automatic contact. Erosion is discussed in detail in section 2.12 on page 17. Alternatively, by specifying a positive FSD and nonzero damage parameters, material ‘‘erosion’’ will be controlled by the accumulated damage parameter $\dot{D}$. Both material erosion methods can be used simultaneously. In this case which every condition is satisfied first will determine erosion.

Material Type 26 (Circumferentially Cracked Elastic-Plastic)

Columns		Quantity	Format
1-10	Card 3	Young's modulus, E	E10.0
1-10	Card 4	Poisson's ratio, ν	E10.0
1-10	Card 5	Yield stress, σ_0	E10.0
11-20		Effective plastic stain at failure, $\bar{\varepsilon}_f^p$	E10.0
1-10	Card 6	Tangent modulus, E_T	E10.0
11-20		Hardening parameter, β	E10.0
1-10	Card 7	Effective plastic strain, $\bar{\varepsilon}_1^p$	E10.0
11-20		Effective plastic strain, $\bar{\varepsilon}_2^p$	E10.0
.	.		.
71-80		Effective plastic strain, $\bar{\varepsilon}_3^p$	E10.0
1-10	Card 8	Yield stress σ_{y1} at $\bar{\varepsilon}_1^p$	E10.0
11-20		Yield stress σ_{y2} at $\bar{\varepsilon}_2^p$	E10.0
.	.		.
71-80		Yield stress σ_{y3} at $\bar{\varepsilon}_3^p$	E10.0

This model is applicable only to axisymmetric structures. The material behavior is similar to material type 3, except that elements of this material cannot carry tensile circumferential stress. By specifying an initial relative volume greater than one on the element cards, the development of compressive circumferential stresses can be delayed or prevented since a gap must close circumferentially before compressive hoop stress develops.

The material behavior is elastoplastic and includes linear or piecewise strain hardening and material failure. The hardening parameter β specifies an arbitrary combination of kinematic and isotropic hardening for linear strain hardening; $\beta = 0.0$ yields purely kinematic hardening, while $\beta = 1.0$ gives purely isotropic hardening. Figure 3 illustrates the effect of β on the uniaxial stress-strain curve. The numerical algorithms used in this model are adapted from (Krieg and Key, 1976).

Material ‘‘erosion’’ and failure may be obtained by defining a nonzero effective plastic strain at failure $\bar{\varepsilon}_f^p$ and specifying, on Control Card 4, that this material is active for automatic contact. Erosion is discussed in detail in section 2.12 on page 17.

The piecewise linear strain hardening can only be used with isotropic hardening -- $\beta = 1$.

EQUATION OF STATE DEFINITION

An equation-of-state defines the volumetric behavior of a material, and must be used *only* in combination with a hydrodynamic material model. Many equation-of-state models allow the user to specify an initial energy per unit initial volume, E_0, and an initial relative volume, V_0. If $V_0 \neq 0$, then E_0 is the energy per unit initial volume (i.e., per unit reference volume for the relative volume computation).

Note that all energies reported by DYNA2D and written to the ORION database are per unit radian for axisymmetric problems and per unit thickness for plane strain problems.

Define an equation-of-state only for Material Types 8, 9, 10, 11, 12, 15, 16, and 22.

Card 9

Columns	Quantity	Format
1-72	Equation-of-state identification	12A6

This equation-of-state title will appear in the printed output. It is often helpful to use this heading to identify the physical material for which the DYNA2D equation of state model was constructed.

Cards 10, . . .

Equation-of-State Form 1 (Linear Polynomial)

Columns		Quantity	Format
1-10	Card 10	Pressure constant, C_0	E10.0
11-20		Linear compression coefficient, C_1	E10.0
21-30		Quadratic compression coefficient, C_2	E10.0
31-40		Cubic compression coefficient, C_3	E10.0
41-50		First energy coefficient, C_4	E10.0
51-60		Second energy coefficient, C_5	E10.0
61-70		Third energy coefficient, C_6	E10.0
71-80		Initial internal energy per unit initial volume, E_0	E10.0
1-10	Card 11	Initial relative volume, V_0 EQ.0.0: default set to 1.0	E10.0

The linear polynomial equation-of-state is linear in internal energy. The pressure is given by:

$$p = C_0 + C_1\mu + C_2\bar{\mu}^2 + C_3\mu^3 + (C_4 + C_5\mu + C_6\bar{\mu}^2)E \qquad (210)$$

where the excess compression μ is given by

$$\mu \equiv \frac{\rho}{\rho_0} - 1\,, \qquad (211)$$

E is the internal energy, ρ is the current density, and ρ_0 is the initial density. The tension-limited excess compression $\bar{\mu}$ is given by

$$\bar{\mu} = max(\mu, 0)\,. \qquad (212)$$

Relative volume is related to excess compression and density by

$$V = \frac{1}{1+\mu} = \frac{\rho_0}{\rho}\,. \qquad (213)$$

This equation-of-state is linear in internal energy, and may be used to fit experimental data for many materials. If $C_1 = K$ (the elastic bulk modulus) and all other $C_i = 0$, then linear elastic volumetric response is obtained.

This form of equation-of-state was adapted from that discussed in (Woodruff, 1973).

Equation-of-State Form 2 (JWL)

Columns		Quantity	Format
1-10	Card 10	A	E10.0
11-20		B	E10.0
21-30		R_1	E10.0
31-40		R_2	E10.0
41-50		ω	E10.0
51-60		Initial internal energy per unit initial volume, E_0	E10.0
61-70		Initial relative volume, V_0 EQ.0.0: default set to 1.0	E10.0

The JWL equation-of-state defines the pressure as

$$p = A\left(1 - \frac{\omega}{R_1 V}\right)e^{-R_1 V} + B\left(1 - \frac{\omega}{R_2 V}\right)e^{-R_2 V} + \frac{\omega E}{V}, \tag{214}$$

where V is relative volume and E is internal energy.

The JWL equation of state is often used for detonation products of high explosives. Additional information in given in (Dobratz, 1981).

Equation-of-State Form 3 (Sack)

Columns		Quantity	Format
1-10	Card 10	A_1	E10.0
11-20		A_2	E10.0
21-30		A_3	E10.0
31-40		B_1	E10.0
41-50		B_2	E10.0
51-60		Initial internal energy per unit initial volume, E_0	E10.0
61-70		Initial relative volume, V_0 EQ.0.0: default set to 1.0	E10.0

The Sack equation-of-state defines pressure p as

$$p = \frac{A_3}{V^{A_1}} e^{-A_2 V} \left(1 - \frac{B_1}{V}\right) + \frac{B_2}{V} E \,, \tag{215}$$

where V is relative volume and E is the internal energy.

This equation-of-state form is often used for detonation products of high explosives, and was adapted from (Woodruff, 1973).

Equation-of-State Form 4 (Gruneisen)

Columns		Quantity	Format
1-10	Card 10	Velocity curve intercept, C	E10.0
11-20		First slope coefficient, S_1	E10.0
21-30		Second slope coefficient, S_2	E10.0
31-40		Third slope coefficient, S_3	E10.0
41-50		Gruneisen coefficient, γ_0	E10.0
51-60		First order volume correction coefficient, a	E10.0
61-70		Initial internal energy per unit initial volume, E_0	E10.0
71-80		Initial relative volume, V_0 EQ.0.0: default set to 1.0	E10.0

The Gruneisen equation-of-state with cubic shock velocity-particle velocity defines pressure for compressed materials ($\mu > 0$) as

$$p = \frac{\rho_0 C^2 \mu \left[1 + \left(1 - \frac{\gamma_0}{2} \right) \mu - \frac{a}{2} \mu^2 \right]}{\left[1 - (S_1 - 1)\mu - S_2 \frac{\mu^2}{\mu + 1} - S_3 \frac{\mu^3}{(\mu + 1)^2} \right]^2} + (\gamma_0 + a\mu)E \quad , \tag{216}$$

and for expanded materials ($\mu < 0$) as

$$p = \rho_0 C^2 \mu + (\gamma_0 + a\mu)E , \tag{217}$$

where C is the intercept of the shock velocity vs. particle velocity ($v_s - v_p$) curve, S_1, S_2, and S_3 are the coefficients of the slope of the $v_s - v_p$ curve, γ_0 is the Gruneisen gamma, and a is the first order volume correction to γ_0. The excess compression μ is defined by

$$\mu \equiv \frac{\rho}{\rho_0} - 1 , \tag{218}$$

where ρ is the current density and ρ_0 is the initial density.

The implementation of the Gruneisen equation-of-state is adapted from (Woodruff, 1973).

Equation-of-State Form 5 (Ratio of Polynomials)

Columns		Quantity	Format
1-16	Card 10	A_{10}	E16.0
17-32		A_{11}	E16.0
33-48		A_{12}	E16.0
49-64		A_{13}	E16.0
1-16	Card 11	A_{20}	E16.0
17-32		A_{21}	E16.0
33-48		A_{22}	E16.0
49-64		A_{23}	E16.0
1-16	Card 12	A_{30}	E16.0
17-32		A_{31}	E16.0
33-48		A_{32}	E16.0
49-64		A_{33}	E16.0
1-16	Card 13	A_{40}	E16.0
17-32		A_{41}	E16.0
33-48		A_{42}	E16.0
49-64		A_{43}	E16.0
1-16	Card 14	A_{50}	E16.0
17-32		A_{51}	E16.0
33-48		A_{52}	E16.0
49-64		A_{53}	E16.0
1-16	Card 15	A_{60}	E16.0
17-32		A_{61}	E16.0
33-48		A_{62}	E16.0
49-64		A_{63}	E16.0

Columns		Quantity	Format
Columns		Quantity	Format
1-16	Card 16	A_{70}	E16.0
17-32		A_{71}	E16.0
33-48		A_{72}	E16.0
49-64		A_{73}	E16.0
1-16	Card 17	α	E16.0
17-32		β	E16.0
33-48		A_{14}	E16.0
49-64		A_{24}	E16.0
1-16	Card 18	Initial internal energy per unit initial volume, E_0	E16.0
17-32		Initial relative volume, V_0 EQ.0.0: default set to 1.0	E16.0

The ratio of polynomials equation-of-state defines the pressure as

$$p = \frac{F_1 + F_2 E + F_3 E^2 + F_4 E^3}{F_5 + F_6 E + F_7 E^2}(1 + \alpha\mu) \tag{219}$$

where the each of the F_i are polynomials in terms of the excess compression μ of the form

$$F_i = \sum_{k=0}^{n} A_{ik}\mu^k \tag{220}$$

with $n = 4$ for F_1 and F_2, and $n = 3$ for F_3 through F_7. The excess compression μ is defined by

$$\mu \equiv \frac{\rho}{\rho_0} - 1\,, \tag{221}$$

where ρ is the current density and ρ_0 is the initial density.

In expanded elements ($\mu < 0$), F_1 in (219) is replaced by $\bar{F}_1$, where $\bar{F}_1$ is defined by

$$\bar{F}_1 = F_1 + \beta\mu^2\,. \tag{222}$$

This equation-of-state was adapted from (Woodruff, 1973).

Equation-of-State Form 6 (Linear Polynomial with Energy Deposition)

Columns		Quantity	Format
1-10	Card 10	Pressure constant, C_0	E10.0
11-20		Linear compression coefficient, C_1	E10.0
21-30		Quadratic compression coefficient, C_2	E10.0
31-40		Cubic compression coefficient, C_3	E10.0
41-50		First energy coefficient, C_4	E10.0
51-60		Second energy coefficient, C_5	E10.0
61-70		Third energy coefficient, C_6	E10.0
71-80		Initial internal energy per unit initial volume, E_0	E10.0
1-10	Card 11	Initial relative volume, V_0 EQ.0.0: default set to 1.0	E10.0
11-20		Load curve number giving energy deposition rate, LC	E10.0

This equation-of-state form is similar to equation-of-state form 1 except that this form allows internal energy to be deposited into the material at a specified rate. The pressure is given by:

$$p = C_0 + C_1\mu + C_2\bar{\mu}^2 + C_3\mu^3 + (C_4 + C_5\mu + C_6\bar{\mu}^2)E \qquad (223)$$

where the excess compression μ is given by

$$\mu \equiv \frac{\rho}{\rho_0} - 1 , \qquad (224)$$

E is the internal energy, ρ is the current density, and ρ_0 is the initial density. The tension-limited excess compression $\bar{\mu}$ is given by

$$\bar{\mu} = max(\mu, 0) . \qquad (225)$$

Relative volume is related to excess compression and density by

$$V = \frac{1}{1+\mu} = \frac{\rho_0}{\rho} . \qquad (226)$$

Internal energy is added into the material at a rate specified by load curve LC. This feature allows energy transfer mechanisms to be included which are not considered in detail in the analysis model.

This equation-of-state is linear in internal energy, and may be used to fit experimental data for many materials.

Equation-of-State Form 7 (Ignition and Growth of Reaction in HE)

Columns		Quantity	Format
1-10	Card 10	R_{1p}	E10.0
11-20		R_{2p}	E10.0
21-30		R_{5p}	E10.0
31-40		R_{6p}	E10.0
41-50		Second ignition coefficient, F_r	E10.0
1-10	Card 11	R_{3p}	E10.0
11-20		R_{1e}	E10.0
21-30		R_{2e}	E10.0
31-40		R_{3e}	E10.0
41-50		R_{5e}	E10.0
1-10	Card 12	R_{6e}	E10.0
11-20		$F_{max,ig}$	E10.0
21-30		F_q	E10.0
31-40		G_1	E10.0
41-50		m	E10.0
1-10	Card 13	a_1	E10.0
11-20		s_1	E10.0
21-30		Heat capacity of reaction products, c_{vp}	E10.0
31-40		Heat capacity of unreacted HE, c_{ve}	E10.0
41-50		η	E10.0
1-10	Card 14	C_{crit}	E10.0
11-20		Q_r	E10.0
21-30		Initial temperature, T_0 (in $^\circ K$)	E10.0
31-40		Minumum fraction reacted, $fcut$	E10.0
41-50		Tolerance for pressure iteration, $ptol$	E10.0
51-60		Maximum reaction per cycle, chi	E10.0

Columns		Quantity	Format
1-10	Card 15	G_2	E10.0
11-20		a_2	E10.0
21-30		s_2	E10.0
31-40		n	E10.0
41-50		$F_{max,\,gr}$	E10.0
51-60		$F_{min,\,gr}$	E10.0

Equation of State Form 7 was developed by Tarver et. al. and is used to calculate the shock initiation and detonation wave propagation of solid high explosive materials. It should be used instead of the programmed burn (ideal burn) options whenever:

- there is a question whether the high explosive will react,
- there is a finite time required for a shock wave to build up to cause detonation,
- there is a finite thickness of the chemical reaction zone in a detonation wave.

At relatively low initial pressures (less than 2 or 3 GPa), this equation of state should be used with DYNA2D Material Type 10 (elastic-plastic hydrodynamic) for an accurate calculation of the stress state in the unreacted HE. At higher initial pressures, the deviatoric stress state in the HE is less important and Material Type 9 (fluid) may be used at lower cost.

In the following description, a subscript ‘‘e’’ denotes quantities for the unreacted explosive, a subscript ‘‘p’’ denotes quantities for the reaction products, p is the pressure, V is the relative volume, and T is the absolute temperature.

The pressure in the unreacted explosive is given by a JWL equation of state,

$$p_e = R_{1e}e^{-R_{5e}V_e} + R_{2e}e^{-R_{6e}V_e} + R_{3e}\frac{T_e}{V_e} \tag{227}$$

where R_{3e} is a given constant related to the specific heat c_{ve} and JWL parameter ω by

$$R_{3e} = \omega_e c_{ve}\,. \tag{228}$$

The pressure in the reaction products is defined by another JWL equation of state,

$$\mathfrak{I}_p = R_{1p}e^{-R_{5p}} + R_{2p}e^{-R_{6p}V_p} + R_{3p}\frac{T_p}{V_p}, \tag{229}$$

and R_{3p} is a given constant related to the specific heat and JWL parameter as above.

As the chemical reaction converts unreacted explosive to reaction products, these JWL equations of state are used to calculate the pressure in the mixture. This mixture is defined by the fraction reacted, F, where $F = 0$ represents no reaction (all explosive) and $F = 1.0$ represents complete reaction (all products). The temperatures and pressures of reactants and products are assumed to be in equilibrium (i.e., $T_e = T_p$ and $p_e = p_p$), and the relative volumes are additive,

$$V = (1 - F)V_e + V_p . \tag{230}$$

The assumed form of the chemical reaction rate for conversion of unreacted explosive to reaction products consists of three physically realistic terms: an ignition term $\dot{F}_1$ which models the reaction of a small amount of explosive soon after the shock wave compresses it, a slow growth of reaction term $\dot{F}_2$ which models the spread of this initial reaction, and a rapid completion of reaction term $\dot{F}_3$ which dominates at high pressure and temperature. The assumed forms for the reaction rate is then

$$\frac{\partial F}{\partial t} = \dot{F}_1 + \dot{F}_2 + \dot{F}_3, \tag{231}$$

where the ignition term is given by

$$\dot{F}_1 = F_q (1 - F)^{F_r} \left[\frac{1}{V_e} - 1 - C_{crit} \right]^{\eta} , \tag{232}$$

the growth term is given by

$$\dot{F}_2 = G_1 (1 - F)^{s_1} F^{a_1} p^m , \tag{233}$$

and the completion term is given by

$$\dot{F}_3 = G_2 (1 - F)^{s_2} F^{a_2} p^n , \tag{234}$$

and F_q, F_r, C_{crit}, η, G_1, s_1, a_1, m, G_2, s_2, a_2, and n are given constants.

The ignition rate $\dot{F}_1$ is set to zero when $F \geq F_{max,ig}$, the growth term $\dot{F}_2$ is set to zero when $F \geq F_{max,gr}$, and the completion term $\dot{F}_3$ is set to zero when $F \leq F_{min,gr}$.

Details of the computational methods and many examples of one and two-dimensional shock initiation and detonation wave calculations can be found in (Cochran and Chan, 1979), (Lee and Tarver, 1980), (Tarver and Hallquist, 1981), (Tarver, Hallquist, and Erickson, 1985), and (Tarver, 1990).

Unfortunately, sufficient experimental data has been obtained for only two solid explosives to develop reliable shock initiation models: PBX-9404 (and the related HMX-based explosives LX-14, LX-10, LX-04, etc.), and LX-17 (the insensitive TATB-based explosive). Reactive flow models for other explosives (such as TNT, PETN, Composition B, propellants) have been developed but

are based on very limited experimental data. The standard models for PBX-9404 and LX-17 (in the centimeters, grams, and microseconds units system) are given in Table 4 and Table 5.

Table 4: Material Type 10 Constants for Two HE Materials

Material	density	shear modulus	yield strength
PBX-9404	1.842	0.0454	0.002
LX-17	1.900	0.0354	0.002

Table 5: Equation of State Form 7 Constants for Two HE Materials

Constant	PBX-9404	LX-17
R_{1p}	8.524	5.31396
R_{2p}	0.1802	0.0270309
R_{5p}	4.6	4.1
R_{6p}	1.3	1.1
F_r	0.667	0.667
R_{3p}	3.8E-6	4.60E-6
R_{1e}	9522.0	778.1
R_{2e}	-0.05944	-0.05031
R_{3e}	2.4656E-5	2.2229E-5
R_{5e}	14.1	11.3
R_{6e}	1.41	1.13
$F_{max,\,ig}$	0.3	0.5
F_q	7.43E+11	4.0E+6
G_1	3.1	0.6
m	1.0	1.0
a_1	0.111	0.111
s_1	0.667	0.667

Table 5: Equation of State Form 7 Constants for Two HE Materials

Constant	PBX-9404	LX-17
c_{vp}	1.0E-5	1.0E-5
c_{ve}	2.7813E-5	2.487E-5
η	20.0	7.0
C_{crit}	0.0	0.22
Q_r	0.102	0.069
T_0	298.0	298.0
G_2	400.0	400.0
a_2	1.0	1.0
s_2	0.333	.333
n	2.0	3.0
$F_{max,gr}$	0.5	0.5
$F_{min,gr}$	0.0	0.0

Equation-of-State Form 8 (Tabulated with Compaction)

Columns		Quantity	Format
1-16	Card 10	ε_{v1}	E16.0
17-32		ε_{v2}	E16.0
33-48		ε_{v3}	E16.0
49-64		ε_{v4}	E16.0
65-80		ε_{v5}	E16.0
1-16	Card 11	ε_{v6}	E16.0
17-32		ε_{v7}	E16.0
33-48		ε_{v8}	E16.0
49-64		ε_{v9}	E16.0
65-80		ε_{v10}	E16.0
1-16	Card 12	C_1	E16.0
17-32		C_2	E16.0
33-48		C_3	E16.0
49-64		C_4	E16.0
65-80		C_5	E16.0
1-16	Card 13	C_6	E16.0
17-32		C_7	E16.0
33-48		C_8	E16.0
49-64		C_9	E16.0
65-80		C_{10}	E16.0
1-16	Card 14	First temperature, T_1	E16.0
17-32		Second temperature, T_2	E16.0
33-48		T_3	E16.0
49-64		T_4	E16.0
65-80		T_5	E16.0
1-16	Card 15	T_6	E16.0

Columns		Quantity	Format
17-32		T_7 E16.0	
33-48		T_8	E16.0
49-64		T_9	E16.0
65-80		Tenth temperature, T_{10}	E16.0
1-16	Card 16	First unloading bulk modulus, K_1	E16.0
17-32		Second unloading bulk modulus, K_2	E16.0
33-48		K_3	E16.0
49-64		K_4	E16.0
65-80		K_5	E16.0
1-16	Card 17	K_6	E16.0
17-32		K_7	E16.0
33-48		K_8	E16.0
49-64		K_9	E16.0
65-80		Tenth unloading bulk modulus, K_{10}	E16.0
1-16	Card 18	γ	E16.0
17-32		Initial internal energy per unit initial volume, E_0	E16.0
33-48		Initial relative volume, V_0	E16.0

Pressure is positive in compression, and volumetric strain ε_v is positive in tension. The tabulated compaction model is linear in internal energy. Pressure is defined by

$$p = C(\varepsilon_v) + \gamma T(\varepsilon_v)E \tag{235}$$

during loading (compression). Unloading occurs at a slope corresponding to the bulk modulus at the peak (most compressive) volumetric strain, as shown in Figure 12. Reloading follows the unloading path to the point where unloading began, and then continues on the loading path described by (235).

The volumetric strain is found from the relative volume V as

$$\varepsilon_v = ln(V). \tag{236}$$

The tabulated functions may contain from 2 to 10 points, and the model will extrapolate using the last two points to find the pressure if required.

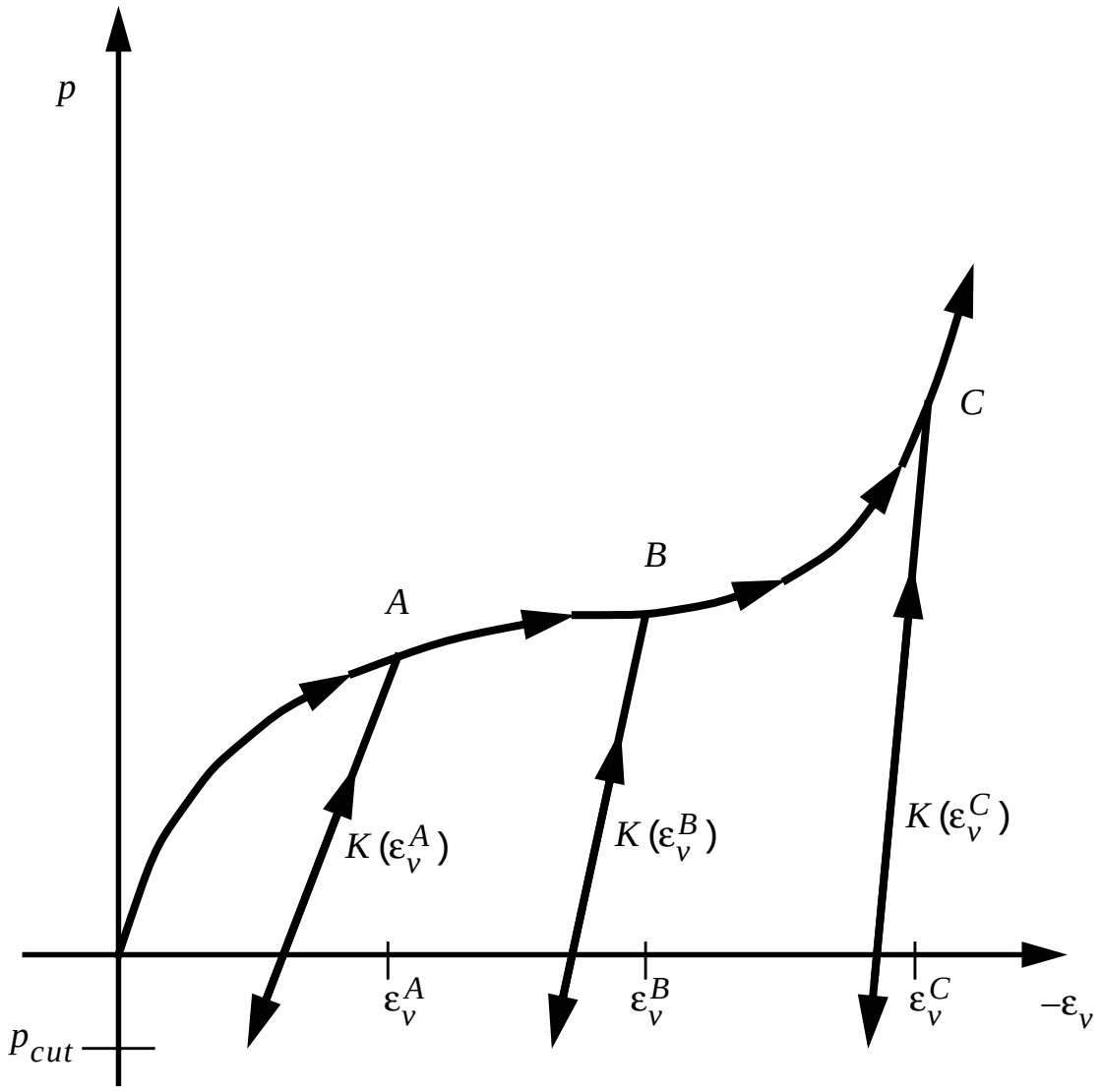

Figure 12

Pressure vs. volumetric strain curve for equation-of-state Form 8 with compaction. The unloading bulk modulus K depends on the peak volumetric strain. The tension limit p_{cut} is defined in the material model definition. Note p is positive in compression and ε_v is positive in tension.

Equation-of-State Form 9 (Tabulated)

Columns		Quantity	Format
1-16	Card 10	ε_{v1}	E16.0
17-32		ε_{v2}	E16.0
33-48		ε_{v3}	E16.0
49-64		ε_{v4}	E16.0
65-80		ε_{v5}	E16.0
1-16	Card 11	ε_{v6}	E16.0
17-32		ε_{v7}	E16.0
33-48		ε_{v8}	E16.0
49-64		ε_{v9}	E16.0
65-80		ε_{v10}	E16.0
1-16	Card 12	C_1	E16.0
17-32		C_2	E16.0
33-48		C_3	E16.0
49-64		C_4	E16.0
65-80		C_5	E16.0
1-16	Card 13	C_6	E16.0
17-32		C_7	E16.0
33-48		C_8	E16.0
49-64		C_9	E16.0
65-80		C_{10}	E16.0
1-16	Card 14	First temperature, T_1	E16.0
17-32		Second temperature, T_2	E16.0
33-48		T_3	E16.0
49-64		T_4	E16.0
65-80		T_5	E16.0

Columns		Quantity	Format
1-16	Card 15	T_6	E16.0
17-32		T_7	E16.0
33-48		T_8	E16.0
49-64		T_9	E16.0
65-80		Tenth temperature, T_{10}	E16.0
1-16	Card 16	γ	E16.0
17-32		Initial internal energy per unit initial volume, E_0	E16.0
33-48		Initial relative volume, V_0	E16.0

Pressure p is positive in compression, and volumetric strain ε_v is positive in tension. The tabulated compaction model is linear in internal energy. Pressure is defined by

$$p = C(\varepsilon_v) + \gamma T(\varepsilon_v) E \ , \tag{237}$$

where E is internal energy.

The volumetric strain is found from the relative volume V as

$$\varepsilon_v = ln(V) . \tag{238}$$

The tabulated functions may contain from 2 to 10 points, and the model will extrapolate to find the pressure if required.

Equation-of-State Form 10 (Propellant)

Columns		Quantity	Format
1-10	Card 10	Burn rate, β	E10.0
11-20		Pressure exponent, α	E10.0
21-30		Form factor, θ	E10.0
31-40		Ratio of specific heats, γ	E10.0
41-50		Solid density, ρ_s	E10.0
41-50		Web thickness, d_{web}	E10.0
1-10	Card 11	Flame temperature, T_f	E10.0
11-20		Gas molecular weight, M_c	E10.0
21-30		Gas constant, R	E10.0
31-40		Specific covolume, η	E10.0
41-50		Igniter mass fraction, f_{mi}	E10.0

Equation-of-State Form 11 (Pore Collapse)

Card 10

Columns	Quantity	Format
1-5	Number of Virgin Loading Curve points, NLD	15
6-10	Number of Completely Crushed Curve points, NCR	15
11-20	Excess Compression required before any pores can collapse, μ_1	E10.0
21-30	Excess Compression point where the Virgin Loading Curve and the Completely Crushed Curve intersect, μ_2	E10.0
31-40	Initial Internal Energy per unit initial volume, E_0	E10.0
41-50	Initial Excess Compression, μ_0	E10.0

Virgin Loading Curve Definition

Cards 11 thru NLD+10

Columns	Quantity	Format
1-15	Excess Compression, μ	E15.0
16-30	Corresponding pressure, p	E15.0

Continue on additional Virgin Loading Curve Definition Cards until all NLD pairs have been defined.

Completely Crushed Curve Definition

Cards NLD+11 thru NLD+NCR+10

Columns	Quantity	Format
1-15	Excess Compression, μ	E15.0
16-30	Corresponding pressure, p	E15.0

Continue on additional Completely Crushed Curve Definition cards until all NCR points have been defined.

The Pore Collapse equation-of-state is based on (Burton, 1982) and uses two curves: the virgin loading curve and the completely crushed curve, as shown in Figure 13. Two critical points are defined: the excess compression point required for pore collapse to begin (μ_1), and the excess compression point required to completely crush the material (μ_2). From this data and the maximum compression the material has attained (μ_{max}), the pressure for any excess compression μ can be determined. Unloading occurs along the virgin loading curve until the excess compression surpasses μ_1. After that, the unloading follows a path between the completely crushed curve and the virgin loading curve. Reloading will follow this curve back up to the virgin loading curve. Once the excess compression exceeds μ_2, then all unloading will follow the completely crushed curve.

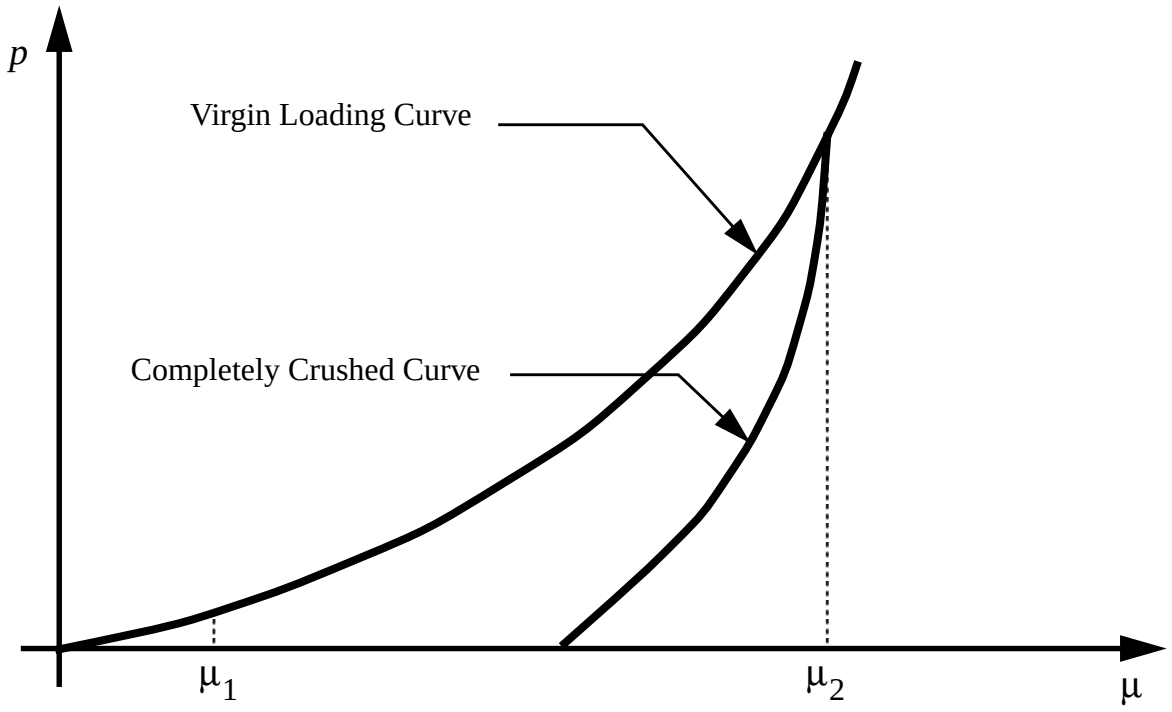

Figure 13
Pressure vs. excess compression for the Pore Collapse equation-of-state. The partially crushed curve lies between the Virgin Loading Curve and the Completely Crushed Curve.

For unloading between μ_1 and μ_2 a partially crushed curve is determined by the relationship:

$$p_{pc}(\mu) = p_{cc}\left[\frac{(1+\mu_B)(1+\mu)}{1+\mu_{max}} - 1\right], \quad (239)$$

where

$$\mu_B = p_{cc}^{-1}(p_{max}) \tag{240}$$

is the excess compression corresponding to a pressure of p_{max} on the completely crushed curve. In the above, subscript pc refers to the partially crushed state and subscript cc refers to the completely crushed state.

In terms of the relative volume V,

$$V = \frac{1}{1+\mu}, \tag{241}$$

$$p_{pc}(V) = p_{cc}\left(\frac{V_B}{V_{min}}V\right). \tag{242}$$

Thus, for a fixed $V_{min} = \frac{1}{\mu_{max}+1}$, the partially crushed curve will separate linearly from the completely crushed curve as V increases to account for pore recovery in the material.

The bulk modulus K is determined as one plus the excess compression times the slope of the current curve,

$$K = (1+\mu)\frac{\partial p}{\partial \mu}. \tag{243}$$

It then follows that the slope for the partially crushed curve is

$$\frac{\partial p}{\partial \mu} = \frac{(1+\mu_B)}{1+\mu_{max}}\frac{\partial p_{cc}}{\partial \mu}\left(\frac{(1+\mu_B)(1+\mu)}{(1+\mu_{max})}\right). \tag{244}$$

The bulk sound speed is determined from the slope of the completely crushed curve at the current pressure to avoid instabilities. The virgin loading and completely crushed curves are modeled with monotonic cubic splines. An optimal vectorized interpolation scheme is then used to evaluate the cubic splines as required during the solution. The bulk modulus and sound speed are derived from a linear interpolation on the derivatives of the cubic splines.

Equation-of-State Form 12 (Composite High Explosive)

Columns		Quantity	Format
1-10	Card 10	JWL coefficient for component 1 products, A_p (mbar)	E10.0
11-20		JWL coefficient for component 1 products, B_p (mbar)	E10.0
21-30		JWL exponent for component 1 products, R_{1p}	E10.0
31-40		JWL exponent for component 1 products, R_{2p}	E10.0
41-50		JWL constant for component 1 products, ω_p	E10.0
1-10	Card 11	JWL coefficient for component 1 explosive, A_e (mbar)	E10.0
11-20		JWL coefficient for component 1 explosive, B_e (mbar)	E10.0
21-30		JWL exponent for component 1 explosive, R_{1e}	E10.0
31-40		JWL exponent for component 2 explosive, R_{2e}	E10.0
41-50		JWL constant for component 1 explosive, ω_e	E10.0
1-10	Card 12	Ambient temperature, T_0 (deg. K)	E10.0
11-20		Viscosity, μ (mbar-microsec/cm^2)	E10.0
21-30		Thermal conductivity, λ (cal/cm microsec deg)	E10.0
31-40		Specific heat, c_p (cal/gm deg)	E10.0
41-50		Pore size (radius), r_0 (cm)	E10.0
51-60		ϕ	E10.0
1-10	Card 13	Activation energy, E_{ac} (cal/mole)	E10.0
11-20		Arrhenius prefactor, K_{0a} (microsec^{-1})	E10.0
21-30		Heat of reaction, Q_a (cal/gm)	E10.0
31-40		Energy of detonation, E_{qa} (mbar)	E10.0
41-50		ρ_a	E10.0
1-5	Card 14	Reaction growth type, IGT EQ.0: Default set to 1 EQ.1: Uses growth formula in (245)	I5
6-15		H_a	E10.0
16-25		X_a	E10.0
26-35		Y_a	E10.0

Columns	Quantity	Format
36-45	Z_a	E10.0
46-55	Mass fraction for explosive component 1, f_{m1} EQ.1.0: one component explosive, input completed LT.1.0: two component explosive; repeat Cards 10-14 for the explosive component two.	E10.0

This equation of state models the shock initiation and reaction growth of solid high explosives. The theoretical derivations and physical foundations for this model are discussed in (Nutt and Erickson, 1984) and (Nutt, 1987).

The initiation is based on viscoplastic heating in the reactant surrounding microscopic pores. The yield strength is compared with the applied stress. Pore collapse begins if the stress exceeds the strength. The rate of collapse is determined by the pressure and the viscosity. The resulting heating rate is calculated. The input for this phase of the calculation is supplied on Card 12. Sources for this data are handbooks, and porosimetry measurements. If the heating rate is greater than the heat conduction rate the local temperature in the neighborhood of the pores will rise until either the pressure is released, or the condition for runaway reaction is reached.

Card 13 supplies the data necessary to calculate critical conditions. The heat of reaction and energy of detonation are similar quantities but not identical because they are measured in different ways. The heat of reaction is tabulated in reports on criticality experiments such as the ODTX test. The heat of detonation is obtained from cylinder tests and is usually listed with equation of state data for the product gases.

At criticality, if $IGT = 1$, the reaction proceeds according to the formula

$$\frac{dF}{dt} = H(1-F)^y p^z \tag{245}$$

for the global chemical reaction rate. The input parameters controlling the reaction are supplied on Card 14. The appropriate values can be obtained from reactive flow Lagrange analysis, or by trial and error fit to whatever appropriate experimental data is available. The formula used for $IGT = 1$ is more or less traditional but has no reliable theoretical basis. Other growth formulas will become available as a user option as our understanding improves.

The equations of state are assumed to have a JWL form because of the widely available fits for many different explosives. The convenient analytic properties of JWL also make its choice appropriate. Hugoniot data for the reactant can be used to find fits to the JWL parameters when they are not already published.

The purpose of this model is to provide the basic physics of high explosive initiation and reaction growth, at least to the extent these processes are presently understood. The user should remember that explosives are generally heterogeneous materials while this model is base on a continuum mechanical description. Thus, there are certain small length scales within which it will not apply.

The input parameters may vary for different samples of the same type of explosive. Some experimentation may be necessary to get satisfactory results. Knowledge of the variability of each explosive will be useful as well as the nominal values for the parameters. It may be found for instance that one particular pore size may control initiation at a certain shock pressure while other pore sizes are required under different shock conditions. A knowledge of the pore size distribution will be very helpful under these conditions.

Where possible, the model is based upon specific physical processes so that the input parameters are related to definite physical quantities, with predictable effects on the results when they are varied. For example, increasing the heat conductivity results in delay between shock arrival and runaway reaction or it may prevent it altogether.

This model may be used for two component composite explosives. If the mass fraction f_{m1} on Card 14 is less than 1.0, DYNA2D will expect Card 14 to be followed by 5 more cards describing the second component in exactly the same way as in Cards 10 through 14. Thus, it will require 10 cards to model a two-component composite explosive.

The two reacting explosives decompose with independent reaction rates, but will remain in pressure equilibrium within each element. At present *it is assumed that the most sensitive component is described by the first five cards*. Once the first component starts reacting it will ignite the second component. One can therefore make Card 17 a duplicate of Card 12. The same goes for Cards 13 and 18 except the heat of detonation must have the appropriate value for the second explosive.

Equation-of-State Form 13 (Pressure vs. Time via Load Curve)

Columns	Quantity	Format
1-10	Load curve defining pressure as a function of time, LC	E10.0

This is a special purpose equation-of-state wherein the pressure in a material is specified *a priori* as a function of time. Thus, this is not a true equation-of-state in the traditional sense since the pressure in the material does not depend on its deformation history. This model has been found useful for simplified models of reacting fluids and in other special modeling circumstances.

Equation-of-State Form 14 (JWLB)

Columns		Quantity	Format
1-10	Card 10	A_1	E10.0
11-20		A_2	E10.0
21-30		A_3	E10.0
31-40		A_4	E10.0
41-50		A_5	E10.0
1-10	Card 11	R_1	E10.0
11-20		R_2	E10.0
21-30		R_3	E10.0
31-40		R_4	E10.0
41-50		R_5	E10.0
1-10	Card 12	$A_{\lambda 1}$	E10.0
11-20		$A_{\lambda 2}$	E10.0
21-30		$A_{\lambda 3}$	E10.0
31-40		$A_{\lambda 4}$	E10.0
41-50		$A_{\lambda 5}$	E10.0
1-10	Card 13	$B_{\lambda 1}$	E10.0
11-20		$B_{\lambda 2}$	E10.0
21-30		$B_{\lambda 3}$	E10.0
31-40		$B_{\lambda 4}$	E10.0
41-50		$B_{\lambda 5}$	E10.0
1-10	Card 14	$R_{\lambda 1}$	E10.0
11-20		$R_{\lambda 2}$	E10.0
21-30		$R_{\lambda 3}$	E10.0
31-40		$R_{\lambda 4}$	E10.0
41-50		$R_{\lambda 5}$	E10.0

Columns		Quantity	Format
1-10	Card 15	C	E10.0
11-20		ω	E10.0
21-30		Initial internal energy per unit initial volume, E_0	E10.0

This equation-of-state was recently developed by Baker (1991) and is further described in (Baker and Orosz, 1991). This equation of state was developed to adequately describe the high pressure regime produced by overdriven detonation while retaining the low pressure expansion behavior required for standard acceleration modeling. The derived form of the equation of state is based on the Jones-Wilkins-Lee (JWL) form due to its computational robustness and asymptotic approach to an ideal gas at high expansions. Additional exponential terms and a variable Gruneisen parameter have been added to adequately describe the high pressure region above the Chapman-Jouguet state. The resulting Jones-Wilkens-Lee-Baker (JWLB) equation of state is

$$p = \sum_{i=1}^{5} A_i\left[1 - \frac{\lambda}{R_i V}\right]e^{-R_i V} + \frac{\lambda E}{V} + C\left(1 - \frac{\lambda}{\omega}\right)V^{-(\omega+1)} \tag{246}$$

where

$$\lambda = \sum_{i=1}^{5} (A_{\lambda i} V + B_{\lambda i})e^{-R_{\lambda i} V} + \omega . \tag{247}$$

In the above, V is relative volume, E is energy per unit initial volume, and A_i, R_i, $A_{\lambda i}$, $B_{\lambda i}$, $R_{\lambda i}$, C, and ω are material constants.

Values for the material constants for octol 75/25 are given in (Baker and Orosz, 1991).

4.3 NODES

Cards 1,2,...,NUMNP

Columns	Quantity	Format
1-5	Node number, n	I5
6-10	Boundary condition code, BCC EQ.0.0: no constraint EQ.1.0: r-constraint EQ.2.0: z-constraint EQ.3.0: r and z constraints If BCC is not any of the above, it is assumed to be the angle in degrees between the positive r-axis and the direction of the motion along a sliding boundary (see Figure 14). The angle is measured in a counterclockwise direction.	F5.0
11-20	r or y-coordinate	E10.0
21-30	z-coordinate	E10.0
31-35	Generation interval KN EQ.0: default set to 1	I5

Node cards do not need to be in order. However, the first card must contain the first node, and the last card must contain the highest node number. Cards containing intermediate node numbers may be omitted (in this case, fewer than NUMNP nodes are specified) and their data is internally generated as follows. Node numbers are generated according to the sequence n^i, n^i + KN, n^i + 2KN,..., n^j where n^i and n^j are the nodal numbers defined on the two consecutive cards, and KN is taken from the first consecutive card. Linear interpolation is used to obtain the coordinate of the generated nodes and the nodal temperatures. The boundary condition code of generated data is set to zero whenever $BCC^i \neq BCC^j$; otherwise, it is assumed to be the same. Unconstrained nodes can be generated between constrained nodes that have the same boundary condition by making the code on the second card (node n^j) negative. After the data is generated the code is reset.

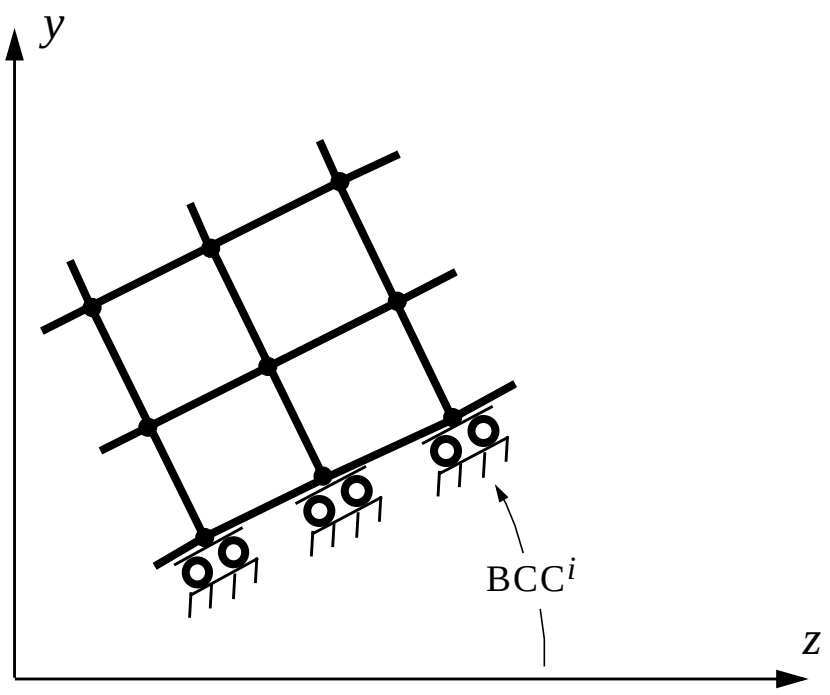

Figure 14
Roller boundary condition that is obtained if BCC^i is not equal to 0, 1, 2, or 3.

4.4 ELEMENTS

Define one card for each element.

Cards 1,2,...,NUMEL

Columns	Quantity	Format
1-5	Element number	I5
6-10	Node n_1	I5
11-15	Node n_2	I5
16-20	Node n_3	I5
21-25	Node n_4	I5
26-30	Material number, *MT* EQ.0: element is deleted	I5
31-35	Generation increment, KN	I5
36-45	Material dependent parameter: MT.EQ.2: angle Ψ in degrees MT.EQ.(8 or 9).and.IHE.EQ.1: input 1.0 if element is lit at time zero MT.EQ.(8 or 9).and.IHE.EQ.3: input lighting time for this element MT.EQ.(10, 11, 12, 15, 16, or 22): initial internal energy per unit radian (axisymmetric) or per unit thickness (plane strain) MT.EQ.(26): initial relative volume (default=1.0)	E10.0

Element cards must be in order. The first card must contain data for the first element and the last card must contain the data for the highest element number. Cards containing intermediate element data may be omitted (in this case, fewer than NUMEL sets of cards are specified), and these elements will be generated internally. Connecting node numbers n_j are generated with respect to the first card prior to omitted data by

$$n_j^{i+1} = n_j^i + \mathrm{KN} \tag{248}$$

Element attributes, such as material number, are taken from this first card. The convention for numbering nodes is shown in Figure 15, where n_1, n_2, n_3, and n_4 are global node numbers. Triangular elements are defined by replacing n_4 by n_3.

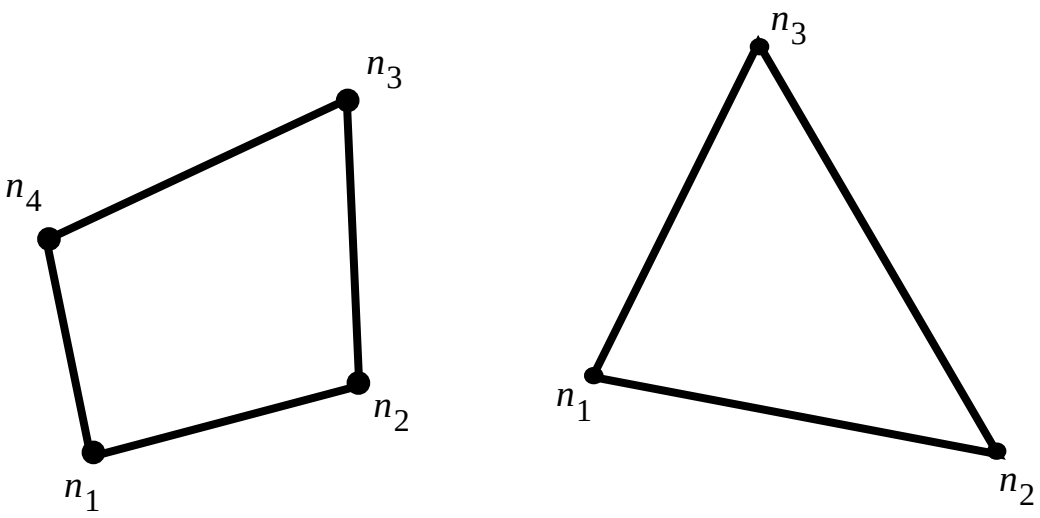

Figure 15
Two-dimensional plane strain and axisymmetric elements available in DYNA2D.

The angle Ψ for orthotropic materials (Material Type 2) is defined in section 4.2 on page 51. This option allows a unique material orientation to be defined for every element.

Note that the initial internal energy may be specified for all hydrodynamic material models except material types 8 and 9. If a nonzero initial internal energy is specified, it should be energy per unit radian for axisymmetric problems and energy per unit thickness for plane strain problems.

4.5 HIGH EXPLOSIVE PROGRAMMED BURN

Skip this section if *IHE* on Control Card 7 is not equal to 2. Four programmed burn options are available: the multiple point detonation, the line detonation, the Huygen detonation, and a layered explosives option.

Card 1

Columns	Quantity	Format
1-5	Programmed burn type, *IBTYP* EQ.0: multiple point detonation EQ.1: line detonation EQ.2: Huygens detonation EQ.3: Layered high explosives	I5
6-10	Number of detonation points, *NUMPTS* *IBTYP*.EQ.0: *NUMPTS* is the number of detonation points (nodes) *IBTYP*.EQ.1: *NUMPTS* is the number of points in detonation line *IBTYP*.EQ.2: *NUMPTS* is the number of detonation points *IBTYP*.EQ.3: *NUMPTS* is the number of layers of explosive	I5

For **point detonation**, $IBTYP = 0$

Repeat the following card *NUMPTS* times:

Cards 2, . . ., NUMPTS

Columns	Quantity	Format
1-5	Node number at detonation point	I5
6-15	Lighting time EQ.0.0: if $IBTYP = 1$	E10.0
16-20	Material number of HE to be lit EQ.0: The possibility of all HE elements being lit by this point is considered.	I5

For **line detonation**, $IBTYP = 1$:

Repeat the following card $NUMPTS$ times to input $NUMPTS$ nodes defining the detonation line. Note that at least two points are required, and that detonation lines always light at time zero.

Cards 2, . . . , NUMPTS

Columns	Quantity	Format
1-5	Node number defining detonation line	I5

For **Huygen's detonation**, $IBTYP = 2$:

Repeat the following set of cards $NUMPTS$ times to input $NUMPTS$ detonation points for Hugyens burn.

Card 2

Columns	Quantity	Format
1-5	Node number at detonation point	I5
6-15	Lighting time for this node	E10.0
16-20	Material number of HE to be lit EQ.0: The possibility of all HE elements being lit by this point is considered.	I5
21-30	Detonation velocity outside shadowed HE, D_{us}	E10.0
31-40	Detonation velocity inside shadowed HE, D_s	E10.0

Card 3

Columns	Quantity	Format
1-5	Number of nodes defining shadow boundary, *NPSS*	I5

Repeat the following card *NPSS* times to define a shadow boundary by *NPSS* nodes.

Cards 4, . . . , 3+NPSS

Columns	Quantity	Format
1-5	Shadow surface point number	I5
6-10	Node number	I5

For **layered explosives**, *IBTYP* = 3:

Input the following set of cards.

Card 2

Columns	Quantity	Format
1-5	Maximum number of points in any detonation line, *MAXPTS*	I5

Repeat the following set of cards *NUMPTS* times to input *NUMPTS* detonation lines for layered explosives.

Card 3

Columns	Quantity	Format
1-5	Number of nodes defining this detonation line, $LPTS$ .EQ.1: point detonation in this layer .GT.1: line detonation in this layer	I5
6-10	Material number lit by this detonation line (required)	I5
11-20	Detonation time for this line	E10.0

Repeat the following card $LPTS$ times to define this detonation point or line.

Cards 4, . . . , LPTS+3

Columns	Quantity	Format
1-5	Detonation line point number	I5
6-10	Node number defining detonation line or point	I5

Explosive materials in DYNA2D are defined by Material Type 8 (see section 4.2 on page 51) along with an appropriate equation of state. During DYNA2D initialization, the lighting time of each element is computed using the selected programmed burn algorithm.

Point detonation is illustrated in Figure 16. The lighting time t_L for an element is computed based on the distance from the center of the element to the nearest detonation point l_d, the detonation velocity D, and the lighting time of that detonation point t_{det}, using

$$t_L = t_{det} + \frac{l_d}{D}. \tag{249}$$

The use of line detonation is illustrated in Figure 17. A line detonation must be defined by at least two points, and nodes that define a detonation line must be given in the order in which they appear as one moves along the line. The lighting time t_L of each element is computed based on the distance from the centroid of the element to the nearest point on the detonation line, l_L, the detonation velocity D, using

$$t_L = \frac{l_L}{D}. \tag{250}$$

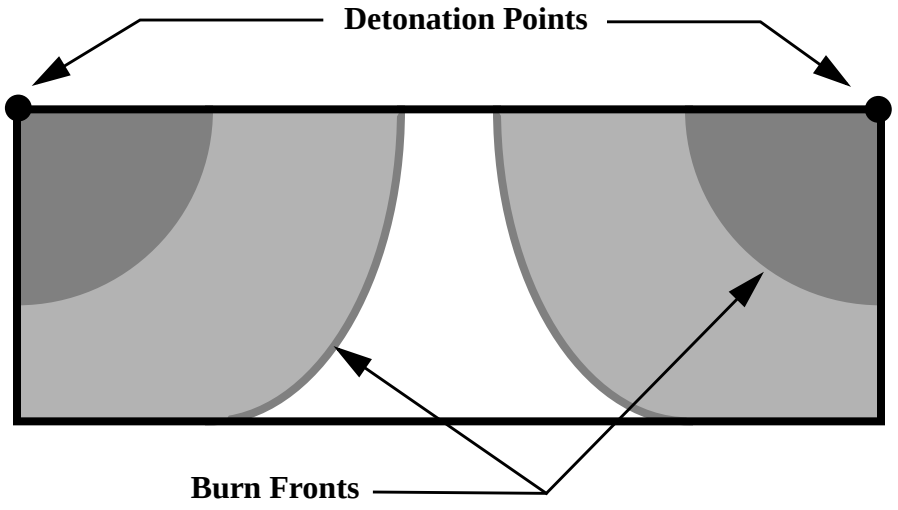

Figure 16
Point detonation (IBTYP=0) for high explosive burn.

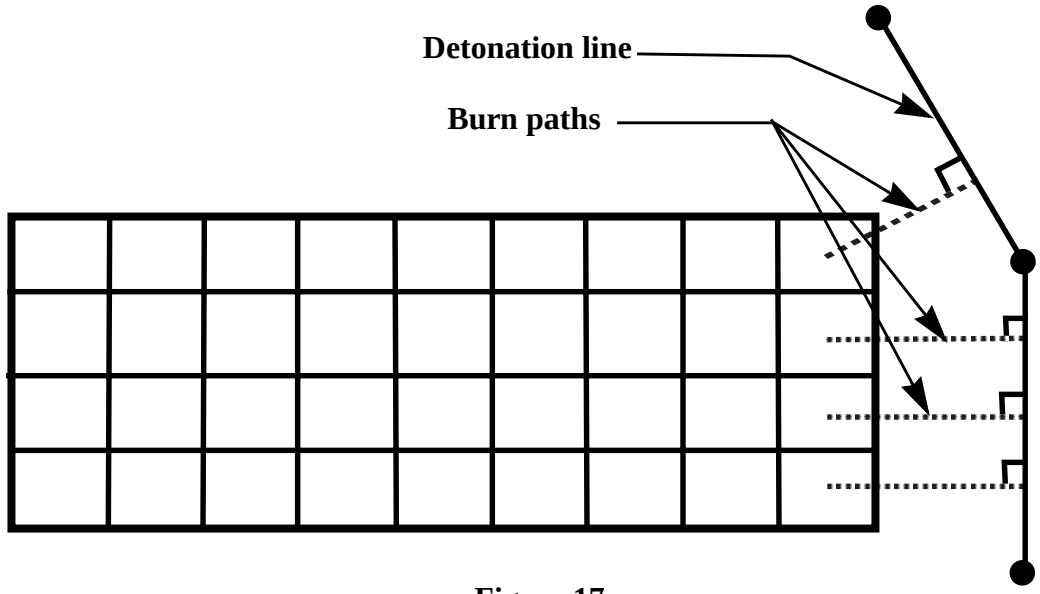

Figure 17
Lighting time computation for line detonation (IBTYP=1) of high explosive.

The use of Huygens detonation is illustrated in Figure 18. In a Huygens detonation, a shadow boundary must be given for each detonation point. The first point on the shadow boundary must be closest to the detonation point or the detonation point itself. The shadow boundary points must be

defined in the order in which they are encountered as one moves along the boundary with the explosive material on the left. Omitted data are automatically generated by incrementing the node numbers by:

$$\frac{(n_i - n_j)}{(sn_i - sn_j)} \tag{251}$$

where sn_i, sn_j are the shadow point numbers on two successive cards and n_i and n_j are their corresponding node numbers.

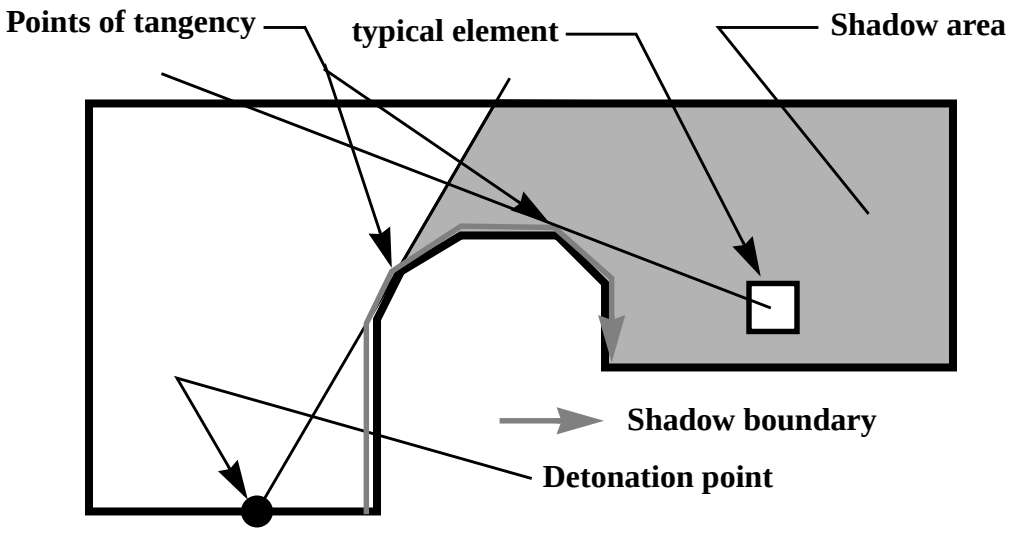

Figure 18
Definition of shadow boundary for Huygen's burn option.

As shown in Figure 19, the Huygen's burn option calculates an element's lighting time by assuming a detonation wave path from the initial lighting point to the first point of tangency of a line drawn from the detonation point to the shadow boundary. The path then follows the shadow boundary until it reaches the point of tangency of a line drawn from the target element to the shadow boundary. From this second tangent point, the burn path is assumed to follow a straight line to the target element. The ''shadow area'' is defined as the region which cannot be reached by a straight line from the detonation point without going outside the region. The element lighting time is computed by

$$t_L = t_{det} + \frac{l_{us}}{D_{us}} + \frac{l_s}{D_s}, \tag{252}$$

where t_L is the lighting time of the target element, t_{det} is the lighting time of the detonation point, l_{us} is the path length in the unshadowed region, D_{us} is the detonation wave velocity in the unshadowed region, l_s is the path length in the shadowed region, and D_s is the detonation wave velocity in the shadowed region.

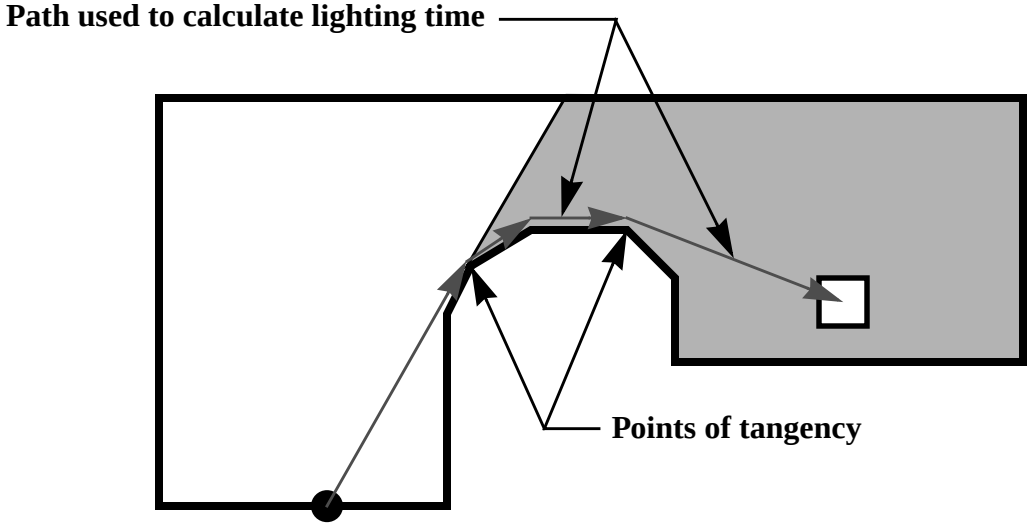

Figure 19
Lighting time computation for Huygens burn option.

The lighting time calculation for the Layered Explosive option is shown in Figure 20 for cases involving either a line detonation or a point detonation within each layer. Each layer is composed of a different material, and therefore may have a different detonation wave velocity. The lighting time for an element in a layer is computed as the sum of the burn time from the detonation point or line in that layer to the element centroid, plus the sum of the burn times from the first layer to the current layer. The burn paths are depicted by gray arrows in Figure 20. For the burn path beginning in layer j, the detonation velocity is d_j (i.e., detonation velocities for a burn path are based on the material in which that burn path *begins*). Clearly, each layer must contain at least one detonation point or line, and detonation points and lines may be arbitrarily mixed within different layers of the same problem.

A good reference for the numerical modeling of explosives is found in (Mader, 1979), and an introductory theoretical review is given in (Fickett, 1985).

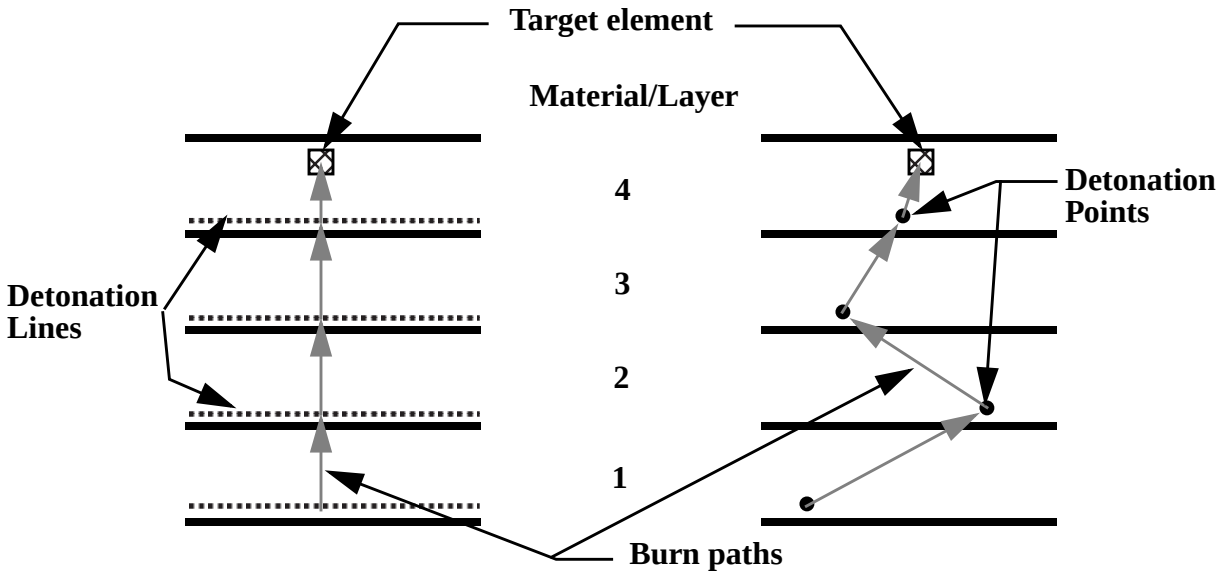

Figure 20
Lighting time calculation for layered explosives.

4.6 NODE TIME HISTORY BLOCKS

Skip this section if the number of node time history blocks is zero on Control Card 6 of section 4.1 on page 37. Otherwise, input the number of cards required to define node time history blocks with eight blocks per card. There is no limit to the number of time history blocks or the total number of nodes.

Columns	Quantity	Format
1-5	First node of first time history block	I5
6-10	Last node of first time history block	I5
11-15	First node of second time history block	I5
16-20	Last node of second time history block	I5
.	.	.
.	.	.
.	.	.
.	.	.

Node time history blocks are used to define sets of nodes for inclusion in the time history plot database. Typically, the time interval between writes to this time history plot database is much smaller than the time interval between writes to the state plot database, which contains information for the complete analysis model at each plot time point (state). Thus, for the nodes included in the time history plot database, much higher frequency resolution is possible in post-processing time history plots than is available in time history plots made from the state plot database. The plot databases are described in more detail in section 3.8 on page 34.

The time history plot database may be post-processed using ORION to generate time-history plots of nodal quantities such as displacement, velocity, or acceleration.

4.7 ELEMENT TIME HISTORY BLOCKS

Skip this section if the number of element time history block is zero on Control Card 6 of section 4.1 on page 37. Otherwise, input the number of cards required to define element time history blocks with eight blocks per card. There is no limit to the number of element time history blocks or the total number of elements.

Columns	Quantity	Format
1-5	First element of first time history block	I5
6-10	Last element of first time history block	I5
11-15	First element of second time history block	I5
16-20	Last element of second time history block	I5
.	.	.
.	.	.
.	.	.

Element time history blocks are used to define sets of elements for inclusion in the time history plot database. The time history plot database is typically written at a much smaller time increment than the state database, and therefore contains more high frequency response information. The plot databases are described in more detail in section 3.8 on page 34.

The time history plot database may be post-processed using ORION to generate time-history plots of element quantities such as stress or strain.

4.8 LOAD CURVES

Define the number of load curves specified on Control Card 2 in section 4.1 on page 37. Repeat the following card set for each load curve.

Card 1

Columns	Quantity	Format
1-5	Load curve number	I5
6-10	Number of points in this load curve, $NPTS$	I5
11-20	Scale factor on time points, $TSCL$ (default=1.0)	E10.0
21-30	Scale factor on function values, $FSCL$ (default=1.0)	E10.0
31-35	Load curve option, $LCOPT$ EQ.0: load curve used in transient dynamic analysis only EQ.1: load curve used in dynamic relaxation solution but not in transient dynamic analysis EQ.2: load curve used in both dynamic relaxation solution and transient analysis. Separate portions of the curve may be optionally specified for the dynamic relaxation solution and transient dynamic analysis.	I5

Cards 2, . . . ,NPTS+1

Columns	Quantity	Format
1-10	Time, t, or independent variable, x	E10.0
11-20	Load value, $f(t)$, or function value, $f(x)$	E10.0

Various options in DYNA2D use load curves to define arbitrary functional relationships. Many loads and boundary conditions are functions of time, and for these options, the specified load curve should relate load (or boundary condition) value $f(t)$ to time t. Some material models require the specification of load curves defining the variation of material parameters $f(x)$ with temperature x. Other models require the specification of load curves defining effective stress $f(x)$ as a function of effective plastic strain or other material variable, x.

If $TSCL$ is input as nonzero, then all time (or independent variable) values are replaced by $TSCL*t$ (or $TSCL*x$). Similarly, if $FSCL$ is input as nonzero, then all load values (or function values) are replaced by $FSCL*f(t)$ (or $FSCL*f(x)$). These scale factors are useful for avoiding redefinition of a large number of points in a load curve if some minor change in units is desired, for example.

Load curve option 2 permits either: 1) a single load curve to be specified and used for both the dynamic relaxation solution and transient analysis, or 2) two distant load curve regimes, combined and referenced by a single load curve number, to be specified. In the later case, the first regime is used only during the dynamic relaxation solution while the second regime is used only during the transient analysis. This option is extremely useful when initializing loads that can be only specified with one load curve number.

Based upon the t and $f(t)$ or x and $f(x)$ pairs entered, DYNA2D automatically determines if one or two load curve regimes are being defined for load curve option 2. The single load curve is defined by entering all the t and $f(t)$ or x and $f(x)$ pairs in ascending t or x order. The dual load curve is defined by entering all the t and $f(t)$ or x and $f(x)$ pairs for the dynamic relaxation regime first followed by all the t and $f(t)$ or x and $f(x)$ pairs for the transient analysis regime. All t or x values must be listed in ascending order, and the last t or x value in the dynamic relaxation curve must be larger than the first t or x value in the transient analysis curve. The number of points in the load curve is the total number of points used in both regimes.

There is no limit on the number of load curves, or on the number of points in a load curve definition.

DYNAMIC RELAXATION STATIC ANALYSIS

DYNA2D contains a limited capability for performing quasistatic analysis using a dynamic relaxation algorithm. This feature is primarily intended to be used to generate a static stress solution as an initial condition for a transient dynamic analysis, but it has been applied with some success to the solution of more general static problems.

During the DR static solution process, ‘‘time’’ is really just a parameter to describe the solution process, and does not correspond to physical time.The current implementation uses a DR time step equal to the standard dynamic time step. Thus, if it is desired to slowly apply the static loads to minimize overshoot in the solution, then a short trial dynamic run can be made to determine the

time step size. The static loads to be applied during the DR solution can then be applied over some number of time steps (typically 5000-10,000 but problem dependent), and this determines the time points to be used on the load curve controlling the static loads.

The current implementation of DR in DYNA2D is susceptable to dynamic overshoot if static loads are applied too quickly. If only history-independent material models (such as elasticity) are used, then the resulting solution will still be correct and this overshoot behavior is of little consequence. If history-dependent material models (such as plasticity) are used, however, this dynamic overshoot can cause yielding which is erroneous, and therefore an incorrect static solution is obtained. Thus, the DR static solution capability can be used with confidence for elastic initialization, but must be carefully used with slowly applied loads to prevent overshoot and inaccuracy in history-dependent static problems.

A DR static solution is activated by specifying the “load curve option” $LCOPT = 1$ for a load curve to control the application of the static loads. The dynamic relaxation factor, the DR time step, and the DR convergence tolerance can be modified from default values in the control cards..

4.9 NODAL FORCES AND FOLLOWER FORCES

Define the number of concentrated nodal loads specified on Control Card 2 in section 4.1 on page 37.

Columns	Quantity	Format
1-5	Node number, m_1, on which this load acts	I5
6-10	Direction in which load acts EQ.1: and IFW.EQ.0: r or y-direction EQ.2: and IFW.EQ.0: z-direction EQ.*n*: and IFW.EQ.1: *n* is a node number that defines a line beginning at *m* and ending at *n*. The force is perpendicular to the line, and points to the right as one moves along the surface from *n* to *m*.	I5
11-15	Load curve number for force vs. time	I5
16-25	Load curve multiplier EQ.0.0: default set to 1.0	E10.0
26-30	Follower force flag, IFW EQ.0: concentrated force acts in either r- or z-direction EQ.1: follower force is defined	I5

For axisymmetric geometries, the force is defined per unit radian; in plane strain, per unit thickness.

Nodal loads and follower forces may be imposed as a prescribed function of time. The time variation is taken from a load curve, and may be arbitrarily scaled in the nodal load or follower force definition.

A follower force remains perpendicular to the line from node n to node m throughout the deformation.

4.10 PRESSURE AND SHEAR LOADS

Define the number of element pressure and shear cards specified on Control Card 2 in section 4.1 on page 37.

Columns	Quantity	Format
1-5	Card number EQ.0: the preceding card number is incremented by one	I5
6-10	Load curve number for pressure or shear vs. time EQ.0: Brode function is used to determine pressure time history EQ -1: HE function is used to determine pressure time history	I5
11-15	Node n_1	I5
16-20	Node n_2	I5
21-30	Multiplier of load curve at n_1 EQ.0.0: default set to 1.0	E10.0
31-40	Multiplier of load curve at n_2 EQ.0.0: default set to 1.0	E10.0
41-50	Arrival time of load on the surface	E10.0
51-55	Generation interval, KN EQ.0: default set to 1	I5
56-60	Loading type flag EQ.0: pressure EQ.1: shear	I5

Each card defines a segment (element side) on which a pressure or shear load (traction) is applied. Segments are specified by nodes n_1 and n_2 as shown in Figure 21. These nodes should be defined in counterclockwise order. Pressure and shear cards must be defined in sequence. Nodes n_j for omitted cards (in this case, fewer than NPSL cards are specified) are generated with respect to the first card prior to the omitted data as

$$n_j^{i+1} = n_j^i + \text{KN} \tag{253}$$

The start times and multipliers are taken from this first card. Equivalent nodal loads are calculated by numerically integrating the tractions along the surface. Traction loads are always evaluated in the current geometry.

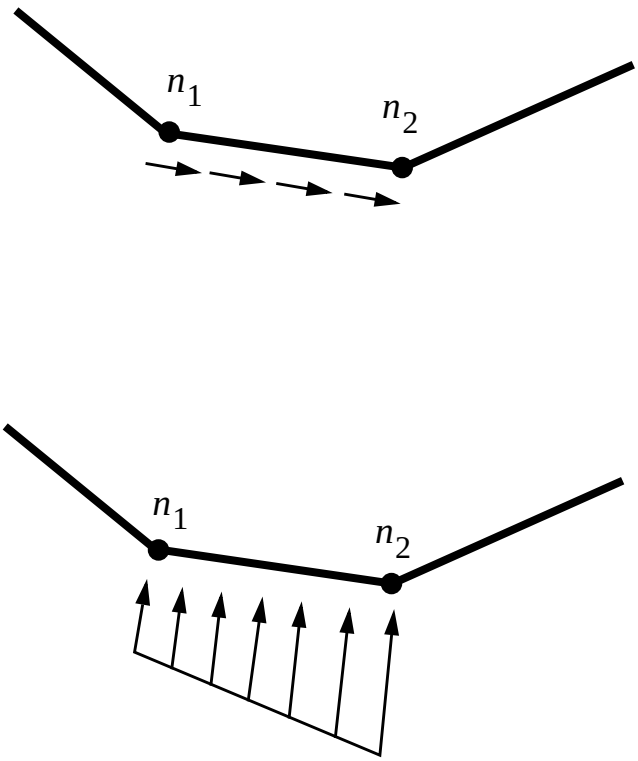

Figure 21
Definition of n_1 and n_2 for the application of traction boundary conditions.

If the load curve number is input as a negative value, then the pressure time history to be applied is computed from the Brode function data given in section 4.21 on page 208. The time-of-arrival of the pressure is then computed based on the distance from the Brode origin to the centroid of the element face receiving the pressure loading.

4.11 PRESCRIBED VELOCITIES

Define the number of cards specified on Control Card 2 in section 4.1 on page 37.

Columns	Quantity	Format
1-5	Node number to which this velocity is applied	I5
6-10	Load curve number for prescribed velocity vs. time	I5
11-15	Direction in which the prescribed velocity acts EQ.1.0: r or y-direction EQ.2.0: z-direction NE.1.0 and NE.2.0: the angle θ, in degrees, counterclockwise between the r-axis and the direction of the prescribed velocity vector	E5.0
16-25	Scale factor	E10.0

Nodal velocities may be imposed as a prescribed function of time. The time variation is taken from a load curve, and may be arbitrarily scaled in the prescribed velocity definition. This is convenient when many nodes have the same velocity or acceleration time history but different amplitudes, since only one load curve needs to be defined in that case. Nodal velocities may be specified with respect to the global axes, or in an arbitrary direction specified by an angle measured counter-clockwise from the r-axis.

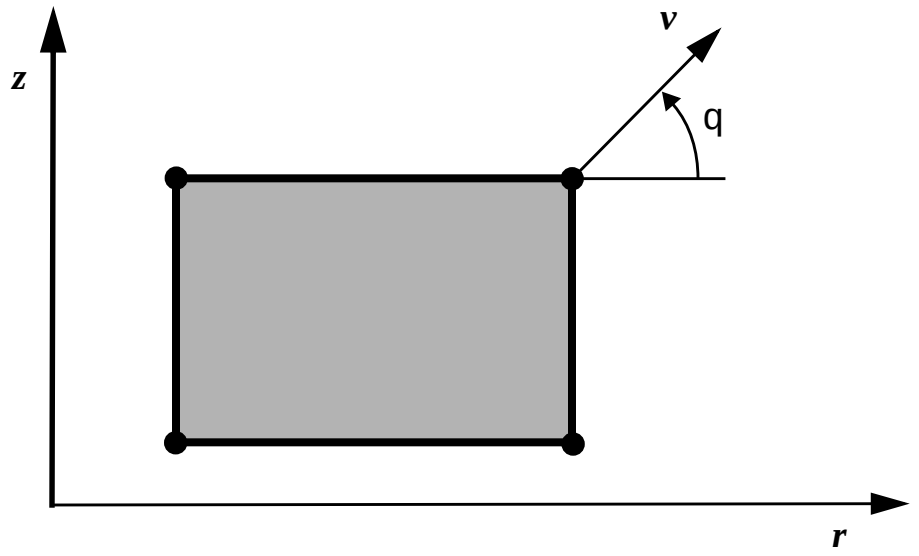

Figure 22
Prescribed velocities applied in an arbitrary direction.

It is not required that velocities be initially zero. However, if zero velocity initial conditions are specified in section 4.15 on page 194 and prescribed velocity load curves are not zero at $t = 0$, then a discontinuity in initial conditions is created, and this may excite very high frequency response in the model.

4.12 PRESCRIBED BASE ACCELERATIONS

Define nonzero base acceleration loads as specified on Control Card 2 in section 4.1 on page 37.

Y-Direction Base Acceleration

Define this card only if a nonzero y-direction base acceleration is specified on Control Card 3.

Columns	Quantity	Format
1-5	Load curve number giving time variation	I5
6-15	Scale factor on y-acceleration EQ.0.0: default set to "1.0"	E10.0

R-direction base acceleration loading is *only available for plane strain geometries*.

Z-Direction Base Acceleration

Define this card only if a nonzero z-direction base acceleration is specified on Control Card 3.

Columns	Quantity	Format
1-5	Load curve number giving time variation	I5
6-15	Scale factor on z-acceleration EQ.0.0: default set to "1.0"	E10.0

Translational base accelerations allow body force loads to be imposed on a structure. Conceptually, base acceleration may be thought of as accelerating the coordinate system in the direction specified, and thus the inertial loads acting on the model are of opposite sign. For example, if a cylinder were fixed to the $z = 0$ plane and extended in the positive z direction, then a positive z-direction base acceleration would tend to shorten the cylinder.

4.13 PRESCRIBED ANGULAR VELOCITIES

Define a nonzero angular velocity about the global z-axis as specified on Control Card 2 in section 4.1 on page 37.

Columns	Quantity	Format
1-5	Load curve number giving angular velocity vs. time	I5
6-15	Scale factor on angular velocity (default = 1.0)	E10.0

Note that this option applies to *axisymmetric geometries only.*

Body force loads due to the angular velocity are always calculated with respect to the deformed configuration, and act radially outward from the axis of rotation. Torsional effects arising from changes in angular velocity are not included. Angular velocity is assumed to have the units of radians per unit time.

The body force density $\boldsymbol{b}$ at a point P in the body is calculated from

$$\boldsymbol{b} = \rho(\omega \times \omega \times \boldsymbol{r}), \tag{254}$$

where ρ is the mass density, ω is the angular velocity, and $\boldsymbol{r}$ is a position vector from the origin to point P. Note that although the angular velocity may vary with time, the effects of angular acceleration are not included in this formulation.

This feature is useful for studying transient deformations of axisymmetric objects which are spinning about their axis of symmetry.

4.14 NODAL CONSTRAINTS

Define the number of nodal constraint sets specified on Control Card 7 in section 4.1 on page 37.

Card 1

Columns	Quantity	Format
1-5	Number of nodes that share degrees-of-freedom, N_c	I5
6-10	Degrees-of-freedom in common, *IDOF* EQ.1: r or y degree-of-freedom EQ.2: z degree-of-freedom EQ.3: r (or y) and z degrees-of-freedom	I5

Cards 2, . . .

Columns	Quantity	Format
1-5	Node number of first node to be tied	I5
6-10	Node number of second node to be tied	I5
11-15	Node number of third node to be tied	I5
.	.	.
.	.	.
.	.	.

Continue on additional cards in the same format until N_c nodes have been specified.

Nodal constraints allow sets of nodes to share a common degree-of-freedom. Any number of nodes may be included in a nodal constraint set.

4.15 NONREFLECTING BOUNDARIES

Define the number of nonreflecting boundaries specified on Control Card 3 in section 4.1 on page 37.

Card 1

Columns	Quantity	Format
1-5	Number of boundary nodes, *NBNS*	I5

Cards 2, . . . ,NBNS+1

Columns	Quantity	Format
1-5	Boundary point number EQ.0: increment last value by 1	I5
6-10	Node number	I5

A nonreflecting boundary must be defined by at least two points. Node numbers must be given in the order in which they appear as one moves along the boundary. Omitted data are automatically generated by incrementing the node numbers by:

$$\frac{(n_i - n_j)}{(bn_i - bn_j)} \tag{255}$$

where bn_i , bn_j are the boundary point numbers on two successive cards and n_i , n_j are their corresponding numbers.

Nonreflecting boundaries are used on the exterior boundaries of an analysis model of an infinite domain, such as a half-space, to prevent artificial stress wave reflections generated at the model boundaries from reentering the model and contaminating the results. Internally, DYNA2D

computes an impedance matching function for all nonreflecting boundary segments based on an assumption of *linear material behavior.* Thus, the finite element mesh should be constructed so that all significant nonlinear behavior is contained within the discrete analysis model.

4.16 INITIAL CONDITIONS

Cards 1, . . .

Define these cards if the initial condition flag is nonzero on Control Card 3 in section 4.1 on page 37.

Columns	Quantity	Format
1-5	Node number	I5
6-15	Initial velocity in r or y-direction	E10.0
16-25	Initial velocity in z-direction	E10.0
26-30	Node number increment, k EQ.0: default set to "1"	I5

Nodal velocity initial conditions are defined in this section. Initial velocities must be input for the first node, node 1, and the last node, $NUMNP$, if the initial condition flag on Control Card 3 is nonzero. Initial velocities for intermediate nodes may be input directly, or may be generated internally using a node number increment k. Linear interpolation between specified values is used to define initial velocities for omitted nodes.

If prescribed nodal velocities (section 4.11 on page 189) are also present in the model, care should be taken to ensure that the given initial velocity agrees with the prescribed nodal velocity at $t = 0$.

4.17 RIGID WALLS

Define the number of rigid walls specified on Control Card 3 in section 4.1 on page 37. Repeat the following set of cards for each rigid wall definition.

Card 1

Columns	Quantity	Format
1-5	Number of slave nodes	I5
6-15	r or y-coordinate of point P (must be on rigid wall) (see Figure 23)	E10.0
16-25	z-coordinate of point P	E10.0
26-35	r or y-coordinate of point Q	E10.0
36-45	z-coordinate of point Q	E10.0

Repeat the following cards for each definition:

Card 2, . . .

Columns	Quantity	Format
1-5	Slave number	I5
6-10	Node number	I5

Omitted slave nodes are automatically generated by incrementing the node numbers by

$$\frac{(n_i - n_j)}{(sn_i - sn_j)} \tag{256}$$

where sn_i and sn_j are slave numbers on two successive cards and n_i and n_j are their corresponding node numbers.

A rigid wall is a flat surface defined by a normal vector ***n***, which extends to infinity. The normal vector is defined from a point P on the surface of the rigid wall to a point Q in space, and must point towards the impacting body. The impacting body is defined by listing nodes which are not permitted to penetrate the rigid wall. Nodes which are *not* listed as slave nodes may penetrate the wall without resistance.

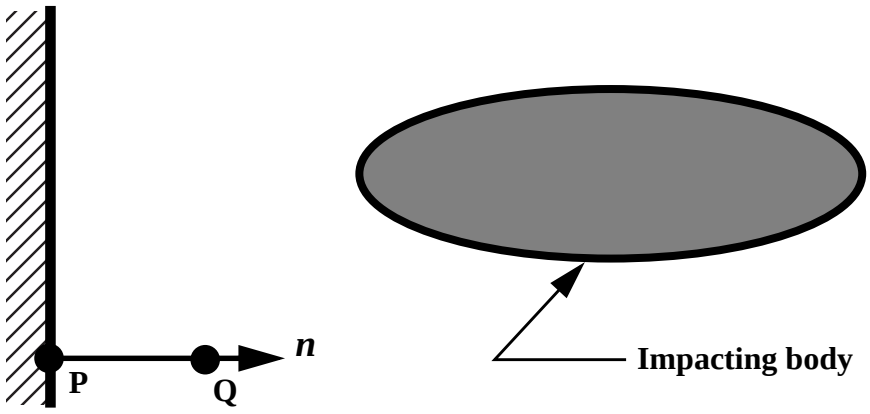

Figure 23
Definition of a rigid wall.

Rigid walls are an inexpensive method for modeling unilateral contact (i.e., contact between a deforming body and a rigid body) when the target surface is planar. The rigid wall feature eliminates the need to discretize the rigid surface and then define a slideline between the rigid surface and the impacting body.

4.18 SLIDING INTERFACE DEFINITIONS

Define *NUMSI* slidelines as specified on Control Card 4 in 4.1. Define all *NUMSI* Slideline Control Cards first, then define slave and master segment cards as needed.

Cards 1, . . . , NUMSI

Columns	Quantity	Format
1-5	Number of slave nodes in slideline, *NSN*	I5
6-10	Number of master nodes in slideline, *NMN*	I5
11-15	Slideline type number, *ISLT* EQ.1: sliding only EQ.2: tied EQ.3: sliding with separation and no friction EQ.4: sliding with separation and friction (penalty formulation) EQ.5: sliding with separation and no friction (penalty formulation) EQ.6: single surface contact (*NMN* = 0) (penalty formulation)	I5
16-25	Tolerance for determining initial gaps, *SLFAC* EQ.0.0: set to *SLFAC* = 0.001	E10.0
26-35	Angle in degrees of slideline extension at first master node, θ_1 EQ.0.0: extension remains tangent to first master segment	E10.0
36-45	Angle in degrees of slideline extension at last master node, θ_2 EQ.0.0: extension remains tangent to last master segment	E10.0
46-55	Scale factor on default penalty stiffness EQ.0.0: default set to 0.10	E10.0
56-60	Slideline extension bypass option EQ.1: slideline extensions are not used	I5

Slideline extensions apply only to the distributed parameter slidelines (*ISLT*.EQ.1, 2, or 3). Angles θ_1 and θ_2 are measured counterclockwise from the r-axis and remain constant (i.e., do not change during deformation). If θ_1 and θ_2 are zero, the extensions are made tangent to the first and last master segments and remain so throughout the calculation. The force exerted by a slave node lying on an extension of the master node at the origin of the extension diminishes to zero as the slave node moves away a distance equal to the length of one slave segment.

Define $NUMSI$ sets of slave nodes and master nodes as specified on the Slideline Control Cards described above. For each slideline, define first the slave nodes, then the master nodes. Repeat this pattern until slave nodes and master nodes are defined for all $NUMSI$ sliding interfaces.

SLAVE NODES

Card NUMSI+1

Define the slave surface using the following *slave node* cards.

Columns	Quantity	Format
1-72	Title card for slideline ($ISLT$.NE.4 only)	12A6
1-10	Static coefficient of friction, μ_s ($ISLT$.EQ.4 only)	E10.0
11-20	Dynamic coefficient of friction, μ_k ($ISLT$.EQ.4 only)	E10.0
21-30	Exponential friction decay constant, β ($ISLT$.EQ.4 only)	E10.0

Repeat the following card as necessary to define NSN slave nodes.

Cards NUMSI+2, . . . , NUMSI+NSN

Columns	Quantity	Format
1-5	Slave number	I5
6-10	Node number	I5

Omitted data are automatically generated by incrementing the node numbers by:

$$\frac{(n_i - n_j)}{(sn_i - sn_j)} \tag{257}$$

where sn_i, sn_j are the slave numbers on two successive cards and ni and nj are their corresponding numbers.

MASTER NODES

Repeat the following card to define NMN master nodes, except that no master nodes are defined for single surface contact ($ISLT = 6$).

Cards NUMSI+NSN+2,...,NUMSI+NSN+NMN

Columns	Quantity	Format
1-5	Master number	I5
6-10	Node number	I5

Sliding interfaces are described by defining one slave surface and one master surface. Each side of the slideline is then described as a list of nodes given in the order in which they appear as one moves along the surface. *The slave surface must be to the left of the master surface as one moves along the master surface, encountering the master nodes in the order they are defined.*

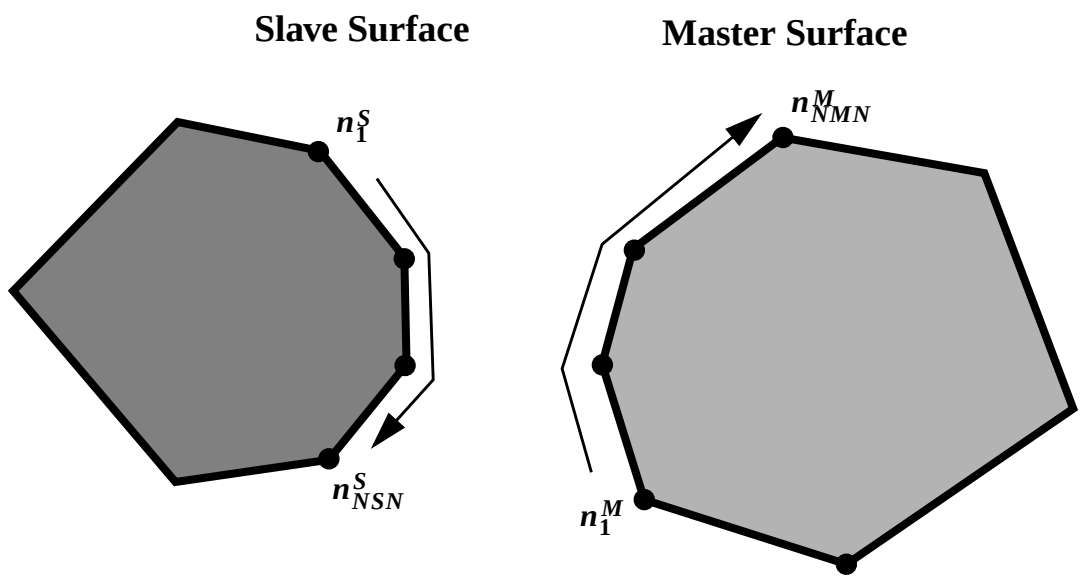

Figure 24
Definition of slideline slave and master surfaces.

SLIDING INTERFACE TYPES

The **sliding only** (type 1) slideline is a two-surface method based on a kinematic formulation. The two surfaces are allowed to slide arbitrarily large distances without friction, but are not permitted to separate or interpenetrate. Surfaces should be initially in contact when type 1 slidelines are used. This option performs well when extremely high interface pressures are present. The more coarsely meshed surface should be chosen as the master surface for best performance.

The **tied** (type 2) slideline is not really a slideline at all, but is a feature for joining two parts of a mesh with differing mesh refinement. This is also a kinematic formulation, so the more coarsely meshed surface should be chosen as the master surface.

The **sliding with separation** (type 3) slideline is a kinematic formulation without friction which permits the two surfaces to separate if tensile forces develop across the interface.

The **sliding with separation (penalty formulation)** (types 4 and 5) slidelines are the most generally applicable option. This implementation is a penalty formulation, so the designation of master and slave surfaces is not important. These slideline options allow two bodies to be either initially separate or in contact. Large relative motions are permitted, and friction is included in Slideline Type 4. Surfaces may separate and come together in a completely arbitrary fashion.

A rate-dependent Coulomb friction model is used in DYNA2D. The coefficient of friction is given by

$$\mu = \mu_k + (\mu_s - \mu_k)e^{-\beta v_{rel}}, \tag{258}$$

where μ_s and μ_k are the static and kinetic friction coefficients, β is a transition coefficient governing the rate of change from static friction to kinetic friction, and v_{rel} is the relative velocity between the two sliding surfaces. Note that if $\mu_k = 0$ and $\beta = 0$, then a rate-independent friction model is recovered with $\mu = \mu_s$.

The **single surface contact** (type 6) slide surface is a penalty formulation used for modeling two portions of the same body which may come into contact. This situation often arises in buckling problems, where one surface develops folds and comes into contact with itself. Frictional sliding is permitted between surfaces in contact. Due to the complexity of this algorithm, it is slightly more expensive than the other slide surface options, and therefore should only be used where necessary. Note that no master surface is defined for single surface contact.

Using Kinematic Formulation Slidelines

The kinematic slidelines in DYNA2D offer advantages over penalty method slidelines in some situations, but also are somewhat more complex to use. In the kinematic formulation, slave nodes are prevented from penetrating master segments, but master nodes may penetrate slave segments without resistance. Thus, when defining slidelines, it is advantageous to define the most finely meshed side as the slave side when kinematic slidelines are used.

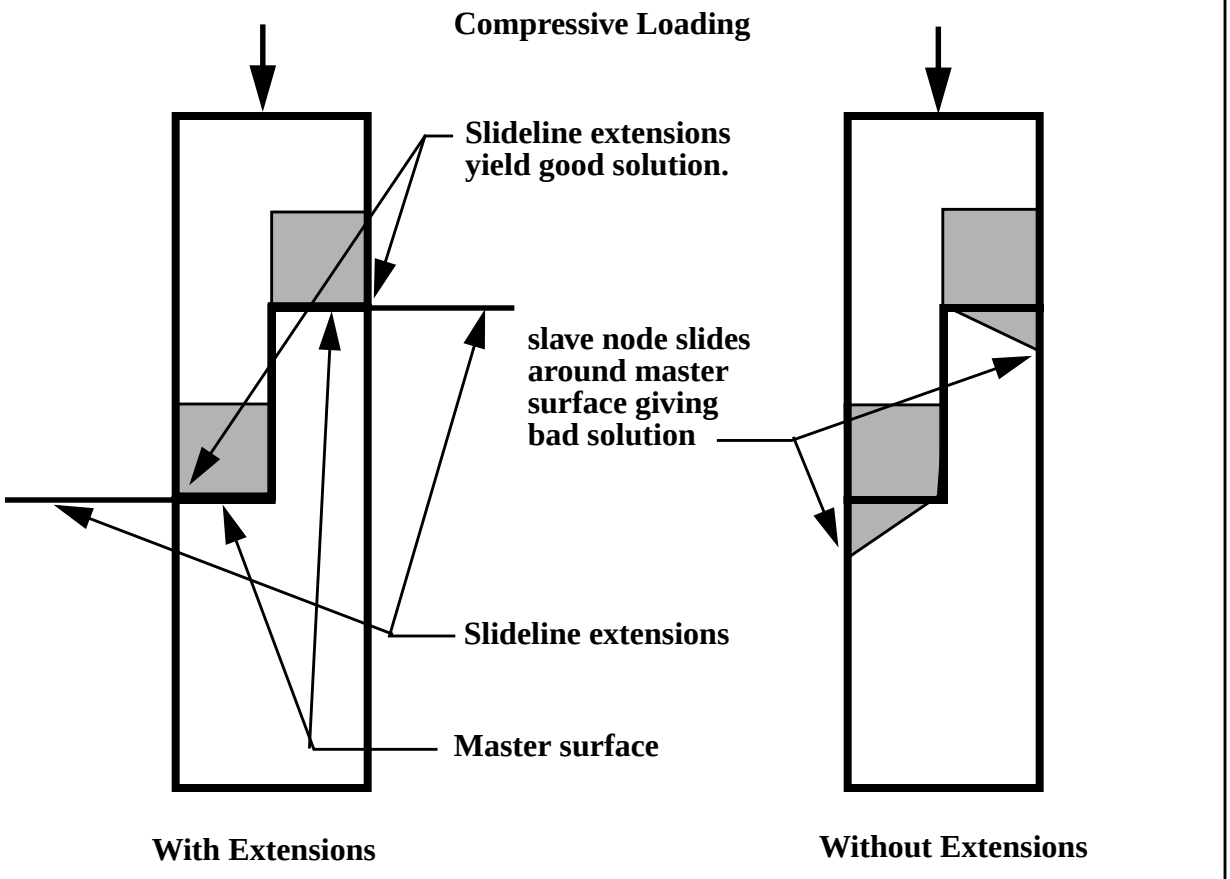

Figure 25
Example showing the use of slideline extensions for kinematic slidelines.

The lack of symmetry in the kinematic formulation also motivates the concept of “slideline extensions.” Slideline extensions are continuations of the master surface of the slideline, and by default are tangent (in the current deformed configuration) to the first and last segments in the master

slideline. These extensions may be oriented differently with respect to the ends of the master slideline by specifying orientation angles in the slideline definition. The force exerted by a slave node lying on an extension of the master slideline diminishes to zero as the slave node moves away a distance equal to the length of one slave segment. Simply described, slideline extensions help prevent slave nodes from “falling off” the edge of master surfaces which end on the edge of a body. An example is shown in Figure 25.

Another important concept unique to kinematic slidelines is the slideline intersection. Slideline intersections are described in section 4.19 on page 205.

4.19 SLIDELINE INTERSECTIONS

Define the number of slideline intersections *NUMSIN* as specified on Control Card 4 in section 4.1 on page 37.

Cards 1, . . . , NUMSIN

Columns	Quantity	Format
1-5	Number of slideline that is intersected	I5
6-10	Number of slideline that intersects the above line	I5

Whenever two slidelines cross such that one node is a slave node common to both slidelines and one node is a slave node to the first slideline and a master node to the second slideline, a slideline intersection should be defined. An example is shown in Figure 26. There must be one node which is a slave node common to both slidelines, and there must be one node which is a slave node to the first slideline and is a master node to the second slideline.

Slideline intersections should *only be defined between kinematic formulation slidelines*. Penalty formulation slidelines automatically account for slideline intersections.

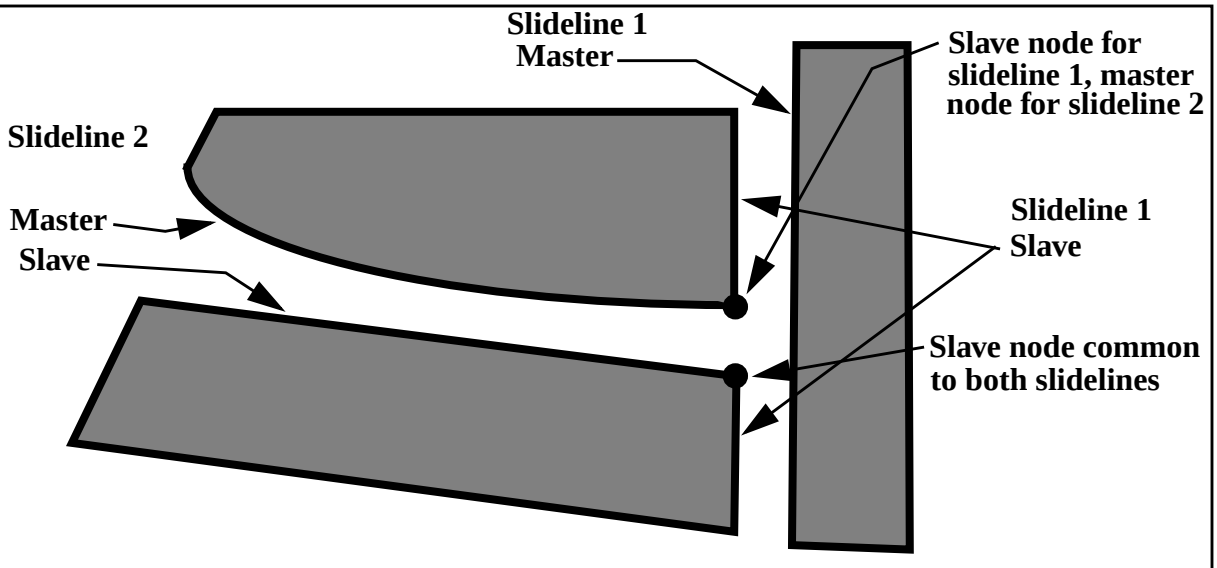

Figure 26
Slideline intersection should be defined for kinematic formulation slidelines.

4.20 GRAVITY STRESS INITIALIZATION

Skip this section if the number of points in the density versus depth curve is zero on Control Card 7 of section 4.1 on page 37. Otherwise, supply $NUMDP + 1$ cards.

Card 1

Columns	Quantity	Format
1-10	Gravitational acceleration	E10.0

Define $NUMDP$ cards giving the mass density as a function of depth.

Cards 2, 3, . . . , NUMDP+1

Columns	Quantity	Format
1-10	Mass density, ρ	E10.0
11-20	Depth (z-coordinate), d	E10.0

Density vs. depth curves are often used to initialize hydrostatic stresses arising in a material due to gravity acting on an overburden material. The hydrostatic pressure acting on a material point at a depth d_0 is given by

$$p = -\int_{d_0}^{d_{top}} \rho(z) g dz , \tag{259}$$

where p is pressure, d_{top} is depth at the top of the material to be initialized (usually $d_{top} = 0$), $\rho(z)$ is the mass density at depth z, and g is the acceleration of gravity. This integral is evaluated numerically for each material to be initialized.

Depth is measured along the global coordinate z-axis, and the sign convention of the global coordinate system should be respected. The sign convention of gravity also follows that of the global coordinate system. For example, if the positive z axis points “up,” then gravitational acceleration should be input as a negative number.

4.21 BRODE FUNCTIONS

Skip this section if columns 21-25 are blank on Control Card 7 in section 4.1 on page 37. Otherwise, enter two cards for the pertinent Brode function data.

Card 1

Columns	Quantity	Format
1-10	Yield (Ktons)	E10.0
11-20	Height of burst	E10.0
21-30	DYNA2D x-coordinate of Brode origin	E10.0
31-40	DYNA2D y-coordinate of Brode origin	E10.0
41-50	DYNA2D z-coordinate of Brode origin	E10.0
51-60	Initiation time for Brode function	E10.0
61-65	Optional load curve no. giving TOA shift vs. range, $LCTOA$	I5
66-70	Optional load curve no. giving yield vs. time for scaling calcs, $LCYLD$	I5

Card 2

Columns	Quantity	Format
1-10	Conversion factor - ft to DYNA length units	E10.0
11-20	Conversion factor - ms to DYNA time units	E10.0
21-30	Conversion factor - psi to DYNA pressure units	E10.0

The Brode functions are internally written in units of feet, milliseconds, and psi. Default conversion factors assume DYNA units are meters, seconds, Pascals. If other units are used in the DYNA2D model appropriate unit conversion factors should be supplied.

The development and limitations of the equations underlying this option are given in (Speicher and Brode, 1987).

4.22 DISCRETE SPRINGS, DAMPERS, AND MASSES

Define discrete springs, dampers, and masses in this section if $INPSD = 1$ on Control Card 2 in section 4.1 on page 37. Discrete element input follows the general organization of the entire DYNA2D input file: first a control card defines the number of discrete element materials, discrete elements, and lumped nodal masses. Next, each discrete element material is defined by a Discrete Element Material Control Card and a Discrete Element Material Data Card. Then, discrete elements are defined on Discrete Element Data Cards, and discrete masses are specified on Lumped Mass Data Cards.

First, define the Discrete Element Control Card:

Card 1

Columns	Quantity	Format
1-5	Number of material definitions for discrete elements, $NDMAT$	I5
6-10	Number of discrete springs and dampers (discrete elements), $NUMELD$	I5
11-15	Number of discrete masses, $NUMMAS$	I5

Next, for each of the $NDMAT$ discrete element materials, define the Discrete Element Material Control Card and the Discrete Element Material Data Card as described below.

The Discrete Element Material Control Card is defined as:

Cards 2, 4, 6, . . .

Columns	Quantity	Format
1-5	Discrete element material number ($\leq NDMAT$)	I5
6-10	Discrete element material type: EQ.1: linear elastic EQ.2: linear viscous EQ.3: isotropic elastoplastic EQ.4: nonlinear elastic EQ.5: nonlinear viscous	I5

The Discrete Element Material Data Card is defined as described below for each discrete element material type.

Cards 3, 5, 7, . . .

Discrete Element Material Type 1: (Linear Elastic)

Columns	Quantity	Format
1-10	Elastic stiffness (spring constant), k (force/displ.)	E10.0

Discrete Element Material Type 2: (Linear Viscous)

Columns	Quantity	Format
1-10	Damping constant (viscosity), c (force/velocity)	E10.0

Discrete Element Material Type 3: (Isotropic Elastoplastic)

Columns	Quantity	Format
1-10	Elastic stiffness, k (force/displ.)	E10.0
11-20	Tangent stiffness, k_T (force/displ.)	E10.0
21-30	Yield, F_Y (force)	E10.0

Discrete Element Material Type 4: (Nonlinear Elastic)

Columns	Quantity	Format
1-10	Load curve number giving force vs. displacement curve	E10.0

Element Material Type 5: (Nonlinear Viscous)

Columns	Quantity	Format
1-10	Load curve number giving force vs. velocity curve	E10.0

Define *NUMELD* Discrete Element Data Cards as specified on the Discrete Element Control Card.

Cards 2+2*NDMAT, . . . , 1+2*NDMAT+NUMELD

Columns	Quantity	Format
1-5	Discrete element number	I5
6-10	First node, n_1	I5
11-15	Second node, n_2	I5
16-20	Discrete element material number	I5
21-25	Generation increment, k	I5
26-35	Scale factor on computed force (default = 1.0)	E10.0

Define *NUMMAS* Lumped Mass Data Cards as specified on the Discrete Element Control Card.

Cards 2+2*NDMAT+NUMELD, . . . , 1+2*NDMAT+NUMELD+NUMMAS

Columns	Quantity	Format
1-5	Node number,	I5
6-15	Mass	E10.0

Lumped nodal masses are added to any existing mass at a node.

Discrete element forces are printed into the ‘‘hsp’’ file at the time history dump interval specified in columns 1-10 on Control Card 6.

Discrete elements (springs and dampers) and lumped nodal masses provide a convenient method for imposing prescribed force-displacement relationships between two nodes. These features may be used alone to allow DYNA2D to solve lumped parameter spring-mass-damper models, or may be used in combination with a finite element model to represent a complex system.

4.23 ALE (ARBITRARY LAGRANGIAN EULERIAN) MATERIALS

Repeat the following set of three cards *NALE* times to activate ALE for *NALE* materials as specified on Control Card 7 in section 4.1 on page 37. For each ALE material, first an ALE Control Card is defined to select the desired algorithms and options for that material. Next, two ALE Data Cards are defined to specify parameter values for the ALE algorithms. The basic assumption in DYNA2D ALE is that each element contains only one material, yielding a so-called ‘‘simple ALE’’ formulation. The applications of this option and other background works are discussed in section 2.14 on page 18.

Card 1

ALE Control Card

Columns	Quantity	Format
1-5	DYNA2D material number (*not* material type)	I5
6-10	Number of time steps between remap (default=1)	I5
11-15	Material advection type EQ.1: Donor cell EQ.2: Quadratic interpolation EQ.3: Modified quadratic interpolation (default)	I5
16-20	Velocity advection type EQ.1: Donor cell EQ.2: Quadratic interpolation EQ.3: Modified quadratic interpolation (default)	I5
21-25	Remap weighting function EQ.0: Volume (default) EQ.1: Area	I5
26-30	Boundary extrapolation option EQ.0: No extrapolation (default) EQ.1: Linear extrapolation	I5
31-35	Mesh relaxation at initialization EQ.0: No initial relaxation (default) EQ.1: Mesh is relaxed at initialization	I5
36-40	Unused at this time	I5

41-45	Number of merged materials (max of 16)	I5
46-50	Boundary relaxation flag EQ.0: Nodes on material boundary are not moved. (defalut) EQ.1: Nodes on material boundary are moved OR EZ does not know ?????????????????????????????????? EQ.1: Equal spacing EQ.2: Normal projection from interior EQ.3: R-constraint EQ.4: Z-constraint EQ.5: Equipotential (symmetric reflection) EQ.6: Equipotential (antisymmetric reflection) EQ.7: Proportional to interior	I5

Card 2

ALE Data Card 1

Columns	Quantity	Format
1-10	Stencil combination factor (default=0.0) EQ.0: Purely equipotential relaxation EQ.1: Purely serendipity stencil**** labeled as ‘bulk q switch’ ****	E10.0
11-20	Remap scaling factor (default=1.0)	E10.0
21-30	Angle criterion, degrees (default=80^o)	E10.0
31-40	Area criterion (default=0.95)	E10.0
41-50	ALE start time for this material	E10.0
51-60	ALE end time for this material	E10.0
61-70	Material death time	E10.0
71-80	Volume Limit (not currently implemented)	E10.0

Card 3

ALE Data Card 2

Columns	Quantity	Format

1-10	Minimum displacement increment for boundary node update	E10.0
11-20	Maximum allowable boundary node displacement increment	E10.0

Define the fourth card only if the number of merged materials is greater than zero.

Card 4

ALE Data Card 3

Columns	Quantity	Format
1-5	First merged material	I5
6-10	Second merged material	I5
.	.	.
.	.	.
.	.	.
76-80	Sixteenth merged material	I5

ALE is activated in DYNA2D on a material basis. For each ALE material, the above set of two cards define the desired algorithm and parameter value options. *Only the material number on the ALE Control Card is required; all other inputs may be specified as zero and thereby set to default values.* This ALE capability was originally developed by (Benson, 1986) but has received little use to date. The theoretical underpinnings of this work are described in (Benson, 1989). Development of this capability is continuing, and users are encouraged to experiment with nondefault parameters and report their experiences.

The following sections describe each of the ALE options and parameters.

Number of Time Steps Between Remaps

By default, the ALE remap is performed every time step. A cost reduction can be achieved by performing the remap only every five to ten time steps, but the effect on accuracy is highly variable. Some problems actually work better with remapping performed only every five time steps, while others exhibit severe accuracy degradation. Generally, the default is recommended as a starting point.

Advection Type

Advection is the actual remap phase of the automatic rezoning, or ALE, algorithm. It takes place after the nodes have been moved and before the next time step.

Three options are available for performing the advection operation: donor cell, quadratic, and modified quadratic. Donor cell advection assumes that all properties being remapped are constant over the element. This assumption is consistent with use of one-point integration in the element formulation, and yields a very stable advection method. Unfortunately, donor cell advection does tend to be quite dispersive and smooths out stress gradients more than the other methods. Quadratic advection uses a parabola fitted over three adjacent elements to interpolate remapped quantities. This method is formally second order accurate, but can be unstable, especially for problems with strong shocks. For example, a square stress pulse will eventually turn into an oscillating signal with this formulation. This method has been found to work reasonably well for problems that do not involve shocks, however. The modified-quadratic advection method uses quadratic interpolation whenever possible, but combines it with donor cell advection whenever the possibility of an instability is detected. This combination method retains most of the advantages of the other two methods while eliminating their weaknesses, and therefore should be used in almost all cases. Modified-quadratic advection is the default algorithm in DYNA2D.

Remap Weighting Function

Two remap weighting functions are available: volume weighting and area weighting. The volume weighting function defines the quantity of a transport variable as its density multiplied by the volume donated from one element to another. This volume approach is consistent with the physics of the problem and with the Bubnov-Galerkin finite element formulation used for plane strain problems in DYNA2D. The area weighting function defines the quantity of a transport variable as its density multiplied by the area fraction donated from one element to another. This area approach

is consistent with the Petrov-Galerkin finite element formulation used for axisymmetric problems in DYNA2D. Volume weighting is the default remap weighting function, and seems to work well for most problems.

Boundary Extrapolation Option

Interpolation error is often largest near the outer boundaries of a problem. This option is an experimental approach to improving the accuracy of interpolation near the boundaries. By default this option is not used, and it should only be activated for experimentation.

Initial Mesh Relaxation

This option smooths the mesh during initialization in DYNA2D. Although inactive by default, this option can be useful for difficult meshes or to improve meshes generated by an automatic meshing program.

Number of Merged Materials

This command activates necessary ALE features for the merged materials listed.

Boundary Relaxation Flag

This option controls nodal relaxation along all material boundaries associated with this definition. The individual options are described further detail in section 4.23 on page 213.

Stencil Combination Factor

Equipotential relaxation is used by default to smooth the mesh. Although this method is stable and quite reliable, it does tend to smooth out grading in the mesh. The serendipity stencil has less effect on mesh gradation, but can be unstable and invert an element during the smoothing process. The stencil combination factor allows a linear combination of equipotential relaxation and the serendipity stencil to be used in the actual smoothing process. Due to its instability, the serendipity stencil should never be used alone, and the stencil combination factor should always be less than 0.5.

Remap Scaling Factor

The remap scaling factor allows the user to scale back the distance a node would be moved by the chosen remap algorithm. The default value is 1.0, but this should be reduced if the serendipity stencil is used. A remap scaling factor greater than one is never recommended.

Remap Angle Criterion

If any of the element vertices surrounding a node forms an included angle less than the specified value, then that node will be moved during the remap phase. The default remap angle criterion is 60^o, but some results in some problems may be improved by reducing this value to 30^o or 45^o.

Remap Area Criterion

If the ratio of the minimum area to the maximum area of all elements connected to a node falls below the specified value, then that node will be moved during the remap phase. The default area criterion is 0.7.

Remap Start and End Time

These values determine the starting and ending time of ALE operations on the current material. The default start time is the beginning of the analysis, and the default end time is the termination time specified for the analysis.

Material Death Time

The material death time is a material deletion time, after which all elements and slidelines associated with the current material are deleted. By setting the number of time steps between remaps to a very large number and specifying a material death time, a material can be automatically deleted without any ALE operations taking place. This option may be used to delete high-explosive materials.

Volume Limit

This control feature is not currently implemented.

Minimum boundary Increment

The minimum boundary displacement increment specifies how much a node, in a boundary segment, must move before it is actually adjusted..

Maximum Boundary Increment

The maximum boundary displacement increment limits how much incremental displacment is permited for nodes in boundary segments. This option is useful in limiting movement of boundary nodes.

4.24 ALE BOUNDARY SEGMENTS

Repeat the following card *NABC* times to define *NABC* ALE boundary segments as specified on Control Card 7 in section 4.1 on page 37. The applications of this option and other background works are discussed in section 2.14 on page 18.

Card 1

ALE Boundary Segment Card

Columns	Quantity	Format
1-5	Beginning node number of boundary segment	I5
6-10	Ending node number of boundary segment	I5
11-15	Material number to which these nodes belong (**what if shared??**)	I5
16-20	Boundary relaxation type EQ.0: No relaxation (default) EQ.1: Equal spacing EQ.2: Normal projection from interior EQ.3: R-constraint EQ.4: Z-constraint EQ.5: Equipotential (symmetric reflection) EQ.6: Equipotential (antisymmetric reflection) EQ.7: Proportional to interior	I5

Nodal relaxation types can be specified for individual material boundary segments. This feature overides the boundary relaxation type prescribed in section 4.23 on page 213 (I thinkkk), and allows greater flexibilty, then the previous method, since the relexation type can uniquely defined for each material boundary segment. One boundary segment should be defined for each material side when relaxation is desired. Node numbers defining the boundary segment should be specified in a counterclockwise order.

Nodal movement along a boundary is conrolled by the boundary relaxation type. By default, all boundary nodes are initially assigned to be type 0.

4.25 AUTOMATIC CONTACT MATERIALS

Skip this section unless $IAUTO = 1$ on Control Card 4. Otherwise, define an automatic contact activity flag for all $NUMMAT$ materials in the model.

Columns	Quantity	Format
1-5	Material 1 automatic contact activity flag EQ.0: material is not active for automatic contact EQ.1: material is active for automatic contact	I5
6-10	Material 2 automatic contact activity flag	I5
.	.	.
.	.	.
.	.	.
76-80	Material 16 automatic contact activity flag	I5

Repeat the above 16I5 format on additional cards as needed to specify an activity flag for all $NUMMAT$ materials. Automatic contact is discussed in detail in section 2.12 on page 17.

5.0 RESTART INPUT FORMAT

The following sections describe the format of the DYNA2D restart input file. The procedure for initiating a DYNA2D restart analysis is described in section 3.5 on page 31.

The specification of a restart input file is optional when restarting an analysis which was terminated before the termination time specified in the initial input file. If no changes to the model or analysis parameters are desired, the restart may be initiated by omitting the restart input file and specifying only the restart dump file which contains the desired starting point data. DYNA2D will then resume execution and continue until the termination time specified in the original input file.

A restart input file is required when restarting a run which completed normally (to, for example, increase the termination time), or when changes to the model or analysis parameters are desired. A restart input file may be used to:

- change the termination time,
- change the time interval between writes of time history plot data,
- change the time interval between writes of state plot data,
- delete slidelines,
- delete materials,
- delete elements,
- reset the time step scale factor.

If a restart input file is used, it should be specified along with the appropriate restart dump file on the DYNA2D command line used to initiate the restart.

All changes made at a restart will be reflected in all subsequent restart dumps.

If a restart is made using a complete DYNA2D input file with the remesh option, the resulting familied files will be re-initialized (`D2PLOT01`, etc.) and a new sequence of files will be created. In all other cases, the familied files for the state plot database, time history database, and restart dump files will retain their original names (by default) and will continue with numbering according to the original sequence. This allows convenient plotting of the entire analysis results using only one family of plot database files.

5.1 TITLE CARD

Card 1

Columns	Quantity	Format
1-72	Heading or problem title	12A6

5.2 RESTART CONTROL

Card 2

Columns	Quantity	Format
1-10	New termination time EQ.0.0: termination time remains unchanged	E10.0
11-20	New time interval between writes of printout or time history plot data EQ.0.0: interval remains unchanged	E10.0
21-30	New time interval between writes of state plot data EQ.0.0: interval remains unchanged	E10.0
31-35	Number of load curves to be redefined	I5
36-40	Number of slidelines to be deleted	I5
41-45	Number of element blocks to be deleted	I5
46-50	Number of materials to be deleted	I5
51-55	Number of slidelines to be redefined	I5
56-60	Number of slideline intersections to be redefined	I5
61-65	Number of materials to be redefined	I5
66-70	Flag for resetting default viscosities, *IRQ* EQ.1.0: new defaults are specified for redefined materials	I5
71-80	New scale factor for computed time step size	E10.0

Note that slidelines and materials to be deleted are simply listed, but elements to be deleted are specified in blocks, or groups of elements. Groups are defined by giving the first and last numbers of a consecutive sequence of elements to be deleted.

5.3 LOAD CURVE REDEFINITIONS

Skip this section if there are no load curves to be redefined at restart. Otherwise, repeat the following set of cards for each load curve to be redefined.

Card 1

Columns	Quantity	Format
1-5	Load curve number to be redefined	I5

Card 2

Columns	Quantity	Format
1-10	Time, t, or independent variable, x	E10.0
11-20	Load value, $f(t)$, or function value, $f(x)$	E10.0

Note: the number of points in a load curve may not change from that specified in the original input.

5.4 DELETED SLIDELINES

Skip this section if there are no sliding interfaces to be deleted at restart.

Columns	Quantity	Format
1-5	Number of first slideline to be deleted	I5
6-10	Number of second slideline to be deleted	I5
.	.	.
.	.	.
.	.	.
.	.	.

Repeat this pattern on additional cards, using 16I5 format, until all deleted slidelines have been listed.

5.5 DELETED ELEMENT BLOCKS

Skip this section if there are no elements to be deleted at restart.

Columns	Quantity	Format
1-5	First element of first block to be deleted	I5
6-10	Last element of first block to be deleted	I5
11-15	First element of second block to be deleted	I5
16-20	Last element of second block to be deleted	I5
.	.	.
.	.	.
.	.	.
.	.	.

All elements with numbers between the first and last numbers of each block are deleted.

5.6 DELETED MATERIALS

Skip this section if there are no materials to be deleted at restart.

Columns	Quantity	Format
1-5	Material number of first material to be deleted	I5
6-10	Material number of second material to be deleted	I5
11-15	Material number of third material to be deleted	I5
.	.	.
.	.	.
.	.	.

When a material is deleted, all elements associated with that material are also deleted. There is no limit to the number of materials which may be deleted. Deleting materials is a way of deleting a group of elements which all share the same material number, and may be more convenient than listing the elements individually if the element numbers are not contiguous.

5.7 SLIDELINE REDEFINITIONS

Skip this section if there are no slidelines to be redefined at restart. Otherwise, the number of slidelines to be redefined must be the total number of slidelines remaining in the problem after restart. Thus, all remaining slidelines must be redefined whether or not their definitions are changed.

For the slidelines remaining in the problem, specify complete slideline input for the new definitions as described in section 4.18 on page 199. This approach allows great flexibility in changing slidelines as the problem evolves. In most cases, much of this slideline redefinition input can be copied from the original DYNA2D input file.

5.8 SLIDELINE INTERSECTION REDEFINITIONS

Skip this section if there are no slideline intersections to be redefined at restart. Otherwise, the number of slideline intersections to be redefined must be the total number of slideline intersections remaining in the problem after restart. Thus, all remaining slideline intersections must be redefined whether or not their definitions are changed.

For the slideline intersections remaining in the problem, specify complete input as defined in section 4.19 on page 205. In most cases, much of this slideline intersection redefinition input can be copied from the original DYNA2D input file.

5.9 DEFAULT VISCOSITY RESET

Skip this section unless the number of materials to be redefined was nonzero and the flag for resetting default viscosities, *IRQ*, was set to ‘‘1.0’’ on the Restart Control Card described in section 5.2 on page 225.

Columns	Quantity	Format
1-5	Hourglass control method EQ.0: default set to “1” EQ.1: standard DYNA2D EQ.2: rotational EQ.3: Flanagan-Belytschko EQ.4: Hancock EQ.4: Hancock	I5
6-15	Hourglass viscosity coefficient, QH (default = .1) IHQ.EQ.1: QH .15 IHQ.EQ.2: QH .20 IHQ.EQ.3: QH .40 IHQ.EQ.4: QH .40	E10.0
16-20	Bulk viscosity type, IBQ EQ.0: default set to “1” EQ.1: standard DYNA2D EQ.2: Richards-Wilkins	I5
21-30	Quadratic viscosity coefficients, Q1 (default = 1.5)	E10.0
31-40	Linear viscosity coefficient, Q2 (default = .06)	E10.0
41-45	Stress rate default reset EQ.0: DYNA2D default stress rate for this material EQ.1: Jaumann rate EQ.2: Green-Nagdi rate	I5

This option allows the user to reset the default values of the above parameters, and these new defaults will be used for each redefined material when no values for these parameters are specified on the Material Control Card. Any parameter value on the Material Control Card used to redefine a material will override the values set on this card.

5.10 RESTART MATERIAL REDEFINITIONS

Skip this section if the number of materials to be redefined is zero. Otherwise, for each material to be redefined, input one set of eight material cards in the format specified in section 4.2 on page 51.

This option can be used to change material parameters during restart. This option must be used with care to obtain physically meaningful results.

6.0 REZONING AND ANALYSIS DISPLAY

The following sections describe the DYNA2D commands used for interactive rezoning, automatic rezoning via a command file, analysis display, and generating MAZE line definitions for remeshing. Interactive rezoning is initiated by typing the `sw5.` sense switch control during program execution. The analyst is next prompted for a TMDS monitor or graphics device number. Commands can then be typed to study current results and rezone the mesh. Automatic rezoning command files should contain similar command sequences, except that the TMDS monitor or graphics device number *should not* be included in the rezone command file. Analysis display commands can be contained in a file or entered interactively as described in section 3.6 on page 32. Commands for creating line definitions for MAZE (for remeshing) should be entered interactively as described in section 3.7 on page 33.

6.1 LIST OF REZONING COMMANDS BY FUNCTION

Rezoning is performed by material. The following commands are useful, but do not in themselves rezone a material:

A, DEB, DMB, DSL, ELPLT, END, F, FR, FRAME, FSET, G, GRID, GSET, IP, MC, MD, MN, NDPLT, NOFRAME, NOGRID, PLOTS, PLTI, PRIT,R,SC, SD, SETF, SN, T, TERM, TR, TV, Z

Materials for which boundaries have been changed by the **SC**, **SD**, **MC**, and **MD** commands must still be rezoned. Commands for rezoning a material (may be used with above commands) are:

B, CN, M, S, TN, V

Commands that are available for adjusting boundary nodes following the **"B"** command are:

BD, BDS, ES, ESS, ER, ERS, EZ, EZS, SLN, SLNS, VS, VSS

The **"B"** command should be used only if a material has been designated for rezoning with the **"M"** command.

6.2 LIST OF ANALYSIS DISPLAY COMMANDS

The following commands are available for the analysis display option:

B, CONTOUR, F, FRINGE, FSET, FSON, G, GO, GRID, GS, GSET, IFD, IFN, IFP, IFS, IFVA, IFVS, LINE, M, MNON, MOLP, NCOL, NDLF, NLOC, NOFRAME, NSDF, NSSDF, NUMCON, O, PLDF, PRIN, PROFILE, RANGE, RPHA, RPVA, UZ, UZG, V, VECTOR, VS, Z.

The command sequence must be terminated by the "**f**" command. The picture generated by the last display command will remain in the graphics window until the display is again refreshed.

6.3 LIST OF COMMANDS FOR REMESHING GEOMETRY DEFINITION

When remeshing an analysis model the definition of the geometry for the new mesh must be consistent with that of the old mesh. This consistency is achieved by defining the boundary of new mesh materials with MAZE using line definitions created while in the DYNA2D rezoner with the old mesh (for a complete description of this process see section 3.7 on page 33). The **LD** and **LDS** commands are used to generate line definitions, and these definitions are written to the MAZE line definition file (specified by **m**=*mlf* on the DYNA2D command line).

The following commands must be preceded by the M and B commands within the rezoner.

LD *n k l*	Generate line definition n for MAZE that consists of boundary from nodes *k* to *l*
LDS *n l*	Generate line definition *n* for MAZE that consists of side *l*

6.4 COMMAND DEFINITIONS

HELP	Enter HELP package and display all available commands. Description of each command is available in the HELP package.
HELP/*commandname*	Do not enter HELP package but print out the description on the terminal of the command following the slash
PHP *ans*	Print help package - If *ans* equals 'y' the package is printed in the high speed printer file.
TV *n*	Use TMDS with monitor number *n*.
TV -n_1 n_2 n_3	Use color TMDS with monitor numbers n_1, n_2, and n_3 for the red, green, and blue channels, respectively. (LLNL only)
T or **END**	Terminate.

F	Terminate interactive phase, remap, continue in execution phase.
FR	Terminate interactive phase, remap, write restart dump, and call exit.
Z *r z* ΔL	Zoom in at point (*r,z*) with window ΔL
UZ *a b* ΔL	Zoom in at point (*a,b*) with window ΔL where *a*, *b*, and ΔL are numbers between 0 and 1. The picture is assumed to lie in a unit square.
UZG	Cover currently displayed picture with a 10 by 10 square grid to aid in zooming with the unity zoom, **"UZ**," command.
FIX	Set TMDS picture to its current window. This window is set until it is reset by the **"GSET**," "**FSET**," or "**SETF**" commands or released by the **"UNFIX**" command.
UNFIX	Release current TMDS window set by the **"FIX**," "**GSET**," **"FSET**" or "**SETF**" commands.
GSET *r z* ΔL	Center TMDS pictures at point (*r,z*) with square window of width ΔL. This window is set until it is reset or the "**UNFIX**" command is typed.
FSET *n* Δr Δz	Center TMDS pictures at node *n* with a rectangular Δr x Δz window. This window is set until it is reset with or the **"UNFIX**" command is typed.
SETF *r z* Δr Δz	Center TMDS pictures at point (*r,z*) with a rectangular Δr x Δz window. This window is set until it is reset or the **"UNFIX**" command is typed.
FR80 *filmtype*	Select FR80 camera. FR80 default filmtype is FICHE48. Other options include: FICH48D, FICHE24, FICH24D, 35mm, COLOR35, DICO35, P16mm, COLOR16, DICO16, CSLIDE35, HARDCOPY, REPORT, VUGRAPH, and VUGRAF11. This command, if used, must precede the **"PLOTS**" command. (LLNL only)
CLASS *level*	Set classification level of FR80 output. The default is UNCLASS. Other levels include: PROGLEV, PARD, ADP, CONFIDNT, SRD, and SYSTEM. This command, if used, must precede the **"PLOTS**" command. (LLNL only)
GIVE	Give the FR80 file to the system for plotting upon termination. This command, if used, must precede the **"PLOTS**" command. (LLNL only)

PLOTS	Create FR80 plotfile containing a record of the TMDS display. (LLNL only)
C	Comment - proceed to next line.
GRID	Overlay displays with a grid of orthogonal lines.
NOGRID	Do not overlay displays with a grid of orthogonal lines (default).
G	View mesh.
GS	View mesh and solid fill elements to identify materials by color
GO	View mesh right of centerline and outline left of centerline.
UG	Display undeformed mesh.
RPVA	Reflect mesh, contour, fringe, etc., plots about vertical axis. Retyping **"RPVA**" turns this option off.
RPHA	Reflect mesh, contour, fringe, etc., plots about horizontal axis. Retyping **"RPHA**" turns this option off.
FRAME	Frame plots with a reference grid (default).
NOFRAME	Do not plot a reference grid.
RJET *n i*	Send a copy of the FR80 file to rjet *n* using plot format *i* where i=1 gives a 5" plot i=2 gives a 8" plot i=3 gives a 10.5" plot i=4 gives the largest possible plot. If i is negative, the plot is sideways, rotated 90 degrees clockwise on the paper. Plots may be sent to either the 11 or 22 inch plotters. (LLNL only)
RESO n_x n_y	Set the x and y resolutions of DYNA2D plots to *nx* and *ny*, respectively. We default both nx and ny to 1024.
LOGO	Put LLNL logo on all plots (default). Retyping this command removes the logo.
O	Plot outlines of all material.
FSON	Plot only free surfaces and slideline interfaces with"**O**" command. [Must be used before "**O**" command.]

FSOFF	Turn off the **"FSON"** command.
MNOFF	Do not plot material numbers with the **"0"**, "**G**", and "**GO**" commands (default).
MNON	Plot material numbers with **"0"**, "**G**", and "**GO**" commands.
CONTOUR *c n m1 m2... mn*	Contour component number *c* on *n* materials including materials *m1, m2,..., mn*. If *n* is zero, only the outline of material *m1* with contours is plotted. Component numbers are given in Table 6.
PRIN *c n m1 m2... mn*	Plot lines of principal stress and strain in the yz plane on *n* materials including materials *m1, m2,..., mn*. If *n* is zero, only the outline of material *m1* is plotted. The lines are plotted in the principal stress and strain directions. Permissible component numbers in Table 6 include 5, 6, 100, 105, 106,...,etc. Orthogonal lines of both maximum and minimum stress are plotted if components 0, 100, 200, etc. are specified.
FRINGE *c n m1 m2... mn*	Fringe component number c on n materials including *m1, m2,..., mn*. If n is zero, only the outline of material m1 with contours is plotted. Component numbers are given in Table 6.
NCOL *n*	Number of colors in fringe plots is n. The default value for n is 6 which includes colors magenta, blue, cyan, green, yellow, and red. An alternative value for n is 5 which eliminates the minimum value magenta.
PROFILE *c n m1 m2...mn*	Plot component c versus element number for n materials including materials m_1, m_2,..., m_n. If n is 0, then component c is plotted for all elements. Component numbers are given in Table 6.
VECTOR *c n m1 m2...mn*	Make a vector plot of component c on n materials including materials m_1, m_2,..., m_n. If n is zero, only the outline of material m_1 with vectors is plotted. Component c may be set to "**D**" and "**V**" for vector plots of displacement and velocity, respectively.
LINE *c n m1 m2...mn*	Plot variation of component c along line defined with the "NLDF", "PLDF", "NSDF", or the "NSSDF" commands given below. In determining variation, consider n materials including material number m_1, m_2,..., m_n.
NLDF *n n1 n2...n3*	Define line for "**LINE**" command using n nodes including node numbers n_1, n_2,...n_n. This line moves with the nodes.
PLDF *n r1 z1...rn zn*	Define line for "**LINE**" command using n coordinate pairs (r_1,z_1), (r_2,z_2),...(r_n,z_n). This line is fixed in space.

NSDF m	Define line for "**LINE**" command as side m. Side m is defined for material n by the "**B**" command.
NSSDF m n	Define line for "**LINE**" command and that includes boundary nodes m to n (counterclockwise) in the interface definitions. This command must follow the "**B**" command.
RANGE r_1 r_2	Set the range of levels to be between r_1 and r_2 instead of in the range chosen automatically by ORION. To deactivate this command, type **RANGE 0. 0.**
MOLP	Overlay the mesh on the contour, fringe, principal stress, and principal strain plots. Retyping "**MOLP**" turns this option off.
NUMCON *n*	Plot n contour levels. The default is 9.
PLOC	Plot letters on contour lines to identify their levels (default).
NLOC	Do not plot letters on contour lines.
IFD *n*	Begin definition of interface n. If interface n has been previously defined, this command has the effect of destroying the old definition.
IFS *m*	Include side m in the interface definition. Side m is defined for material n by the "**B**" command.
IFN *m n*	Include boundary nodes m to n (counterclockwise) in the interface definition. This command must follow the "**B**" command.
IFP *c m*	Plot component c of interface m. Component numbers are given in Table 7.
IFVA r_c z_c	Plot the angular location of the interface based on the center point (r_C,z_C) along the abcissa. Positive angles are measured counterclockwise from the y axis.
IFVS	Plot the distance along the interface from the first interface node along the abcissa (default).
A	Display all slidelines. Slave sides are plotted as dashed lines.
SN *n*	Display slideline n with slave node numbers.
SC *n*	Check slave nodes of slideline n and put any nodes that have penetrated through the master surface back on the master surface.
SD *n*	Dekink slave side of slideline n - after using this command, the **SC** or **MC** command is sometimes advisable.

MN *n*	Display slideline n with master node numbers.
MC *n*	Check master nodes of slideline n and put any nodes that have penetrated through the slave surface back on the slave surface.
MD *n*	Dekink master side of slideline n. After using this command, the **SC** or **MC** command is sometimes advisable.
DE e_1 e_2	Delete elements e_1 to e_2.
DM *n* m_1 m_2... m_n	Delete n materials including m_1, m_2,..., and m_n.
R	Restore original mesh.
DEB *n* f_1 g_1...f_n g_n	Delete n element blocks consisting of element numbers f_1 to g1 f_2 to g_2..., and f_n to g_n inclusive. These elements will be inactive when the calculation resume.
DMB *n* m_1 m_2... m_n	Delete n material blocks consisting of all elements with material numbers m_1, m_2,...,and m_n. These materials will be inactive when the calculations resume.
DSL *n* g_1 g_2...g_n	Delete n slidelines including slideline numbers g_1, g_2,..., and g_n.
TERM *t*	Reset the termination to t.
PRTI Δt	Reset the node and element printout interval to Δt.
PLTI Δt	Reset the node and element data dump interval to Δt
M *n*	Material n is to be rezoned.
NDPLT	Plot node numbers on mesh of material n.
ELPLT	Plot element numbers on mesh of material n.
V	Display material n on TMDS.
VSF	Display material n on TMDS and solid fill elements
S	Smooth mesh of material n. To smooth a subset of elements, a window can be set via the "**GSET**", "**FSET**", OR "**SETF**" commands. Only the elements lying within the window are smoothed.
BLEN *s*	Smooth option where s=0 and s=1 correspond o equipotential and isoparametric smoothing, respectively. By letting 0 s 1 a combined blending is obtained.
TN *r z* ΔL	Type node numbers and coordinates of all nodes within window (r +ΔL / 2, z + ΔL/ 2).

CN *m r z*	Node m has new coordinate (r,z).
B	Determine boundary nodes and sides of material n and display boundary with nodes and side numbers on TMDS.
ER *m n*	Equal space in r-direction boundary nodes m to n (counter-clockwise).
ERS *s*	Equal space in the r-direction boundary nodes on side s.
EZ *m n*	Equal space in z-direction boundary nodes m to n (counter-clockwise).
EZS *s*	Equal space in the z-direction boundary nodes on side s.
ES *m n*	Equal space along boundary, boundary nodes m to n (counter-clockwise).
ESS *s*	Equal space along boundary, boundary nodes on side s.
SLN *m n*	Equal space boundary nodes between nodes m to n on a straight line connecting node m to n.
SLNS *n*	Equal space boundary nodes along side n on a straight line connecting the corner nodes.
VS *m n r*	Vary the spacing of boundary nodes m to n such that r is the ratio of the first segment length to the last segment length.
VSS *s r*	Vary the spacing of boundary nodes on side s such that r is the ratio of the first segment length to the last segment length.
BD *m n*	Dekink boundary from boundary node m to boundary node n (counterclockwise).
BDS *s*	Dekink side s.
TR *t*	DYNA2D will stop and enter interactive rezoning phase at time *t.*

The following commands apply to line plots, interface plots, etc.

ASET *amin amax*	Set minimum and maximum values on abscissa to amin and amax, respectively. If amin=amax=0.0 (default) DYNA2D determines the minimum and maximum values.
OSET *omin omax*	Set minimum and maximum values on ordinate to omin and omax, respectively. If omin=omax=0.0 (default) DYNA2D determines the minimum and maximum values.

ASCL f_a Scale all abscissa data by f_a. The default is f_a=1.

OSCL f_o Scale all ordinate data by f_o. The default is f_o=1.

SMOOTH *n* Smooth a data curve by replacing each data point by the average of the 2n adjacent points. The default is n=0.

Table 6: Component numbers for element variables.

No.	Component	No.	Component
1	y	21 *	ln (V/Vo) (volumetric strain)
2	z	22 *	y-displacement
3	hoop	23 *	z-displacement
4	yz	24 *	maximum displacement
5	maximum principal	25 *	y-velocity, y-heat flux
6	minimum principal	26 *	z-velocity, z-heat flux
7	von Mises	27 *	maximum velocity, max. heat flux
8	pressure or average strain	28	ij normal
9	maximum principal-minimum principal	29	jk normal
10	y minus hoop	30	kl normal
11	maximum shear	31	li normal
12	ij and kl normal	32	ij shear
13	jk and li normal	33	jk shear
14	ij and kl shear	34	kl shear
15	jk and li shear	35	li shear
16	y-deviatoric	36 *	relative volume V/Vo

Table 6: Component numbers for element variables.

No.	Component	No.	Component
17	z-deviatoric	37*	Vo/V-1
18	hoop-deviatoric	38*	bulk viscosity, Q
19*	effective plastic strain	39*	P + Q
20*	temperature	40*	density

Note that by adding 100, 200, 300, 400, and 500 to the component numbers in Table 6 not super-scripted by an asterisk, component numbers for infinitesimal strains, Green-St. Venant strains, Almansi strains, strain rates, and extensions are obtained, respectively. Maximum and minimum principal stresses and strains are in the y-z plane; the corresponding hoop quantities must be examined to determine the overall extremum.

Table 7: Component Numbers for Interface Variables

No.	Component
1	pressure
2	shear stress
3	normal force
4	tangential force
5	y-force
6	z-force

Note that for axisymmetric geometries the force components in Table 7 are per unit radian.

7.0 REMESHING

7.1 OVERVIEW

Remeshing is a new capability in this release of DYNA2D. It is a useful technique for extending Lagrangian analysis to problems with very large shape changes, such as those found in bulk metal forming and some projectile penetration problems. Remeshing can even be useful to simply control element distortion and prevent the time step reduction that occurs when elements become severely distorted.

The DYNA2D remeshing capability works by allowing the user to stop an analysis, enter the rezoner, and write out MAZE line definitions defining the deformed boundary of each material. These line definitions are then read into MAZE where a completely new mesh is developed for the deformed part, along with appropriate boundary conditions, loads, and slidelines. The resulting new analysis model is then input to DYNA2D along with the restart file from the old analysis model. All stresses, velocities, accelerations, and material history variables are initialized from the old model, and the analysis then continues using the new model. This process is described in more detail in section 3.7 on page 33.

7.2 CONSIDERATIONS IN DEVELOPING A NEW MESH

There are few restrictions on the new mesh to be used in a remeshed DYNA2D analysis. However, a few guidelines should be observed in its construction to obtain the best results. These guidelines and some notes on interpreting the results of a remeshed analysis are given in the following paragraphs.

The new mesh may contain a different number of nodes and elements with completely different connectivity than the original mesh. In the new mesh, all elements of a particular material must either:

a) lie completely outside any materials in the old mesh at $t = t_{remesh}$ (i.e., this is a new body in the analysis), or

b) lie completely inside one of the materials in the old mesh at $t = t_{remesh}$. In this case, the elements comprising the material in the new mesh must completely fill the volume of the old mesh material. This condition is ensured by generating line definitions (material

boundaries) in the DYNA2D rezoner at $t = t_{remesh}$ using the commands described in section 6.3 on page 238.

For new mesh materials satisfying case (b) above (i.e., which are remeshed versions of materials present in the old mesh), the material parameters (including density) and the DYNA2D material number should be the same for the new mesh as for their old mesh counterpart. Boundary conditions on new mesh materials satisfying case (a) above may be specified as desired. Boundary conditions on new mesh materials satisfying case (b) should usually be consistent with their old mesh counterparts. For consistency, new mesh load curves evaluated at $t = t_{remesh}$ should have the same value as old mesh load curves evaluated at $t = t_{remesh}$. Nonzero initial velocities should *not* be specified for the new mesh. Velocities for nodes with materials satisfying case (b) above will automatically be remapped onto the new mesh. Velocities for nodes of materials satisfying case (a) above will be initialized to zero. For materials which existed in the old mesh, this procedure assures that velocity will be continuous at $t = t_{remesh}$.

It should remembered that using DYNA2D with the remesh option is still a restart procedure, and therefore the termination time t_f in the new mesh input file should be absolute. A remeshed analysis with the new mesh model will run for $t_{remesh} < t \leq t_f$.

The new mesh model will create a new set of binary plotfiles from DYNA2D (note: these new files will overwrite existing plotfiles if a new plotfile name is not specified on the DYNA2D execution line - see section 3.5 on page 31). In these new plotfiles, state 1 will correspond to $t = t_{remesh}$. Configuration (position), velocity, acceleration, stresses, effective plastic strain, strain rate, and global variables are absolute in that they represent the actual value at the stated time. Displacement and strain are relative in that they are computed with respect to the configuration at $t = t_{remesh}$. Thus, care must be used in the interpretation of displacements and strains from a remeshed analysis.

7.3 REMESHING EXAMPLE 1: ROD IMPACT

To illustrate the continuity achieved in a simulation undergoing a remesh, the standard DYNA2D rod impact problem is analyzed three ways: using a coarse mesh, using a fine mesh, and starting with a coarse mesh and remeshing to a fine mesh at $t = 40\mu s$. The total simulation time for each analysis is $81\mu s$. Figure 27 and Figure 28 show the initial and deformed geometry for the coarse mesh only and the fine mesh only simulations, respectively. Figure 29 shows the mesh configuration of the remeshed analysis at various times. Here, both the coarse (‘‘old mesh’’) and fine (‘‘new

mesh'') models are shown at $t = t_{remesh} = 40\mu s$. Note that the boundaries of the rod at $t = 40\mu s$ in the old mesh and new mesh are coincident. This compatibility is a result of using the DYNA2D rezoner at $t = 40\mu s$ with the coarse mesh to create line definitions to be used in the fine mesh command file for MAZE. The MAZE command files used for the coarse mesh model at $t = 0$ and the fine mesh model at $t = 40\mu s$ are shown in Figure 30 and Figure 31 respectively.

Time histories of the velocity at the free end of the bar for each of the coarse, fine, and remeshed analyses are shown in Figure 32. Note the continuity of the velocity time history for the remeshed analysis. Time histories of kinetic energy for each of the analyses are shown in Figure 33, and again good continuity is achieved.

STACK 3 COARSE MESHES IN HERE, HORIZONTALLY

Figure 27
Rod impact problem using coarse mesh: initial mesh (top), deformed mesh at $t = 40\mu s$ (middle), and deformed mesh at $t = 81\mu s$ (bottom).

STACK 3 FINE MESHES IN HERE, HORIZONTALLY

Figure 28
Rod impact problem using fine mesh: initial mesh (top), deformed mesh at $t = 40\mu s$ (middle), and deformed mesh at $t = 81\mu s$ (bottom).

STACK COARSE/FINE REMAP MESHES IN HERE, HORIZONTALLY

Figure 29
Rod impact problem using remeshing option: initial old mesh at $t = 0\mu s$ (top), deformed old mesh at $t = t_{remap} = 40\mu s$ (upper middle), initial new mesh at $t = t_{remap} = 40\mu s$ (lower middle), and deformed new mesh at $t = 81\mu s$.

Figure 30
MAZE command file used to generate ‘‘old mesh’’ input file for DYNA2D.

Figure 31
MAZE command file used to generate the ‘‘new mesh’’ input file for DYNA2D. Note the line definitions which were written by the DYNA2D rezoner and incorporated into this file.

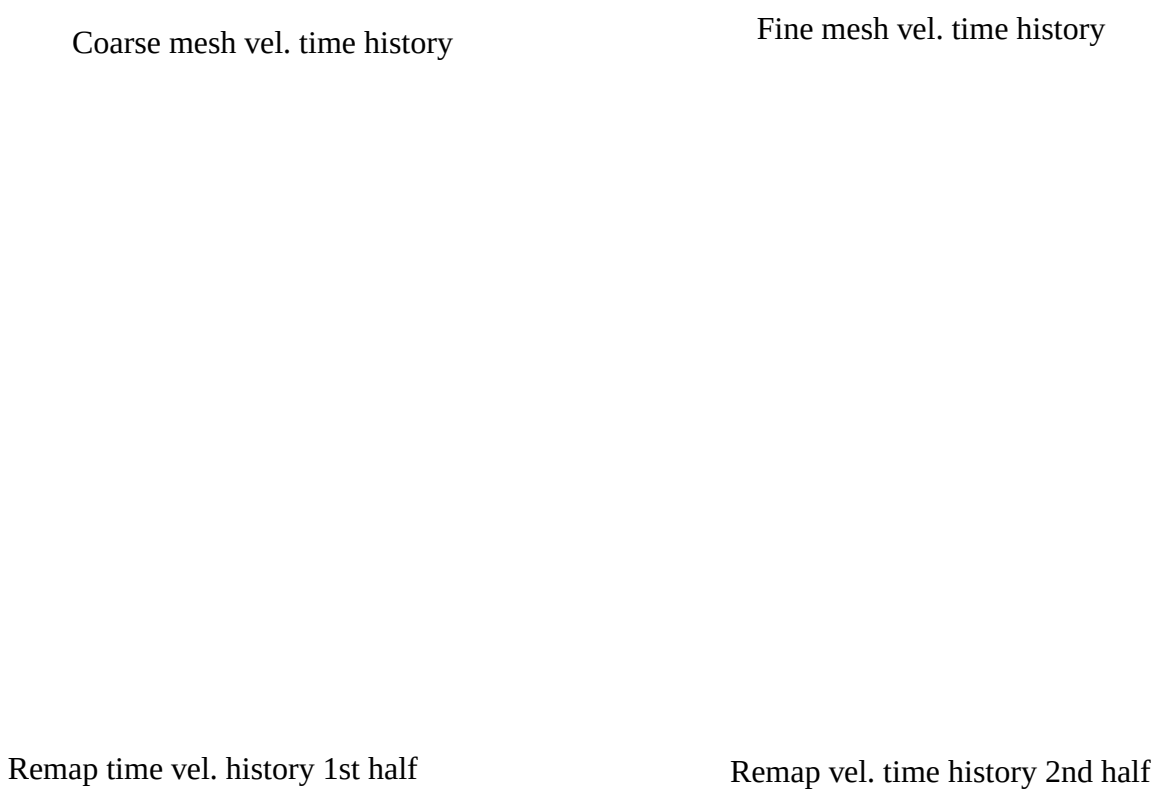

Figure 32
Time history of the axial velocity at the free end of the bar: coarse mesh only (top left), fine mesh only (top right), and coarse to fine remesh (bottom).

Figure 33
Time history of total kinetic energy: coarse mesh only (top left), fine mesh only (top right), and coarse to fine remesh (bottom).

7.4 REMESHING EXAMPLE 2: PASTE EXTRUSION

In this simulation, a paste is extruded through a nozzle by action of a piston. The extruded paste is then used to fill a borehole. This analysis was performed by Doug Faux at LLNL and makes excellent use of the remesh feature in two ways. First, since the paste undergoes large shape changes, remeshing is required to limit element distortion and continue the simulation. Second, the remesh feature allows the entire simulation to be divided into several phases. The model used for each phase contains only components necessary to analyze the response of the paste during that phase.

The axisymmetric model used for the first phase of the analysis includes the cylinder, piston, nozzle, and paste as shown in Figure 34. The cylinder, piston, and nozzle are modeled as elastic materials and the paste is modeled as a compressible inviscid fluid in this example. Figure 35 shows the deformed mesh of the cylinder, nozzle, and paste at the end of Phase 1 ($t = 4.5ms$). The piston was deleted from the model by interactive rezoning at $t = 3.2ms$ to reduce the cost of the analysis.

A remesh was performed at $t = 4.5ms$. The Phase 2 model does not include the cylinder or nozzle since they will have no further effect on the response of the paste. The new model, shown in Figure 36, does include the paste and a new part representing the borehole. Figure 37 zooms in on the Phase 1 and Phase 2 representations of the paste at $t = t_{remesh} = 4.5ms$. The Phase 2 representation includes a finer mesh in the bottom region where most of the deformation is expected to occur. Note that although the mesh topology of the paste varies from one phase to the next, the paste boundaries are exactly preserved.

The Phase 2 simulation continued until $t = 6.2ms$ at which point the paste is deformed as shown in Figure 38. To begin Phase 3, the paste was again remeshed to account for the substantially distorted shape. Figure 39 shows a close-up view of the Phase 2 and Phase 3 representations of the paste. In addition to the new paste mesh, Phase 3 includes the specification of a single-surface slideline to account for the anticipated contact of the paste material with itself. The simulation was terminated at $t = 7.35ms$. Figure 40 shows the deformed paste material and highlights the contact of the paste material with itself, and thus the importance of the added single-surface slideline.

This example provides a graphic demonstration of the power of DYNA2D's new remeshing capability for extending the domain of Lagrangian analysis. The large shape changes in this problem would have once rendered it intractable to Lagrangian codes, forcing a move to Eulerian

codes with substantially increased cost and less precise material boundary definitions. This class of problems is now easily solved with DYNA2D. The authors anticipate that analysts will continue to find new and innovative applications for DYNA2D's new remeshing capability.

Figure 34
Material outline (left) and initial mesh (right) for the first phase of the paste extrusion simulation. Each plot shows the piston at top left, paste at bottom left, cylinder at top right and center right, and nozzle at bottom right

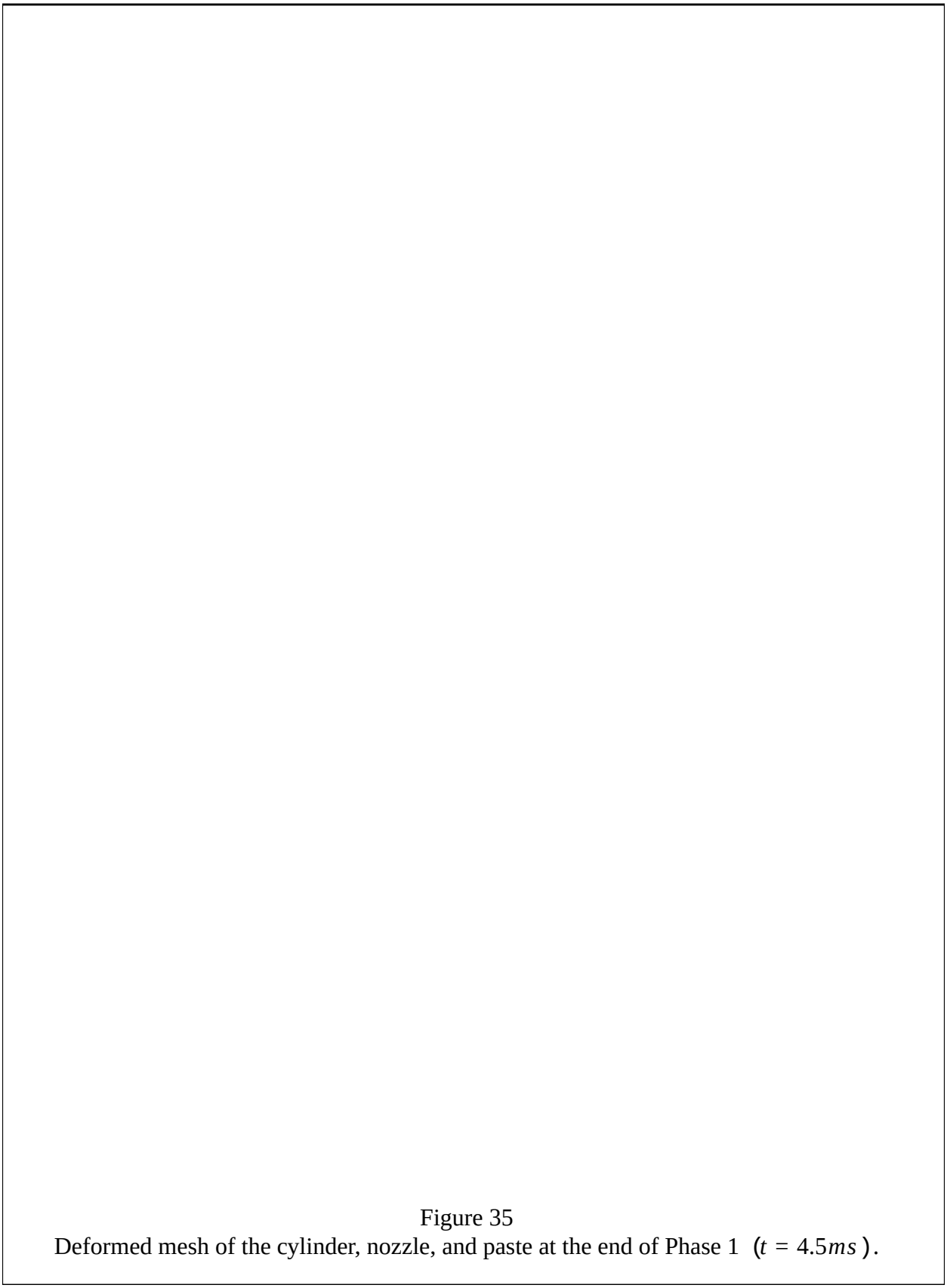

Figure 35
Deformed mesh of the cylinder, nozzle, and paste at the end of Phase 1 ($t = 4.5ms$).

Figure 36
Initial mesh configuration (at $t = 4.5ms$) for the Phase 2 model showing paste and borehole.

Figure 37
Phase 1 (left) and Phase 2 (right) mesh representations of the paste at $t = t_{remesh} = 4.5ms$

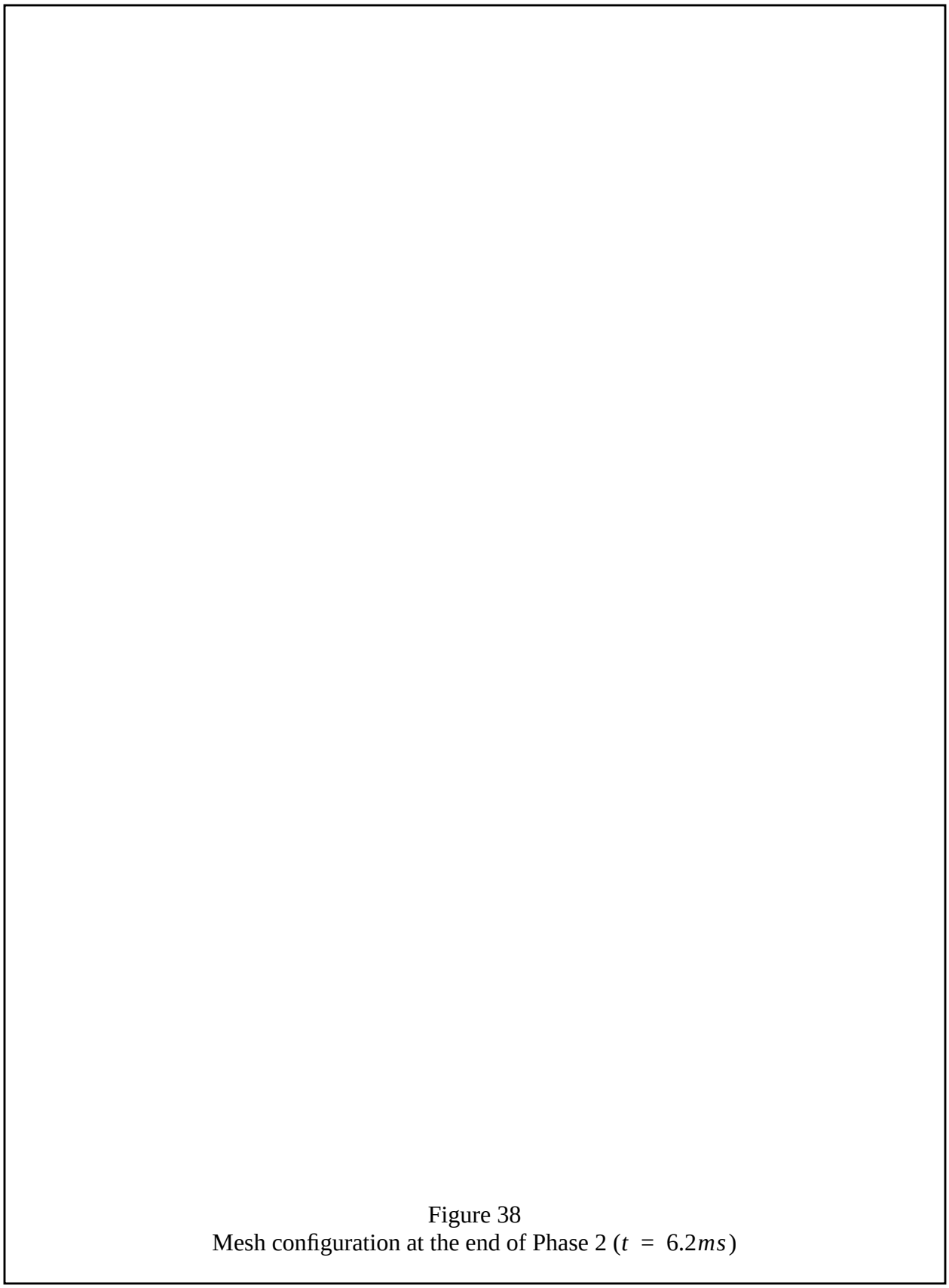

Figure 38
Mesh configuration at the end of Phase 2 ($t = 6.2ms$)

Figure 39
Phase 2 (left) and Phase 3 (right) mesh representations of the paste at $t = t_{remesh} = 6.2ms$

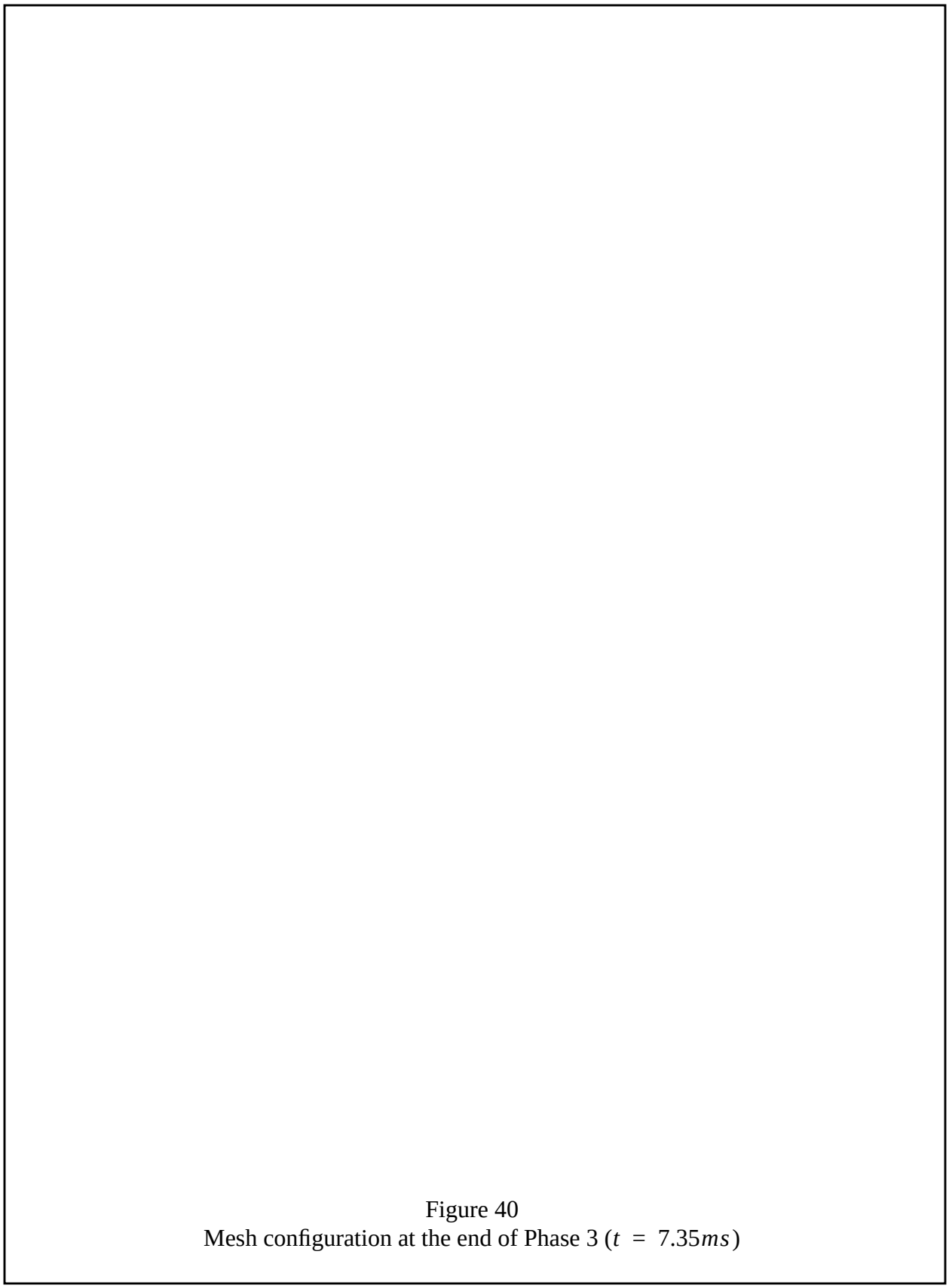

Figure 40
Mesh configuration at the end of Phase 3 ($t = 7.35ms$)

8.0 MATERIAL MODEL DRIVER

8.1 OVERVIEW

This section describes a Material Model Driver which is incorporated into DYNA2D. The Material Model Driver allows interactive plotting of the stress-strain response predicted by a material model under a given load path. This feature is particularly useful when fitting complex material models to experimental data, or when using a material model for the first time. The interactive graphics plotting capability of the Material Model Driver allows the simulated material stress-strain behavior to be easily compared with actual material test results or theoretical predictions.

The material model driver works with any DYNA2D material model and computes the stress history corresponding to a given strain history without including the effects of dynamic response. The dynamic equations of motion are not used by the material model driver, and therefore the material behavior is simulated independent of inertial effects. These inertial effects would be present and complicate the interpretation of the results if a "one-element" problem were used to demonstrate the material model behavior. Rate dependence in the constitutive model is included, so realistic strain rates must be used with the Material Model Driver for rate-dependent materials.

8.2 INPUT DEFINITION

The Material Model Driver is invoked by setting the number of nodes and elements to zero in a standard DYNA2D input file (described in Chapter 4 of this manual). The number of load curves should be set to five, and the termination time should be set to the desired length of the simulation. The state plot dump interval (Control Card 6) is interpreted as the time step to be used in the Material Model Driver run. This value should be chosen in conjunction with the strain vs. time description in the load curves to yield realistic strain increments at each step of the simulation. Plotting information is saved at every step of a Material Model Driver run.

The remainder of the DYNA2D input file should be as specified in Chapter 4 up through the material model definition. Immediately after the material definition, five load curves describing the strain path should be defined. These five curves describe the time history of the displacement gradient components shown in Table 1, where x, y, and z represent three orthogonal coordinate directions and u, v, and w represent displacement fields in those directions, respectively. For

axisymmetry, x is assumed to be the hoop direction, and z is the axis of symmetry. For plane strain, ε_{xx} is set to zero regardless of the value of load curve three. Note that if a rate-dependent model is used, then the "time" in the Material Model Driver corresponds to physical time and must yield realistic strain rates. If a rate-independent material model is used, then "time" is really a nonphysical quasi-time used to parameterize the strain history, and any convenient scale may be used (such as a Driver time step size of 1.0 and a termination time equal to the number of steps desired).

Table 8: Load Curve Component Definitions

Load Curve Number	Component Definition
1	$\frac{\partial v}{\partial y}$
2	$\frac{\partial w}{\partial z}$
3	$\frac{\partial u}{\partial x}$
4	$\frac{\partial v}{\partial z}$
5	$\frac{\partial w}{\partial y}$

The strain rate, or rate of deformation in a finite strain context, is found by taking the symmetric part of a finite difference time derivative of the gradient components specified by the load curves. For example, if the above components are considered to form a tensor $\boldsymbol{S}$, then a tensor $\boldsymbol{L}$ at time t_k (corresponding to step k) is calculated from

$$\boldsymbol{L}(t_k) = \frac{\boldsymbol{S}(t_k) - \boldsymbol{S}(t_{k-1})}{(t_k - t_{k-1})} \quad , \tag{260}$$

and then the rate of deformation $\boldsymbol{d}$ is found from

$$\boldsymbol{d} = \frac{1}{2}(\boldsymbol{L} + \boldsymbol{L}^T) \tag{261}$$

and the spin is found from:

$$\mathbf{W} = \frac{1}{2}(\boldsymbol{L} + \boldsymbol{L}^T). \tag{262}$$

In a small strain context, load curves 1-4 may be used to specify strain time histories, and load curve 5 simply defined as zero throughout the duration of the simulation. *All five load curves must be defined in all cases, and must be defined over the entire time interval of the simulation.* The small strain interpretation of the load curve quantities is given in Table 2.

Table 9: Small Strain Load Curve Definitions

Load Curve Number	Small Strain Interpretation
1	ε_{rr} or ε_{yy}
2	ε_{zz}
3	$\varepsilon_{\theta\theta}$
4	γ_{yz} (engineering)
5	not used

8.3 INTERACTIVE COMMANDS

The Material Model Driver contains an integral plotting package to allow immediate display of simulation results. After reading the input file and completing the calculations, DYNA2D gives a command prompt to the terminal. A summary of the available interactive commands is given in this section. An on-line help package is available by typing **help** at the prompt. Refer to the notational conventions described in section 2.1 on page 7.

- **ASCL** - scale all abscissa data by f. default is $f = 1$.
- **OSCL** - scale all ordinate data by f. default is $f = 1$.
- **ASET** - *amin omax* - set minimum and maximum values on abscissa to *amin* and *amax*, respectively. If *amin*=*amax*=0, scaling is automatic.
- **OSET** - *omin omax* - set minimum and maximum values on ordinate to *omin* and *omax*, respectively. If *omin*=*omax*=0, scaling is automatic.

- **GRID** - tmds or graphics display will be overlayed by a grid of orthogonal lines
- **NOGRID** - tmds or graphics displays will not be overlayed by a grid of orthogonal lines
- **LOGO** - puts LLNL logo on all plots (default). Retyping this command removes the logo.
- **TV** *n* - use tmds *n* or graphics device *n*, where *n* is the monitor or device number
- **TV** - *n1 n2 n3* - (LLNL only) use color tmds with monitor numbers *n1*, *n2*, and *n3* for red, green, and blue channels, respectively.
- **PLOTS box** *ann* - (LLNL only) create a plotfile for box number *ann* that contains a record of the tmds display
- **CLASS** *lev* - (LLNL only) reset classification level of hardcopy output from default unclassified to: proglev, pard, adp, confidnt, srd, or system. This command must precede the plots command if used.
- **RJET** *n* - (LLNL only) send a copy of the fr80 file to rjet *n*
- **TIME** *c* - plot component *c* versus time
- **CROSS** *c1 c2* - plot component *c1* versus *c2*
- **PRINT** - print plotted time history data in file "pamper." Only data plotted after this command is printed. File name can be changed with the “FILE” command. The “pampers” file contains 2-column ASCII data suitable for plotting with other software.
- **FILE** *name* - change pampers filename to *name*.
- **RDLC** *m n r1 z1 ... rn zn* - redefine load curve *m* using *n* coordinate pairs (*r1,z1),(r2,z2),...,(rn,zn*)
- **CONTINUE** - reanalyze material model
- **ECOMP** - display component numbers on the tmds or graphics display. The component numbers are also shown in Table 3.
- **CHGL** *n* - change label for component *n*. Program will prompt for new label.
- **QUIT, END, T** - exit the material model driver

9.0 EXAMPLE PROBLEM

This example, taken from (Randers-Pehrson and Juriacs, 1968) illustrates the analysis of a type of shaped charge called a ‘‘self-forging fragment.’’

Figure 41
Initial mesh used in shaped charge calculation.

Calculations were performed to study the formation of the fragment produced by the upper plate. The initial mesh is shown in Figure 41. Slidelines are initially placed between the plate-HE and cylinder-HE interfaces. By $t = 10\mu s$ the HE has burn has completed. Between $t = 12\mu s$ and $t = 50\mu s$ elements at the outer edges of the plate become elongated and cause a significant decrease in the time-step size, so these elements are eliminated prior to $t = 50\mu s$. By $t = 50\mu s$ the pressure in the HE has dropped to negligible levels, so at $t = 50\mu s$ all elements except those in the upper plate are eliminated from the calculation. In addition, at this time a new slideline is defined along the upper surface to prevent the plate from penetrating through itself as it folds.

Figure 42 shows a view of the deformed shape at $t = 50\mu s$. The formation of the fragment is shown in Figure 43, which contains a sequence of deformed shapes at $20\mu s$ intervals.

Figure 42
Deformed shape at $50\mu s$.

Figure 43
Formation of fragment.

ACKNOWLEDGEMENTS

The authors first wish to acknowledge the many suggestions and requests from the DYNA2D user community. Collaborative feedback from analysts and researchers, both inside LLNL and in industry, has been invaluable in contributing to this manual and to the continuing evolution of DYNA2D.

In particular, thanks to Dr. Glenn Randers-Pehrson of the Ballistic Research Laboratory for his many suggestions and contributions, especially in regards to the material models in DYNA2D. Thanks also to Dr. Len Schwer and Ms. Barbara Lewis (Aptek, Inc.) for their day-to-day feedback and suggestions for the improvement of DYNA2D, especially the improvements to Material Type 5 and ALE. The assistance of Mr. Ernie Moor (LLNL) with the documentation of Material Type 16 is gratefully acknowledged. Appreciation is also extended to Dr. Phil Church of RARDE in the U. K. for the contribution of the Armstrong-Zerilli material model. In addition, many thanks to all of the LLNL analysts, whose discussions, experiences, and frustrations have shaped the continuing development of DYNA2D.

The automatic contact and eroding slideline algorithms were developed from 1987 to 1988 by Dr. John Hallquist during his tenure at LLNL. Slightly modified versions of these algorithms have been incorporated into this release of DYNA2D. The documentation of these capabilities should greatly expand their impact on the user community.

The contributions of Dr. David Benson during his tenure as co-developer of DYNA2D from 1984 to 1987 are gratefully acknowledged. In particular, the ALE capabilities developed by Dr. Benson during that period have proven a valuable addition to DYNA2D.

The authors also wish to acknowledge their colleagues in the Methods Development Group at LLNL. Dr. Jerry Goudreau, Dr. Brad Maker, Mr. Tom Spelce, and Dr. Mark Christon all provided ideas, technical insight, and encouragement. In particular, the authors wish to acknowledge Tom Spelce, who served as lead developer on DYNA2D from mid-1988 to September of 1990 and implemented the Rate-Dependent Steinberg-Guinan-Lund model and significantly improved the Material Model Driver.

Finally, the authors wishes to again acknowledge Dr. John Hallquist for his pioneering work on the DYNA2D code and his contributions to the field of computational mechanics.

REFERENCES

1. Armstrong, R. W., and Zerilli, F. J., ‘‘Dislocation Mechanics Based Analysis of Material Dynamics Behavior,’’ *Journal de Physique, Colloque C3,* Vol. 49, pp. 529-534, **1988**.
2. Baker, E. L., ‘‘An Explosives Products Thermodynamic Equation of State Appropriate for Material Acceleration and Overdriven Detonation: Theoretical Background and Formulation,’’ Technical Report ARAED-TR-91013, U. S. Army Armament Research, Development and Engineering Center, Picatinney Arsenal, New Jersey, **1991**.
3. Baker, E. L., and Orosz, J., ‘‘Advanced Warheads Concepts: An Advanced Equation of State for Overdriven Detonation,’’ Technical Report ARAED-TR-91007, U. S. Army Armament Research, Development and Engineering Center, Picatinney Arsenal, New Jersey, **1991**.
4. Bammann, D. J., “Modeling Temperature and Strain Rate Dependent Large Deformation of Metals,” *Applied Mechanics Reviews,* Vol. 43, pp. 312-319, **1990**.
5. Bammann, D. J., Johnson, J. C., and Chiesa, M. L., “A Strain Rate Dependent Flow Surface Model of Plasticity,” Sandia National Laboratories, Report SAND90-8227, **1990**.
6. Bammann, D. J., Chiesa, M. L., McDonald, A., Kawahara, W. K., Dike, J. J., and Revelli, V. D., “Prediction of Ductile Failure in Metals,” in *Failure Criteria and Analysis in Dynamic Response,* H. E. Lindberg, ed., ASME AMD Vol. 107, pp. 7-12, November, **1990**.
7. Bammann, D. J., Chiesa, M. L., Horstemeyer, M. F., and Weingarten, L, I., “Failure in Ductile Materials Using Finite Element Methods,” in Structural Crashworthiness and Failure, N. Jones and T. Wierzbicki, eds, Elsevier Applied Science Publishers, **1993**.
8. Benson, D. J., ‘‘Simple ALE in DYNA2D,’’ Unpublished LLNL Notes, **1986**.
9. Benson, D. J., ‘‘An Efficient, Accurate, Simple ALE Method for Nonlinear Finite Element Programs,’’ *Computer Methods in Applied Mechanics and Engineering*, Vol. 72, pp. 305-350, **1989**.
10. Burton, D.E. et al., “Physics and Numerics of the TENSOR Code,” University of California, Lawrence Livermore National Laboratory, Report UCID-19428, July, **1982**.
11. Chen, W. F., and Baladi, G. Y., *Soil Plasticity: Theory and Implementation*, Elsevier, New York, **1985**.
12. Church, P. D., and Cullis, I., ‘‘Development and Application of High Strain Rate Constitutive Models in Hydrocodes,” *Journal de Physique IV, Colloque C3,* Vol. 1, pp. 917-922, **1991**.
13. Cochran, S. G. and J. Chan, “Shock Initiation and Detonation Models in One and Two Dimensions,” University of California, Lawrence Livermore National Laboratory, Rept. UCID-18024, **1979**.
14. Desai, C. S., and Siriwardane, H. J., *Constitutive Laws For Engineering Materials With Emphasis On Geologic Materials*, Prentice-Hall, Chapter 10, **1984**.

15. Dilger, W. H., Koch, R., and Kowalczyk, R., "Ductility of Plain and Confined Concrete Under Different Strain Rates," ACI Journal, January-February, **1984**.

16. Dobratz, B.M., and Crawford, P. C., "LLNL Explosives Handbook: Properties of Chemical Explosives and Explosive Simulants," University of California, Lawrence Livermore National Laboratory, Rept. UCRL-52997, Rev. 2, **1985**.

17. Engelmann, B. E., and Hallquist, J. O., "NIKE2D: A Nonlinear, Implicit, Two-Dimensional Finite Element Code for Solid Mechanics - User Manual," University of California, Lawrence Livermore National Laboratory, UCID Report, **1991**.

18. Fickett, W., *Introduction to Detonation Theory*, University of California Press, Berkeley, **1985**.

19. Flanagan, D.P. and T. Belytschko, "A Uniform Strain Hexahedron and Quadrilateral and Orthogonal Hourglass Control," *Int. J. Numer. Meths. Eng.*, 17, pp. 679-706, **1981.**

20. Ghosh, S., and Kikuchi, N., ''An Arbitrary Lagrangian-Eulerian Finite Element Method for Large Deformation Analysis of Elastic-Viscoplastic Solids,'' *Computer Methods in Applied Mechanics and Engineering*, Vol. 86, pp. 127-188, **1991**.

21. Giroux, E.D. "HEMP User's Manual," University of California, Lawrence Livermore National Laboratory, Rept. UCRL-51079, **1973**.

22. Goldthorpe, B. D., ''Constitutive Equations for Annealed and Explosively Shocked Iron for Application to High Strain Rates and Large Strains,'' *Journal de Physique IV, Colloque C3,*, Vol. 1, pp. 829-835, **1991**.

23. Goudreau, G.L. and J.O. Hallquist, "Recent Developments in Large Scale Finite Element Lagrangian Hydrocode Technology," *J. Comp. Meths. Appl. Mechs. Eng.*, 30, **1982**.

24. Haber, R. B., ''A Mixed Eulerian-Lagrangian Displacement Model for Large-Deformation Analysis in Solid Mechanics,'' Computer Methods in Applied Mechanics and Engineering, Vol. 43, pp. 277-292, **1984**.

25. Hallquist, J.O. "A Procedure for the Solution of Finite Deformation Contact-Impact Problems by the Finite Element Method," University of California, Lawrence Livermore National Laboratory, Rept. UCRL-52066, **1976**.

26. Hallquist, J.O. "A Numerical Treatment of Sliding Interfaces and Impact," in: K.C. Park and D.K. Gartling (eds.), *Computational Techniques for Interface Problems*, AMD Vol. 30, ASME, New York, **1978**.

27. Hallquist, J. O., ''DYNA2D - An Explicit Finite Element and Finite Difference Code for Axisymmetric and Plane Strain Calculations (User's Guide),'' University of California, Lawrence Livermore National Laboratory, Report UCRL-52429, March, **1978a**.

28. Hallquist, J. O., "MAZE - An Input Generator for DYNA2D and NIKE2D," University of California, Lawrence Livermore National Laboratory, Rept. UCID-19029, Rev. 2, **1983**.

29. Hallquist, J. O., ‘‘User’s Manual for DYNA2D - An Explicit Two-Dimensional Hydrodynamic Finite Element Code with Interactive Rezoning and Graphical Display,’’ University of California, Lawrence Livermore National Laboratory, Report UCID-18756, Revs. 1-3, (1980-1988), Rev. 3, **1988**.

30. Hallquist, J.O., G.L. Goudreau, and D.J. Benson, “Sliding Interfaces with Contact-Impact in Large Scale Lagrangian Computations,” *Comp. Meths. Appl. Mech. Eng.*, 51, pp. 107-137, **1985**.

31. Hallquist, J. O. and Levatin, J. L., “ORION: An Interactive Color Post- Processor for Two Dimensional Finite Element Codes,” University of California, Lawrence Livermore National Laboratory, Rept. UCID-19310, Rev. 2, **1985**.

32. Hancock, S. L., “An Hourglass Subtraction Procedure,” TCAM Tech. Memo 73-6, Physics International Co., San Leandro, California, **1973**.

33. Hancock, S. L, “Equations for Forces in Axisymmetric Lagrange Zones,” Proceedings of the Second International Conference on Computational Methods in Nonlinear Mechanics**, 1979**.

34. Hill, R., *The Mathematical Theory of Plasticity*, Clarendon Press, Oxford, **1950**.

35. Isenberg, J., Vaughn, D. K., and Sandler, I., “Nonlinear Soil-Structure Interaction,” EPRI Report MP-945, Weidlinger Associates, December, **1978**.

36. Johnson, G. C. and Bammann, D. J., “A Discussion of Stress Rates in Finite Deformation Problems,” Sandia National Laboratories, Livermore, California, Rept. 82-8821, **1982**.

37. Johnson, G.R. and W. H. Cook, “A Constitutive Model and Data for Metals Subjected to Large Strains, High Strain Rates and High Temperatures,” Presented at the Seventh International Symposium on Ballistics, the Hague, The Netherlands, April, **1983**.

38. Johnson, G. R., and Stryk, R. A., ‘‘User Instructions for the EPIC-2 Code,’’ AFATL-TR-86-51, **1986.**

39. Johnson, G. R., and Stryk, R. A., ‘‘Eroding Interface and Improved Tetrahederal Element Algorithm for High-Velocity Impact Computations in Three Dimensions,’’ *International Journal of Impact Engineering*, Vol. 5, pp. 411-421, **1987**.

40. Kenchington, G.J., “A Non-Linear Elastic material Model for DYNA3D,” Proceedings of the DYNA3D Users Group Conference, published by Boeing Computer Services (Europe) Limited, September, **1988**.

41. Key, S.W. “HONDO - A Finite Element Computer Program for the Large Deformation Dynamic Response of Axisymmetric Solids,” Sandia National Laboratories, Albuquerque, N.M., Rept. 74-0039, **1974**.

42. Kimsey, K. D., and Zukas, J. A., ‘‘Contact Surface Erosion for Hypervelocity Problems,’’ BRL-MR-3495, **1986**.

43. Krieg, R.D. and S.W. Key, "Implementation of a Time Dependent Plasticity Theory into Structural Computer Programs," Vol. 20 of *Constitutive Equations in Viscoplasticity: Computational and Engineering Aspects*, American Society of Mechanical Engineers, New York, N.Y., pp. 125-137, **1976**.

44. Lee, E.L. and C.M. Tarver, "Phenomenological Model of Shock Initiation in Heterogenous Explosives, *Phys. Fluids*, Vol. 23, p. 2362, **1980**.

45. Liu, W. K., Belytschko, T., and Chang, H., ''An Arbitrary Lagrangian-Eulerian Finite Element Method for Path-Dependent Materials, *Computer Methods in Applied Mechanics and Engineering*, Vol. 58, pp. 227-245, **1986**.

46. Mader, C., Numerical Modeling of Detonations, University of California Press, Berkeley, **1979**.

47. Maenchen, G. and Sack, S., "The Tensor Code," in *Methods in Computational Physics*, Vol. 3, Academic Press, New York, **1964**.

48. Maker, B. N., Ferencz, R. M., and Hallquist, J. O., "NIKE3D: A Nonlinear, Implicit, Three-Dimensional Finite Element Code for Solid and Structural Mechanics - User's Manual, University of California, Lawrence Livermore National Laboratory, Report UCRL-MA-105268, January, **1991**.

49. Moor, E., University of California, Lawrence Livermore National Laboratory, Private Communication, April, **1991**.

50. Nutt, G. L., "A Reactive Flow Model for a Monomolecular High Explosive", University of California, Lawrence Livermore National Laboratory, Report UCRL-97601, **1987**.

51. Nutt, G. L., and Erickson, L. M., "Reactive Flow Lagrange Analysis in Plastic Bonded Explosives", JOEM, Vol. 2, No. 263, **1984**.

52. Pagano, N. J., "Exact Moduli of Anisotropic Laminates," Mechanics of Composite Materials, Vol. 2, G. P. Sendickyj, ed., Academic Press, New York, pp. 23-44, **1974**.

53. Randers-Pehrson, G., and Juriaco, I. P., *Computer Aided Self-Forging Fragment Design*, U.S. Army Science Conference Proceedings, West Point, N.Y., **1968**.

54. Richards, G. T., "Derivation of a Generalized Von Neuman Psuedo-Viscosity with Directional Properties," University of California, Lawrence Livermore National Laboratory, Rept. UCRL-14244, **1965**.

55. Sackett, S.J., "Geological/Concrete Model Development," Private Communication, **1987**.

56. Sandler, I.S. and D. Rubin, "An Algorithm and a modular subroutine for the cap model," *Int. J. Numer. Analy. Meth. Geomech.*, 3, pp. 173-186, **1979**.

57. Schwer, L. E., **"**Viscoplastic Augumentation of the Smooth Cap Model," *Nuclear Engineering and Design*, 150, pp. 215-233, **1994**.

58. Schwer, L. E., and Murray, Y., **"**A Three-Invariant Smooth Cap Model with Mixed Hardening,'' *International Journal for Numerical and Analytical Methods in Geomechanics*, 18, pp. 657-688, **1994**.

59. Schwer, L. E., Rosinsky, R., and Day, J., ''An Axisymmetric Lagrangian Technique for Predicting Earth Penetration Including Penetrator Response,'' *International Journal for Numerical and Analytical Methods in Geomechanics,* Vol. 12, pp. 235-262, **1988**.

60. Shapiro, A. B., "TOPAZ3D - A Three Dimensional Finite Element Heat Transfer Code," University of California, Lawrence Livermore National Laboratory, Report UCID-20484, **1985**.

61. Shapiro, A. B., and Edwards, A. L., "TOPAZ2D Heat Transfer Code Users Manual and Thermal Property Data Base," University of California, Lawrence Livermore National Laboratory, Report UCRL-ID-104558, May, **1990**.

62. Simo, J. C., J.W. Ju, K.S. Pister and R.L. Taylor, "An assessment of the cap model: Consistent return algorithms and rate-dependent extension,: *J. Eng. Mech.*, Vol. 114, No. 2, pp. 191-218, **1988**.

63. Simo, J. C., J.W. Ju, K.S. Pister and R.L. Taylor, "Softening Response, Completeness Condition, and Numerical Algorithms for the Cap Model," Int. *J. Numer. Analy. Meth. Eng.*, **1990**.

64. Speicher, S. J., and Brode, H. L., Pacific-Sierra Research Corporation, Report PSR-1630, April, **1987**.

65. Steinberg, D.J. "Equation of State and Strength Properties of Selected Materials," University of California, Lawrence Livermore National Laboratory, Report UCRL-MA-106439, **1991**.

66. Steinberg, D.J. and M.W. Guinan, "A High-Strain-Rate Constitutive Model for Metals," University of California, Lawrence Livermore National Laboratory, Rept. UCRL-80465, **1978**.

67. Steinberg, D.J. and C. M. Lund, "A Constitutive Model for Strain Rates from 10^{-4} to 10^{6} S^{-1}**,"** *Journal of Applied Physics,* Vol. 65, p. 1528, **1989**.

68. Spelce, T., and Hallquist, J. O., "TAURUS: An Interactive Post-Processor for the Analysis Codes NIKE3D, DYNA3D, TOPAZ3D, and GEMINI, University of California, Lawrence Livermore National Laboratory, Report UCRL-MA-105401, May, **1991**.

69. Snow, P., ''KEPIC-2,'' Kaman Sciences Corporation, Report K82-46U, **1982**.

70. Stecher, F. P., and Johnson, G. R., ''Lagrangian Computations for Projectile Penetration into Thick Plates,'' in *Computers in Engineering*, W. A Grover, Ed., Vol. 2, ASME, pp. 292-299, **1984**.

71. Stillman, D. W. and J. O. Hallquist, "INGRID: A Three-Dimensional Mesh Generator for Modeling Nonlinear Systems," University of California, Lawerence Livermore National Laboraotry, Rept. UCID-20506, **1985**.

72. Tarver, C. M., and Hallquist, J. O., *Proceedings of the Seventh Symposium on Detonation*, Naval Surface Weapons Center, NSWC MP82-334, Annapolis, MD, p. 488, **1981**.

73. Tarver, C. M., Hallquist, J. O., and Erickson, L. M., *Proceedings of the Eighth International Symposium on Detonation*, Naval Surface Weapons Center, NSWC MP86-194, Albuquerque, NM, p. 951, **1985**.

74. Tarver, C. M., *Propellants, Explosives, and Pyrotechnics*, Vol. 15, p. 132, **1990**.

75. Whirley, R. G., and Engelmann, B. E., “A Vectorized Numerical Implementation of a Two-Invariant Cap Model including Kinematic Hardening,” University of California, Lawrence Livermore National Laboratory, UCID Report, **1991b**.

76. Wilkins, M. L., “Calculation of Elastic-Plastic Flow,” University of California, Lawrence Livermore National Laboratory, Rept. UCRL-7322, Rev. I, **1969**.

77. Wilkins, M. L., “The Use of Artificial Viscosity in Multidimensional Fluid Dynamics Calculations,” University of California, Lawrence Livermore National Laboratory, Rept. UCRL-78348, **1976**.

78. Wilkins, M.L., R.E. Blum, E. Cronshagen, and P. Grantham, "A Method for Computer Simulation of Problems in Solid Mechanics and Gas Dynamics in Three Dimensions and Time," University of California, Lawrence Livermore National Laboratory, Rept. UCRL-51574, **1974**.

79. Woodruff, J.P. "KOVEC User's Manual," University of California, Lawrence Livermore National Laboratory, Rept. UCRL-51079, **1973**.